THE CONCEPTUAL DESIGN OF A TIDAL POWER PLANT IN THE BROUWERSDAM

Author   M.H. van Saase

Date   12 January 2018

Status   Final report

THE CONCEPTUAL DESIGN OF A TIDAL POWER PLANT IN THE BROUWERSDAM

Final Report

Student

M.H. van Saase

Student ID: 4080319

mark_saas@hotmail.com

Tel. +316 51 92 41 14

Thesis committee:

Prof. dr. ir. S.N. Jonkman,	TU Delft
Ir. W.F. Molenaar,	TU Delft
Dr. ir. Drs. C.R. Braam	TU Delft
Ir. B. Reedijk,	BAM Infra

TU Delft

Faculty of Civil Engineering an Geosciences

Date: 12-1-2018

PREFACE

After more than seven years studying at the faculty of Civil Engineering at the TU Delft, this master thesis finalizes my master programme in Hydraulic Engineering at the Delft university of Technology. This master thesis represents a conceptual design of a Tidal Power Plant in the Brouwersdam, in the province Zeeland, the south-west of the Netherlands.

In the search of a satisfying graduation topic, I found myself back at BAM, one of the largest contractor of The Netherlands. After completing an internship at BAM International in Dubai in 2015, I decided to elaborate my thesis at BAM Infraconsult. BAM provided me with a design topic, a Tidal Power Plant in the Brouwersdam.

Special thanks for Bas Reedijk and Erik ten Oever for providing me with information and their knowledge of previous performed research to the Tidal Power Plant.

Secondly, I would like to thank my daily supervisor from the Delft University of Technology: ir. W.F. Molenaar. Thanks to his advice, knowledge, encouraging me to keep up the pace and the pleasant meetings, I was able to write this thesis. I would also like to acknowledge Dr. ir. Drs. C.R. Braam for helping me with the structural elements in this thesis. Furthermore, I would like to thank Prof. dr. ir. S.N. Jonkman for chairing my committee and for the critical advice during the meeting.

Finally, during the months spent at the section Coastal Engineering at BAM Infraconsult in Gouda, I had the pleasure of collaborating with many interesting and very kind colleagues. My gratitude extends to every one of the Coastal Engineering department for contributing to the pleasant time I have had.

CONTENTS

SUMMARY

Zeeland, located in the south west of The Netherlands, has suffered major casualties and damage due to the flood in 1953. After the disaster, the Dutch Government appointed the so-called Deltacomittee, provided with the task of advising on the execution of the Deltaplan. As part of the Deltaplan, North Sea estuaries has been closed off from the North Sea in order to provide sufficient safety against flooding in the future.

The 11000 hectare Lake Grevelingen was one of the closed off North Sea estuaries. Two dams and two islands enclose the lake and prevent fresh water flowing in. Characteristic of former estuaries are deep gullies that remain intact as any kind of sediment transport is prevented. Contact with the North Sea is prevented due to the construction of the Brouwersdam, the western border of Lake Grevelingen. Direct after finishing the construction works of the Brouwersdam, Lake Grevelingen showed reducing oxygen gradients and thus a decreasing water quality, especially at the deep gullies. The construction of a stop lock, the Brouwerssluice, was conducted to prevent the further decrease of the oxygen gradient.

Today, more than 40 years after finalizing the Brouwerssluice, the low oxygen gradient tends to rise to shallower areas and reaches critical values. Measures, such as a water inlet system are due to be constructed.

Introducing a tidal range of 50 cm has shown to be a valid solution to overcome the decreasing water quality. The tidal range allows thinking of power generation when water flowing in or out Lake Grevelingen. Generating tidal energy produces revenues and provides renewable energy. Therefore, the design of a Tidal Power Plant in the Brouwersdam has become the goal of this thesis.

Since caissons were used to close Lake Grevelingen off from the North Sea, as a starting point, it has been determined whether these caissons allow reusing with a new function; forming the powerhouse of a Tidal Power Plant. Mainly due to the concrete cover of the caisson, has shown to be inappropriate. Adapting the caissons becomes expensive and very time-consuming.

The starting point of the power plant construction was found in the turbine dimensions. In total six turbine types have been analyzed. Based on their efficiency, fish friendliness and ability to generate power in two directions, two optimal turbine types for low head power generation have been found: free-stream (Tocardo) and a modified bulb turbine (Pentair Fairbanks Nijhuis).

Due to the low head differences between lake Grevelingen and the North Sea, maximum energy generation will be required even for very low head differences. Hence, turbines able to generate energy at such low head differences will be required. In the Preliminary turbine design, two turbine types provided the most promising features: The Pentair Fairbanks modified Bulb turbine and the Tocardo free-stream turbine.

A total cross-sectional discharge area of 960 m2 would lead to a tidal range of 50 cm at Lake Grevelingen. Applying in total 18 turbines in a squared sluiceway with an inner space of 8.24 meter allows introducing a tidal range of 50 cm at the lake.

The free-stream turbine has already proven to generate power in low head environments in previous projects. The PFN modified bulb turbine has not yet been tested on such scale, but due to the expected higher efficiency rate, the energy

generation of the PFN lies supposedly much higher than the Tocardo free-stream turbine. Therefore, it has been decided to temporarily apply the free-stream turbine until the PFN turbine has shown to meet the fish friendly requirements while ensuring high efficiencies. With current knowledge, the annual production of the Tocardo and PFN turbine has been estimated at 20 GWh and 80 GWh respectively. The energy production of the freestream turbine is based on the tidal data obtained from 2016. The same tidal data has been applied to the PFN turbine while accounting for the sea level rise as well. Since it is expected the PFN turbine will be in commission at 2030, an estimated sea level rise of 25 cm has been added to the 2016 tidal data.

The dimensions of the powerhouse, the structure containing all Tidal Power Plant components, have consequently been determined using the turbine dimensions as a starting point. A water retaining gate at the North Sea side, designed to prevent water flowing in when maximum or minimum allowed water level at Lake Grevelingen is reached, resulted together with the overtopping requirement in a height of +10.04 meter NAP. Including the turbine maintenance room based on the turbine dimensions and a highway on top the sluiceway resulted in the 1D transverse cross-section as shown in Figure 1.
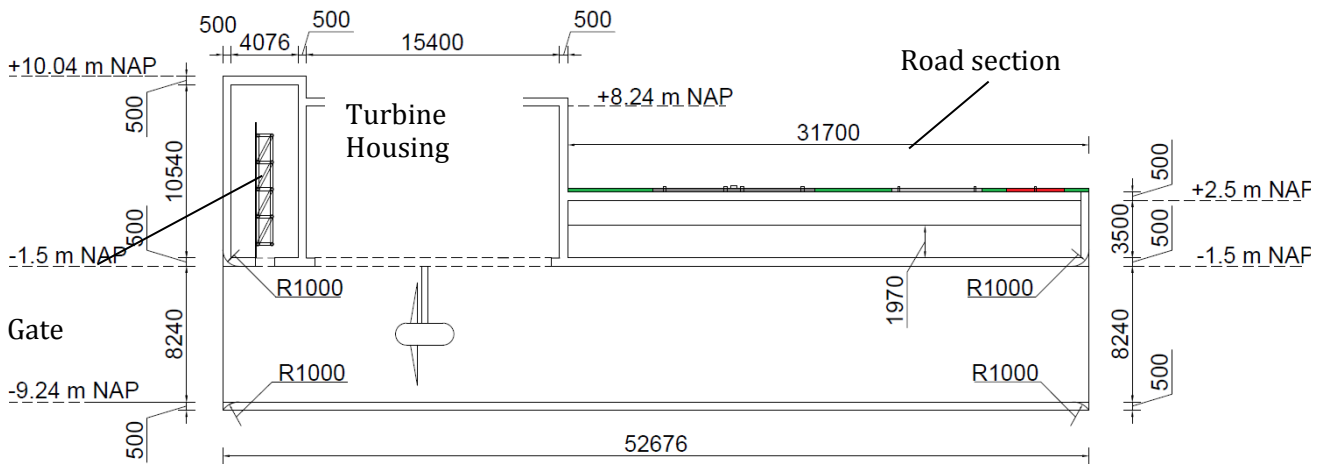
FIGURE 1: CROSS SECTION TIDAL POWER PLANT IN TRANSVERSE DIRECTION

The Tidal Power Plant will be constructed in the northern section of the Brouwersdam. A top view of the full structure located in the Brouwersdam is provided in Figure 2.
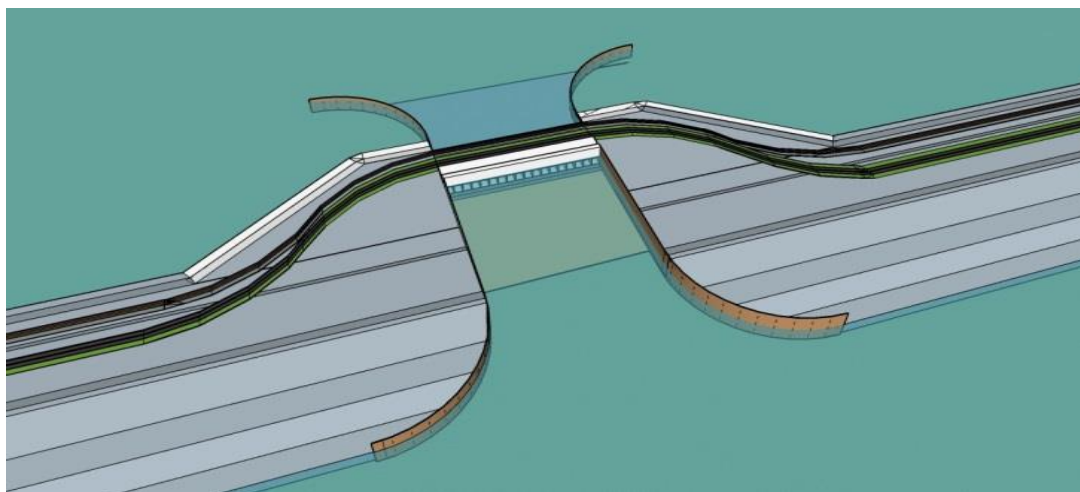
FIGURE 2: NORTH SEA SIDE TOP VIEW TIDAL POWER PLANT IN THE BROUWERSDAM

The thickness of the concrete members in the preliminary design has been set at 500 mm. The conceptual design of structural elements has been dedicated to checking the assumption. In total four base cases have been studied, providing local and global forces emerged from uneven bedding of the rubble foundation layer. The rubble foundation layer functions as a bed protection foundation on which the Tidal Power Plant is located.

The influence of uneven bedding of the rubble foundation bed has been computed by considering the Tidal Power Plant as a beam on an elastic foundation. Due to an uneven bedding, one-dimensional base cases Hogging and Sagging are introduced. Sagging represents a beam on elastic foundation subject to a reduced foundation stiffness at the midsection of the beam. Hogging has been described as the opposite situation of sagging, a reduced bedding stiffness at the beam edges.

The structure's strength has been determined while applying the hogging and sagging bases cases together with external and local forces. The external forces emerged from the hydraulic pressures in transverse direction and lateral earth pressures in longitudinal direction. The local forces concern the self-weight of an element or locally applied loads, such as the ballast load or road construction. The bending and shear resistance of the concrete members has been checked accordingly.

In addition to the forces obtained from hogging and sagging, a coupled 2-dimensional approach has been applied. Two base cases have been considered in the 2-dimensional plane. The uneven bedding induces the rise of torsional moments in the beam on an elastic foundation. The torsional resistance of the concrete members has been checked. Together with local and global one-dimensional forces, the governing reinforcement ratio has been determined for relevant concrete members. Combining the findings of the one-dimensional approach with the two-dimensional approach has resulted in reinforcement ratios exceeding 3%. Comparing this with the 1 % economical reinforcement ratio value, it has been concluded the 500 mm thickness of the concrete member is insufficient.

In further analyses, it is recommended to provide a cost estimation including revenues made from the energy production. The feasibility of the Tidal Power Plant will be determined by this cost estimation.

1 INTRODUCTION

In 2013 Rijkswaterstaat opened a tender for the reconstruction of the Brouwersdam. As a consequence of a low oxygen rate in Lake Grevelingen, the Brouwersdam was due to be reconstructed to increase the water quality in the lake. Before the tender became public Rijkswaterstaat and many engineering institutes have provided many researches to determine current issues at Lake Grevelingen.

This chapter will primarily give insight to the location and general information from the Brouwersdam and its surroundings. The Characteristics of the Grevelingendam, Lake Grevelingen and Brouwersdam will provide information regarding the current situation.

1.1 GENERAL INFORMATION

Zeeland, located at the Southwest of The Netherlands, consisting of islands connected by dams and barriers. These dams do not only form a connection between the islands, but provide the hinterland safety against flooding. During the 1953 flood, the majority of Zeeland suffered from casualties and major damages. Due to high tide under the extra influence of a hurricane moving towards the Dutch coast, the sea level rose to + 4.55 meter NAP. Primary flood defence systems were not designed to protect the hinterland against such conditions and failed. Breaching of the dikes led to the understanding of the necessity of dike improvements. As a consequence, the Dutch Government formed a committee, named the Deltacomittee, provided with the task of advising the execution works of the Deltaplan. The Deltaplan proposed the construction of several hydraulic structures (The Deltaworks) prohibiting floods in the future.

The proposal included closing off estuaries by closure dams. The Brouwersdam was one of these closure dams. Prior to the construction of the Brouwersdam, the Grevelingendam was constructed (finished in 1965), providing favourable conditions for construction works at the Brouwersdam, Haringvliet barrier and the Eastern Scheldt barrier. Constructing the Brouwersdam (finished in 1971) led to the formation of Lake Grevelingen. Figure 3 on the next page, provides an overview of the location of both the Brouwersdam and Grevelingendam with respect to the Netherlands and Sealand [www.deltawerken.nl].

The lake's northern border has been formed by the island Goeree-Overflakkee, positioned in the southwest of the province South-Holland. The Southern border has been formed by the island Schouwen-Duiveland, positioned in the province Sealand. Both island are connected by the Grevelingendam at the eastern side and the Brouwersdam at the west side.

With the western border formed by the Brouwersdam, the lake has been completely shut off from the North Sea. Consequently, the water quality of Lake Grevelingen deteriorated disastrously. Therefore, a decade after finishing the Brouwersdam, the Dutch Government decided to construct a stop lock within the southern part of the Brouwersdam, named the Brouwerssluice. The Brouwerssluice introduced a small tide on Lake Grevelingen and provided the lake with a small amount of incoming fresh water. In addition, the Grevelingendam has been equipped with a syphon type stop lock connecting Lake Grevelingen with the Eastern Scheldt.

More detailed features of the Grevelingendam, Lake Grevelingen and the Brouwersdam will be discussed in the succeeding paragraphs.

FIGURE 3: OVERVIEW LAKE GREVELINGEN, WITH (A) THE LOCATION OF THE BROUWERSDAM AND (B) THE LOCATION OF THE GREVELINGENDAM

Figure 3 provides a clear overview of Lake Grevelingen and the two adjacent relevant municipalities; Schouwen-Duiveland and Goeree-Overflakkee. The relevant surrounding waters, illustrated with blue tints, are he Volkerak, Haringvliet and Eastern Scheldt. Brouwersdam, Grevelingendam, and the Haringvliet barrier are indicated with respectively A, B and C. Next to that, four sandbanks are located in Lake Grevelingen such as the 'Hompelvoet' (indicated with no. 1), 'Veermansplaat' (no. 2), 'Stamperplaat' (no. 3), and 'Dwars in den Weg' (no. 4). These sand banks provide habitat to large diversity in flora and fauna. Furthermore, the construction dock Bommenede has been indicated by β. This construction dock will come up in the construction method of the Brouwersdam.

1.1.1 GREVELINGENDAM

The Grevelingendam will not be of high importance in this thesis, therefore the features of this dam are described briefly.

As mentioned, the Grevelingendam was constructed to provide favourable site conditions for construction closure works, such as: Haringvliet barrier, Brouwersdam and the Eastern Scheldt barrier. Construction of the Brouwersdam would have led to major current flowing from Lake Grevelingen towards the Haringvliet barrier and the Eastern Scheldt barrier. These currents would have complicated the construction works of the Haringvliet barrier and the Eastern Scheldt barrier. Obstructing these currents became a priority, resulting in the construction of the Grevelingendam.

The dam was divided into three parts; northern, middle and southern part with a total length of 6 km. The middle part consisted of a sandbank which was raised using suction dredgers. Raising the middle part led to a reduction of the water depth of the 600 meter long northern part, allowing caissons to be used for closure. Due to the length and depth of the southern part the Deltacommittee decided to use an innovative construction technique; a cableway dropping concrete blocks into the water. Construction works started in 1958 and took in total 7 years to finish.

Furthermore, the Grevelingendam has been equipped with a stop lock and a chamber lock. The chamber lock was designed to provide access from the Eastern Scheldt towards Lake Grevelingen during the Brouwersdam construction works. The stop lock renovation works, finished in 2017, has resulted in a bi-directional discharge system. Hence, the water quality at the eastern part of Lake Grevelingen will be increased thanks to the renovation works. The renovation of the syphon type stop lock, included the design of a Tidal Test Centre. In 2018 this Tidal Test Centre should become fully operational.

The Grevelingendam is in addition accommodated with the N59, a highway running connecting Goeree-Overflakkee and Schouwen Duiveland at the east side of Lake Grevelingen. The locations of the Tidal Test centre, stop lock, chamber lock and N59 are simply illustrated in Figure 4.

FIGURE 4: TOP VIEW GREVELINGENDAM [GOOGLE MAPS]

1.1.2 LAKE GREVELINGEN

Lake Grevelingen has originated the moment the Brouwersdam was finalized. General characteristic of Lake Grevelingen will be discussed in this paragraph first, in section 1.1.2.1.

The second part of this paragraph, 1.1.2.2 will be dedicated to describe recent development in Lake Grevelingen. It will come forward the water quality has been reducing to an alarming level in the last decades. The influence of the water quality reduction on the main activities at the Lake will be described in paragraph 1.1.2.3.

1.1.2.1 GENERAL CHARACTERISTICS

Enclosed by the Brouwers- and Grevelingendam Lake Grevelingen stretches in total 14000 ha, of which 3000 ha is occupied by dry land or sandbanks. Hence, the total water surface of Lake Grevelingen stretches 11000 ha. The construction of the Brouwerssluice has led to a small tidal range of 5 cm, while the lake's average water level equals -0.20 meter NAP.

Since the lake has been a former estuary of the North Sea, several deep gullies located adjacent to the sandbanks have been originated over time. The locations of the sandbanks has already been presented in Figure 3. Due to the lack of currents and sand transport within the lake, these gullies are still present as can be seen from the bathymetry in Figure 5. Due to the deep gullies, sandbanks and calm water, the lake has become attractive for a number of activities as will be described below.
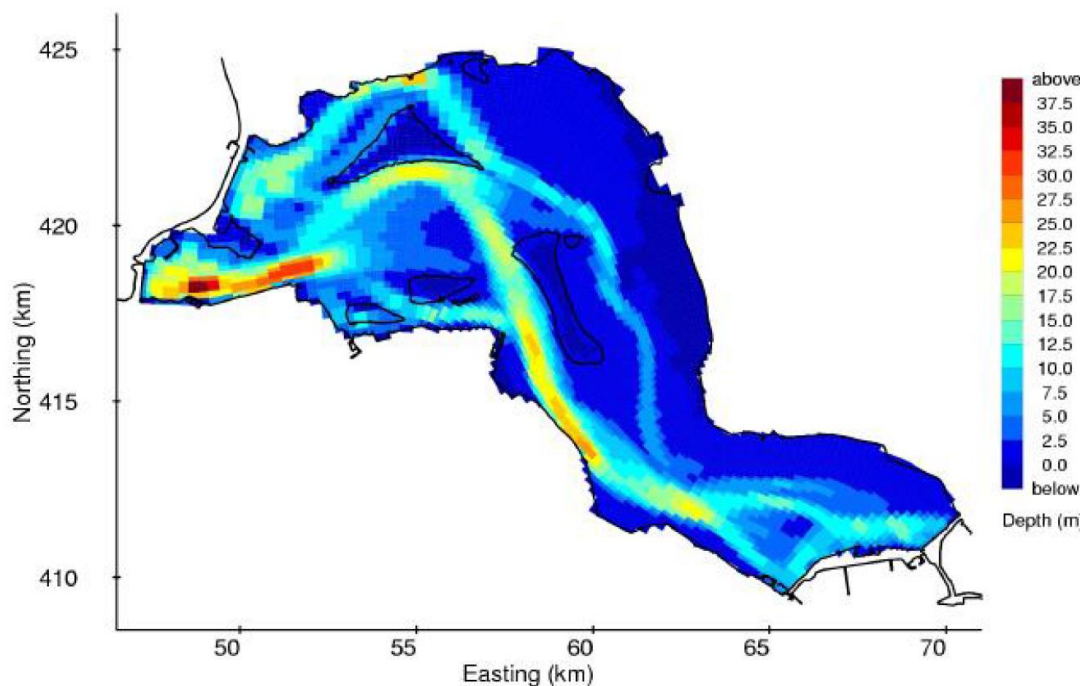
FIGURE 5: BATHYMETRY LAKE GREVELINGEN [SPITERI AND NOLTE, 2010]

TOURISM AN RECREATION

Lake Grevelingen provides recreational activities such as surfing, swimming, diving, sailing, sports fishing etc. Tourism and recreation are the most important income resources of the local area. In total, it is estimated the lake is visited by approximately 2

million visitors. The diversity of flora and fauna, but also the clear water of the lake, make the lake such an attractive recreational area. According to Natuur- en Recreatieschap de Grevelingen [2006], 75 per cent of the visitors find their recreational needs at the shores, while approximately 20 percent is active on the water, the last five per cent concerns sports fishery, divers or take a boat trip. This is quite remarkable since the lake is especially attractive for diving and boat trips, due to the clear water and diversity in flora and fauna.

In total six official swimming locations and ten official diving locations are present at the lake. Next to that, the lake accommodates ten recreational harbours with a total capacity of approximately 3800 ships. It is clearly noticeable from Figure 6, tourism and water sport activities are widely represented within Lake Grevelingen. The chamber sluice in the Grevelingendam makes it also possible to sail between Lake Grevelingen and the Eastern Scheldt.
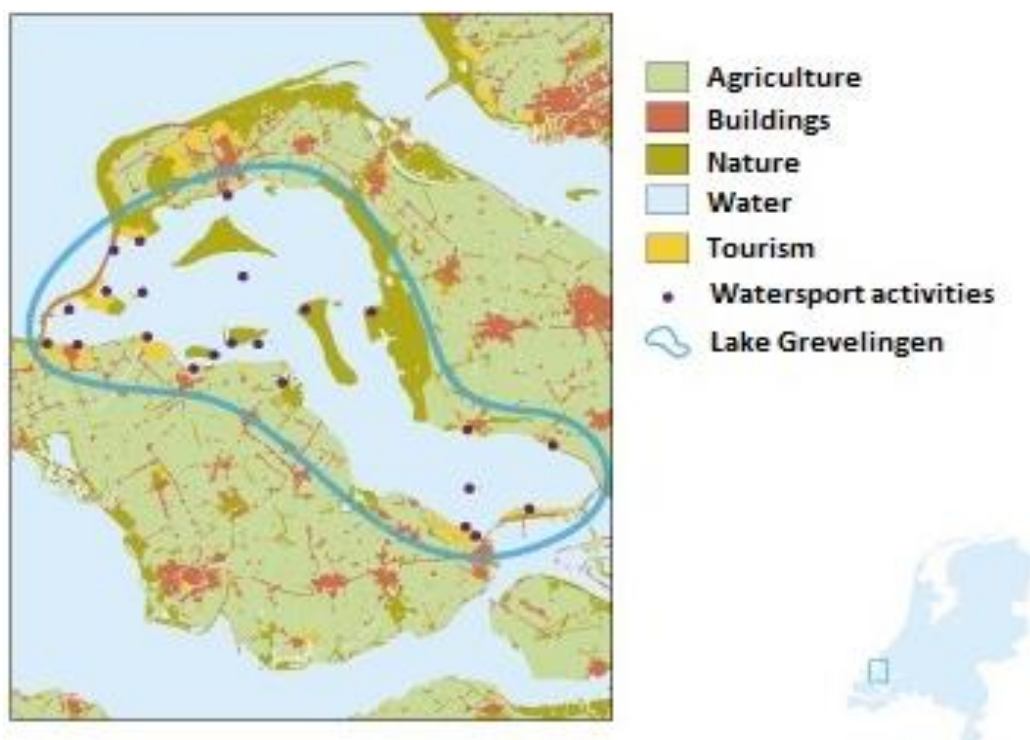
FIGURE 6: OVERVIEW LAKE GREVELINGEN 2009 [BPL, 2009]

FLORA AND FAUNA

Thanks to the many mud flats, the calcium content, and the salinity gradient, the Grevelingen is very rich in a diversity of its flora and fauna. A combination of scarce vegetation on the shores, fishy areas, and the dried mud flats makes the lake an perfect environment for birds and lots of different species of protected animals. The dry mud flats and shores the area are intensely used for incubating, especially by birds living in these areas. In addition, migrating birds use Lake Grevelingen as a stop when migrating towards the north or Africa. The stop is required to recuperate, thus sufficient nourishment is preferred.

FISHERY INDUSTRY

Initially, after constructing the Brouwersdam and the resulting still standing water, oyster and mussel production seemed to become impossible as the salty water in the

lake became sweet. However, due to the construction of the stop lock in the Brouwersdam and the reintroduction of a small tide in the lake, oyster production became feasible again [Wijsman et al. 2014]. Today, in 2017, Lake Grevelingen consists of multiple oyster farms (550 ha). The total revenues of the oyster production in the Netherlands reaches 5 million euro, generated by 30 companies. 75% Of the total oyster production is realized in Lake Grevelingen (500 ha) and the Eastern Scheldt (1550 ha). In Strattelligence [2014] an estimation of the revenues regarding the fishery industry at Lake Grevelingen has been made. In total a revenue of 1.3 million euro is generated by both the oyster production and fishing on eel and lobster.

1.1.2.2 RECENT DEVELOPMENT LAKE GREVELINGEN

Deep gullies and a small amount of fresh incoming seawater induce water quality problems in Lake Grevelingen. These water quality problems are described in this section. In addition, Room for the River project in the Netherlands has appointed several basins to become water storage facilities during extreme water levels. The role of Lake Grevelingen within this plan will be described in this section as well.

WATER QUALITY

In the Natura-2000 management plan [Rijkswaterstaat and Royal Haskoning DHV, 2015] the water quality in Lake Grevelingen has been described as a big issue. While the algae population, macro fauna, and fish population comply with the prescribed norms, though the fish migration is during summer periods negatively influenced by the salinity gradient. The remaining water flora does not comply with the norms. Due to the still standing water, there is a lack of currents in the lake. Especially in the deeper parts of the lake the different layers are therefore not able to mingle, which is called stratification. Moreover, at the surface oxygen exchange takes place, obviously, this is not the case in the deep parts of the lake. Hence the deep sections of the lake suffer from a very poor oxygen gradient. Rotting processes at the lake bottom has been an additional feature of the low oxygen gradient. Dead organic material sinks to the bottom of the lake where it is decomposed by micro-organisms. These rotting processes require oxygen, resulting in a downward spiral of the oxygen gradient and thus the water quality. If this situation continues, the lack of oxygen will extend to the shallower areas with very negative consequences for i.e. nature, tourism, fishery etc.

As described above, oyster production in Lake Grevelingen is an important income source. Growing oysters requires an oxygen gradient of 7 mg O_2/l. Wetsteijn [2011] described the ecological developments in Lake Grevelingen. The report mentions the lake's management strives to have a total bottom area of less than 5% that is poor in oxygen (<3 mg O_2/l), with a distinction layer at -15 m NAP. This distinction layer is the layer that gives a clear difference in temperature and oxygen gradient. The value < 3 mg O_2/l has been used in further conclusions since exposure for approximately a week to an oxygen gradient of <3 mg O_2/l leads to mortality for most of the bottom organism

At certain areas in the lake, presence of the distinction layer appeared already at areas shallower than -15 m NAP. Especially during hot springs and summer periods, more than 10% of the bottom area becomes poor in oxygen [Bouma et al., 2008, Lengkeek et al., 2010, Wetsteijn, 2011]. Nolte et al. [2008] have even shown that in the current situation a total area of 1,300 ha is poor in oxygen (1 meter above bottom level, oxygen gradient <3 mg O_2/l) for a continuous period of more than 7 days.

The poor oxygen gradient has already been present since the closure of Lake Grevelingen. However, the water conditions have become worse in the past decade. According to the available data between 1990 to 2010 it has appeared the poor oxygen gradients even occur during winter periods. In addition, the poor oxygen areas are increasing as well [Wetsteijn, 2011] and are extending to shallower areas [Bouma et al., 2008]. Spitoni and Nolte [2010] provided a validation of a 3D model describing the oxygen gradient in Lake Grevelingen, including the effect of stop lock in the Grevelingendam, one meter above the bottom level in the year 2000. The result of this model is shown in Figure 7.
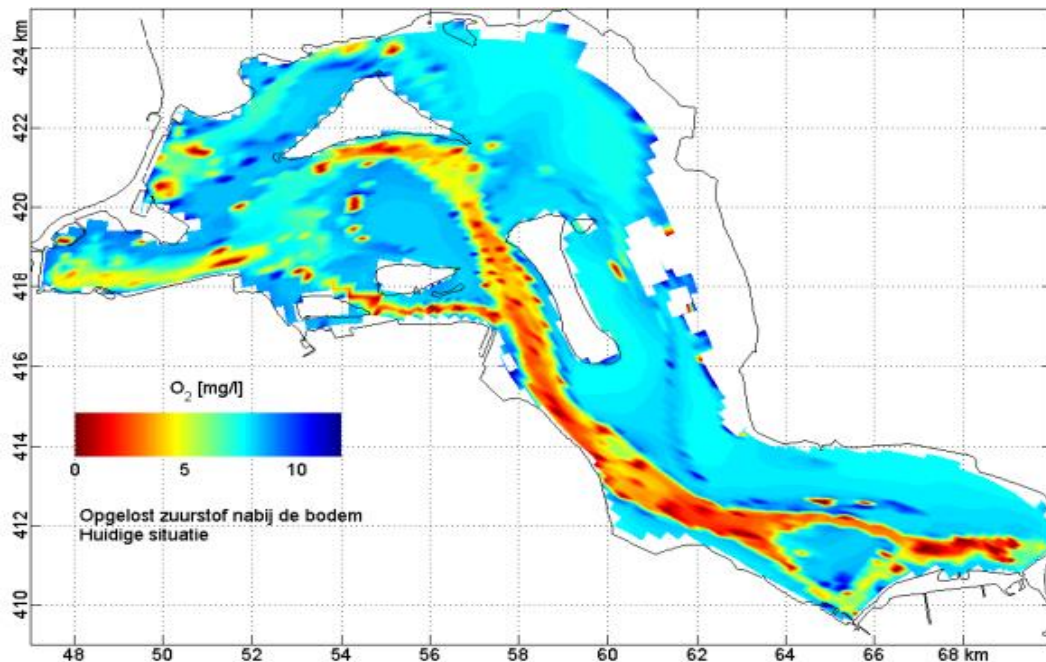
FIGURE 7: OXYGEN LEVEL CURRENT SITUATION INCLUDING STOP LOCK GREVELINGENDAM [SPITERI AND NOLTE, 2010]

ROLE LAKE GREVELINGEN IN ROOM FOR THE RIVER PROGRAMME

In the context of 'Room for the river', the project 'Water storage Volkerak-Zoommeer' has been introduced. This project strives to create extra water storage facility in case of very high water levels in the Rijn-Maas estuary. However, no connection between Lake Grevelingen and the Volkerak-Zoommeer has been realized (yet). Therefore, prior to function as part of a water storage system, the connection between the two lakes must be provided. However, it is wise to bear in mind that these plans are in discussion. The probability of occurrence is set to 1/1400, according to the national structural concept Grevelingen and Volkerak-Zoommeer. Hence with a probability of 1/1400 the sluices in the Brouwersdam should be able to discharge a large amount of water from the lake to the North Sea. No final decisions have been made to use the Grevelingen as a bearing lake, though plans have been investigated thoroughly with positive results. This should especially be kept in mind in case of designing the tidal power turbines, discharging the water from Lake Grevelingen to the North Sea would then be an additional requirement.

1.1.2.3 CONSEQUENCES REDUCING WATER QUALITY

A reduction in water quality will influence the lake activities. Engineering companies have performed many researches regarding the consequences of the reducing water quality. Results of these researches will be described in this section for each activity separately.

TOURISM AND RECREATION

Due to the lack of oxygen in the deeper parts of the lake, the diving experience is decreasing. Since the shallower parts of the lake suffer from the oxygen gradient as well, it will become less attractive for tourism to recreate at the shallow areas.

Another problem has been arising recently, rotting sea lettuce has been washed ashore progressively, this might not be a consequence of the reducing oxygen gradient, but could have a negative influence on recreational activities. Next to that, the Japanese oysters decrease the attractiveness of swimming in the lake due to their sharp edges. Hence a decline of touristic and recreational activities is predicted if the reducing oxygen gradient will not be counteracted.

FLORA AND FAUNA

Without any measures the reduction of the water quality will continue, leading to reduction of the amount and variety of nourishment. The oxygen problems might threat the fish populations as well. The lake is rich in migrating fish from sweet to salt water and the other way around. During these migrating processes a lot of oxygen is required [Kranenbarg, 2004]. Unfortunately there is no clear data regarding the fish population available. Still, a decrease in fish population will be expected. Thanks to these two situations fish- and plant-eating birds will slowly disappear as well.

Since the poor oxygen gradient is extending to the shallower areas, mortality of bottom organism becomes inevitable. Bottom organism form an important player in filtering water, but functions as nourishment for animals as well. Thus, mortality of the bottom organism has a big influence on both the water quality and the lake's ecosystem.

It may be concluded the reduction in water quality has a large negative influence on the ecosystem of the lake. It is expected fish, birds, bottom organism, vegetation and other wildlife will slowly disappear.

FISHERY INDUSTRY

As mentioned in the 'Flora and Fauna' section, it is expected the fish populations will decrease. The commercial fishery is suffering from the static situation in the lake. According to Bouma et al. [2007], oyster farmers announced an oyster mortality of 30% during the summer of 2005 and 60-90% during the summer of 2006. The mortality was a result of the poor oxygen gradient present at the lake. There is, however, one positive side regarding the harvesting of the Japanese oyster, their population seems to increase. These oysters are also caught for commercial fishing. Though, they are not as much wanted as the flat oysters grown in the oyster farms.

CONCLUSION

The consequences of the reducing water quality are significant for Lake Grevelingen and its surroundings. Revenues from fishery and tourism and recreational activities will decrease progressively. Moreover, the rich diversity in Flora and Fauna will be due to

disappear. Hence oxygen gradient increasing measures are required to improve the recent development at lake Grevelingen.

1.1.3 BROUWERSDAM

General information regarding the Brouwersdam will be treated in this paragraph. More detailed information of the Brouwersdam is provided in chapter two, where construction methods, cross sectional illustrations and an overview of the local activities are given.

The Brouwersdam functions as part of a primary flood defence system, protecting the hinterland from the North Sea and forming a complete flood defence system with the Deltaworks. The total length of the Brouwersdam is 6.5 km and provides a connection between Goeree-overflakkee and Schouwen-Duiveland. On top of the Brouwersdam the N57 is located, a highway running from the north of Middelburg to the west of Roozenburg (Europlein) where it connects with the A15/N15. In addition on both the North Sea and Lake Grevelingen side two parallel roads are positioned.

The Brouwersdam can be divided into two separate sections; these sections are based on the construction of the Brouwersdam which will be treated later. The deterioration of the water quality led to the construction of the Brouwerssluice, a stop lock constructed in the southern part of the dam. This stop lock was supposed to provide Lake Grevelingen with fresh (salt) water, resulting in an increase of the water quality. Fresh water flows from the 'Voordelta' into Lake Grevelingen, see Figure 8.

The Brouwerssluice has currently a daily average discharge of approximately 120 m^3/s, this discharge leads to a water level variation of approximately 5 cm in the middle of Lake Grevelingen [Nolte et al. 2013]. However, as mentioned earlier, this amount of incoming water has been insufficient to increase the oxygen gradient in the lake adequately.

FIGURE 8: OVERVIEW BROUWERSDAM FOCUSSED ON THE BROUWERSSLUICE
[WWW.IZI.TRAVEL.NL]

The general information following from the Grevelingendam, Lake Grevelingen and the Brouwersdam has described one major problem; reducing water quality as a consequence of a low oxygen gradient. In this conclusion the results regarding the reducing water quality are summarized. Moreover, the solution to this problem will be treated, forming the goal of this thesis.

PROBLEM DEFINITION

The construction of the Brouwersdam has led to a lack of incoming fresh water. The succeeding construction of the Brouwerssluice did counteract the problem slightly, but has still shown to be insufficient. Especially the deep gullies are subject to the low oxygen gradient. Research has even shown the low oxygen gradient extends to shallower areas, while in the past decade the low oxygen gradient has arose in winter periods as well.

Main activities at Lake Grevelingen, such as: tourism and recreation, fishery industry and flora and fauna, will suffer from the deteriorating oxygen gradient. Since these three activities contribute to revenues of local enterprises, the entire Lake environment suffers from the reducing water quality.

Due to the renovation works on the stop lock in the Grevelingendam, water exchange at the eastern part of the lake with the Eastern Scheldt counteracts the low oxygen gradient locally. However, contribution from this stop lock will not be observable in deep gullies at the western part of the lake. Hence, at the western part of the lake the reducing oxygen gradient will remain in a downward spiral.

COUNTER THE PROBLEM

Several studies are performed concerning the water quality in Lake Grevelingen. Conclusions of these studies are discussed here. Since the studies are done by professional engineering companies it assumed these studies can be considered as trustworthy.

In 2008 the first relevant report regarding the water quality was published [Nolte et al., 2008]. It concerns an exploration of solutions regarding the water quality in Lake Grevelingen including several water quality models. One year later a collaboration between Witteveen en Bos and Rijkswaterstaat [R. Nieuwkamer et al. 2009] resulted in a concluding report regarding the water quality solutions and their consequences. The model from Nolte et al. [2008] produced an overview of the water quality in the Grevelingen. The model results were translated by Bouma et al. [2007] to ecological consequences. From this analysis, it appeared that several guidelines concerning the water quality, according to KRW and Natura 2000, were already met.

Calculations, from the mentioned reports, have shown by increasing the water exchange with the North Sea will have a positive influence on the oxygen gradient. In addition, the reports mention the introduction of a 50 cm tidal range. Introducing such tidal range would comply with the required effects. Establishing a tidal range is possible by increasing the discharge area by approximately a factor 8 of the current discharge capacity of the Brouwerssluice.

Spitoni and Nolte [2010] provided a validation of a 3D model including a 50 cm tidal range at lake Grevelingen, including the effect of stop lock in the Grevelingendam, one

meter above the bottom level obtained with data from the year 2000. The results of applying a discharge structure at the northern part of the dam has been provided in Figure 9. Chapter 2 will provide a clear understanding of the separation between the southern and northern part of the Brouwersdam.
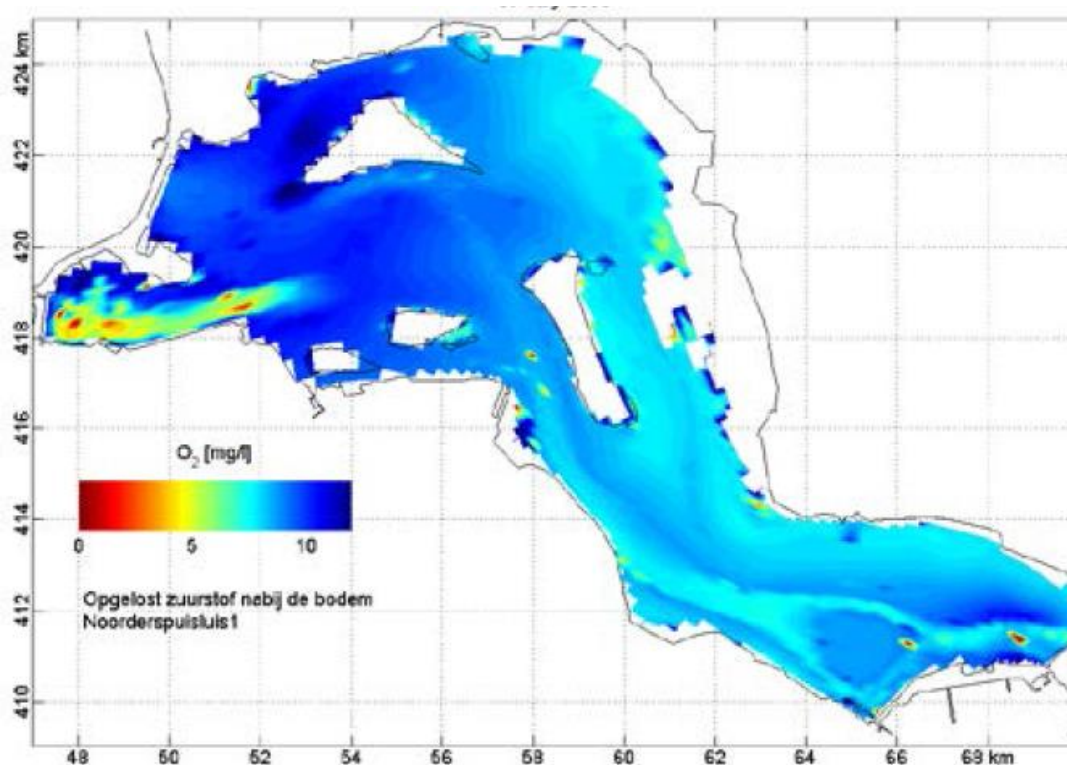
FIGURE 9: RESULTS INRODUCING 50 CM TIDAL RANGE WITH DISCHARGE STRUCTURE AT NOTHERN PART OF THE DAM [HOUTEKAMER & VAN KLEEF, 2016]

Thus, a discharge structure in the Brouwersdam is due to be designed enabling the increase of the oxygen gradient in Lake Grevelingen. Introducing a tidal range of 50 cm results in the required oxygen gradients.

The construction costs of a sluice complex will be rather expensive, whereas the tide could be used to lower the overall construction cost. In La Rance, France, a large tidal range is present enabling a tidal power plant to generate energy which leads to reduction in overall construction costs. At the North Sea such large tidal difference is not available, but with the recent techniques it might become possible to generate energy even with a very low tidal range.

A tidal range at the Brouwersdam of approximately 2.5 meter from the North Sea, and a tidal range of 50 cm at Lake Grevelingen, allows thinking of a very low head Tidal Power Plant. This very low head Tidal Power Plant generates energy while allowing passage of fresh sea water from the North Sea to Lake Grevelingen and adversely. The generated power suffices as a cost reducing measure plus the generation of nowadays strongly wanted green energy.

The goal of this thesis has thus become:

Design a very low head Tidal Power Plant in the Brouwersdam, which enables the introduction of a 0.5 meter tidal range at Lake Grevelingen.

2 BROUWERSDAM

Prior to design considerations more detailed information regarding the Brouwersdam is required. The previous chapter already described some general information regarding the Brouwersdam, but this will not suffice to have a clear understanding of what to expect from the Brouwersdam. This chapter will therefore be solely dedicated to the Brouwersdam.

First, the current environment of the Brouwersdam will be discussed, here a separation between the Northern and Southern part arises. This separation is more elucidated in the second paragraph; the construction method. In the construction method the final cross-sectional figures of the dam are dealt with.

Prior to designing a Tidal Power Plant in the Brouwersdam, the optimal location within the dam is examined in paragraph 2.3. The Northern part of the dam will become the optimal location. Since the construction method of the northern part has provided the use of caissons, the ability of reusing these caissons will be checked in paragraph 2.4 and 2.5. Where 2.4 will provide a clear understanding of the currently available caissons, In paragraph 2.5 will the ability of reusing the caissons be checked based on general requirements.

2.1 ENVIRONMENT BROUWERSDAM

The Brouwersdam is surrounded by beach clubs and surfspot/clubs, especially at the North Sea side. Moreover at the midsection of the dam, a large recreational park has been constructed. In total four recreational ports are located adjacent to the dam, of which one is the large Marina Port Zélande. Moreover, at the North Sea side a large beach has been developed where lot of (wind)surf activities take place, but is also intensely visited by tourism during summer periods. Figure 10 on the next page, gives a clear overview of the occupation of the Brouwersdam.

The dam has been divided into two sections; the Northern section and the Southern section. A distinction between these two sections has been made due to the varying construction methods at both sections, explained in the succeeding paragraph. Clearly noticeable from Figure 10 on the next page, is the location of the Brouwerssluice at the southern part of the dam.
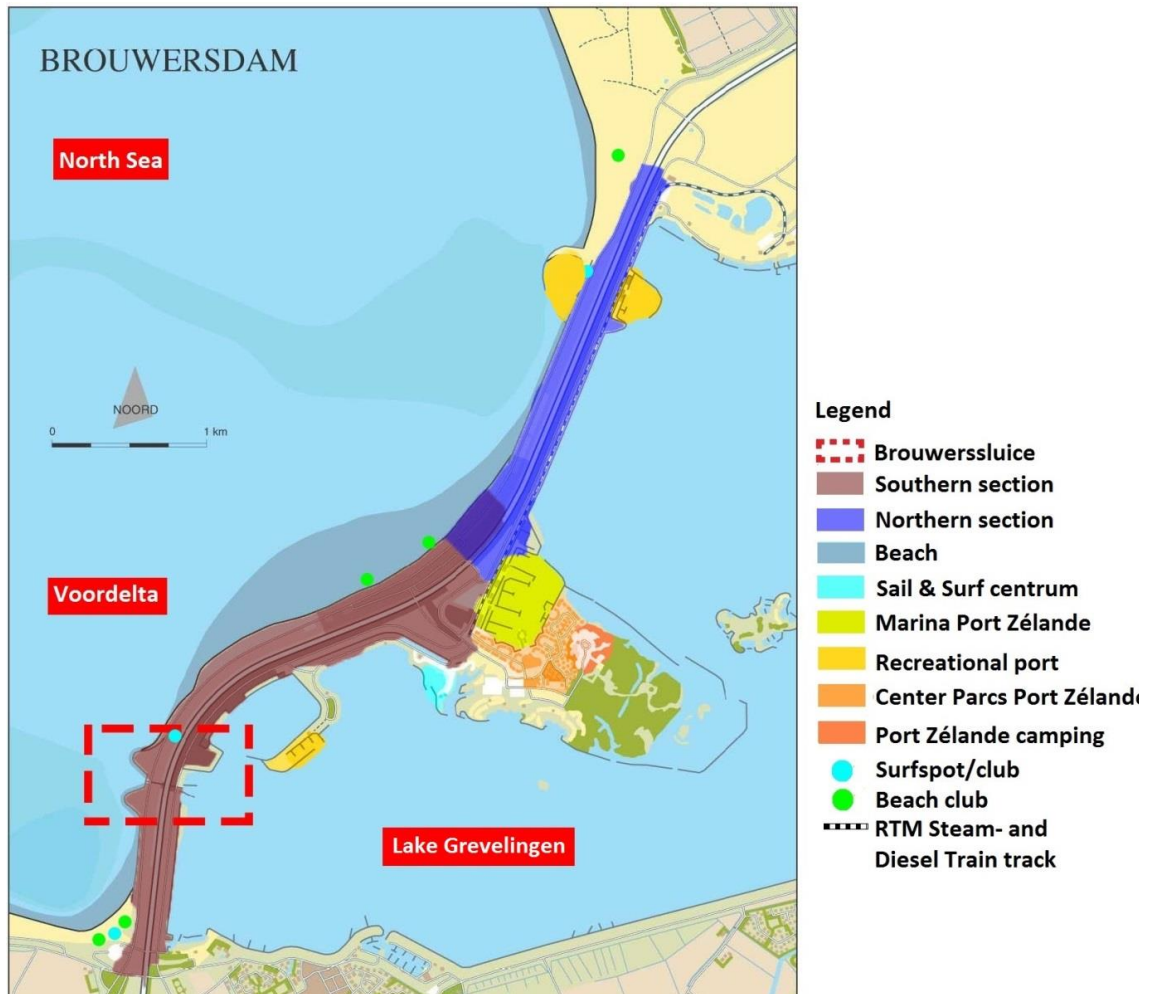
FIGURE 10: OVERVIEW BROUWERSDAM AND ADJACENT RECREATIONAL FACILITIES [MINISTERIE VAN VERKEER- EN WATERSTAAT, 2007]

2.2 CONSTRUCTION METHOD BROUWERSDAM

The construction methods are useful when elaborating a new design in more detail, it might become feasible to reuse current structural elements from the dam. The construction method of the Brouwersdam is separated into two sections; a Northern and a Southern section. In the succeeding subparagraphs the general construction method will be discussed, followed by the Northern and Southern section. Finally the construction method of the Brouwerssluice will be treated as an example of modifying the Brouwersdam.

2.2.1 GENERAL

The construction of the dam started in 1964 and was finalized in 1971. The current crest height of the Brouwersdam is at +11.00 meter NAP (Normative Amsterdam level). As mentioned, the construction of the dam was performed at two section, a northern and southern section. The reason for the split up was the presence of two sandbanks (Middelplaat and Kabbelaarsplaat) in the middle of the dam. The sandbanks were merged, while the much deeper southern trench required a different approach compared with the shallower northern section [Stichting Deltawerken Online, 2004]. Figure 11 and Figure 12 on the next page illustrate cross-sections of the Brouwersdam.
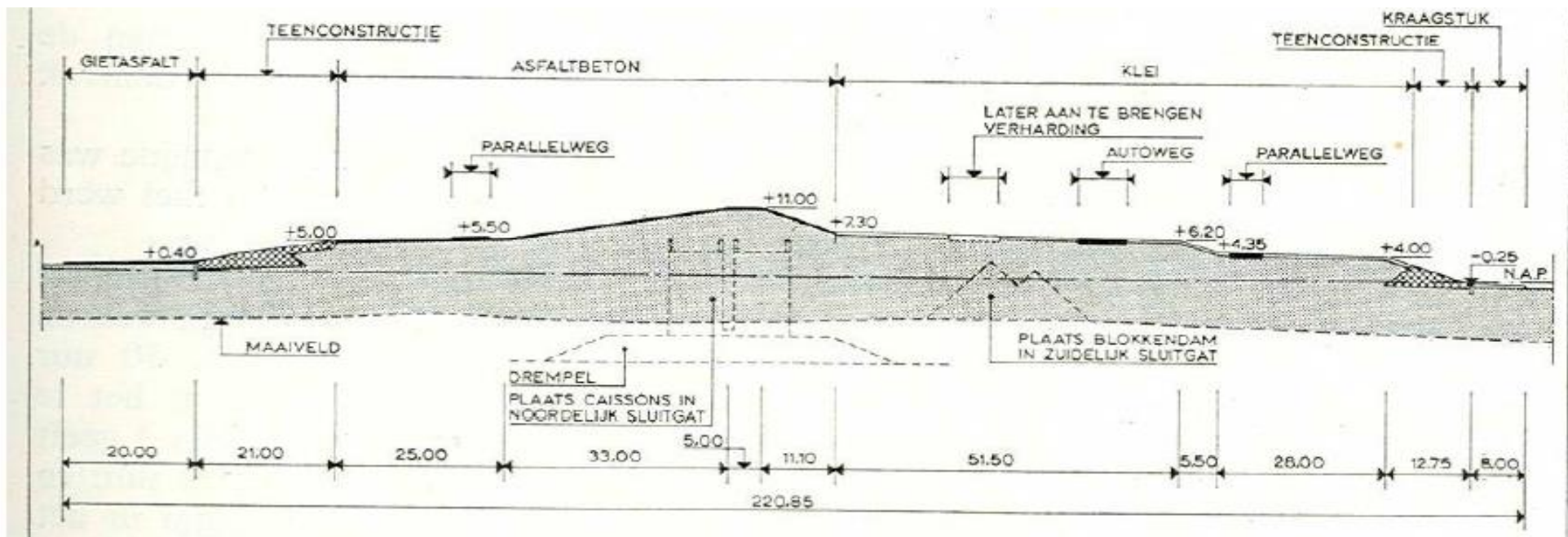
FIGURE 11: CROSS-SECTION BROUWERSDAM [MALDEGEM, 1973]

Legend:
- Mine stone
- Clay
- Crushed rubble material
- Asphalt
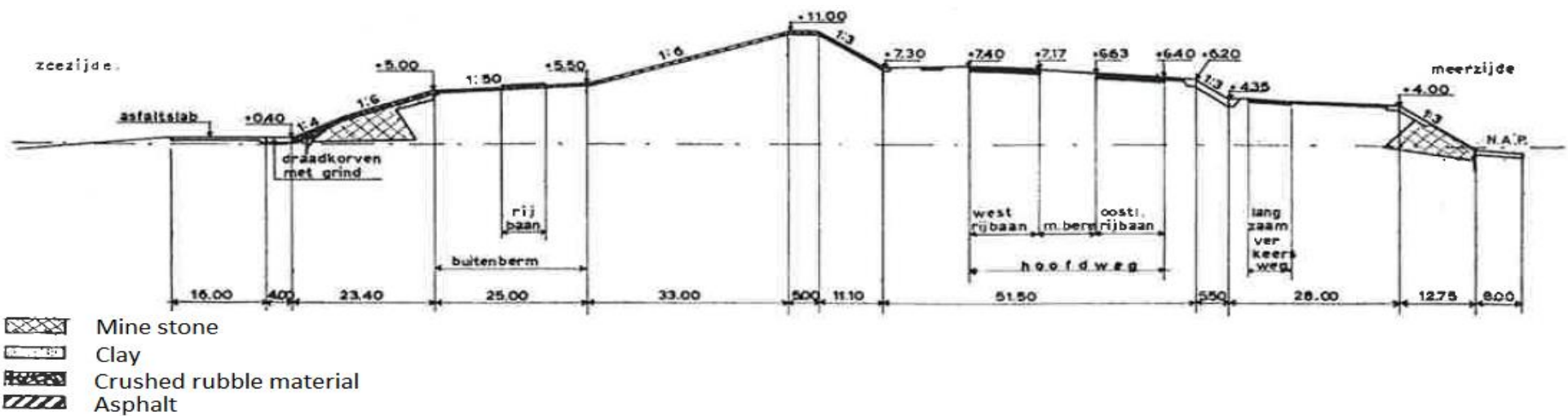
FIGURE 12: CROSS-SECTION BROUWERSDAM [WESTEN, 1972]

2.2.3 SOUTHERN SECTION

Due to the deep southern gully, a cableway was used to close this trench. From the cableway one cubic meter concrete blocks were dropped in the water. The hollow sections between these blocks were backfilled with gravel (30 to 100 mm diameter). Prior to dropping the concrete blocks a bed protection was constructed. This bed protection consisted of a 30 cm thick mastic asphalt on which a rubble mound layer (300 kg/m^2) was placed. On both sides of the bed protection, an extra scour protection was constructed. This scour protection consisted of classical matrasses reaching 165 to 100 meter at the lake and sea side respectively. The bed profile at the southern section has been illustrated in Figure 13, from where it can be noticed the depth reaches -23 meter NAP.
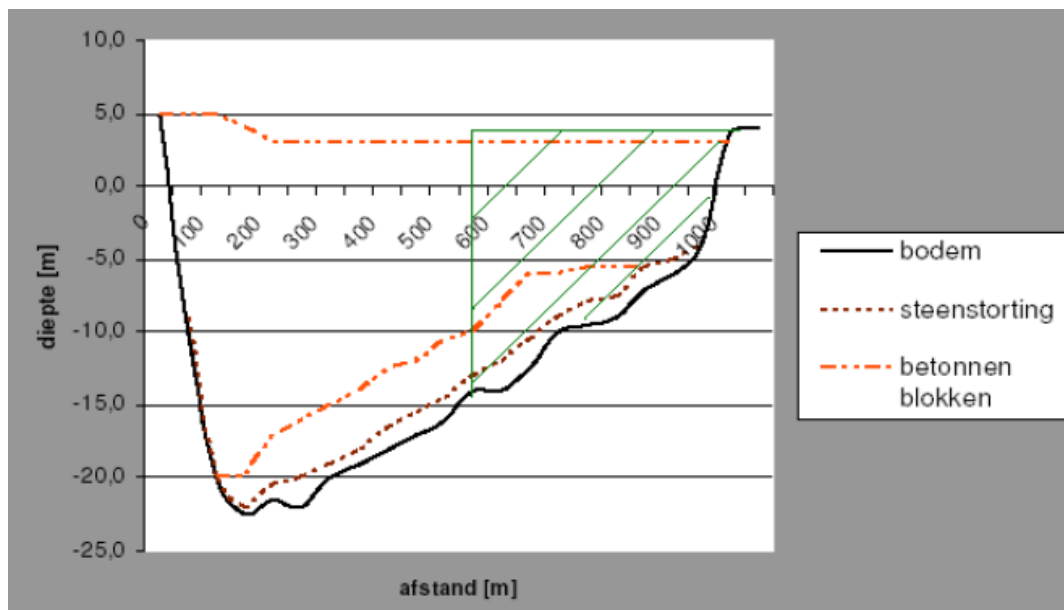
FIGURE 13: BOTTOM PROFILE SOUTHERN SECTION [VRIJLING ET AL. 2008]

2.2.4 BROUWERSSLUICE

As mentioned before, the stop lock inside the Brouwersdam, the Brouwerssluice, is located in the southern section of the dam. This sluice consists of two 195 meter long cylindrical sleeves. These two sluices can be used for both discharging and sluicing of salt water between Lake Grevelingen and the North Sea. Next to the stop lock a fish passage was constructed to maintain the fish population in the lake. Each sleeve is constructed as a venturi-shape tube, ensuring a high discharge coefficient. The orifice dimensions are 6.0 meter in width and 4.5 meter in height (bottom at -11.0 m NAP, top at -6.5 m NAP).The shape of the sleeves becomes wider at the end, therefore the orifice dimensions at tube ends are: 12.85 meter wide and 8.0 meter high (bottom at -11.0 meter NAP and top at -3.00 meter NAP). To construct the sleeves in the dam, a part of the dam section had to be removed. The construction method in the dry was performed to construct the Brouwerssluice. The sluice is founded on steel, with the foundation located in a sand layer with sufficient bearing capacity.

2.2.2 NORTHERN SECTION

The northern section gullies reached a maximum depth of -14 meter. By flattening the bed using both fine and coarse gravel, it was decided to apply open caissons. The use o open caissons would not lead to major flow velocities as the flow area would somehow remain the same. Applying closed caissons would induce major flow velocities during placement of the latter caissons. Hence, by applying open caissons the favourable site conditions remain unchanged during closure works.

The open caissons were constructed in a dry construction dock at Bommenede, located at the North shore of island Schouwen-Duiveland, see Figure 3. From here the caissons have been transported over water and sunk to its final position on top of a rubble material bed. Bulkheads were applied to close the open caissons of from water during transport. As soon the submerging process was initiated. In total twelve caissons were used to close the Northern part, each provided with a height of 16.2 meter, a width of 18 meter and a length of 68 meter. Each caisson had 12 openings with a heart-to-heart distance of 5 meter [Vrijling et al. 2008].

Prior to submerging the caissons to its final position, a 2.75 m thick rubble material bed was constructed at a depth of -10 meter NAP. The total width of the rubble material bed reached 35 meter. The rubble material bed consisted of a filter layer containing layers of rubble-mound material. First a filter layer of 50 cm fine gravel (2-5 mm) was placed, on top a 75 cm coarse gravel layer (30-63 mm), and a final 1.5 meter protection layer of stone (60-300 kg) finishes the bed protection. Underneath, and adjacent to the rubble material bed a bed protection was constructed at a depth of -12.75 m NAP, reaching a width of 130 meter at both the North Sea and like side, measured from the centre line of the protection. The abutments required an increased bed protection width, and reach 160 meter from the centre line. The bed protection consists of a 24 centimetre thick mastic mat on which the rubble mound layer has been placed. The bed protection has been designed for a head difference of 2.5 to 3 meter. Figure 15 and Figure 16 on the next page illustrate cross-section and the top view of the applied bed protection respectively.

As soon all caissons were in place the caissons were closed off by gates and filled with sand and rocks. The caissons were placed between so-called abutment caissons with a height of 16.6 meter, a width of 20 meter and a length of 47 meter [Hydraulic structures lecture notes, 2011. The cross section of the open caissons is given in Figure 14. The right figure shows a steel gate in the middle of the cross section. Back in the days, this was a technical innovation which ensured the stability of the caissons during transport through the water. More detailed information regarding the caisson design will follow in paragraph 2.4.

FIGURE 14: CROSS-SECTIONS OF OPEN CAISSONS BROUWERSDAM [HYDRAULIC STRUCTURES LECTURE NOTES, 2011]

FIGURE 15: CROSS-SECTION RUBBLE MATERIAL BED [MALDEGEM, 1973]
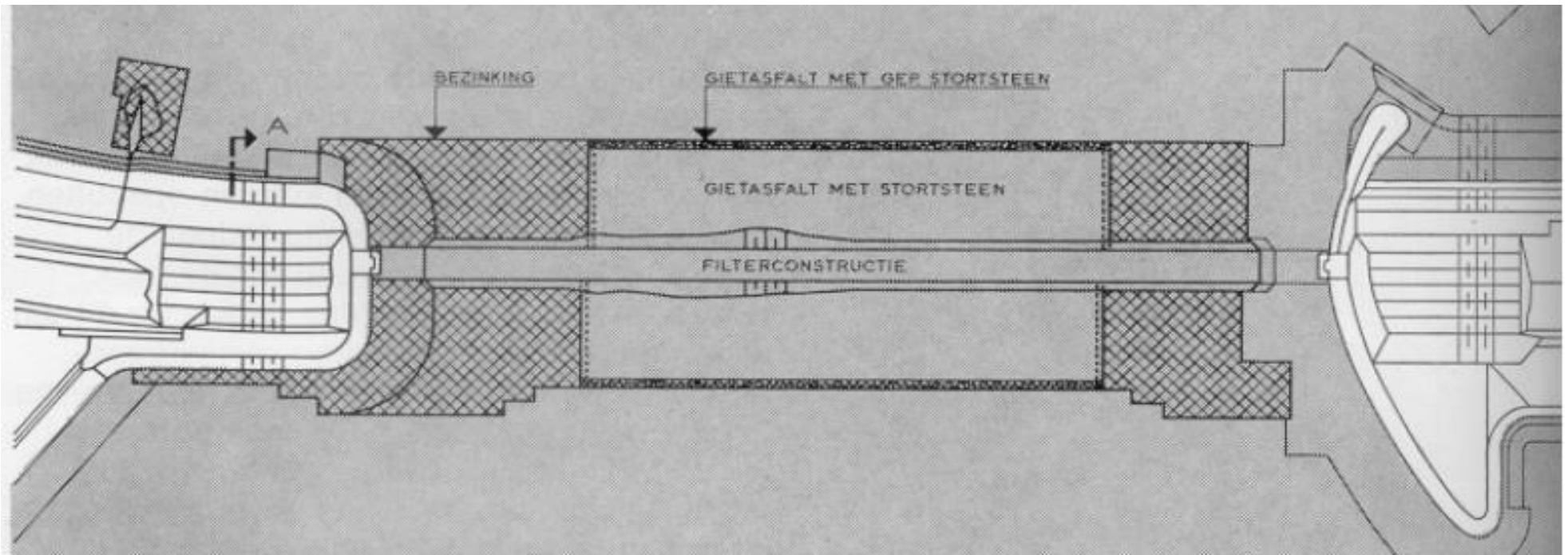
FIGURE 16: TOP VIEW BED PROTECTION NORTHERN SECTION BROUWERSDAM [MALDEGEM, 1973].

In a location study performed by Smale et al. [2008]. The optimal location for the construction of a very low head tidal power plant has been obtained. At both the northern and the southern section of the Brouwersdam, gullies are present. Refreshing water at these gullies has a positive influence on the morphology and hydrodynamics in Lake Grevelingen.

The caissons present at the northern section of the Brouwersdam might emerge into difficulties regarding the construction conditions. If these caissons do not allow reusing, the caissons will have to be removed using heavy machinery. On the other hand, removing the bed protection reaching -12.75 meter NAP, if required, should be feasible without applying heavy machinery. If the caissons allow reuse, it is assumed the caissons require major adaptations.

The southern section was constructed using concrete blocks backfilled with gravel. Reaching a depth of -23.0 meter NAP removal of the concrete blocks will be difficult and very time consuming. Moreover, applying a proper foundation at such depth is complex and irregularities in foundation bed level are very likely to occur. However, the deeper gully might allow to apply more or larger turbines.

Smale et al. [2008] concluded both sections of the Brouwersdam are considered suited for the construction of a Tidal Power Plant. Constructing the Tidal Power Plant will become challenging at both sections. Comparing both sections it seems the construction works at the southern sections are greater. The structure of the Tidal Power Plant becomes much higher and it is doubtful whether applying more and larger turbines becomes more economically beneficial. Next to that, the available space at the southern section is restricted by a recreational harbour and the Brouwerssluice, see Figure 10. The extra work at the northern section is formed by the presence of the caissons and its bed protection. These caissons and bed protection might, however, be suited for reuse, which will be determined in the succeeding paragraph. In addition, the available space at the northern section is not restricted by any local constructions or recreational ventures, see Figure 10.

The qualitative reasoning from above is based on assumptions. These assumptions tend to prefer construction at the northern section. The possibility of reusing the caissons makes the construction at the northern section even more favoured. It has therefore been decided to construct the Tidal Power Plant at the Northern section of the Brouwersdam, see Figure 17
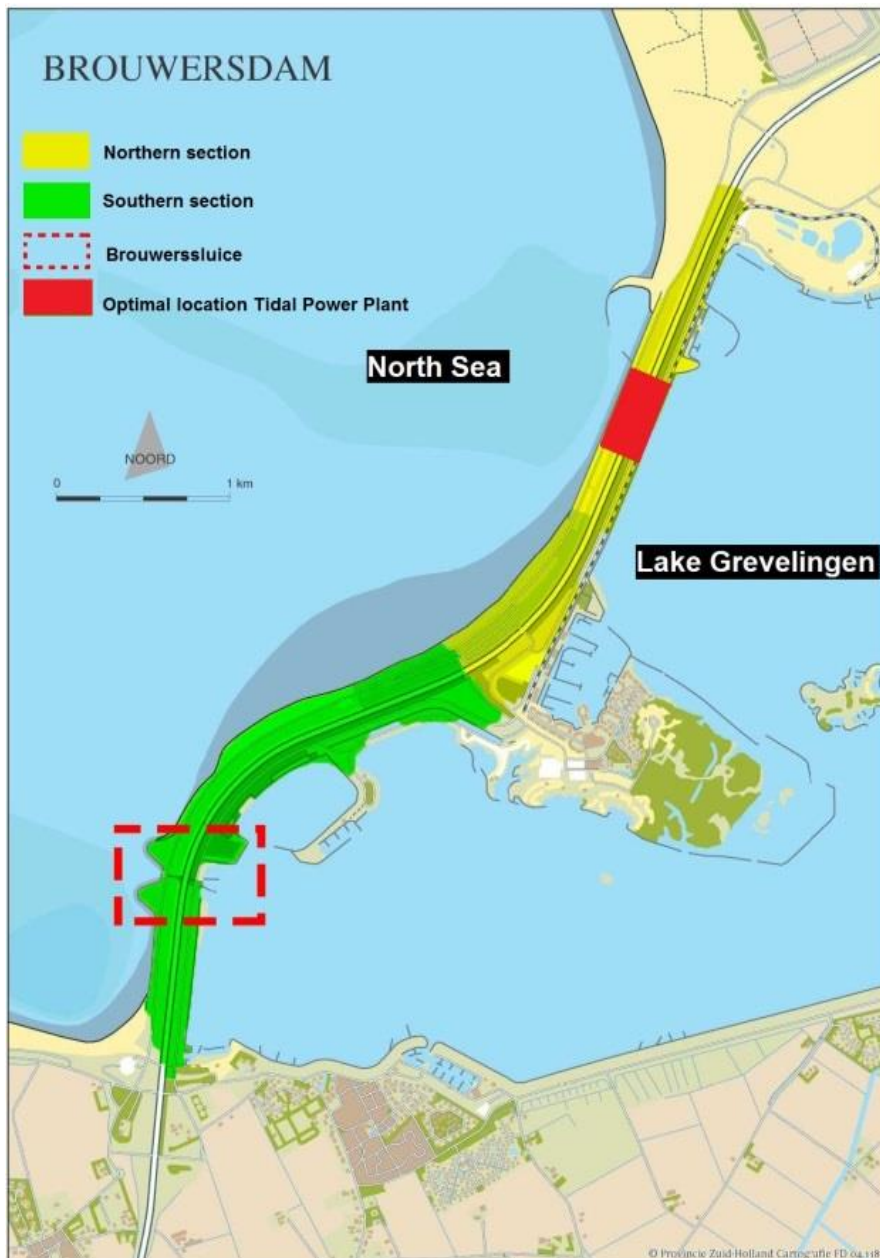
FIGURE 17: TOP VIEW LOCATION TIDAL POWER PLANT IN BROUWERSDAM [GOOGLE MAPS]

2.4 REUSING CAISSONS

From a cost perspective it might become beneficial to reuse the current available caissons in the Brouwersdam. The feasibility of reusing these caissons will be considered in this paragraph.

First, more detailed information regarding the caissons currently located in the Brouwersdam will be required, section one will therefore be dedicated to the caissons currently present in the Brouwersdam. Secondly, with the detailed information available, the caisson are examined with respect to the requirements set to the concrete elements of the caissons.

2.4.1 CURRENTLY PRESENT CAISSONS

The construction of the caissons took place between 1968 and 1970. A special dry dock was excavated nearby the Brouwersdam to manufacture the caissons. From this dry construction dock the caissons were towed by tug boats towards their final positions. In total twelve open caissons were sunken into place, with a total longitudinal length (parallel to the North Sea) of 828 meter. Each caisson has a height of 16.2 meter, a width of 18 meter and a length of 68 meter. The caissons are provided with 12 openings with a c.t.c. of 5 meter [Vrijling et al. 2008]. Each caisson weighted 7800 ton and had a draught of 6.25 meter. The metacentric height during transport is 1.20 meter, whereas this becomes 0.85 m at the start of the sinking process to 1.60 m when reaching the bottom. Due to the draught and the clearance required underneath the caissons, a special trench was dug. The total towing distance became 12 km through a trench with a width of 65 meter and a bottom level at -12.0 meter NAP. During the placement of the caissons a margin of 0.25 meter was used as safety margin between each caisson. An exception was made for the final caisson, in total 2.0 meter was reserved, ensuring the caisson to enter its final position safely. After construction it appeared a gap of 2.20 meter between the edges of the final caisson and the adjacent one was left. Due to placing the first caissons against the abutment without any margin, this larger gap was available.

The concrete type used for the construction of the caissons has a strength class K300, with a characteristic design compression force of 19 N/mm² [Rijkswaterstaat, 2013]. This corresponds to the currently known C20/25.

The construction of the caissons can be schematized as a skeleton-construction of reinforced concrete and steel. In between the two closed sides eleven parallel vertical reinforced walls are casted. For stiffening purposes each of the eleven vertical walls were connected with cross shaped steel H-profiles, two on top of each other. The bottom section consists of a 2.5 meter height concrete box, whereas the top section consists of a 2.20 meter high ballast box. As a consequence of high swell, which could lead to delay of the caisson transport, a curving shape was designed (with a slope of 1:5 towards the caisson side, functioning to increase the discharge coefficient) in the bottom box. The curving shape ascertained the caisson was able to reach a total length of 68 meter. A cross-section, cross section A-A from Figure 14, in transverse direction (perpendicular on the North Sea) of the caisson is shown in Figure 18. Included in the middle of this cross-section is a steel gate. Back in the days this was an innovative technical feature which ensured the stability of the caissons during transport through the water.
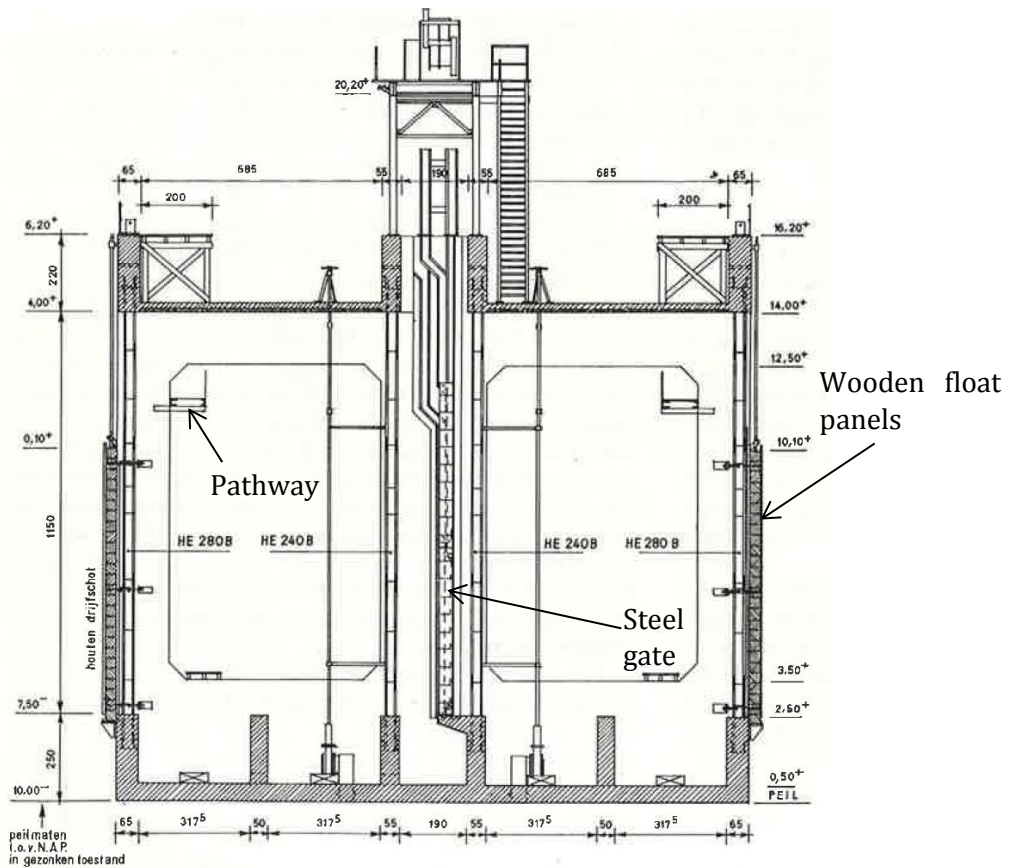
FIGURE 18: CROSS SECTION A-A[NIEUWENDIJK, 1968].

2.4.2 REUSING CURRENT CAISSONS

The presence of the caissons in the Brouwersdam raises the question whether these caissons can be reused or not. Recent studies, mentioned in Appendix B.1, have already drawn some conclusions regarding the reuse of caissons. However, since the reuse of the caissons might be a very interesting and maybe a cost saving solution this option is discussed here.

Due to changing climate conditions the Dutch Government has modified the safety standards for Dutch hydraulic structures, likewise the safety standard for the Brouwersdam. Multiple hydraulic structures did not comply with these new safety standards and were due to be adapted or completely rebuild. Next to the modifications within the safety standards, also the functionality of the structure adapts. Due to sea level rise safety standards might change in the future (let's say in 50 to 100 years) as well. Hence, in the future a similar situation might occur where structures lose their functionality due to changing conditions.

In the case of the Brouwersdam, caissons are already present. These caissons are more than 55 years old, but have not been exposed to significant wave actions since completing the dam. Therefore the caissons might still be sufficiently strong to maintain its current function for another 50 years. As the new Tidal Power Plant will be constructed in a caisson type structure, would it not be ideal if the current caissons can be reused with a new functionality? This could function as a reference for other hydraulic structures exposed to changing conditions as well. Enabling the hydraulic

structure to adapt to new functions or conditions reduces demolition works and enhances the environmental friendliness of the Tidal Power Plant.

The objective in this subparagraph is to determine whether the currently present caissons allow reusing for the Tidal Power Plant. If this is not possible the caissons could be used for other purposes.

The analysis will be based on drawings and information obtained from both Rijkswaterstaat archives and a master thesis concerning the reuse of caissons in the Port of Rotterdam [Danad, 2015]. Conclusions from these two sources are discussed below.

Concrete in marine environments

The permeability of concrete structures could allow aggressive chemical ions to enter to penetrate into the concrete. Permeability of the concrete could result in corrosion of the reinforcing steel. The permeability of the concrete gives an indication of the ability of porous material to let liquids and gasses commence the concrete. Since concrete is a porous material with a certain permeability, influenced by the curing period and the water-cement ratio, it is likely liquids and gasses have commenced the concrete of the current caissons. The water-cement factor used in the concrete of the caissons lies between 0.37 and 0.40. The NEN 8005 describes a maximum allowed water-cement factor of 0.45 for concrete exposed to sea water. Thus, the water cement-ratio of the concrete used in the caissons complies with the NEN 8005 norm. Since the permeability is, among other things, depending on the water-cement factor, which complies with the European norm, it may be concluded the permeability of the concrete is sufficiently low.

Cracks could increase the permeability, initiating deterioration and decrease the service lifetime of concrete structures. Overloaded concrete structures tend to crack, but still function as long the crack width do not exceed a certain limiting value. Protrusion by chlorides, oxygen and humidity into the reinforcement bars, exposed due to cracks in the reinforced concrete, will start corroding. As a consequence of cracks or a high permeability, the reinforcing steel expands and loses its bond with the surrounding concrete, initiating cracks in the concrete cover.

After finishing the installation of the caissons, gates on each side were used to close the caisson off from water. As soon the gates were in place the caissons were filled by sand and sand was deposited around the caissons to form the dam as we know it today Deposition of sand took until October 1971, while finishing of the complete dam took until March 1972, which means the dam has not been exposed to extreme design conditions for a significant amount of time. It is therefore assumed the concrete caissons only had a retaining function until the complete finish of the dam. Hence, the caissons in were exposed to the North Sea for the time being of approximately 2 years. Solely during transport and the sinking process chlorides, water and oxygen have had their chance to commence into the concrete structure.

From the above it is concluded the caissons were designed for a two year lifespan in extreme marine conditions. This means durability measures, such as a large concrete cover were probably not applied. An increased concrete cover would lead to an increase in construction costs, it is therefore plausible the cover does not comply with the current requirements for structures in marine environments. This thought was supported by drawings and documents obtained from the Rijkswaterstaat archives. It was clearly noticeable the concrete cover used for the outer reinforcing bars is 20 mm. A

concrete cover of 20 mm does not comply with the current requirements for concrete structures in marine environments, which is due to be at least 45 mm [NEN 8005].

Strength after 50 years

In the master thesis of Danad [2015] reuse study for caissons in the Port of Rotterdam has been performed. It was concluded the strength of the caissons had increased over the past years compared to the initial design strength of the caissons. The characteristic strength of concrete after 28 years became much higher compared with the characteristic strength after 28 days, reaching a ratio of 1.3 to 1.4 times the initial.

In 1962 new guidelines (GBV 1962) for concrete structures provided a restriction on the water-cement ratio of 0.6, which is much higher compared with the current requirements (0.45). The water-cement ratio is an important factor with respect to the strength and permeability. A lower water-cement ratio would increase the strength, but decrease the workability. On the other hand, after many years a higher water-cement ratio could result in a higher strength of the structure, especially in submerged conditions. However, from the documents and drawings obtained from the Rijkswaterstaat archives, the water cement-ratio used in the caissons complies with the current requirements. Hence, the water-cement ratio does not form a threat for the strength of the current caissons.

Back in the 70's coarser cement was used, leading to slow development of the hydration process compared with what is possible nowadays. This insinuates a higher characteristic strength after a couple of years resembling it with the characteristic strength after 28 days. This was also proven by research regarding the compressive strength of structures build more than 25 years ago, a significant increase of the compressive strength was found. Moreover, the strength of concrete in wet conditions increases during it lifetime.

Thus regarding the strength after 50 years, it is expected the caissons strength have increased.

Conclusion reusing concrete

Due to the small concrete cover of 20 mm, which does not comply with the required concrete cover from NEN 8005, it is concluded the caissons may not be reused as the base structure of the Tidal Power Plant. There are no problems expected regarding a reduction in strength and corrosion of the reinforced bars due to the permeability. Therefore, the caissons may be reused at a different location, with a different function, not exposed to a marine environment. Danad [2015] has mentioned several possible functions for reusing caissons. It does however mean that the caissons will not be reused in the design of the very low head Tidal Power Plant in this thesis.

The Brouwersdam is surrounded by small venues and recreational harbour with at the intersection of the southern and northern section of the dam a large recreational park including a relative large harbour.

The dam has been divided into two major sections; the Northern and Southern section. Based on the closure methods, applying caissons (northern) or one cubic meter concrete blocks dropped from a cableway (southern), the distinction has been made.

In recent literature the optimal location for constructing a Tidal Power Plant has been discussed. Both sections were concluded to be well suited to construct the Tidal Power Plant. From qualitative reasoning it was concluded the northern section will be the optimal location of construction the Tidal Power Plant. The favourable depth and available space will be more beneficial compared with the southern section and with respect to the construction costs. Moreover, the reuse of caissons might be an additional asset.

This asset has unfortunately been countered by the results from paragraph 4. The caissons are, mainly due to the low concrete cover, not suited for reuse in a marine environment. It has been assumed that adaptations to the concrete caissons would lead to high costs. Moreover, the dimensions of the caissons would restrict the dimensions of turbines and the total amount of turbines.

Still, due to the available space at the northern section and the relative favourable bottom depth it is chosen to construct the Tidal Power Plant at the northern section.

Since the restriction of the caissons do not form a starting point of the Tidal Power Plant design, the succeeding chapters will determine a proper starting point from where the preliminary design of the Tidal Power Plant will be elaborated. As a base the requirements for the Tidal Power Plant set by MIRT Grevelingen will be discussed in chapter 3.

The dam has thus been divided into two sections; the northern and southern section. The optimal Tidal Power Plant location has been assumed at the Northern Section. Caissons present at this section do not allow reuse due to the required concrete cover.

3 REQUIREMENTS AND BOUNDARY CONDITIONS

Prior to the preliminary design stage of the very low head Tidal Power Plant, acknowledge of the requirements is recommended. With the prerequisites a primary idea of the very low head Tidal Power Plant features will be provided. The requirements function as starting point for the preliminary design stage and will be described in paragraph 3.1. Part of the requirements are especially of importance in the preliminary design of the Tidal Power Plant, these are summarized in paragraph 3.2.

In addition boundary conditions obtained from the in the literature study executed analysis will be provided in paragraph 3.3.

3.1 REQUIREMENTS FROM MIRT GREVELINGEN [2011]

The design of the very low head Tidal Power Plant is due to comply with the requirements set in this paragraph. The MIRT Grevelingen, a governmental institute which focusses on multiannual programme for infrastructure, space and transport, has set a number of requirements for the project outline of a Tidal Power Plant in the Brouwersdam. The requirements formulated by MIRT Grevelingen [2011], were set in the year 2011. Hereafter several studies have been performed; therefore the list of requirements is slightly updated according to findings from the relevant studies in a later stadium. Appendix A provides the full list of requirements set by MIRT Grevelingen. Solely the most requirements that contribute to the preliminary turbine and powerhouse design will be provided. The requirements are distinguished in three components:

FUNCTIONAL REQUIREMENTS

Water passage	The Tidal power plant needs to allow passage of water from the North Sea to lake Grevelingen and adversely.
Flow rates	The Tidal Power Plant needs to: • Facilitate passage of minimal 3500 m³/s (time average) of water in ebb-mode. • Facilitate passage of minimal 3500 m³/s (time average) of water in flood-mode.
Water barrier	The tidal power plant must be able to withstand (hold) also in case of a 1/4000, the norm-frequency for maximum conditions at the North Sea.
Level Control	During normal operation: • Targeted water level at lake Grevelingen on average NAP -0.20 m with variation between -0.45 and +0.05 m NAP. • The mean sea water level during lifetime shall be based on sea level rise predictions. The tidal power plant must facilitate control of the water level in lake Grevelingen, between maximum and minimum level, with prescribed average level.
Traffic	The tidal power plant needs to facilitate road traffic on the Brouwersdam, also from the N57 and parallel road, at least with today's traffic quality.

Fish friendliness	The tidal power plant fish mortality rate must be lower than 0.01 %.
Availability water passage	Non-availability of the tidal power plant, in relation to water passage, must be less than 0.5 %. Non-availability includes: • Foreseeable non-availability (maintenance). • Non foreseeable, non-availability as a result of closure of the gates due to malfunctioning.
Discharge capacity during maintenance	Reduction of water passage capacity due to planned maintenance must be less than 50 %.
Availability traffic connection	Non-availability of the tidal power plant in relation to road traffic must be equal or less than 0.5 %.
Life time tidal power plant	The tidal power plant must be constructed with a lifetime for functional use of at least 100 years.
Life time components	Components must have a life time: • Civil works: 100 years • Steel construction components: 50 years • Mechanical engineering components: 50 years.
Max. overtopping flow rate	Maximum overtopping flow rate during MHW must be less than 0.1 $m^3/s/m$.
Water safety during construction	During construction of the tidal power plant, the water holding function of the Brouwersdam must at all times be fulfilled.
Dismantling	Moving construction components needs to be demountable with reasonable effort

EXTERNAL INTERFACE REQUIREMENTS

Cables and conduits	Functions of existing cables and pipe work on the Brouwersdam must be maintained.
Interface traffic roads	Roads inside the tidal power plant system boundary need to connect to surrounding roads.

3.2 REQUIREMENTS WITH RESPECT TO PRELIMINARY DESIGN

From the requirements in total five requirements will be used to determine the Tidal Power Plant dimensions.

- Flow rate
- Fish friendliness
- Level control
- Max. overtopping flow rate
- Traffic

The flow rate and fish friendliness will be used to determine the turbine dimensions and the type of turbine respectively. The level control will be included in this computation to

determine the total discharge area of the Tidal Power Plant. These three requirements will thus lead to the preliminary design of the turbine type, turbine dimensions and total number of turbines. Which will be treated in chapter 4

The dimensions of the Tidal Power Plant structure will, among other things, be determined using max. overtopping flow rate and required infrastructure dimensions. Which will be treated in chapter 5.

3.3 BOUNDARY CONDITIONS

Two main boundary conditions have been obtained from the in the literature study performed analyses. These boundary conditions are summarized briefly in this paragraph.

1. The document 'Hydraulische randvoorwaarden 2006 voor het toetsen van primaire waterkeringen [2007] provides design data for primary water defence systems in the Netherlands. This document was elaborated by Rijkswaterstaat. The provided data obtained from the document, regarding the Brouwersdam, has been presented in Table 1 below.

Location	Design water level [m NAP]	Significant wave height H_s	Wave period $T_{m-1.0}$	Incoming wave β
Northern section	+5.0	2.6	7.5	10°
Middle section	+5.0	2.3	8.2	0°
Southern section	+5.0	2.2	7.9	10°

TABLE 1: OBTAINED DATA FROM HYDRAULISCHE RANDVOORWAARDEN 2006 VOOR HET TESTEN VAN PRIMAIRE WATERKERINGEN [MINISTERIE VAN VERKEER EN WATERSTAAT, 2006]

2. Current water levels obtained from www.waterbase.nl between October 2015 and October 2016 are considered governing for 2017. Table 4 gives an overview of the obtained data.

Parameter	Value	Unit	Parameter	Value	Unit
North Sea					
Average water level	0.00	m NAP	Maximum Tidal range	3.44	m
Maximum High water level	+2.05	m NAP	Average tidal range	2.511	m
Minimum High water level	+0.87	m NAP	Average low water slack	6.26	Hours
Minimum Low water level	-1.49	m NAP	Average high water slack	5.59	Hours
Maximum Low water level	-0.65	m NAP			
Average high water level	+1.456	m NAP			
Average low water level	-1.055	m NAP			
			Average Head flood	1.906	m
Lake Grevelingen			Average Head ebb	1.005	m
Average water level lake	-0.20	m NAP			
Minimum water level lake	-0.45	m NAP			
Maximum water level lake	+0.05	m NAP			

TABLE 2: OVERVIEW CURRENT WATER LEVELS LAKE GREVELINGEN

3. With the available CPN tests it was concluded soil mainly composes of fine to coarse sand. The sand has a particle diameter of $0.063 < D < 2\ mm$. The D_{b85} is approximated using soil tests close to the Brouwersdam. The particle size distribution of the sand close to the Brouwersdam has been presented in Figure 19.

At the Southern section of the Brouwersdam thin layers of clay have been detected. The soil composition at the northern section is set to a combination of coarse and fine sand. The properties of fine to coarse sand are presented in Table 3 below.

Properties		Fine Sand	Coarse Sand	
Specific weight dry	γ_d	16	16	$[kN/m^3]$
Specific weight wet	γ_w	20	20	$[kN/m^3]$
Grain density	ρ_k	2650	2650	$[kg/m^3]$
Permeability coefficient	k	$10^{-3} - 10^{-4}$	$10^{-5} - 10^{-6}$	$[m/s]$
Grain size	d_{50}	0.063 - 0.3	0.3 - 2	$[mm]$
Angle of repose	ϕ	25°-35°	35°-45°	$[-]$
Character flow	-	Laminar	Laminar	$[-]$

TABLE 3: SOIL PROPERTIES BROUWERSDAM
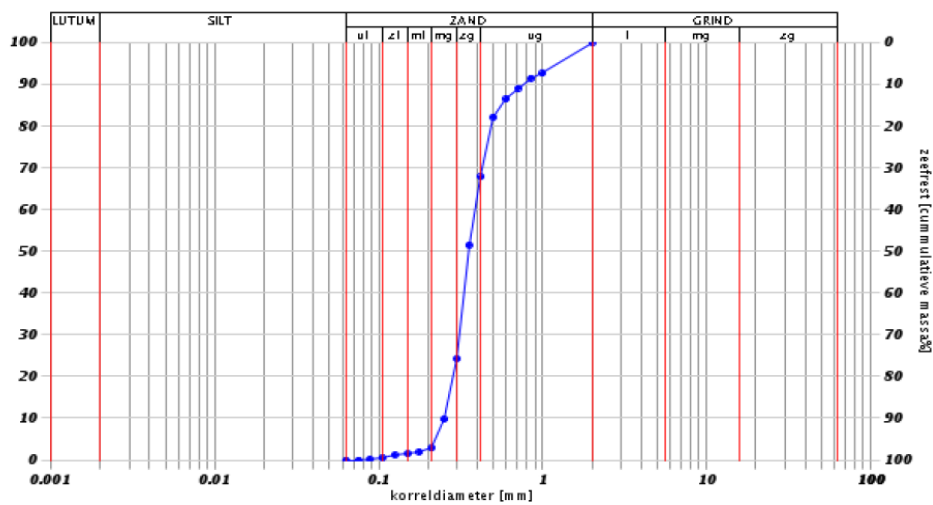
FIGURE 19: PARTICLE SIZE DISTRIBUTION CLOSE TO THE BROUWERSDAM [DINOLOKET].

4 PRELIMINARY TURBINE DESIGN

It has been mentioned the head difference between the North Sea and Lake Grevelingen is relatively low. Normally power plants require a much higher head difference. The most common turbine type such as the Kaplan, Bulb and Francis turbine are applied at head differences of at least 10 meter. The proper turbine type for the very low head Tidal Power Plant in the Brouwersdam will therefore be elaborated in paragraph 4.1.

Including the water level restrictions from the requirements set by MIRT Grevelingen (chapter 3), the final turbine dimensions are computed in paragraph 4.2. At last, paragraph 4.3 will provide a clear conclusion regarding the turbine design.

4.1 TURBINE SELECTION

As mentioned above, the most common turbine techniques require a head difference exceeding the head difference between the North Sea and Lake Grevelingen by a factor 5. Determination of the optimal turbine type therefore starts with setting with several requirements. For example, the ability of generate power at low head differences, but also the in the previous chapter mentioned fish friendliness. The room for the river programme includes a third requirement, namely the ability to pump a large amount of water from Lake Grevelingen towards the North Sea. In addition, from a cost and revenue perspective, two more requirements are set. These requirements are summarized in subparagraph 1. In the Literature study performed analysis regarding the available turbine types and techniques, it was already concluded that multiple turbine types or techniques are suited for low head hydro power generation. The most promising techniques will be treated in subparagraph 2.

Since the new techniques have in most cases not been proven on a proper scale yet, the turbine selection will be based on assumptions. As the turbines have a design lifetime of 50 years, variations in water levels will be included in the turbine design as well. Therefore, three scenarios are set in subparagraph 3, based on sea level rise as a consequence of global warming. With these three scenarios and the assumed optimal turbine types, three alternatives are considered at paragraph 4. From these three alternatives a final turbine selection will be made in paragraph 5.

4.1.1 REQUIREMENTS

The requirements set by MIRT Grevelingen and additional requirements regarding costs and revenues, and the Room for the River programme are described in this subparagraph.

GENERATE POWER WITH A VERY LOW HEAD

The hydraulic analysis of the water level at the North Sea performed in the Literature study, has shown an average water level at 0.00 meter NAP. The tidal range of the North Sea fluctuates between -1.59 meter NAP and +2.05 meter NAP. These data has been obtained from www.waterbase.nl for the year 2016. Next to that, the water level at the Grevelingen Lake fluctuates with approximately 20 cm, due the currently present Brouwerssluice. The head difference, or head, may thus be considered very low (which is defined for head differences lower than 5 meter. Thus the applicability of the turbine is based on the ability of generating power with a very low head.

FISH FRIENDLY

As mentioned in the General information of Lake Grevelingen (Section 1.1.2.1), fish migration between the North Sea and Lake Grevelingen will be required to enhance the fish population in Lake Grevelingen. Therefore, the applied turbine will have to allow fish to pass without being damaged or killed. Moreover, the requirements set by MIRT Grevelingen, which comply with the maximum fish mortality described by the Dutch Government [Dronkers, 2015], mention a maximum mortality of 0.01%. Accordingly, proven fish friendly turbines are preferred.

EFFICIENCY

The higher the turbine efficiency, the higher the energy production and thus the higher the revenues. Making the new design economical feasible, the construction, operational and maintenance costs of the turbine should be minimal, whereas revenues become to the utmost. Therefore, a proven high efficiency rate will be attractive from a revenue point of view. Lower efficiency rates could become beneficial when compensated with very low construction and maintenance costs. Therefore, the efficiency, in combination with the construction and operational costs, is the most important criterion when selecting the turbine type.

PUMP AND TURBINE FUNCTION

According to the programme of 'Room for the river', set by the Dutch Government, Lake Grevelingen could function as a water storage basin in the future. In that case pumping water out of the Grevelingen is of importance to maintain a proper water level in the lake. Next to that, to maximise the energy generation, it will be beneficial to apply bi-directional turbines. Bi-directional turbines generate power in both directions, resulting in water flowing from the North Sea to the lake during spring tide and adversely during neap tide. It becomes feasible if the following features apply:

- Efficiency must be high in both flow directions.
- The maximum efficiency of the turbines lie at a lower flow velocity rate compared with the maximum efficiency during pumping. Variable runner velocities are in that case required.
- The depth at which the runner will be positioned during pumping is based on the cavitation. Research should be carried out during both pump and turbine operation whether cavitation may occur. Presence of cavitation could lead to significant turbine damage.

COSTS

The costs are related to the efficiency, the higher the efficiency, the higher the revenues and thus reducing the overall costs. However, construction and maintenance costs should be reduced as much as possible. For each turbine type only a small qualitative indication of the costs, based on the maintenance and construction, will be described. The efficiency will be treated separately.

The importance of reducing the costs emerge even more when behold recent development in renewable green energy. For example windmill parks, the windmill parks in the North Sea are able to deliver energy for €72,70 per MWh, achieved at Borselle in front of the South-West Dutch coast [Grol, 2016]. It has taken almost a decade to achieve this low price for a windmill park. It is thus not expected the Tidal Power Plant will be able to deliver energy at the same price. But it remarks the urge of

lowering construction costs, to make the tidal power plant still feasible and an attractive renewable energy source.

4.1.2 TURBINE TYPES AND TECHNIQUES

The generally applied turbine type and techniques have been treated in the literature study. Turbines examined in previous research have been summarized in Appendix B.1 and will contribute to determine the optimal turbine type. With the mentioned turbine requirements, a selection of the most promising techniques has been made and will be discussed in this subparagraph. Based on the requirements a conclusion and recommendation will be made.

4.1.2.1 BULB TURBINE

The name bulb-turbine is based on the shape of the turbine. Bulb turbines are provided with a horizontal axis. Both the generator and auxiliary equipment are accommodated in a torpedo-shaped casing, surrounded by water. The runner used in bulb-turbines is similar to the Kaplan turbine, only more suited for lower heads. Efficiency rates of 90% for head difference between 0.5 to 30 meter have been claimed by Andritz, manufacturer of bulb-turbines [www.andritz.com]. The concrete foundation below the bulb supports the bulb at it sides. The bulbs are accessible via shafts located above the bulb, these shafts accommodate cables and hydraulic pipelines as well. Discharge regulation is done by guide vanes, which are located at the outside.
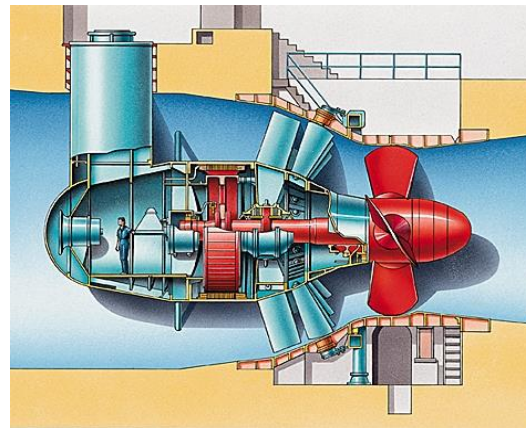
FIGURE 20: BULB TURBINE SKETCH [GOOGLE]

Some other bulb-turbine characteristics:

- The bulb turbine support will not be extremely stiff, this makes the bulb-turbine more sensitive to vibrations.
- The bulb shape limits the generator dimensions, this on its turn, limits the flywheel effect and with that the stability of the grid.
- The water depth has to be at least two times the runner diameter.
- Able to work bi-directionally, both pump and turbine operation.
- Several bulb turbines have shown to be fish friendly, depending on the number of runner blades and the distance between them.

Maintenance work at the bulb turbine may be performed in-situ, providing a dry maintenance area. Watertight closure of the turbine's sluiceway might become an expansive operation, depending on the availability of closure gates. The construction costs of the bulb turbine on the other hand are quite large, since large civil constructions are required.
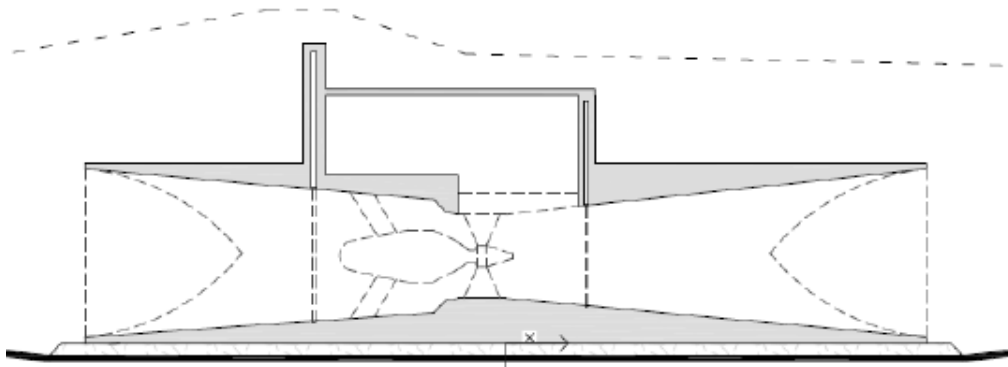
FIGURE 21: BULB-TURBINE SKETCH DESIGN [WELSINK, 2014]

4.1.2.2 FISH FRIENDLY BI-DIRECTIONAL TURBINE BY PENTAIR FAIRBANKS NIJHUIS (PFN TURBINE)

The design of the PFN turbine is quite similar to common bulb-turbines and may therefore be referred to as a modified bulb turbine. Fairbanks Nijhuis has presented positive tests regarding the fish mortality of the bi-directional turbines. Results have shown a fish mortality of 0.0%, for tests performed with a blade diameter of 800 mm and three fish species. Thanks to the undisturbed distance between the propeller vanes and the generated favourable flow, these test results are achieved. In addition, efficiency tests have shown the efficiency of the turbine is not affected by the applied fish friendly technique compared to conventional turbines (up to 90% at the design point). The ability of blades rotating 180 degrees around its horizontal axis in the flow direction contribute to the high efficiency rate. The PFN turbine van be both custom designed and manufactured.
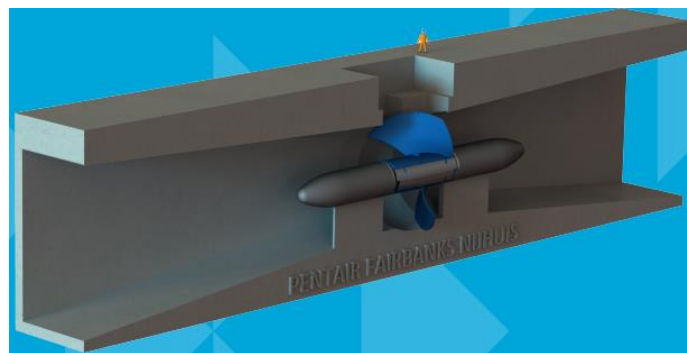
FIGURE 22: CROSS-SECTION PFN TURBINE [ESCH, 2015]

Unfortunately the PFN turbine has not been tested or applied at a significant scale yet. The test results of small scale tests have shown to be promising.. It is therefore assumed future development results in very promising features. Furthermore Pentair Fairbank Nijhuis has announced in 2015 the fish friendly bi-directional turbine will be applied in the Brouwersdam using an 8 meter diameter turbine with a capacity of 4000 kW and a discharge capacity of 340 m³/s.
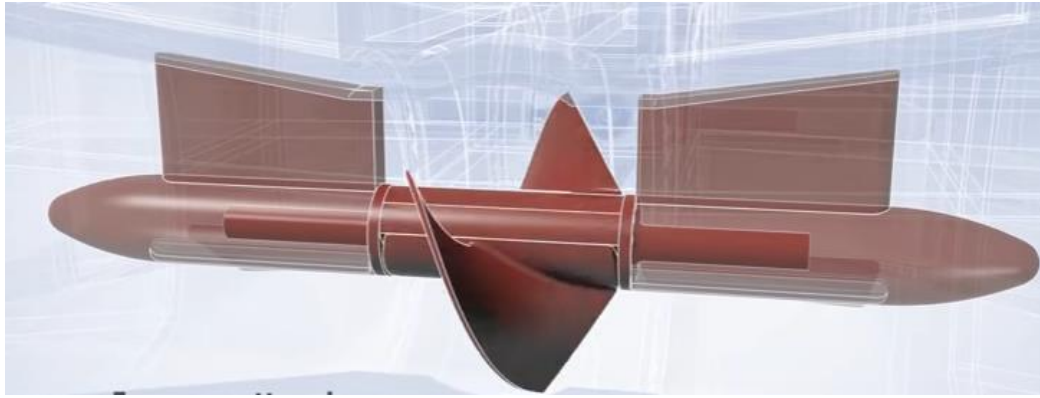
4.1.2.3 HORIZONTAL AXIS FREE STREAM TURBINES (HAWT)

In-shore free stream turbines (Horizontal axis turbine) have been recently (2015) installed by Tocardo at the Eastern Scheldt barrier, Figure 24. The turbines are bulb shaped like the earlier mentioned bulb turbines, but constructed in a free-stream area. At the Eastern Scheldt five turbines were placed attached to a horizontal steel beam, allowing the turbines to be suspended into the water. The turbines are able to rotate around the horizontal steel beam, allowing to apply maintenance works above water. In addition, by constructing the turbines on a single beam, removing the turbines can be removed quite easily. It is therefore assumed the maintenance and operational costs are rather low. The investment costs together with specific technical data remain uncertain. Tocardo has mentioned the turbine costs are proportional to the turbine diameter. Also, output charts for two types of turbines by Tocardo as well. These charts do apply solely for turbines located in a free-stream environment. the Eastern Scheldt,

For the standard turbine placed in a 100% confined flow, a theoretical efficiency is claimed at 59%. Due to the free space required between the turbine blade tips and walls, the fish should theoretically be able to pass the turbines without any damage. This was tested at Den Oever in 2006. No evidence of any fish injuries or mortality due to the turbines was found here.

FIGURE 24: TOCARDO IN-SHORE TIDAL TURBINES INSTALLED AT EASTERN SCHELDT [WWW.TOCARDO.NL].

4.1.2.4 VERTICAL AXIS FREE STREAM TURBINES (VAWT)

Vertical free-stream turbine are the second type of free-stream turbines in this selection. Darius and Well designed an omnidirectional tidal turbine with fixed blades (vertical axis turbine), see Figure 25. The pre-commercial scale prototype, C-energy, was installed in 2009 at the Western Scheldt. The turbines have an estimated efficiency of 16%. Improvements in the rotor design could lead to a further increase in efficiency.

Fish mortality has not been investigated yet, however due to the low rotational speed a very low fish mortality has been assumed. The beneficial shape allows the sluiceway to be rectangular instead of singular as is required for many other turbine types. In addition the relative simple design results in low investment costs. Large civil constructions are not required, whereas the turbines are relatively light and easily lifted out of the Tidal Power Plant. The low efficiency rate and lack of fish mortality tests make the applicability of these turbines uncertain.

FIGURE 25: FREE STREAM VERTICAL AXIS TURBINE[VAN BERKEL, 2014]

4.1.2.5 VENTURI-ENHANCED TURBINE TECHNOLOGY (VETT)

With the venturi-enhanced turbine technology, VerdErg Renewable Energy, designed an innovative low head turbine. The technology is based on the Bernoulli's 18th century Venturi principle, driving a primary flow of water through the device creating a pump without any moving parts. VETT's venturi pump drives a higher velocity secondary flow which drives a conventional axial flow turbine, the only underwater moving part. This allows it to function at an amplified drop under a higher efficiency. An overview of the VETT is given in Figure 26.
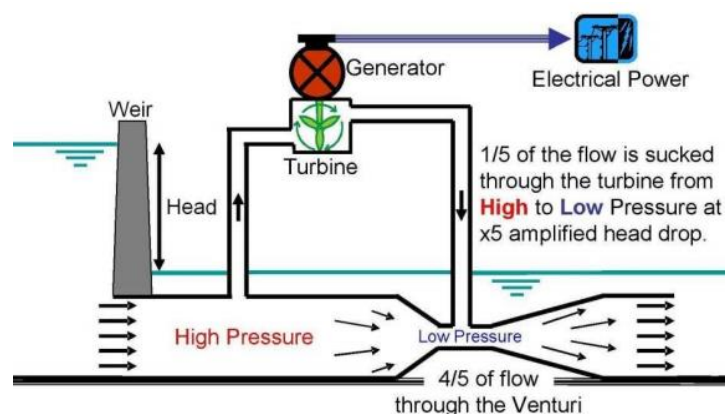
FIGURE 26: SCHEMATIZATION VETT[VAN SPENGEN AND REIJNEVELD, 2015]

The Venturi-enhanced turbine technology requires a simple concrete structure and thus leading to relative low construction costs. In addition, test observations show zero fish damage. The theoretical maximum efficiency according to VerdErg Renewable energy lies between 70-75%, including viscosity in real fluids and other losses a theoretical

efficiency of 65% has been suggested. While applying several adaptations, field and laboratory tests have shown an efficiency of approximately 55%. Due to the relative small turbine diameter the energy output is expected to be relatively low comparing to bulb turbines.

In 2015 VedErg started testing a bi-directional VETT. Within 12 months a complete design was set-up. Three designs were elaborated and still due to be tested. For these designs the efficiency rate, the fish friendliness and the costs remain uncertain.

4.1.2.6 VERY LOW HEAD HYDRO TURBINE (VLH TURBINE)

A French patent application has been filed for the VLH turbine in 2003. In 2004 MJ2 Technologies was founded in order to develop the new concept. MJ2 Technologies aimed to reduce the inlet and outlet structures as much as possible with this VLH turbine.
A rotating trash rake cleaner is mounted on top of the turbine unit to prevent trash flowing in. Under this rake, the bulb is formed by the turbine runner containing the direct-driven variable-speed permanent-magnet generator. This Kaplan-type turbine contains 8 adjustable blades according to the water level upstream and the flow velocity. Moreover, the VLH is able to stop water flowing through by closing its blades, hence no heavy gates are required. The VLH is placed in inclined position, as can be seen in Figure 27, while hydraulic lifting jacks are mounted to the turbine allowing the turbine to be lifted into horizontal position for maintenance purpose. The turbine has performed positive tests concerning fish migration, showing results of a 100% fish survival rate. Furthermore, existing structure sites have shown an efficiency rate of approximately 80%.
It is uncertain whether the turbine will able to work as a two-way operating turbine. The manufacturer aims to be flexible towards their clients, hence it might therefore possible the turbine becomes bi-directional operative in future development. This was already elaborated in Welsink and Yazici [2014] where the different positions of the VLH turbine were considered in such way the turbine was able to work bi-directionally.

FIGURE 27: VLH TURBINE IN FINAL POSITION[WWW.VLH-TURBINE.COM]

4.1.2.7 CONCLUSIONS AND RECOMMENDATIONS

The provided information from the previous sections will be appraised to the mentioned requirements in the conclusion first. The final recommended turbine type will be treated secondly.

4.1.2.7.1 CONCLUSION

Within this conclusion the turbines are qualitatively appreciated for each requirement separately.

GENERATE POWER WITH A LOW HEAD

Both the free-stream and bulb turbine have shown to be able to generate power with a low head. Also the PFL, VLH and VETT turbines are tested in low head environments. Solely the free-stream turbine has not shown clear test data regarding energy generation. However, since these turbines have been installed at the Eastern Scheldt barrier, it is expected energy generation for free-stream turbines will be possible.

FISH FRIENDLY

The fish friendliness is an important factor for turbine selection. Bulb turbines have shown to be fish friendly for larger diameters, whereas free-stream turbines are fish friendly even for smaller diameters. Since a significant space between the turbine blade tips and the sluiceway walls will be present for free-stream turbines, fish will be able to swim freely around the turbine blades.

The VLH, VedErg and PFL turbine have shown to be fish friendly in scaled tests. Based on those tests it is assumed the fish friendliness of each turbine is sufficient.

EFFICIENCY

The amount of energy generation induces the reducing overall costs and will therefore be the crucial requirement in determining the optimal turbine type. In Scheijgrond et al. [2014] the efficiency and energy generation is described by the manufacturers, which makes that information quite reliable.

For bulb turbines available literature have mentioned an efficiency reaching more than 90%. In literature obtained from PFN, an efficiency rate for the modified bulb turbine (PFN turbine) reaching 80% has been described for small scale models. For large scale turbines this efficiency rate seems to increase even more according to PFN [Pentair-Nijhuis, 2015].

Similar to the PFN turbine, the VedErg and VLH turbines have not been applied on full scale in any tidal power project yet. For these turbines the information regarding the efficiency has been obtained from the manufacturers' website. Yet, it remains unknown whether these efficiencies are obtained from situations using a continuous head difference or bi-directional flow.

PUMP AND TURBINE FUNCTION

Solely the VedErg bi-directional syphon turbine is still due to be tested. The remaining five turbines have shown to be able to work bi-directionally from scald tests or modified set-up.

COSTS

The costs remain the most important factor for choosing a certain turbine type. The investment costs of bulb turbines seems to be higher compared with the free-stream or other turbine types. However, the energy generation by bulb-turbines is exceeds energy generated by free-stream turbines. It should be noted that this is based on assumptions, scaled tests and previous performed studies. For each turbine an optimum can be illustrated for construction costs and energy generation. This will be elaborated in a later design stage.

4.1.2.7.2 RECOMMENDATION

In the conclusion it already appeared the bulb-turbine, PFL turbine and free-stream turbines comply with all requirements. Based on the conclusions the final recommendation will be described here.

The bulb turbine is applicable as soon as large diameter turbines are used. The PFL is a modified bulb turbine, tests have shown the turbine is fish friendly thanks to the number of runner blades and the distance between the blades, even for smaller diameters. Due to the weight of the bulb turbine a relatively large cut-in velocity, the flow velocity for which the turbine starts generating power, will be required. The amount of generated energy might thus be reduced as a very low head is present at the dam. Hence, it is recommended to use the PFL turbine when a high efficiency turbine is preferred while a relatively 'large' low head difference is available.

The vertical axis free-stream has not been tested on its fish friendliness and provides a low efficiency, therefore the vertical axis free-stream turbine is not recommended. For small head differences the horizontal axis free-stream turbine seems to be always available for power generation. The relatively light turbines will generate power even for low velocities (in contrast to bulb turbines). The efficiency of the free-stream turbine leaves a lot to be desired, but generating power even for low velocities might compensate the efficiency loss somewhat. Free-stream turbines are fish friendly and able to generate power bi-directionally. Hence, the light free-stream turbines are recommended for lower flow velocities and thus low head differences.

The overall head differences at the Brouwersdam are thus to be examined. During the 100 year lifetime of the structure, optimal turbine type(s) will be applied to result in optimal total construction costs. Therefore, a number of scenarios regarding the hydraulic conditions at the Brouwersdam will be considered. With these scenarios an optimal turbine design will be computed. The following subparagraphs will therefore be dedicated to determine the scenarios, optimal applicable turbine design alternatives and the final recommended type of turbine with the current available knowledge.

A side note must be made regarding the turbine selection; it has strongly been influenced by the fish mortality rate prescribed by the Dutch Government. The extreme low mortality rate seems to be almost unreachable for turbines. Therefore, the exact definition of the fish mortality rate must be more clarified. For example, does the fish mortality mean direct loss of life when passing the turbine or should loss of life as a consequence of damage due to turbine blades be included even after some time. Hence, should the mortality rate be adapted, or should be decided to construct adjacent fish migrating measures?

4.1.3 SCENARIOS

In the near future water levels at the North Sea are expected to rise as a consequence of global warming. This induces variations in head differences during the structure's lifetime. Mainly the sea level rise and basin storage capacity required for the 'Room for the river' program give an uncertain future vision. This subparagraph will treat three scenarios of the hydraulic variations in the near future.

4.1.3.1 SCENARIO 1: 2017

In the current situation the tidal differences as described in the literature study are used. From www.waterbase.nl the North Sea water levels are obtained. These sea levels consist of minima, maxima and mean water levels for one year (October 2015 to October 2016).

The Dutch government has not taken a formal decision with regard to assigning Lake Grevelingen as a storage basin for the 'Room for the River' program. The question arises whether the option, incidental rise of the water level of Lake Grevelingen to +1.50 m NAP, should be still available since this solution has shown to be less cost efficient. In addition, since shores in Lake Grevelingen are not able to cope with such high water levels, it would negatively influence the regional developments,

In the current climate conditions the probability of using a water storage basin is 1/1400 year [Programmabureau zuidwestelijke Delta, 2014]. Since there is no decision taken by the Dutch Government, and it is not very likely this decision will be taken within a couple of years, Lake Grevelingen will not function as a storage basin the first scenario

The water levels obtained from www.waterbase.nl between October 2015 and October 2016 are governing in this first scenario. Table 4 gives an overview of the obtained data.

Parameter	Value	Unit	Parameter	Value	Unit
North Sea					
Average water level	0.00	m NAP	Maximum Tidal range	3.44	m
Maximum High water level	+2.05	m NAP	Average tidal range	2.511	m
Minimum High water level	+0.87	m NAP	Average low water slack	6.26	Hours
Minimum Low water level	-1.49	m NAP	Average high water slack	5.59	Hours
Maximum Low water level	-0.65	m NAP			
Average high water level	+1.456	m NAP			
Average low water level	-1.055	m NAP			
			Average Head flood	1.906	m
Lake Grevelingen			Average Head ebb	1.005	m
Average water level lake	-0.20	m NAP			
Minimum water level lake	-0.45	m NAP			
Maximum water level lake	+0.05	m NAP			

TABLE 4: RELEVANT WATER LEVELS SCENARIO 1

The head difference during flood is defined as the head difference between the higher water level at the North Sea and the lower water level at Lake Grevelingen. The opposite counts for head differences during ebb.

KNMI mentions the expected sea level rise in 2030 is approximately 10 to 25 cm[KNMI, 2014]. A sea level rise of this magnitude might result in an obliged water level rise of Lake Grevelingen. The average low water level of the North Sea is still below the minimum low water level at Lake Grevelingen, thus tidal energy generation will still be possible. Table 5 gives a clear overview of all the required water levels.

As mentioned in scenario 1, in the current climate conditions the probability of using a water storage basin is 1/1400 year. It is therefore assumed scenario 2 is comparable with scenario 1 and Lake Grevelingen will not function as a storage basin.

Parameter	Value	Unit	Parameter	Value	Unit
North Sea					
Average water level	+0.25	m NAP	Maximum Tidal range	3.44	m
Maximum High water level	+2.30	m NAP	Average tidal range	2.511	m
Minimum High water level	+1.02	m NAP	Average low water slack	6.26	Hours
Minimum Low water level	-1.24	m NAP	Average high water slack	5.59	Hours
Maximum Low water level	-0.41	m NAP			
Average high water level	+1.706	m NAP			
Average low water level	-0.805	m NAP			
			Average Head flood	2.156	m
Lake Grevelingen			Average Head ebb	0.755	m
Average water level lake	-0.20	m NAP			
Minimum water level lake	-0.45	m NAP			
Maximum water level lake	+0.05	m NAP			

TABLE 5: RELEVANT WATER LEVELS SCENARIO 2

4.1.3.3 SCENARIO 3: 2050

KNMI expects a sea level rise of 40 cm in 2050. The Delta committee uses the KNMI expectations for future sea level rise. Therefore, these expectations will be used in this scenario as well. At a sea level rise of 40 cm the average low water level of the North Sea still remains underneath the minimum water level of Lake Grevelingen. Hence energy generation will be possible and might even increase since the head difference during spring tide increases, which will increase in larger flow velocities and thus an increase in energy generation.

As mentioned in scenario 1, in the current climate conditions the probability of using a water storage basin is 1/1400 year. Due to the climate changes from 2050 this probability could become 1/550 year. In that case it might be required to use Lake Grevelingen as a storage basin which is therefore assumed to be the actual case in this scenario. It means the water level in Lake Grevelingen could reach +1.50 m NAP incidentally. Powerful two-way turbines will be required to ensure the water level in Lake Grevelingen decreases to the original water level.

As a consequence of the increase of water level at Lake Grevelingen foreshore dams and other current protective measures in the lake require elevation to maintain their protective function against erosion. Table 6 provides an overview of the relevant water levels in scenario 3.

Parameter	Value	Unit	Parameter	Value	Unit
North Sea					
Average water level	0.40	m NAP	Maximum Tidal range	3.44	m
Maximum High water level	+2.45	m NAP	Average tidal range	2.511	m
Minimum High water level	+1.27	m NAP	Average low water slack	6.26	Hours
Minimum Low water level	-1.09	m NAP	Average high water slack	5.59	Hours
Maximum Low water level	-0.25	m NAP			
Average high water level	+1.856	m NAP			
Average low water level	-0.655	m NAP			
			Average Head flood	2.700	m
Lake Grevelingen			Average Head ebb	0.905	m
Average water level lake	0.00	m NAP			
Minimum water level lake	-0.25	m NAP			
Maximum water level lake	+0.25	m NAP			
Maximum storage water level lake	+1.50	m NAP			

TABLE 6: RELEVANT WATER LEVELS SCENARIO 3

In the future up to 2100 the Delta committee has set a scenario which indicates a sea level rise of 120 cm excluding a 10 cm tectonic subsidence [www.knmi.nl]. This rise is much higher compared with the scenario's set by the Meteorology bureau: 85 cm in 2100. This difference is based on the expected increase in temperature: the Delta committee expects a temperature increase of 6 °C, whereas KNMI expects a 4°C temperature rise. An additional fourth scenario in 2100 has been excluded due to these diverging theories. Moreover, with an increase of another 45 cm the possibility of generating energy becomes lower and lower, since the water level at the North Sea exceeds the minimum water level at lake Grevelingen. One could argue if the shores and foreshores require protection or elevation, in order to enable generating energy. This will not be considered ant further in this thesis.

4.1.3 ALTERNATIVES

In section 4.1.2.7 two turbine types have been recommended; the PFN turbine and Free-stream turbine. The other turbines might be very advantages during in the considered scenarios as well, but require additional tests and research. With the two recommended turbines and the advantages of the remaining turbines, three alternatives are set, based on the described scenarios from the previous paragraph. Furthermore, the alternatives are based on an additional concept; RINK. As described in Appendix B.1.3, the RINK method outlines the ability of the tidal power plant to adapt itself to the changing conditions described in the scenario's.

4.1.3.1 ALTERNATIVE 1: ONE TURBINE TYPE, ONE DIAMETER DURING LIFESPAN

The three scenarios have shown some deviations regarding the sea level rise and discharge capacity due to the 'Room for the river' program. The first alternative is based on a single turbine type that should be able to generate a continuous amount of energy, in each scenario. This turbine type should therefore be flexible regarding the head difference. Since the PFN turbine requires a certain cut-in velocity to start generating energy, the PFN turbine shall not be able to deliver a continuous amount of energy.

The free-stream turbines, however, are not constrained to a significant flow velocity due to their lower weight. Therefore, for this alternative the free-stream turbine is considered as best applicable. The free-stream turbines will always be able to generate electricity as they will be designed on the most unfavourable situation during the three scenarios. Moreover, since the free-stream turbines manufactured by Tocardo also allow being easily disposed into maintenance position, it should be possible to adapt the rotor blades. Adapting the rotor blades for different scenarios results in potential higher efficiencies.

4.1.3.2 ALTERNATIVE 2: MULTIPLE TURBINES TYPES DURING LIFESPAN

The idea of alternative 2 is based on the RINK system. Adapt the tidal power plant to changing conditions during its lifetime. This means the tidal power plant will first be equipped with a turbine which seems most suited for scenario 1, while not having significant impact on the civil construction. This allows adaptations to be easily applied.

The one type having minor impact on the civil construction is the VETT turbine. Therefore, for the first scenario the VETT turbine will be applied. The VETT is not recommended from the chapter 'turbine Selection' due to the uncertainties regarding a bi-directional VETT. Hence, the bi-directional turbine should be more elaborated and tested, before actually installing it on the Tidal Power Plant. In the second scenario the head difference during ebb becomes smaller, whereas the head difference during flood increases. Conditions in which the PFN turbine will function. With future scaled tests the PFN turbine will even be more optimized to the low head differences at the Brouwersdam and therefore be best suited.

Scenario 3 has shown to have an even larger head difference at flood and the head difference during ebb decreases again. The final type of turbine to be installed is therefore a bulb turbine. In order to comply with all the requirements and the bulb turbine should undergo a transformation regarding its weight and efficiency. It is expected in 30 years the bulb turbine will be properly developed making it a cost efficient turbine at that moment. In that way the bulb turbine will be able to produce

energy with small head differences while having the highest efficiency rate of all considered turbine types.

4.1.3.3 ALTERNATIVE 3: MULTIPLE TURBINE TYPES DIFFERENT DIAMETERS

Alternative three is based on the two recommended turbines; the modified bulb-turbine and the free-stream turbine are recommended. Since there are still a lot of uncertainties regarding the costs, performance and efficiencies of the turbines it is chosen to design a tidal power plant in which any turbine type can be applied with different diameters. Based on the RINK method, the tidal power plant should become a kind of construction box. Adaptations to the tidal power plant should be applicable. The initial installed turbines will be replaced by turbines better suited for the concerned scenario. It has been assumed for scenario 1 the relatively cheap free-stream turbine will be most favourable, due to the low head and corresponding low flow velocities. In scenario two the PFN turbine will be applied, assumed scaled tests and optimal performance studies have been executed.

4.1.4 FINAL TURBINE TYPE RECOMMENDATION

The three mentioned alternatives allow installation and seem to be reasonable. Due to the uncertainties regarding the turbine design and the developments during the past decades, the mentioned turbines will be further optimized in the near future. For now it seems most reasonable using turbines from which the most reliable information has been available. This induces the lack of information for the turbines mentioned in alternative 2. Alternative 1 will not able to adapt itself to future developments. Therefore, it has been decided to apply alternative 3.

Thus, the new design should be able to adapt by changing the turbine diameters and/or turbine type. The turbine dimensions should be chosen in such matter the requirements are still met. The fish mortality is an important factor regarding both the turbine diameter and the turbine type. For free-stream turbines this will probably not be a very problematic matter as there will be sufficient free space available around the turbines. The PFN turbine requires a higher velocity in order to start turbining, especially for larger diameters. However, the fish mortality for small diameter turbines largely exceeds the requirement of 0.01%. Hence, for the PFN turbine, the applied diameter should be as large as possible. Therefore, the succeeding paragraph will determine the required turbine dimension

4.2 TURBINE DIMENSIONS

With the chosen alternative; applying a free-stream turbine in the time period between scenario 1 and 2 and applying a PFN turbine from scenario 2 during the remaining lifespan of the structure, the required turbine dimensions require computation. This paragraph will therefore be dedicated to the turbine dimensions. First, the water level restrictions are considered, resulting in the maximum level of the sluiceway top. Secondly the required cross-sectional discharge area of the Tidal Power Plant will be elaborated while considering a tidal range of 50 cm at Lake Grevelingen. Third, the optimal turbine diameter for both turbine types will be computed. The combined outcome will result in the preliminary turbine design.

4.2.1 WATER LEVEL RESTRICTIONS

At the North Sea side the minimum low water level lies at -1.50 meter NAP. The significant wave height contains 2.6 meter. Turbulent water flowing into the sluiceway results in a reduced energy generation. Therefore the top of the inlet sluice will lie at the low water level occurring once a year; -1.5 meter NAP. In the succeeding scenario's this minimum water level will increase, the minimum water level from scenario 1 has therefore been considered as governing.

At the lake side the level restriction will be based on the wind set-down of the water level or the significant wave height. Both are determined using the wind velocity. In Appendix B.2 the wind velocity has been calculated. Resulting in:

$$H_s = 1.17\ m$$

$$H_{set-down} = 0.57\ m$$

The design water level at the inner side of the Brouwersdam is calculated using the maximum water level of the lake. During ebb the tube at the lake side will function as inlet tube, while during flood it will function as outlet tube. Therefore the design water level for the top of the inlet tube should be maximum water level in the lake (+0.05 m NAP) minus the significant wave height divided by two (0.59 m). For simplicity the design level of the top of the tube at the lake side becomes: -0.55 meter NAP.

4.2.2 REQUIRED CROSS-SECTIONAL AREA

To determine the required cross-sectional area, the non-homogeneous solution for a system with a discrete storage and resistance will be applied. From Vrijling et al. [2008] it followed, to introduce a tide of 50 cm at Lake Grevelingen, an average discharge capacity of 3500 m³/s should be available at a bi-directional Tidal Power Plant. Both the basin and the channel are short compared with the tidal wave length. The required discharge surface will be determined using the following equations, obtained from Battjes and Labeur [2014]:

$$\hat{Q} = A_k \omega \xi_k$$

$$\xi_k = r * \xi_s$$

$$r = \cos(\theta) = \frac{1}{\sqrt{2}\Gamma}\sqrt{-1 + \sqrt{1 + 4\Gamma^2}}$$

$$\Gamma = \frac{8}{3\pi} \chi \left(\frac{A_k}{\mu A_s}\right)^2 \frac{\omega^2 \xi_s}{g}$$

$$\chi = \frac{1}{2} + c_f \frac{L}{R}$$

In which ½ gives a value for the expansion losses. Furthermore:

$\hat{Q} = discharge\ through\ the\ system$

$A_k = Lake\ Grevelingen\ surface = 117\ km^2$

$\omega = tidal\ frequency = 1.41 * 10^{-4}\ rad/s$

$\xi_k = Tidal\ amplitude\ lake = 0.25$

$r = tidal\ response$

$\xi_s = tidal\ amplitude\ North\ Sea = 1.25\ m$

$\Gamma = dimensionless\ parameter, containing\ all\ independent\ variables\ playing\ a\ role$

$\mu = contraction\ coefficient$

$A_s = discharge\ surface$

$g = gravitational\ constant = 9.81\ m^2/s$

$\chi = dimensionless\ loss\ coefficient$

$c_f = friction\ coefficient\ concrete = 0.003$

$L = channel\ length = 53\ m$

$R = hydraulic\ radius = D_{tube}/4\ for\ a\ cilinder\ shaped\ tube$

$D_{tube} = diameter\ of\ the\ tube$

This approach does not take into account the real (measured) water level at the North Sea, or the allowable water levels at Lake Grevelingen. It assumes a sinusoidal tide. The result will thus be considered as indicative and must be used as a minimum.

In this calculation for several parameters some assumptions have been made. For a first estimation the dimensionless loss coefficient was set to 0.55. Since the channel length and hydraulic radius are not known yet, and comparing it with recent literature such as Spengen et al. [2015] and Boon and Roest [2008] this seems quite reasonable. This was checked in a later stadium of the design stage and corrected if necessary.

The contraction loss coefficient is set to 0.9, since the sluiceway will be designed in to overcome any head losses.

For safety reasons a free space around the turbine of 1.0 meter will be applied, leading to additional loss in efficiency. The free-flow turbine influences the flow velocity flowing through the sluice way. Therefore a reducing factor of the ratio between the velocity in front of the turbine and behind the turbine, named the loss in head difference, is

included in the formula as well. Together with the contraction coefficient it influences the tidal response in the dimensionless parameter Γ:

$$\frac{v_2}{v_1} = \sqrt[3]{\frac{A_s - \eta * C_p A_{turb}}{A_s}}$$

With:

$A_s = wet\ cross\ sectional\ area\ sluiceway$

$\eta * C_p = turbine\ efficiency = 0.35\ (assumed\ for\ free-stream\ turbine)$

It leads to a required discharge capacity of approximately 960 m² for the free-stream turbines.

The minimum discharge area for the modified bulb turbine will be determined using a similar approach. However, the discharge coefficient requires a different calculation method. Mooyaart and Noortgaete [2010] performed this calculation using a reference bulb turbine in Alphen aan de Maas, The Netherlands. From their method the design discharge has been computed with only the rated head and turbine diameter. The rated head is defined as the head difference for which the full capacity of the energy generation of the turbine is reached. Meijnen en Arnold [2015] applied a rated head of 1.25 for the current situation at the Brouwersdam for design calculations of the PFN turbine. As was mentioned earlier, the PFN turbine will be applied for scenario 2, with a sea level rise of 25 cm, the rated head has been increased by 25 cm. Combining the properties of the bulb turbine at Alpen aan de Maas with general turbine equations results in an expression for the design discharge:

$$Q_d = \frac{Q_{d,Alphen}\sqrt{H_{rated}}}{\sqrt{H_{rated,Alphen}}} * \frac{D^2}{D^2_{Alphen}} = 100 * \frac{\sqrt{H_{rated}}}{\sqrt{4}} * \frac{D^2}{4^2} = 3.125\sqrt{H_{rated}}D^2$$

Subsequently, the discharge coefficient will be determined by dividing the design discharge by the actual discharge of the turbine:

$$\mu_{bulb} = \frac{Q_d}{A_{bulb}\sqrt{2gH_s}}$$

For a continuous sinusoidal tide and a loss in hydraulic head $(1 - \mu_{bulb})$ this results in a required discharge area of approximately 960 m² as well.

4.2.3 TURBINE DIAMETER

The description of alternative 3 already mentioned installation of turbines with varying diameters over the structures lifetime. The turbine dimensions are depending on the water velocity. Another limiting factor is the fish mortality, the larger the diameter the lower the damage to fish and thus the fish mortality. The requirements in section 4.1.1 have shown a fish mortality of 0.01% is allowed.

TOCARDO FREE-STREAM TURBINES

Tocardo offers two types of bi-directional hydro-turbines: T100 (100 kW output) and the T200 (200 kW output). The dimensions of those turbines strongly depend on the

water velocity. Therefore, the required cross-sectional area will be obtained first. With the determine cross-sectional area and design discharge, the water velocity can be computed. The required 960 m^2 leads to a design water velocity of 4.3 m/s. Corresponding to this design velocity, are a 3.4 meter diameter T100 or a 49 meter diameter T200. The total diameter of the T100 becomes then 4.43 meter, while the total diameter of the T200 becomes 6.24 meter. The length of the T100 and T200 is respectively 4.25 meter and 5.85 meter. For safety reasons, a margin between blade tips and walls of 1.0 meter shall be applied, which is recommended by Tocardo as well. Since a maximum output is generated while applying the T200, it has been chosen to apply this model. The total required cross-sectional area becomes 8.24 meter. To introduce a tidal difference of 50 cm at Lake Grevelingen, a cross-sectional area of 960 m^2 will be required which is reached by applying in total 18 turbines.

PFN turbine

The Pentair Fairbanks bi-directional turbine shall be applied at scenario 2, a sea level rise of 25 cm. Whereas the free-stream turbine will be applied first, the construction restricts the maximum diameters of the PFN turbine. Adaptations to the construction would lead to an increase in costs and are therefore assumed to be non-taken. The dimensions of the PFN turbine are not bounded and can be customized within practical boundaries. Therefore, the dimensions of the PFN bi-directional turbine will be based on the dimensions of the free-stream turbine and the fish mortality rate. Resulting in a maximum diameter of 8.24 meter. PFN handles a safety margin between the blade tip and the turbine housing of D/1000. A very small safety margin for practical reasons, this also means the foundation for the PFN turbine should be very stiff, since any movements could lead to blade damage. In total 18 turbines will be constructed to reach a cross sectional discharge area of 960 m^2.

4.2.4 FISH MORTALITY

Free-stream non-ducted turbines have shown to be fish friendly at Den Oever, tests performed by Tocardo. Quantitive results have not been published. Ducted free-stream turbines have not been tested on fish mortality a lot. One test, provided by the Electric Power Research Institute [Jacobson, 2014], was executed to determine the fish mortality of a ducted free-stream turbine with a diameter of 1.5 meter. When applying multiple free-stream turbines in the caissons it might act somehow as a ducted free-stream turbine. Hence, the mentioned test is therefore used as a reference. By varying the flow velocity the fish mortality was checked, resulting in a fish passage of approximately 99-100%. It appeared the higher the flow velocity through the ducted turbine, the higher the mortality rate. It is assumed increasing the turbine diameter has a positive influence on the fish mortality.

The PFN turbine, requires a large diameter to become fish friendly. Even with the low head differences the fish friendliness is not expected to be significantly low with a turbine diameter of 8.24 meter. Model tests performed by Pro-Tide (Esch, 2015], using the Fairbanks Pentair Nijhuis turbine, diameter 1 meter and discharge 1 m^3/s, have shown for certain fish species the mortality rate of < 0.1% might be reached. The mortality rate of bass lied a bit higher 0.19%. Therefore, measures might have to be taken to reach a fish mortality rate of 0.01%.

4.2.5 ENERGY GENERATION

With the computed turbine diameters and input information from Tocardo and PFN the total energy generation will be calculated in this section. At first an overview of the turbine properties will be given, this data will be sued to determine the actual energy generation. The energy generation for each turbine will be considered separately, with data obtained from waterbase.nl

From information obtained from Tocardo and PFN a summary has been provided in Table. Since the PFN turbine has not been developed on scale yet, no clear information is available and certain properties will have to be assumed.

Tocardo T200			PFN		
Rated water velocity	4.00	[m/s]	Diameter	8.24	[m]
Blade D	4.9	[m]	Swept area	35.7	[m^2]
Swept Area	19.0	[m^2]			
Rated grid power	180	[kW]			
Rated Revs	41	[rpm]			
Cut-in water speed	0.9	[m/s]			
Cut-out water speed	6.0	[m/s]			
Survival water speed	8.0	[m/s]			
Power output	180	[kW]			

TABLE 7: PRESCRIBED PROPERTIES CHOSEN TURBINES

Determining the generated energy per turbine type, the tidal situation of the North Sea in 2016, at measuring point Brouwershavensche gat 08 (Figure 28), has been used. The PFN turbine shall be applied for scenario 2, meaning a mean sea level rise of 25 cm. The data from 2016 has thus been increased by 25 cm. As a starting point the average water level at Lake Grevelingen was taken; -0.2 m NAP. Head losses will be calculated in a later design stage, but have already been applied to the power generation calculations on the succeeding pages.

FIGURE 28: MEASURING POINTS CLOSE TO BROUWERSDAM

The maximum efficiency of the Free-stream turbine is assumed to be 59% in optimal conditions. The Tocardo turbines offer a power output of 180 kW, as prescribed by Tocardo. It remains unknown how this power output has been defined. Common energy production equations do not result in the given power output provided by Tocardo. However, the power output obtained from Tocardo has been measured for situations in a free-stream non-ducted environment. Therefore, the blockage ratio should be included for determination of the power output for at the ducted Tidal Power Plant. The blockage ratio increases the power output of the turbine and thus the prescribed output is reached for a smaller rated flow velocity. With the following equations the final energy generation has been determined.

$$Q_{in} = \Delta H * A_s * \sqrt{2 * g * H} * n$$

$$U_{in} = \frac{Q_{in}}{A_s}$$

$$U_{rated} = U_{ratedtocardo} * \left(1 - \frac{A_t}{A_s}\right)^2$$

$$dh_{lake} = Q_{in} * t / A_{lake}$$

$$P_{free-stream} = \frac{U_{in}}{U_{ratedtidal}} * P_{tocardo}$$

$$E_{free-stream} = \frac{\sum P_{free-stream}}{60*60}$$

In which:

Q_{in} represents the incoming flow from North Sea or Lake Grevelingen

H represents the head difference

n represents the number of turbines = 18

ΔH represents the head losses in sluiceway = 0.9

U_{in} represents the incoming flow velocity

U_{rated} represents therated flow velocity for the free stream turbine including

       the blockage ratio

$U_{ratedtocardo}$ represents therated velocity prescribed by Tocardo

A_t represents the swept area $Free - stream\ turbine = 19\ m^2$

A_s represents the *wet cross sectional area sluiceway* $= 8.24 * 8.24 = 67,9\ m^2$

A_{lake} represents the surface area Lake grevelingen $= 117\ km^2$

$P_{tocardo}$ represents the power output prescribed by Tocardo

$P_{free-stream}$ represents the generated power $free - stream\ turbine$

$E_{free-stream}$ represents the generated energy $free - stream\ turbine$

The cut-out velocity of the Tocardo T200 turbine contains 6 m/s. This means at an incoming velocity of 6.0 m/s the turbine stops generating energy. This velocity is not reduced by the blockage coefficient, since the blockage coefficient solely increases the efficiency of the turbine, but does not increase the flow velocity.

Varying the cut-in velocity could result in an increase in the energy production. The optimal cut-in velocity is computed using Figure 29. It may be concluded the cut-in velocity prescribed by Tocardo results in the optimal energy production of 19.22 GWH per year.

The discharge development and the water levels at both Lake Grevelingen and the North Sea during 3 days are illustrated in Figure 30 and Figure 31 respectively.
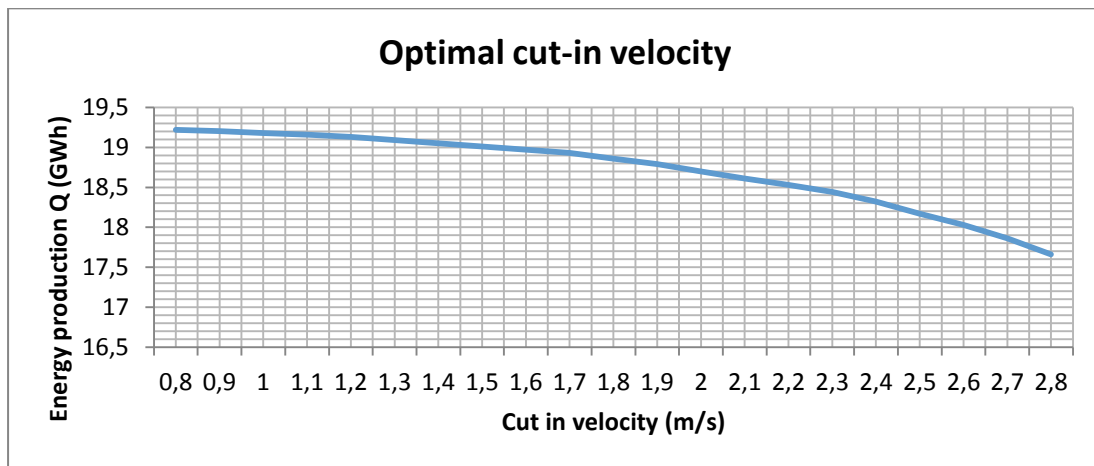
FIGURE 29: OPTIMAL CUT-IN VELOCITY
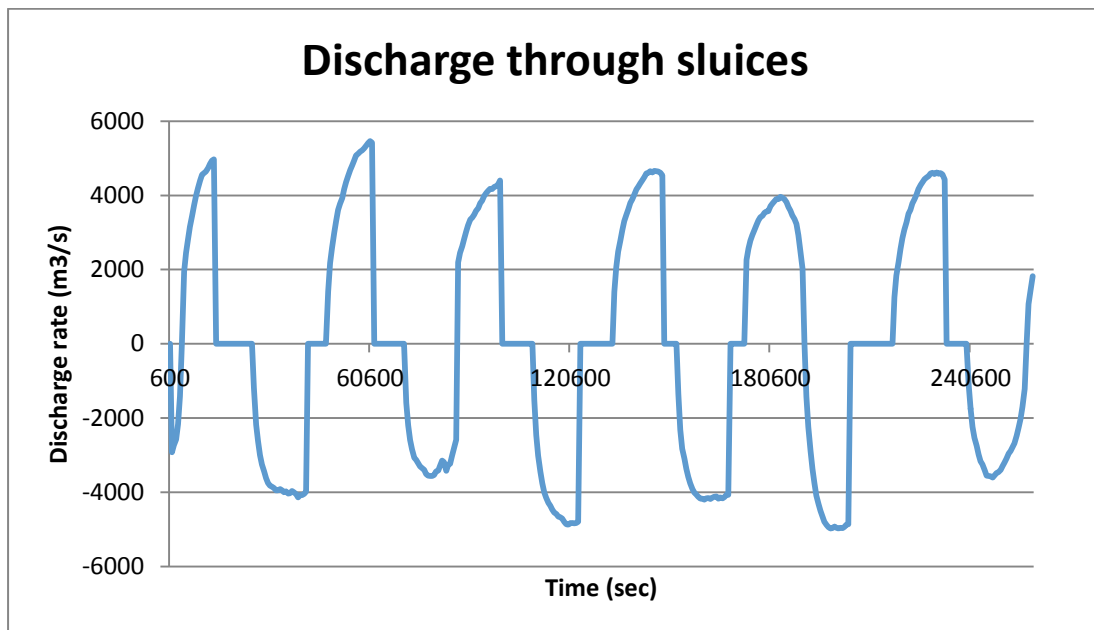
FIGURE 30: DISCHARGE THROUGH TIDAL POWER PLANT DURING INTERVAL OF 3 DAYS
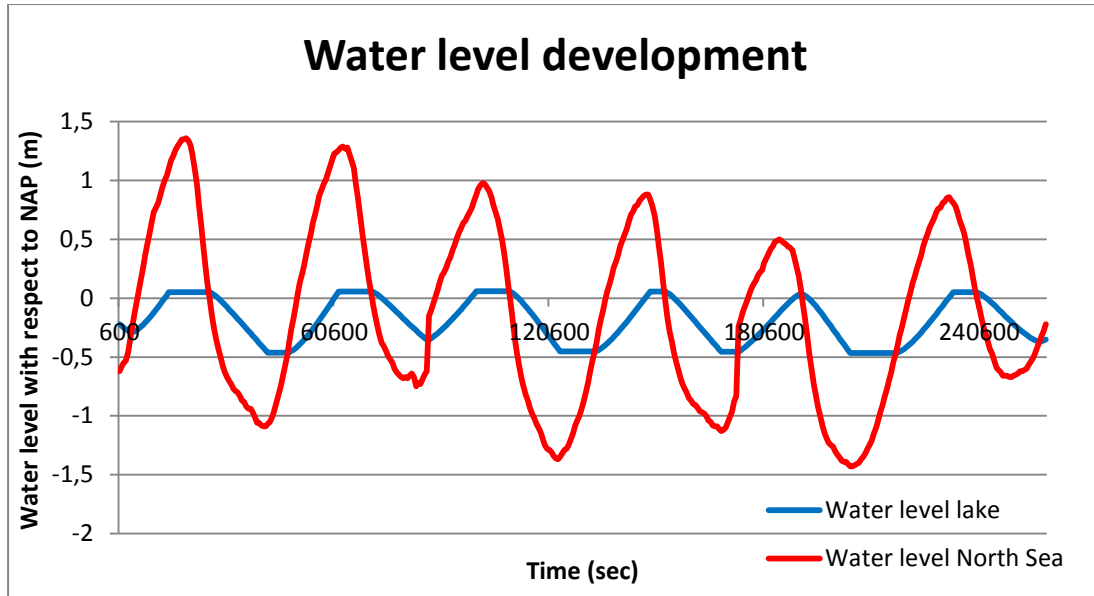
FIGURE 31: WATER LEVEL DEVELOPMENT DURING 3 DAYS

In Figure 30 one may observe horizontal lines for a discharge of 0.0 m³/s and abrupt discharge decrease, these points indicate the maximum or minimum water level at lake Grevelingen has been reached and thus the gate will be lowered and the discharge becomes zero. The blue line from Figure 31, water level lake Grevelingen, supports the discharge line by showing a constant water level the moment the discharge becomes zero.

BULB TURBINE

The calculation of the bulb turbine will be similar to the calculation of the free-stream turbine. Similar tidal data as used for the free-stream turbine will be applied. The North Sea water level, however, is adapted to the proposed water level according to Scenario 2. The opening head of the PFN turbine has been assumed at 0.5 meter. The rated head is due to be determined by the turbine manufacturer. Since PFN has not developed turbines with such diameter yet, no clear data is available regarding the rated head, the efficiency and the maximum generated power. Therefore, the rated head has been determined according to the highest energy generation, where the rated head influences the installed power of the turbine as well. PFN assumes a turbine efficiency of 90% for their currently developed turbines.

$$Q_{in,turb} = Q_{rated} * n * \sqrt{\frac{H}{H_{rated}}}$$

$$P_{installed} = H_{rated} * \rho * g * 3.125 * \sqrt{H_{rated}} * A_{PFN}$$

$$\eta_{PFN} = \frac{H}{H_{rated}} * 0.9$$

$$P_{PFN} = \rho * g * Q_{in} * H * \eta_{PFN}$$

$$E_{PFN} = \frac{\sum P_{PFN}}{60 * 60}$$

64

In which:

$Q_{in,turb}$ represents the incoming discharge applied to the turbine

Q_{rated} *represents* rated discharge $= 3.125 * \sqrt{H_{rated}} * A_{PFN}$

$P_{installed}$ *represents the installed rated power PFN Turbine*

A_{PFN} *represents* the wet cross section area PFN turbine $= 0.25 * \pi * 8.23^2$

$= 53.2 \text{ m}^2$

H_{rated} *represents* the rated head

η_{PFN} represents the efficiency PFN turbine with a maximum of 0.9

P_{PFN} *represents generated power PFN turbine with a maximum of the installed*

power

E_{PFN} represents the total generated energy PFN turbine

From Figure 32 the rated head corresponding with its produced energy has been illustrated. From thus figure an optimal rated head of 1.1 meter has been obtained, resulting in a maximum energy generation of 81.54 GWh per year, with an installed power of 2.46 MW per turbine. The openings percentage of the PFN turbine contains 40 percent. The discharge and water levels development for the applied PFN turbine are given in Figure 33and Figure 34 respectively.
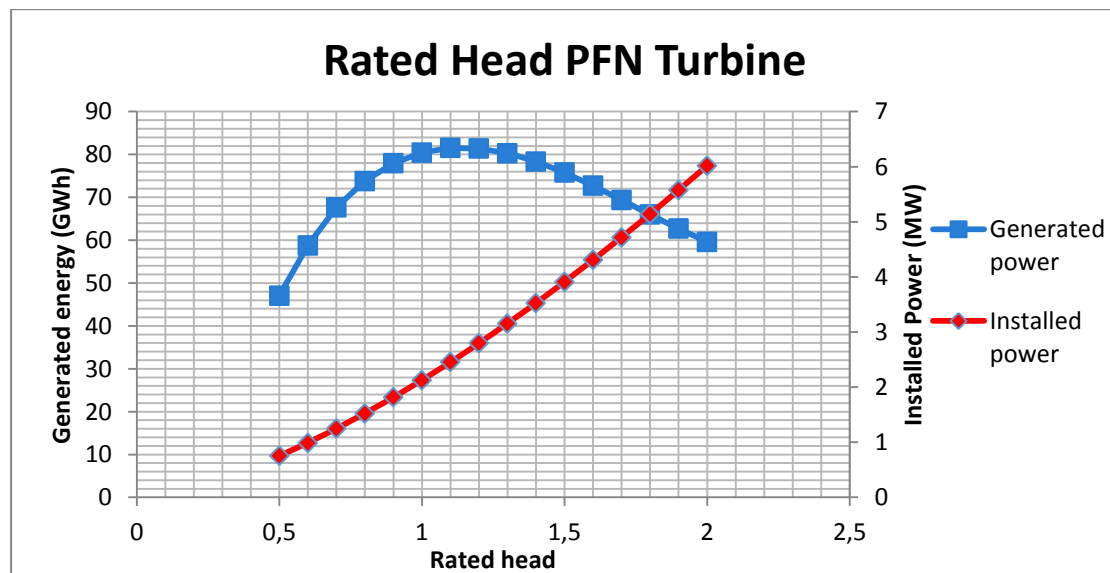
FIGURE 32: RATED HEAD PFN TURBINE
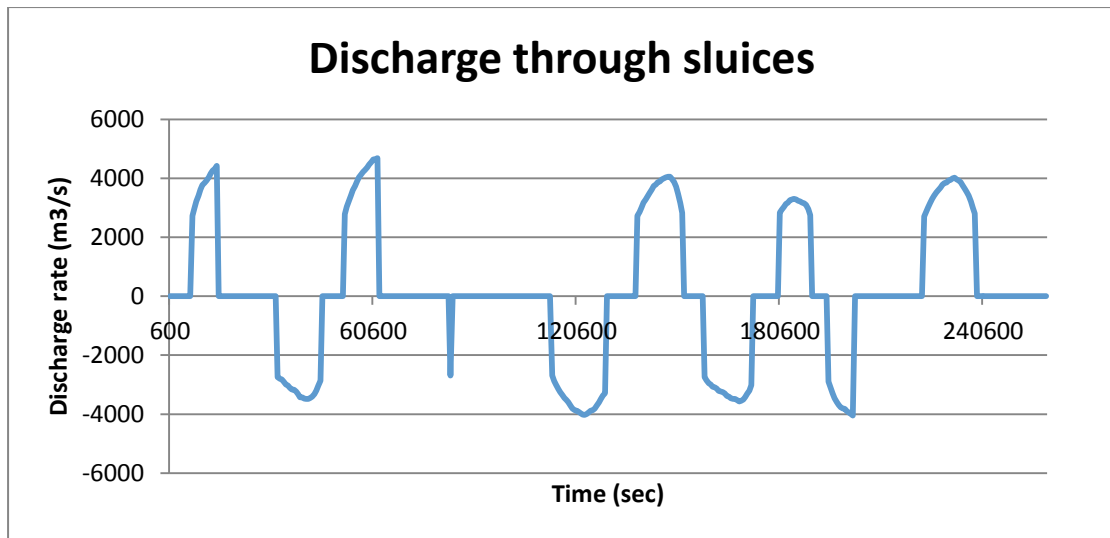
FIGURE 33: DISCHARGE DEVELOPMENT PFN TURBINE DURING 3 DAYS
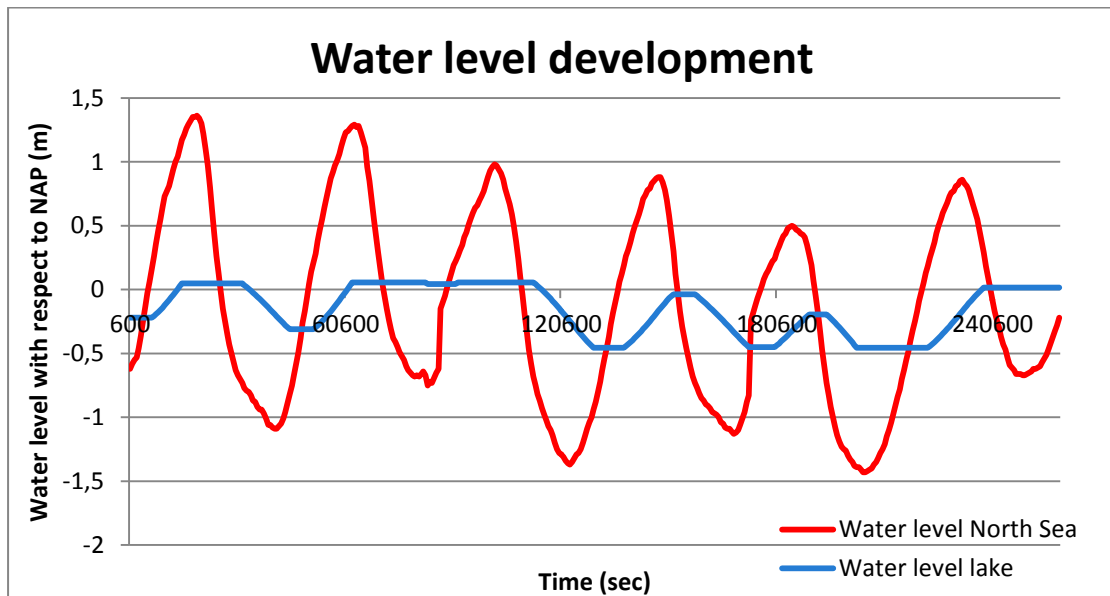
FIGURE 34: WATER LEVEL DEVELOPMENT DURING 3 DAYS PFN TURBINE

In Figure 33 one may observe horizontal lines for a discharge of 0.0 m³/s and abrupt discharge decrease, these points indicate the maximum or minimum water level at lake Grevelingen has been reached and thus the gate will be lowered and the discharge becomes zero. The blue line from Figure 34, water level lake Grevelingen, supports the discharge line by showing a constant water level the moment the discharge becomes zero.

The determination of the optimal turbine type was based on five requirements:

- Generate power with a very low head
- Fish friendly
- Efficiency
- Pump and turbine function
- Costs

Two turbine types complied with the five requirements; the PFN turbine and free-stream turbine.

During the 100 year lifetime of the structure, an optimal turbine type will be applied to result in optimal total construction costs. Therefore, three scenarios regarding the hydraulic conditions at the Brouwersdam were considered:

- 2017; water levels according to data obtained from 2016
- 2030; a sea level rise of 25 cm added to the data from 2016
- 2050; sea level rise of 40 cm and Lake Grevelingen functioning as storage basin

Three alternatives were described to determine the optimal turbine selection during the Tidal Power Plant's lifetime. It resulted in combination of the PFN and free-stream turbine. Where the PFN will be applied from scenario 2. The properties and results of these turbines are summarized below:

	Free –stream	PFN turbine	
Model	T200	Custom	[-]
Required discharge area	960	960	[m^2]
Blade diameter	4.9	-	[m]
Safety margin between blade tip and walls	1.0	D/1000	[m]
Total required diameter	8.24	8.24	[m]
Total number of turbines	18	18	[-]
Installed power	0.18	2.46	[MW]
Total generated energy	19.22	81.54	[GWh]

TABLE 8: SUMMARY TUBRINE PROPERTIES

5 PRELIMINARY POWERHOUSE DESIGN

With the conclusion from the preliminary turbine design the complete housing of the turbines and thus the full Tidal Power Plant will be determined. Within the Tidal Power Plant a number of components are present. The composition of all components results in the powerhouse of the Tidal Power Plant. The Tidal Power Plant's powerhouse may thus be described as the cross-sectional area in which all functions and required components are located. Figure 35 provides an overview of a Tidal Power Plant cross-sectional area. This chapter will be dedicated to design the complete
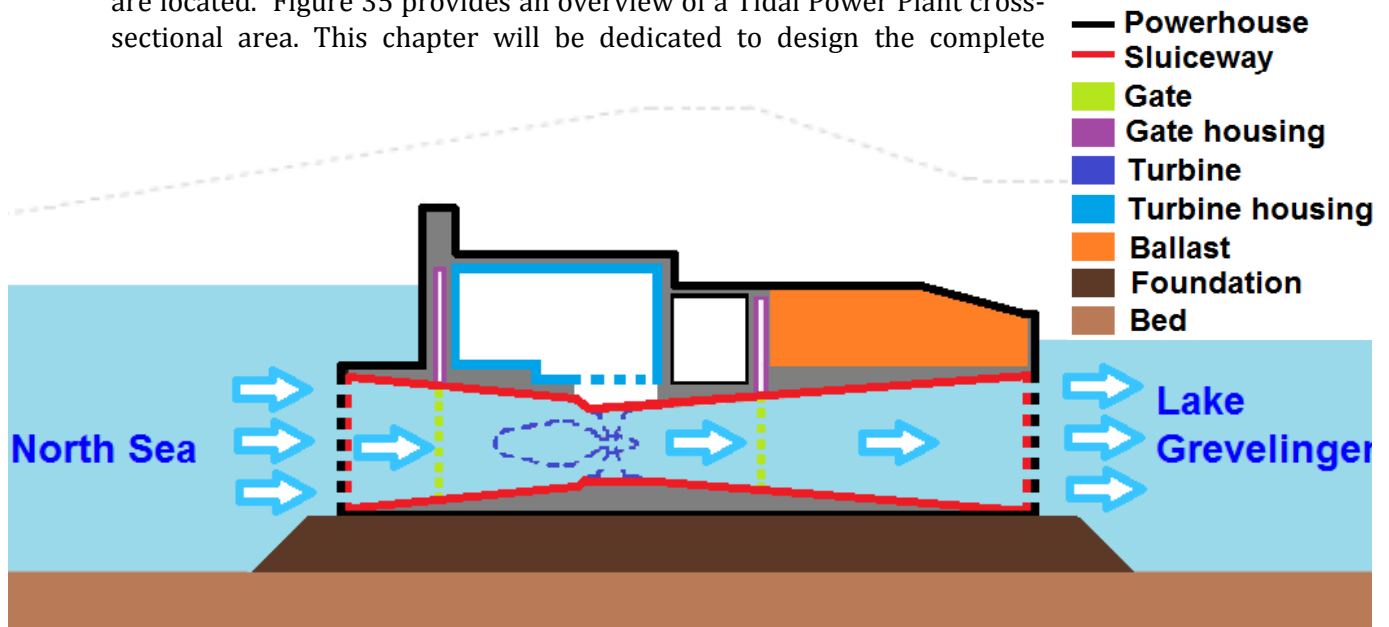
FIGURE 35: SIMPLE SKETCH OF CROSS SECTIONAL AREA TIDAL POWER PLANT AND ITS COMPONENTS IN TRANSVERSE DIRECTION (DIRECTION PERPENDICULAR TO THE BROUWERSDAM)

powerhouse within the cross-sectional area of the Tidal Power Plant including the turbines from the previous chapter.

This chapter will determine the dimensions of the powerhouse. To determine the transverse length (length perpendicular to the Brouwersdam) the required sluiceway length will be computed in paragraph one. This sluiceway length depends on multiple factors:

- Infrastructure width
- Turbine Housing
- Gate housing
- Piping

The second paragraph will be dedicated to the required height of the water retaining structure. Overtopping and wave run-up criteria will be two principal factors determining the required height.

In other words, the powerhouse required at each turbine will be oupled into one structure; the Tidal Power Plant. The required longitudinal length (length parallel to the Brouwersdam) of the complete Tidal Power Plant will therefore be determined in paragraph three.

A summary of the required dimensions and cross-sectional areas of the powerhouse and thus the Tidal Power Plant will be provided in paragraph 4.

With the computed Tidal Power Plant dimensions the stability checks are summarized in paragraph 5. From the stability checks it will come forward whether additional measures are required to ensure the dynamic and static stability of the Tidal Power Plant.

Paragraph 6 will provide a final conclusion regarding the preliminary powerhouse design.

5.1 TRANSVERSE LENGTH

As mentioned, the sluiceway length determines the transverse length of the Powerhouse. The length of the sluiceway will be determined per feature separately. Section 5.1.1 will discuss the required infrastructure cross section, determined using the requirements set MIRT Grevelingen; *The tidal power plant needs to facilitate road traffic on the Brouwersdam, also from the N57 and parallel road, at least with today's traffic quality.*

Section 5.1.2 describes the required space for the turbine housing as a consequence of changing the turbines and for maintenance purposes. Section 5.1.3 will compute the required gate housing area, obtained from a conceptual gate design. Finally, piping will be considered in section 5.1.4, due to piping an increase of the sluiceway length or piping measures might be required.

The sluiceway shape strongly influences the energy losses. In general, energy losses from the sluiceway lead to a reduction in flow velocity, which results in a reduction in energy generation and thus less revenues. Therefore, the design of the sluiceway should avoid any type of energy loss as much as possible. Section 5.1.5 will therefore treat the sluiceway shape modifications.

5.1.1 INFRASTRUCTURE

The maximum speed allowed on this highway is 100 km/h. In Lammens et al. [2016] the traffic intensity as a consequence of the construction of the Brouwerseiland, a small recreational island located west of the Kabbelaarsbank at the middle of the Brouwersdam, was investigated. The maximum expected traffic intensity has been estimated at 1250 equivalent motor vehicles per hour (mvh/h) at maximum during the Tidal Power plant's lifetime. An one-way highway allows a capacity of 1900 (mvh/h) [Rijkswaterstaat, 2015]. This means the current capacity of the N57 is expected to be sufficient and thus a 2x1 way highway will be reconstructed on top of the sluiceway.

In the current situation two parallel roads adjacent to the N57 are present as well, both allowing cyclists to occupy the road. At least one of these parallel roads should be present in the new situation according to requirement set by MIRT Grevelingen. This road has a maximum allowable speed of 60 km/h and available space for cyclists. The safety of these cyclists is discussable, especially when appears that the maximum speed is being exceeded in 85% of the time' [Lammens et al. 2016]. In addition, as a consequence of the assumed increase in recreational activities, an intensity reaching 3000 cyclists per day in busy summer periods has been expected [Lammens et al., 2016]. Therefore, a safe separate bicycle path is preferred.

The parallel road will be constructed for agriculture and local traffic. An obstacle free space between the main road and the N57 of 6.0 meter should be available. In the design no emergency lane is included for now. One could decide to apply small emergency spots with a length of 25 meter within the obstacle free zone. These emergency lanes could function as a stop area as well. The width of these emergency lanes contains 3.0 meters. These emergency lanes shall be located at the right side of the roads' travelling direction. The complete road layout complies with the design criteria set by the Dutch Government [Rijkswaterstaat, 2015].

The final infrastructure top view layout has been illustrated in Figure 37 on the next page. The total obtained infrastructure width is equal to 30.7 meter. For now the sluiceway part at the lake side will be set equal to the road width plus one meter adjacent to the cycling path at the Lake Grevelingen side. Safety measures or other obstacles could be placed within this additional meter, protecting cyclists from descending into the lake. Hence the total infrastructure width contains 31.7 meter.

Due to the water level in Lake Grevelingen, the road must be located at least above +1.50 meter NAP, which is the maximum lake water level according to scenario 3. Due to the water level rise as a consequence of wind waves, which may reach a wave height of 1.17 meter (determined in Appendix B.2), and including a safety margin, the bottom of the road foundation construction shall be located at +2.5 meter NAP. This foundation concerns a 500 mm thick concrete slab on which the road will be constructed The cross-section of the infrastructure or ballast housing has been provided in Figure 36.

From the stability checks it will appear a ballast layer will be required. Between the top of the sluiceway at the lake side and the road, room for additional ballast measures will be available. Therefore the cross-section as illustrated in Figure 36 will be appointed as the ballast housing from now on.

The total infrastructural length contains 31.7 meter, laying at +2.5 meter NAP. The full cross-section has been appointed as the ballast housing.
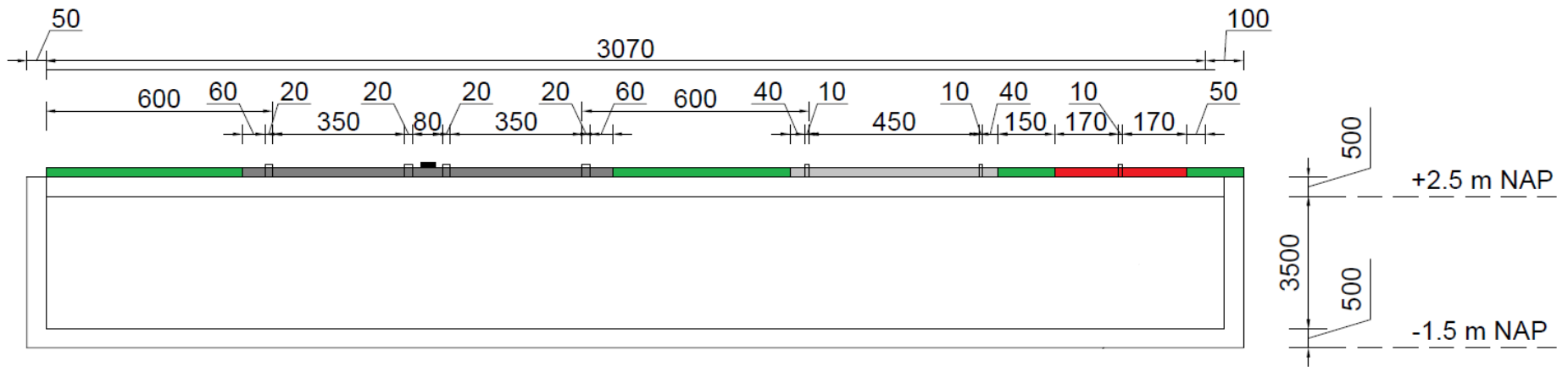
FIGURE 36: TRANSVERSE CROSS-SECTION BALLAST HOUSING (DIMENSIONS IN MM)
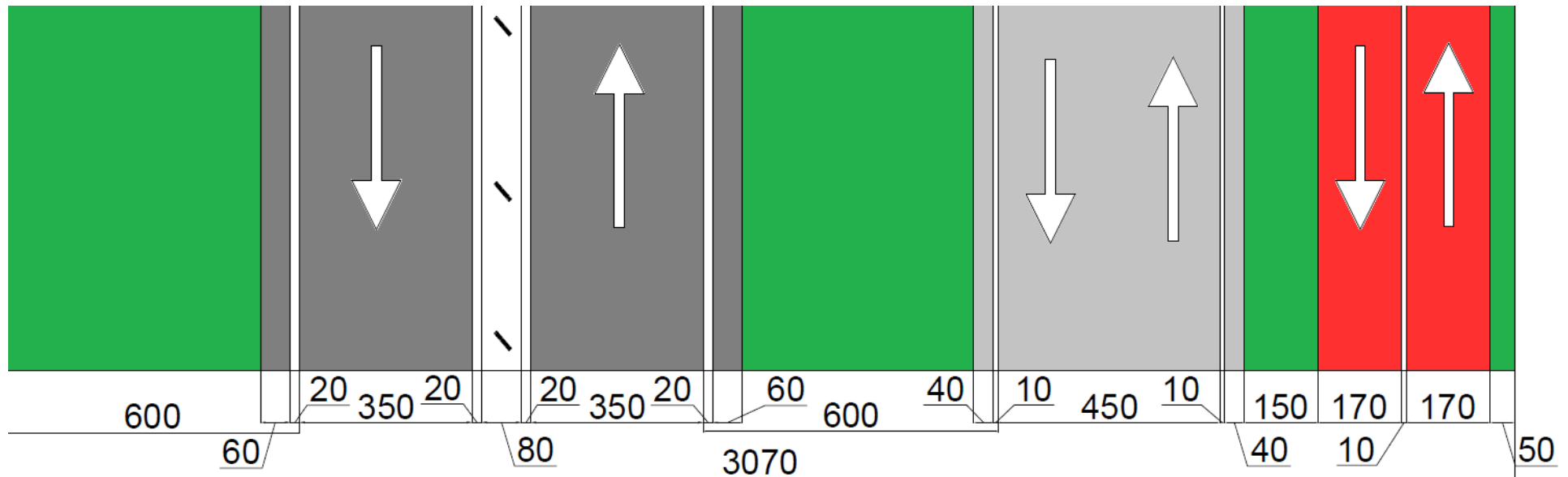
FIGURE 37: TOP VIEW LAYOUT INFRASTRUCTURE (IN CM). BICYCLE PATH LOCATED AT THE LAKE SIDE

Direction seperation obstacle
N57 Highway (80 km/h)
Parallel road (60 km/h)
Roadside
Bicycle path
Road lines

5.1.2 TURBINE HOUSING

According to the recommended alternative for turbine selection, the initial turbines will be removed in 2030. The dimensions of the PFN turbine are governing for the required space during removal.

From drawings in Meijen and Arnold [2015], whom provided a study regarding the optimal sluiceway shape, the length/diameter ratio has been assumed at approximately 1.75. Thus a length of 14.4 meter should be reserved for the maintenance or removal of the governing PFN turbine. Removal of the turbines should not disturb any functions of the Brouwersdam.

The turbine housing could also be classified as the turbine maintenance room. It will be positioned above the turbine position when in commence. The classification 'turbine maintenance room' explains its function; a space available for large turbine maintenance works (i.e. bade removal or large painting jobs). A lifting mechanism will therefore be installed within the turbine housing. To avoid any disturbance to traffic at the N57, the N57 will be located adjacent to the turbine housing.

The lifting mechanism such as a gantry crane will be located in this turbine maintenance room. An additional 0.5 meter at both sides, adjacent to the turbine location within the turbine housing, will be reserved to place the gantry crane.

The lifting mechanism of the gantry crane requires additional space above the turbine when located in the turbine housing. It has been assumed an additional 1.0 meter above turbine's height should be sufficient to ensure the manoeuvrability of the gantry crane. This leads to total height of the turbine maintenance room of **9.24** meter excluding walls and a total width of **15.4** meter excluding walls. Thickness of the walls has been assumed at 0.5 meter, the resistance to external and local forces of these 500 mm thick walls will be checked in chapter 7. A cross-sectional overview of the turbine housing has been illustrated in Figure 38
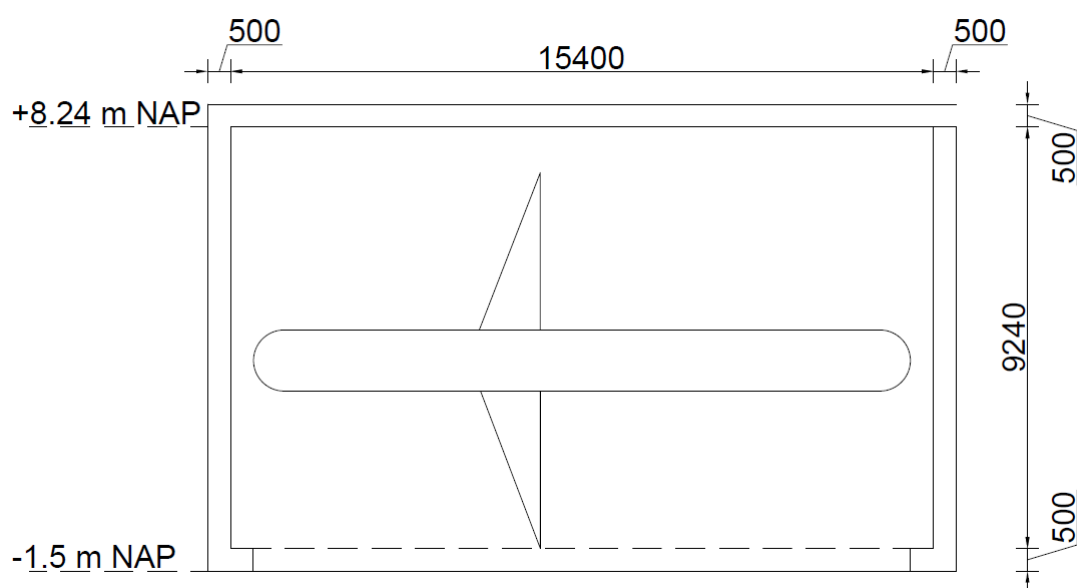
FIGURE 38: TRANSVERSE CROSS-SECTION TURBINE HOUSING WITH PFN TURBINE

5.1.3 GATE HOUSING

This paragraph will determine the gate design and the required gate housing. Two main features of the gate are:

- Protecting the hinterland against flooding
- Closure the moment the restricted water levels at Lake Grevelingen is reached

In this subparagraph first the optimal gate types constructed in each sluiceway will be obtained. Second, prior to computing the gate dimensions, the governing load conditions will be determined. With the governing load conditions the properties of the gate will be determined using Erbisti [2015]. Third, as a compact gate and light is preferred in order to reduce the sluiceway length and the required gate lift mechanism respectively, a gate optimization will be applied. From this gate optimization the final gate dimensions follow and the required gate mechanism properties will be computed in section four. Finally a estimation of the required space required for the gate housing will be discussed in the fifth section.

5.1.3.1 OPTIMAL GATE TYPE

In the lectures of the course Hydraulic Structures 2, a number of gates have been treated. The requirements to the gate form the basis of the optimal gate type. The major factor within the requirements is reducing the possibility of reducing energy production. Therefore two requirements are set:

- Streamlining
  Streamlining both the inlet and outlet sluice of the TPP is essential in order to produce as much energy as possible. Any obstacle could lead to turbulence in the inlet sluice, leading to a reduction in energy generation. The gate should therefore be able to be located in a concrete wall in its rest position.
- Available space
  In order to place as much turbines as possible, maximizing the energy production, the gate should be positioned in the sluiceway's walls or other concrete components while in rest. To this extent, water flows freely into the sluiceway. Gates located in the wall of the inlet sluice would mean the wall needs some additional thickness to bear the gate.

From the course 'Hydraulic Structures 2' two gate types comply with the above mentioned requirements:

1. **Vertical translating** (Figure 39)
   The vertical translating gate moves from its rest position above the inlet sluice downwards towards its water retaining position. Thus additional space is required above the sluice gate, which could be beneficial as the Brouwersdam needs a certain height to prevent overtopping.
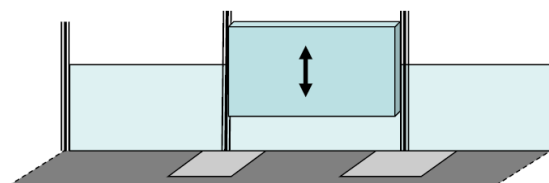
Vertical lifting door
FIGURE 39: VERTICAL TRANSLATING GATE

2. **Radial gates** (Figure 40)

Squared radial gates, named Tainter gates, rotate around a horizontal axis located in the top of the inlet sluice. A disadvantage is the horizontal axis requires a significant amount of space to rotate properly. The required space is not necessarily in vertical direction, but mostly in width direction, mostly due to the required systems to enable rotation.
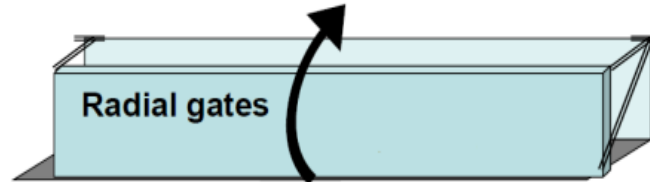
FIGURE 40: RADIAL GATE

The Tainter gate requires a significant amount space in longitudinal direction ensuring the ability to rotate freely. Establishing a streamlined shape of the sluiceway becomes very complex. Since the Tidal Power Plant requires a certain height, in vertical direction a sufficient margin will be available to bear the gate in rest. With the gate located in its rest position above the sluiceway, the sluiceway remains streamlined. The top of the sluiceway should in that case be provided with closing strips. The vertical translating gate will therefore be considered as the optimal gate type at the Tidal Power Plant.

5.1.3.2 GATE DESIGN

Since the maximum water level and thus the maximum water pressures will be present at the North Sea side of the dam, the gate will be constructed at the North Sea side of the Tidal Power Plant.

The gate will close for two reasons:

- The restricted water level at Lake Grevelingen has been reached
- Extreme weather conditions at the North Sea and thus protecting the hinterland from flooding.

During the Tidal Power Plant's lifespan, the gate will thus be exposed to various load combinations. Three of those load combinations will be considered here. From these three load combinations a governing situation will be obtained and applied to the gate dimensioning approach.

LOAD SITUATIONS

A gate housing will be constructed above the gate in when located in closed positon. In rest the gate will be positioned within this gate housing. The gate in rest position will thus not be subject to wave or wind loads. Therefore, three load situations for a closed gate or during closure have been described in Appendix C.1. Summarized, these load situations read:

1. **Gate closure with extreme weather conditions**

In this load situation the gate will considered as closed and will thus be subject to incoming waves. Hence the wave impact will be added to the hydraulic pressures on the gate.

2. **During maintenance in sluiceway**

   Assuming the Lake side will be closed off from water during maintenance by applying temporary closure methods, the gate will solely be exposed to hydrostatic pressures from the North Sea. In Appendix C.1 it has appeared this situation will lead to gate loads almost twice as high compared with situation 1.

3. **During gate closure**

   During closure underflow of sea water will introduce a force on the gate. Due to the pressure difference between the upstream and the downstream side of the gate, the flow velocity under flowing the gate will increase. Consequently, the gate bottom section will be subject to a vertical thrust forces. However, Knapp [1960] stated the following rule: 'all surfaces of a gate located in regions of high water velocity and which form a sharp slope with the direction of the corresponding motion present the possibility of formation of hydrodynamic forces'. The skin plate of the gate moves in the same direction as the flow direction. Therefore, according to Knapp's rule, there is no formation of low-pressure areas, and consequently, vertical thrust forces are not created [Erbisti, 2015].

Instead of designing the gate according to the governing load situation described in situation 2, it has been decided design the gate according to load situation 1. The presence of forces as described in situation 2 will occur once or twice in the gate's lifespan. These forces will induce an increased gate design strength and thus a more expensive gate. It has thus been decided to allow sluiceway maintenance works in periods where the hydraulic pressures do not exceed the governing hydraulic pressures from load situation 1; illustrated in Figure 41.

Combining the wave impact, calculated using Sainflou, and the hydrostatic pressures, lead to the following design values at the positions shown in Figure 116:

$$q_{ed1} = 19.61 \ kN/m^2$$

$$q_{ed2} = 98.42 \ kN/m^2$$

$$q_{ed3} = 93.41 \ kN/m^2$$
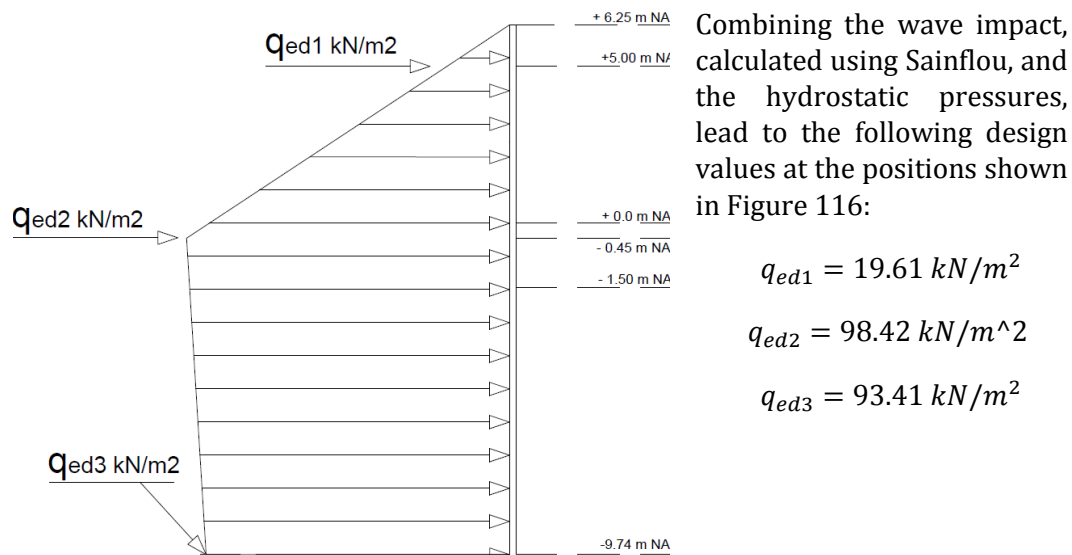
FIGURE 41: RESULTING FORCE LOAD SITUATION 1

Since the gate will be located between -1.5 m NAP and -9.74 m NAP, the governing load within this surface contains:

$$q_{ed,gate,1} = 97.76 \ kN/m^2$$

Load situation 1, as illustrated in Figure 41, will be considered as governing in the gate design approach.

The gate will be subject to large hydraulic pressures, consequently large tensile stresses while emerge. Resistance to large tensile stresses will be optimally achieved by applying a steel gate. Considering the high material costs of steel, reducing the required material has become a preference. Applying a high strength steel class contributes to a material reduction. Therefore the steel class S355 has been chosen. In addition, providing high strength steel member with minimal material, the gate will be designed using hollow tubular beams.

As a starting point of the gate design approach the method described by Erbisti [2015] will be applied. Erbisti [2015] prescribes the use of trusses to reduce the overall gate weight and the total amount of steel. The truss design starts with determining the transverse length:

$$d_{truss} = \frac{1}{10} W_{gate} = \frac{1}{10} * 8.24 = 0.824 \, m$$

Where:

W_{gate} *represents the gate length in longitudinal direction*

The maximum moment present in the gate has been calculated by setting the design load equal over the whole gate height, resulting in a maximum design moment:

$$M_{ed} = \frac{1}{8} q_{ed} l^2 = 6836.83 \, kNm$$

At first it is assumed the steel plate of the gate is vertically supported by two beams, the optimization will show the optimal amount of vertical beams later.

The earlier mentioned steel class S355 has a design yield stress of $\sigma = 355 \, N/mm^2$. This allowable stress is reduced by a safety factor from Table 9. This results in the allowable yield stress:

$$\sigma_{Rd} = 355 * 0.76 = 269.8 \, N/mm^2$$

Type of Stress	Load Case		
	Normal	Occasional	Exceptional
Tension and bending stress	0.68	0.76	0.89
Bending stress if a stability proof is required	0.59	0.68	0.79
Shear	0.39	0.44	0.51
Combined stress	0.76	0.82	0.92
Combined stress in the skin plate	0.87	0.87	0.92

TABLE 9: COEFFICIENTS FOR ALLOWABLE STRESSES, STRUCTURAL ELEMENTS [ERBISTI 2004]

The resulting design force in the truss can be determined using:

$$F_{ed} = \frac{M_d}{z} = \frac{6836.83}{0.9 * 0.824} = 9219.02 \, kN$$

This resulting design force represents a first estimation, as soon as the design of the gate is further optimized, this design force may differ due to changes in the trusses transverse length.

Primarily to computations, as a first assumption two trusses are applied. Calculations will provide whether the number of trusses should be optimized. Next to that, as a first estimation the diameter of the hollow beams contains 200mm with a wall thickness of 15 mm. To provide resistance against buckling the diameter over wall thickness ratio should not exceed 59.6. This value is based on a situation for which in the cross-section the maximum stress is determined by local buckling and the stress in outer fibre is lower than the yield strength [Wardenier, 2010]. Exceeding this value will lead to buckling of the beam.

The gate will cover an area with a longitudinal and vertical length of 8.24 meter (height and width respectively). Consequently, the vertical and longitudinal beam lengths equal these lengths.

To provide a check whether these dimensions are sufficient, the moment of inertia is computed, providing the following equations:

$$I_{beam} = \frac{\pi}{64} * \left(D_{outer}^4 - D_{inner}^4\right) = \frac{\pi}{64} * (200^4 - 170^4) = 3.75 * 10^7 mm^4$$

$$A_{beam} = \frac{\pi}{4}(D_{outer}^2 - D_{inner}^2) = \frac{\pi}{4}(200^2 - 170^2) = 8.72 * 10^4 \ mm^2$$

The centre of gravity from the beam does not coincide with the centre of gravity of the truss tubes and therefore, to define the moment of inertia, the Steiner rule is applied:

$$I_{Steiner} = A_{beam} * (0.5 * d_{truss}^*)^2 = 8.72 * 10^4 * (0.5 * (200 - 0.824 * 1000)^2$$

$$= 8.49 * 10^8 \ mm^4$$

$$d_{truss}^* = d_{truss} - D_{beam} = 824 - 200 = 624 \ mm$$

$$I_{total} = No.beams * I_{beam} + No.beams * I_{Steiner} = 2 * 3.75 * 10^7 + 2 * 8.49 * 10^8$$

$$= 1.77 * 10^9 \ mm^4$$

$$\sigma_{steel} = \frac{M_{ed} * 0.5 * d_{truss}^*}{I_{total}} = \frac{6836.83 * 10^6 * 0.5 * 624}{1.77 * 10^9} = 1196.14 \ N/mm^2$$

The steel stress exceeds the steel resistance stresses ($\sigma_{Rd} = 269.8 \ N/mm^2$). Therefore, a beam with mentioned properties will be insufficiently strong, a design optimization will be applied to reach a steel stress below, but close to the steel resistant stress.

Detailing the trusses will be performed by computing the dimensions of the main components of the trusses. These are defined as:

a. Skin plate
b. Transverse girder
c. Vertical girder
d. Diagonal girder

Both the approach of the skin plate and horizontal girder are elaborated below. The computation of the transverse, vertical and diagonal girders will performed in a similar. An overview of the truss system and its main components has been illustrated in Figure 42.

SKIN PLATE

The required number of trusses allows computation of the gate steel skin plate, the plate in direct contact with the North Sea water. The skin plate is reinforced by the trusses located at the lake side of the plate. These calculations are done according to the NBR-8883 standard: the plate bending stresses from water pressure are calculated with the theory of plates based on the theory of elasticity, using [Beristi, 2014]:

$$\sigma_{steel} = \frac{k}{100} p \frac{a^2}{t^2}$$

Where:

k *represents the non − dimensional*

       factor obtainable from Table 10 *and is*

       defined as a function of the ratio

       b/a (support length of the modulus formed by the beams and/or

       stiffeners) and the support conditions of the module.

p *represents the water pressure relative to the module centre*

a *represents the minor support length*

t *represents the plate thickness*
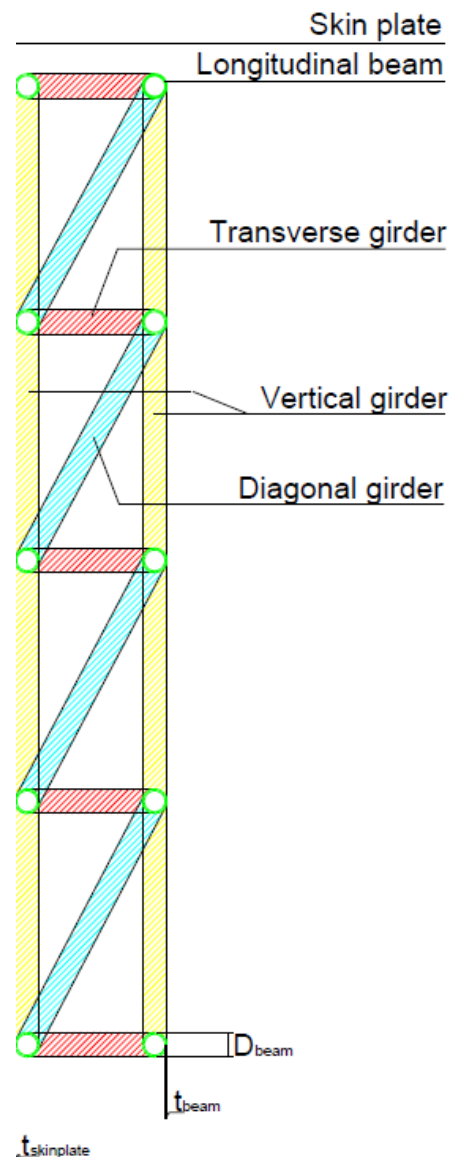
FIGURE 42: OVERVIEW GATE TRUSSES SYSTEM COMPONENTS

b/a	Unfixed mounting of the 4 edges (a)		Rigid fixing of the 4 edges (b)				Rigid fixing of 3 edges and unfixed mount of the fourth edge (c)				(d)			
	$\pm\sigma_{1x}$	$\pm\sigma_{1y}$	$\pm\sigma_{1x}$	$\pm\sigma_{1y}$	$\pm\sigma_{4y}$	$\pm\sigma_{3x}$	$\pm\sigma_{1x}$	$\pm\sigma_{1y}$	$\pm\sigma_{4y}$	$\pm\sigma_{3x}$	$\pm\sigma_{1x}$	$\pm\sigma_{1y}$	$\pm\sigma_{2y}$	$\pm\sigma_{3x}$
∞	75.0	22.5	25.0	7.5	34.2	50.0	37.5	11.3	47.2	75.0	25.0	7.5	34.2	50.0
3.00	71.3	24.4	25.0	7.5	34.3	50.0	37.4	12.0	47.1	74.0	25.0	7.6	34.2	50.0
2.50	67.7	25.8	25.0	8.0	34.3	50.0	36.6	13.3	47.0	73.2	25.0	8.0	34.2	50.0
2.00	61.0	27.8	24.7	9.5	34.3	49.9	33.8	15.5	47.0	68.3	25.0	9.0	34.2	50.0
1.75	55.8	28.9	23.9	10.8	34.3	48.4	30.8	16.5	46.5	63.2	24.6	10.1	34.1	48.9
1.50	48.7	29.9	22.1	12.2	34.3	45.5	27.1	18.1	45.5	56.5	23.2	11.4	34.1	47.3
1.25	39.6	30.1	18.8	13.5	33.9	40.3	21.4	18.4	42.5	47.2	20.8	12.9	34.1	44.8
1.00	28.7	28.7	13.7	13.7	30.9	30.9	14.4	16.6	36.0	32.8	16.6	14.2	32.8	36.0
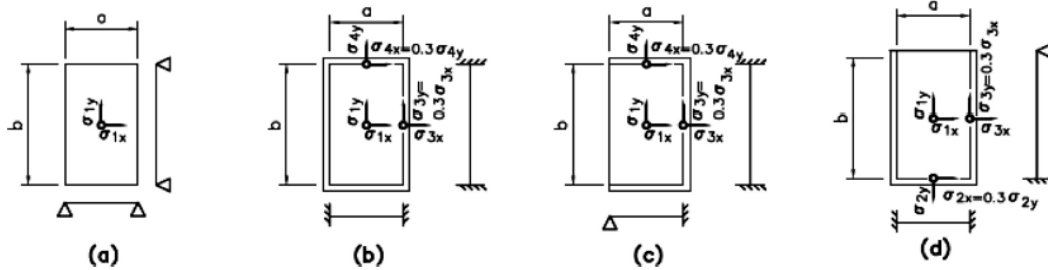
TABLE 10: K-COEFFICIENT

Both the vertical and horizontal spacing between the vertical and horizontal beams has neen assumed to be equal to 8.24 meter;

$$\frac{b}{a} = \frac{8.24}{8.24} = 1$$

The plate is considered as a rigidly fixed plate at 4 edges. This results in values for k:

$$k_{1x} = 13.7$$

$$k_{3x} = 13.7$$

$$k_{1y} = 30.9$$

$$k_{4y} = 30.9$$

With these parameters and the water pressure obtained from Figure 41, where the governing load is located at -1.5 m NAP (top of the gate), the value for the steel stress will be determined. Similar to determining the stresses the allowable stress has to be compensated with a safety factor (obtained from Table 9). The load may be considered as a normal load and a combination of stresses within the skin plate, resulting in:

$$\sigma_{steel} = 0.87 * 355 = 308.85 \; N/mm^2$$

Substituting this value into the plate bending stress equation, will result in the required plate thickness. The design steel stress should not exceed the resistance steel stress. For four governing locations within the plate, the plate thickness has been computed with the provided 'k' values:

$t_{1x} = 54.26 \; mm$ $t_{3x} = 54.26 \; mm$ $t_{1y} = 81.49 \; mm$ $t_{4y} = 81.49 \; mm$

The governing required plate thickness equals t_{3x} and $t_{4y} = 81.49\ mm$. Hence, a plate thickness of 82 mm will applied providing the considered truss design from the previous sections. The plate thickness shall be optimized with the truss optimization as well.

GIRDERS

The girders are all designed in a similar approach. The transverse girder, the girder located between the longitudinal beam directly behind the plate and the longitudinal beam at 824 mm parallel to the skin plate, will be elaborated here. The length of the transverse girder may be considered as the length in transverse direction and the distance between the two parallel longitudinal beams.

The governing force to determine the dimensions of the transverse girder equals half the load acting on the longitudinal beam: $F_{ed} = \frac{1}{2} q_{ed.depth} l$. Where $q_{ed,depth}$ equals the governing load times the spacing between the parallel located longitudinal beams. The final location of the longitudinal beams will be determined later. The governing diameter and wall thickness of the transverse girder has been found using the buckling criteria:

$$\frac{f_{b,rd}}{\sigma_d} \leq 1$$

$$f_{b,rd} = \frac{F_{ed}}{A}$$

$$A_{req} = F_{ed}/\sigma_d = 6.15 * 10^{-3}\ m^2$$

The corresponding dimensions of these girders will be determined in the optimization.

To prevent buckling the limit of the diameter over thickness ratio of a hollow tube is 59.6.

5.1.3.3 GATE OPTIMIZATION

In Table 11 below the final optimization of the steel truss has been executed. For material costs purposes and machinery strength requirements, it is desired to use a minimum amount of steel in the gate design. The optimization has been performed by applying variations in the number of trusses. For the steel beam properties, reference is made to the provided data by TATA Steel for S355 structural hollow sections [TATA Steel, 2016].

Optimization					
Transverse length trusses	d_x	824.00	950.00	1050.00	[mm]
Design load	q_{ed}	805.55	805.55	805.55	[kN/m]
Design moment	M_{ed}	6836.83	6836.83	6836.83	[kNm]
Length longitudinal beams	L_{beam}	8240.00	8240.00	8240.00	[mm]
Longitudinal beams	$\sigma_d = 269.8 \, N/mm^2$				
Buckling limit	$D_{l,beam}/t_{l,beam} \leq 59.6$				
No. of longitudinal beams		6	8	10	[−]
Design resulting force	$F_{l,ed}$	1649.23	1099.49	824.62	[kN]
Beam thickness	$t_{l,beam}$	24.00	25.00	24	[mm]
Beam diameter	$D_{l,beam}$	406.40	244.50	168.30	[mm]
Buckling limit	$D_{l,beam}/t_{l,beam}$	33.87	19.56	14.03	[mm/mm]
Moment of inertia	$I_{l,beam}$	2.89E+08	6.15E+07	2.81E+07	[mm⁴]
Cross-sectional area	$A_{l,beam}$	1.49E+04	9.11E+03	5.89E+03	[mm²]
Steiner rule	$I_{l,Steiner}$	6.48E+08	1.13E+09	1.15E+09	[mm⁴]
Total moment of inertia	$I_{l,tot}$	5.63E+09	9.56E+09	1.16E+10	[mm⁴]
Stress in beam	$\sigma_{steel.l.beam}$	252.20	250.69	259.10	[N/mm²]
Volume beam	$V_{l.beam}$	0.74	0.60	0.49	[m³]
Transverse Girder					
Req. cross-sectional area	A_{req}	6.11E+03	4.10E+03	3.08E+03	[mm²]
Thickness	$t_{t,girder}$	20.00	16.00	12.60	[mm]
Diameter	$D_{t,girder}$	219.10	193.70	168.30	[mm]
Buckling limit	$D_{t,beam}/t_{t,beam}$	21.19	24.21	26.71	[mm/mm]
Cross-sectional area	$A_{t,girder}$	6.57E+03	4.67E+03	3.21E+03	[mm²]
Volume transverse girder	$V_{t,girder}$	0.017	0.0263	0.0275	[m³]
Volume vertical girder	$V_{v,girder}$	0.20	0.14	0.10	[m³]
Volume diagonal girder	$V_{d,girder}$	0.07	0.06	0.05	[m³]
Skin plate	$\sigma_d = 308.85 \, N/mm^2$				
No. of longitudinal beams		3.00	4.00	5.00	[−]
Load	P_{ed}:	97.76	97.76	97.76	[kN/m²]
Spacing ratio	b/a	1.00	3.00	4.00	[−]
Horizontal spacing	b	8.24	8.24	8.24	[m]
Vertical spacing	a	4.12	2.75	2.06	[m]
	k for:				
	σ_{1x}	24.70	25.00	25.00	[−]
	σ_{1y}	9.50	7.50	7.50	[−]
	σ_{4y}	34.30	34.30	34.20	[−]
	σ_{3x}	49.90	50.00	50.00	[−]
	$t_{\sigma_{1x}}$	36.43	24.43	18.33	[mm]
	$t_{\sigma_{1y}}$	22.59	13.38	10.04	[mm]
	$t_{\sigma_{4y}}$	42.93	28.62	21.43	[mm]
	$t_{\sigma_{3x}}$	51.78	34.55	25.92	[mm]
	t_{gov}	52.00	35.00	26.00	[mm]
Volume skin plate	V_{plate}	3.53	2.38	1.77	[mm³]
Total gate volume	V_{total}	4.54	3.20	2.42	[m³]
Total weight		35658.25	25137.82	19022.42	[kg]

TABLE 11: GATE DESIGN OPTIMIZATION

An optimal gate design has been computed when applying 10 longitudinal beams (5 direct behind the skin plate and five 1050 mm parallel to the skin plate) with a diameter of 168.3 mm and wall thickness of 24 mm. Resulting in a total gate weight of 19022.42 kg.

BEAM LOCATION

Optimally loading the trusses will be accomplished by equally loading the longitudinal beams. Hence, the location of the beam will be found in order to provide each beam with such contact area the resulting force on the beam for each beam is equal. Figure 43 provides a clear representation of the resulting force location when 5 longitudinal beams are applied constructed directly behind the skin plate. The arrow point of engagement indicates the beam contact point. The actual values for H_1 to H_5 are shown in the final design; Figure 44 and Figure 45.
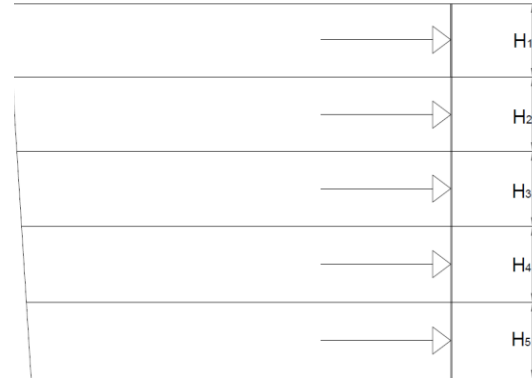
FIGURE 43: LOCATION RESULTING FORCE FOR GATE WITH 5 LONGITUDINAL BEAMS
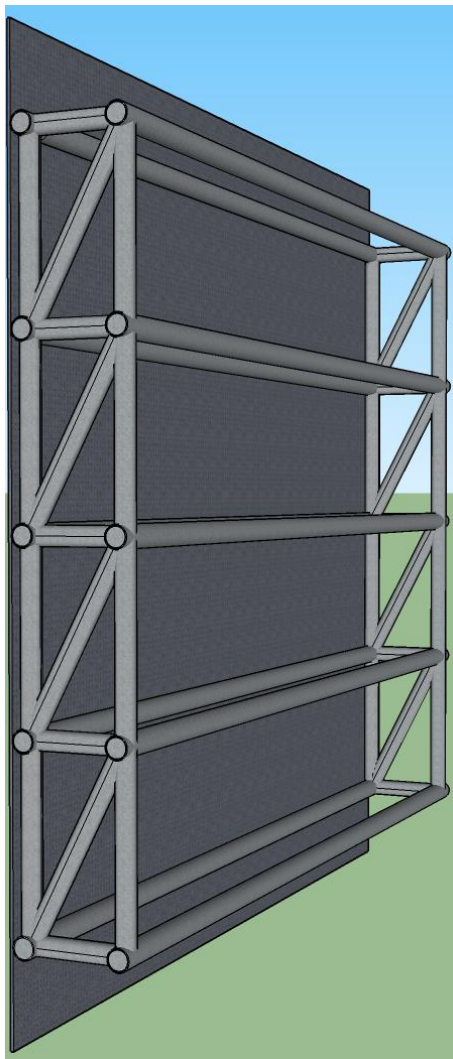
FIGURE 44: 3D REPRESEN-TATION FINAL GATE DESIGN
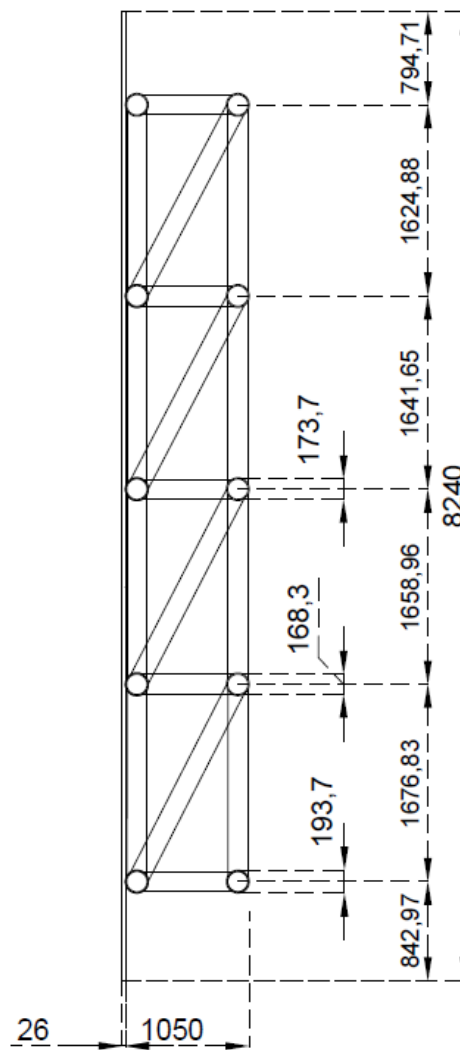
FIGURE 45: 2D REPRESENTATION CROSS SECTION FINAL GATE DESIGN

5.1.3.4 GATE LIFT MECHANISM

The dead weight requires a lifting mechanism consisting of two cylinders. The cylinders are able to extend, retract and deliver the required force to provide gate movement by means of oil pressure. Several parameters need to be taken into account to determine the cylinder design. The design of the cylinder will not be treated in this thesis, therefore solely the results of the required gate operational forces are summarized in Table 12. For elaboration of the gate lift mechanism forces, reference is made to Appendix C.1.3.

Load Type		Force [kN]
Dead weight	G	204.25
Buoyancy	E	101.56
Wheel Load	F_r	10.96
Seal friction	F_v	338.67
Hydrodynamic force	F_h	0

TABLE 12: OVERVIEW LIFT FORCES

To ensure gate water tightness, seals shall be applied. The seal friction becomes rather high due to the J-seal which will be applied at each gate edge.

The governing lifting force for the cylinders reads $452.3\ kN$. *Due to the buoyancy and the friction forces the required force to 'push' the gate into the water is* $246.94\ kN$.

5.1.3.5 GATE HOUSING

Due to the higher water levels and thus larger hydraulic forces at the North Sea side, the gate and its gate housing will be constructed at the North Sea side of the Tidal Power Plant. The gate housing will be constructed above the gate located in closed position, allowing the gate to move vertically between its rest position and its closed position. It will therefore also function as the primary water retaining wall of the Tidal Power Plant.

Gate maintenance work requires sufficient space adjacent to the gate within the gate housing. Maintenance work includes painting, strength checks and replacing or strengthening components. A free space of 1.5 meter adjacent to the gate has been assumed to be sufficient to allow equipment to enter the available space. A free space of 0.5 meter above the gate should be sufficient to construct the gate lift mechanism or other functional components. Figure 46 provides the preliminary gate housing design. As a first estimation a wall thickness of 500 mm will be applied. Whether this wall thickness will be sufficient to bear external and local forces will be checked in chapter 7.
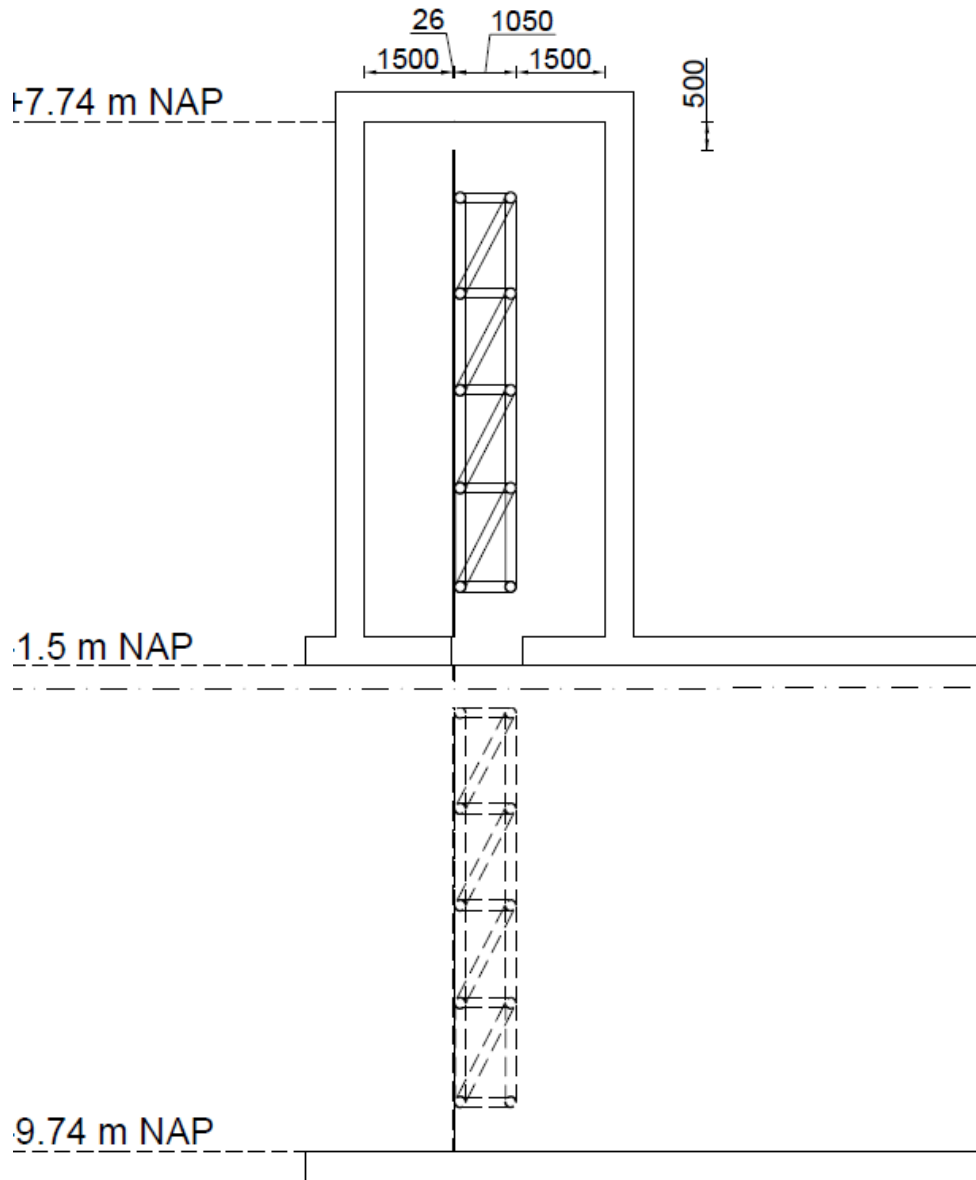
FIGURE 46: PRELIMINARY DESIGN GATE HOUSING AND GATE IN CLOSED POSITION

5.1.4 PIPING

The definition of piping reads; flow of water through a pipe-like channel that has been created by internal erosion. As a consequence of piping the stability of structure fails due to eroding sand particles. failure in the structure's stability. Two calculation methods determine the occurrence of piping; Bligh and Lane, shown in Table 13.

Piping method:	Bligh		Lane	
Safe seepage distance:	$L \geq \gamma \cdot C_B \cdot \Delta H$		$L \geq \gamma \cdot C_L \cdot \Delta H$	
True seepage distance:	$L = \sum L_{vert} + \sum L_{hor}$		$L = \sum L_{vert} + \sum \frac{1}{3} L_{hor}$	
	C_B	i_{max}	C_L	i_{max}
Soil type:				
Very fine sand / silt /sludge	18	5.6 %	8.5	11.8 %
Fine sand	15	6.7 %	7.0	14.3 %
Middle fine sand	-	-	6.0	16.7 %
Coarse sand	12	8.3 %	5.0	20.0 %
(fine) gravel (+sand)	5-9	11.1 – 20.0 %	4.0	25.0 %

TABLE 13: SAFE SEEPAGE DISTANCE FOR PIPING

Due to the potential rise of vertical piping lines, in the Netherlands Lane's method applies for piping underneath water retaining structures. The applied piping safety factor for primary flood defence systems in the Netherlands equals: $\gamma = 2.0$ [NEN 9997-1]

The theoretical maximum head difference in the three described scenarios reaches 2.95 meter. The literature study provides the governing soil types at the Brouwersdam; fine to coarse sand appears to be the governing soil type over the full Tidal Power Plant area.

The safe seepage length has been computed in Table 14

Method of Lane				Method of Bligh		
Soil type	C_L	$\gamma\ [-]$	**L [m]**	C_B	$\gamma\ [-]$	**L [m]**
Fine sand	7.0	2.0	41.3	15	1.0	44.25
Middle fine sand	6.0	2.0	35.4	-	-	-
Coarse sand	5.0	2.0	29.5	12	1.0	35.40

TABLE 14: DETERMINING SAFE SEEPAGE LENGTH

From Table 14 it may be concluded a safe seepage length will be assured for a structure having a length in transverse direction (from North Sea towards Lake Grevelingen) of at least 41.3 meter (Lane) or 44.25 meter (Bligh).

5.1.5 SHAPE SLUICEWAY

Energy losses resulting from head losses as a consequence of the sluiceway shape are strongly unwanted since it induces a reduction in energy production revenues. The sluiceway shape will therefore be treated in this sub-paragraph.

Pentair Fairbanks Nijhuis has provided a report regarding the shape and dimensions of the sluiceway [Meijen and Arnold, 2015]. The design by Meijen and Arnold [2015] has been used as a reference regarding the design considerations for the PFN turbine. Two types of sluiceway shapes are discussed in this report: ducted shape and a venturi shaped. The venturi shaped consists of a converging inlet part and a diverging outlet part, whereas the ducted shaped sluiceway consists of complete straight sluiceway. At

the centre of the turbine a small notch has been constructed, this ensures some free-space between the propeller tip and the wall of the tube.

A venturi shaped sluiceway results in a larger inlet cross-sectional area and thus increased flow velocities at the turbine. Applying a venturi shaped sluiceway confined by the restricted water levels and the currently present bed level, the available turbine diameter decreases significantly. Dredging the current bed level would make it possible to increase the turbine diameter, but increases the construction costs significantly. It has therefore been decided to apply a straight ducted sluiceway.

Water entering the sluiceway, flowing towards the turbine from the reservoir (sea or lake), results in losses arising as soon the flow enters the sudden contraction point. The flow contracts from the reservoir into the tube. Eddies origin close to the entry point and cause loss of energy. Modifying the inlet shape from a straight edges to rounding the corners reduces the inlet losses. Stuwo Modeling Studio [2005] produced a formula for the entry loss coefficient, see Figure 47.

$$\varepsilon_e = \left(\frac{2d}{3d + 25r}\right)^2$$

$\xi i = 0,6 - 1,3$ $\xi i = 0,3 - 0,5$ $\xi i = 0,25$ $\xi i = 0,05 - 0,1$ $\xi i = \left(\frac{2d}{3d + 25r}\right)^2$
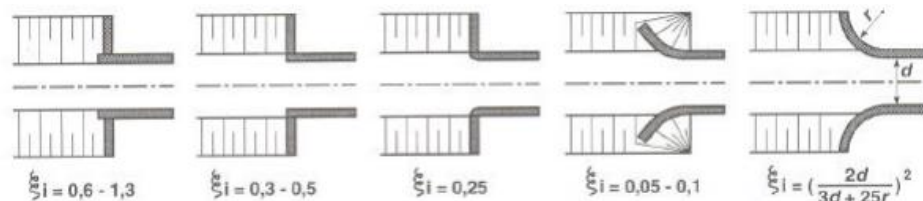
FIGURE 47: EQUATIONS FOR ENTRY LOSSES DEPENDING ON THE SHAPE [STUWO MODELLING STUDIO,2005]

The turbine diameter equals the inlet diameter; 8.24 meter. The value of r for which ε_e becomes minimal will be obtained from Figure 48.
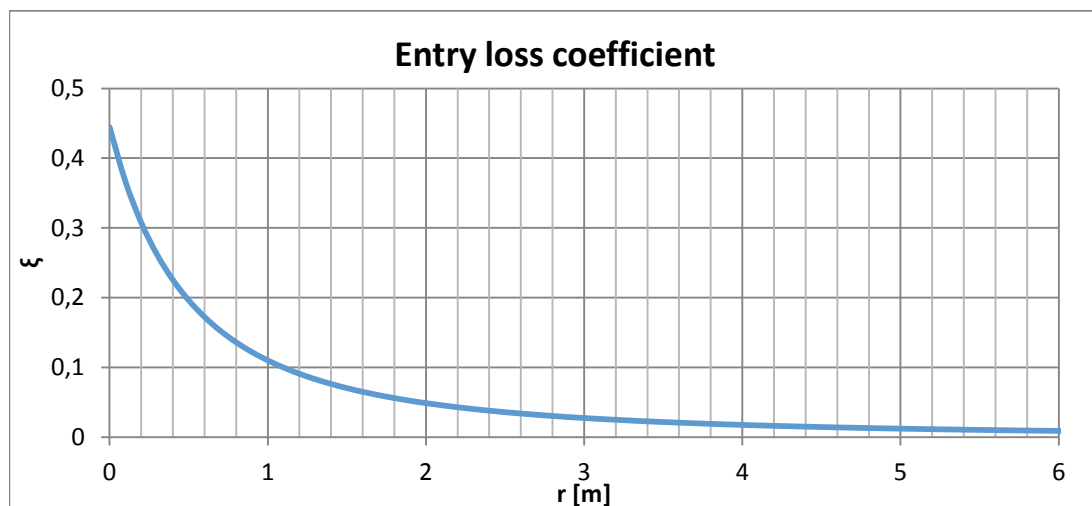
FIGURE 48: ENTRY LOSS COEFFICIENT FOR D=8.24M[EXCELL].

Due to the structural restrictions; wall thickness of 0.5 meter. The maximum applicable radius contains: $r = 1\ m$. The corresponding entry loss coefficient results becomes: 0.11 meter.

5.2 HEIGHT

In computing overtopping two approaches are possible, the gentle slope approach and the steep slope approach. A gentle slope would induce an unintentional increase in the overall transverse length of the Tidal Power Plant. Therefore, the steep slope approach will be used to determine the overtopping.

With the A57 constructed at the lake side of the Tidal Power Plant, significant overtopping of the Tidal Power Plant would lead to shutting off the highway. Therefore, minimal overtopping values are allowed. According to the overtopping manual [2016] the overtopping limits in Table 15 should not be exceeded.

Cars on seawall/dike crest	q (l/s per m)	Max volume V_{max}
$H_{m0} = 3m$	<5	2000
$H_{m0} = 2m$	10-20	2000

TABLE 15: OVERTOPPING LIMITS

However, the requirements from the MIRT Grevelingen in Appendix A, mention: *Maximum overtopping flow rate during MHW must be less than 0.1 m³/s/m.*

An overtopping rate of 0.1 m³/s/m while cars are parked or driving with 60 km/h over the Tidal Power Plant seems rather high and dangerous. Therefore, this requirement has been adapted to a maximum flow rate of 0.01 m³/s/m at the design water level of +5.0 meter NAP. This will prevent closure of the N57 and establishes a road connection between the islands Goerree-Overflakkee and Schouwen-Duiveland at any time.

The Tidal Power Plant will be considered as a vertical wall during gate closure. The incoming waves from the North Sea are considered as plunging waves. According to the overtopping manual [2016] the equation for vertical walls without influence of a foreshore with steep slopes ($\cot(\alpha) \leq 2$), reads:

$$\frac{q}{\sqrt{g * H_{m0}^3}} = 0.054 * \exp\left(-\left(2.12\frac{R_c}{H_{mo}}\right)^{1.3}\right) for\ non-breaking\ waves$$

Where:

$\frac{q}{\sqrt{g*H_{m0}^3}}$ *represents the dimensionless overtopping discharge*

$\frac{R_c}{H_{mo}}$ *represents the relative crest freeboard*

q *represents the maximum overtopping discharge* $= 0.01\ m^3/s/m$

R_c *represents the crest height*

H_{mo} *represents an estimate of significant wave height from spectral analysis*

$= 4\sqrt{m_0} \approx H_s = 2.6\ meter$

For a vertical wall (90 degrees), hence the slope is 90 degrees a crest height R_c of 3.74 meter is required. The wave run-up will not exist for a vertical wall and is therefore not treated any further.

With a design water level of +5.0 meter NAP, and a significant wave height of 2.6 meter the final height of the Tidal power plant becomes: +10.04 meter NAP.

Since this equation is valid for non-influencing foreshores, the influence of oblique waves and a small berm in front of the structure have not been taken into account.

The conditions are considered as non-compulsive, which complies with the in the Overtopping Manuel [2016] described equations, resulting in a minimum required freeboard of 3.67 meter. Hence, the freeboard from the equation of a non-influencing foreshore could be reduced slightly. However, it is chosen to continue with the larger freeboard. The height of the Tidal Power Plant could therefore be considered as slightly over-dimensioned.

The height of the gate housing, which is in direct contact with the North Sea, will be increased to +10.04 meter NAP.

5.3 LONGITUDINAL LENGTH

The longitudinal length of the Tidal Power Plant is simply determined by multiplying the required longitudinal cross-sectional area of one turbine by the total amount of turbines required. The cross-sectional area of one turbine has been illustrated in Figure 49.
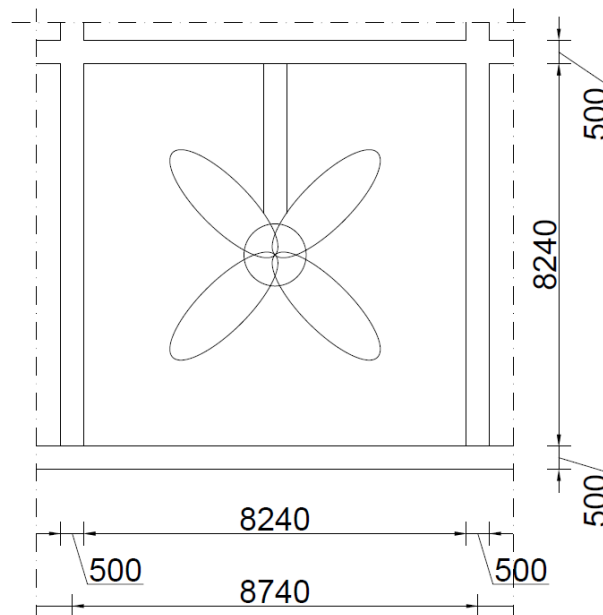
FIGURE 49: LONGITUDINAL CROSS-SECTION SINGLE FREE-STREAM TURBINE IN SLUICEWAY

To reach the required 960 m² discharge area, in total 18 turbine openings will be applied, as was mentioned in chapter 4.2. Between each turbine a 500 mm thick concrete wall will be constructed. The two outer walls, will be constructed with a thickness of 500 mm. The resistance of a 500 mm wall to local and external forces will be checked in chapter 7.

The total longitudinal length of the Tidal Power Plant becomes 157.82 meter.

5.4 RESULTS PRELIMINARY POWERHOUSE DESIGN

In the antecedent three paragraphs the transverse length, height and longitudinal length of the Tidal Power Plant has been determined. This paragraph will summarize the dimensions and provide drawings illustrating the preliminary powerhouse design in transverse and longitudinal direction.

5.4.1 SUMMARY DETERMINED DIMENSIONS

TRANSVERSE LENGTH

- Gate housing: 5.076 meter
- Turbine housing: 16.4 meter
- Infrastructure: 31.7 meter.

To reduce the total transverse length, the turbine housing wall at the North Sea side will be constructed within the gate lake side gate housing wall. Hence the total transverse length becomes: 52.676 meter. The required horizontal length to prevent piping from Bligh and Lane are 41.3 and 44.25 meter respectively. According to these results, piping will not occur thanks to the transverse length of the Tidal Power Plant.

HEIGHT

- The height complying with overtopping requirements contains: +10.04 m NAP.

LONGITUDINAL LENGTH

- In total 18 turbines
- Inner and outer wall thickness 0.5 meter
- Total longitudinal length: 157.82 meter.

5.4.2 ILLUSTRATIONS

The components are now combined into one main Tidal Power Plant element. Figure 50, Figure 51, Figure 52 and Figure 53 provide simple schematizations of the proportions of respectively the width and length cross-sections of the Tidal Power Plant. In Each concrete element has an assumed thickness of 500 mm. The ability to resist local and external loads of these concrete elements will be determined in chapter 7.
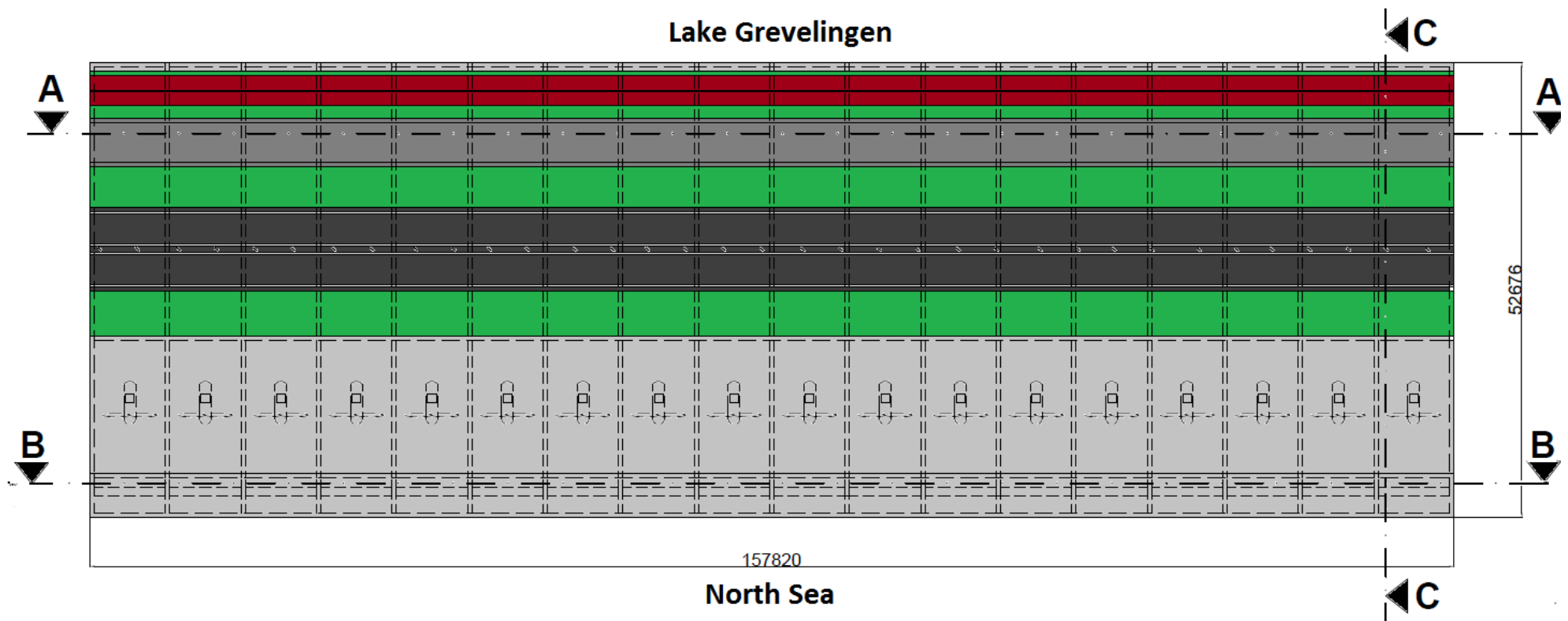
FIGURE 50: TOP VIEW TIDAL POWER PLANT
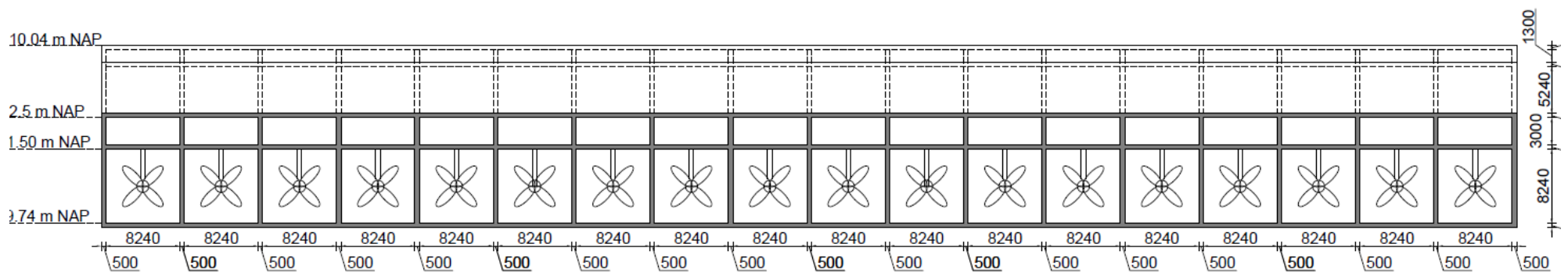
FIGURE 51: PRELIMINARY POWERHOUSE DESIGN, DIMENSIONS CROSS-SECTION A-A

91

FIGURE 52: PRELIMINARY POWERHOUSE DESIGN, DIMENSIONS CROSS-SECTION B-B

FIGURE 53: POWERHOUSE FIRST ESTIMATION OF DIMENSIONS, CROSS SECTION C-C

92

5.5 STABILITY CHECKS

The computed powerhouse dimensions allow performing several stability checks. Since the construction method is still due to be determined, the stability checks during transport an immersion of a caisson, and while in commission are executed. Hence, multiple load situations are considered. The governing load situation(s) will be used to carry out the final checks. Appendix C.2 describes the stability checks in more detail, this paragraph will give a brief description of the results.

If the Tidal Power Plant will be constructed as a caisson, it means it will be prefabricated at an external dry dock and transported through water towards its final position. It is assumed a dry dock adjacent to Lake Grevelingen will be available, and thus load conditions in the lake are governing for stability checks during transport. In Voorendt et. Al [2011] the best length width ratio of a caisson has been discussed based on the manoeuvrability of caisson navigations in the past. The lecture notes conclude a length width ratio between 3/1 and 3.8/1 would suffice in tidal areas. The required width of the caisson contains 52.676 meter, hence a length between 159.53 to 202.07 m will be preferred. The total length of the Tidal Power plant contains 157.82 meter. Especially when assuming the Brouwersdam will not be demolished before transportation. The caisson will thus be transported through the relative still standing water in Lake Grevelingen, improving the transportation conditions. Moreover, the length of the caisson almost equals the preferred length width ratio and therefore assumed to be sufficient for favourable navigation conditions.

In addition, from a constructive point of view, constructing the Tidal Power Plant as one single caisson will be beneficial as well. No stiff connections will be required between adjacent elements. These connection points require major attention since forces from each section are combined in those connecting sections. Such construction joints should be avoided, since the joints bring extra risks during construction. Large tensions and/or compressive forces in small connecting points mean challenging design issues. The joints should be constructed such that all stress and strains can be accommodated. Additional reinforcement will be required, reducing the durability and inducing risks when construction has not been done probably. Therefore, constructing the Tidal Power Plant as a whole will be considered the optimal design option of the Tidal Power Plant.

Within this paragraph the load situations will be considered in subparagraph 5.5.1. Secondly, in 5.5.2, the stability of a floating element will be computed. Both the static and dynamic stability will be checked here. Third, in 5.5.3, the stability of a hydraulic structure on a shallow foundation will be checked. Finally a conclusion will be drawn regarding the dimensions and possible required measures to ensure the overall stability of the Tidal Power Plant in 5.5.4.

5.5.1 LOAD SITUATIONS

Two load situations have been distinguished during the construction and transportation of the Tidal Power Plant.

DURING TRANSPORT AND IMMERSION

During transport the in- and outlet sluice will be closed off from water. In that way the buoyancy of the caisson will be increased. To determine the load during transport first the buoyancy should be determined. The load situation enhances hydrostatic pressures

and the deadweight of the caisson. For construction simplicity the N57 highway will be constructed in situ. To reach a stable situation ballast sand will be deposited on top of the sluice at the lake side, underneath the final highway location, within the ballast housing. The required amount of ballast sand will be determined in the stability checks below. This is than coupled to the buoyancy of the caisson and the rotational stability.

During immersion water will flow gradually into the sluice from both sides of the caisson. This means the total caisson weight increases, while the draught increases as well. It is expected this will not lead to stability problems, it will be checked in the stability checks as well.

IN COMMISSION AT EXTREME CONDITIONS

During extreme conditions the gate in the Tidal Power Plant will be lowered. The horizontal loads on the tidal power plant will be at maximum and are equal to the loads mentioned in the gate design, Appendix C.2.1. In this load situation all the elements of the Tidal Power Plant are installed. An additional 10% of the caisson weight will be added to the total dead weight of the caisson. The additional 10% accounts for all the required operational equipment of the Tidal Power Plant. The sluiceway will be completely filled with water and the amount of required ballast sand will remain unchanged.

5.5.2 STABILITY OF FLOATING ELEMENTS

The stability of floating elements has been separated into a static and dynamic stability in the succeeding sections.

5.5.2.1 STATIC STABILITY

In order to maintain the static stability of the caisson during transport the weight of each side of the caisson requires equality. Therefore the amount of sand located beneath the N57 shall be as much as required to ensure rotational stability. A discrepancy in rotational stability would lead to tilting of the caisson which could lead to major damage. To find the total static stability during transport three equilibrium situations are considered:

EQUILIBRIUM OF VERTICAL FORCES

The equilibrium of vertical forces will be reached when the buoyancy equals the dead weight of the caisson during transportation. During transport a keel clearance of at least 1.00 meter should be available [Voorendt et al., 2011]. Consequently, certain parts of the transportation route require dredging operations.

EQUILIBRIUM OF MOMENTS

Preventing tilting of the caisson in an unacceptable degree during the floating transport or the immersing procedure, an equilibrium of moments will be required. To enhance this situation the sum of moments around the point of rotation equals zero. By adding a ballast sand layer ($\gamma_s = 16 \, kN/m^3$) of 1.97 meter within the ballast housing this requirement will be achieved.

The equilibrium of moments will be sufficient when an element floats in still water, in reality this will, however, not be the case. Therefore the sensitivity to tilting has to be taken into account. The metacentric height (h_m) provides an expression of the tilting sensitivity. If $h_m > 0$ the caisson will be theoretically stable, whereas $h_m > 0.5$ is preferred. Calculations have shown a metacentric height of 30.28 meter will be reached during transport. In immersing conditions the metacentric height will vary between $h_m = 30.28 \ to \ 17.39 \ m$. Thus the static stability regarding the tilting sensitivity will comply with the preferred value for h_m. In these calculations the ballast layer has been included.

5.5.2.2 DYNAMIC STABILITY

During transport over water, floating elements will be affected by waves or swell. This may cause the caisson to sway which may result in navigable and clearance problems. For now it will be assumed the caisson will be prefabricated at a location adjacent to Lake Grevelingen. Therefore, it is not very likely significant swell waves will arise. Anyway, the dynamic stability should be assured. The wave conditions generated by wind for Lake Grevelingen are used. The wind velocity has been determined in Appendix B.2, resulting in a value of $U_w = 22.13 \ m/s$ in the direction of the Brouwersdam at extreme conditions.

SWAY

The dimensions of the caisson are compared with the wave length of the swell waves. The following rules of thumb should be applicable to ensure the dynamic stability with respect to sway:

$l_w < 0.7 l_e$ and $l_w < 0.7 b_e$

l_w *represents the wave length* (m)

l_e *represents the length of the floating element* (m)

b_e *represents the width of the floating element* (m)

With the determined wind velocity, the wave period and thus the wave length allows computation. The wave period has been calculated using the wind wave formula based on the Sverdup-Munk-Brettschneider method [SPM,1984]. This formula required the fetch and water depth as well, both discussed in Appendix B.4. Results have shown for a fetch of 10 km, the wave period $T_s = 3.99 \ sec$, whereas a fetch of 9 km leads to a wave period $T_s = 3.92 \ sec$.

The governing wave length has been determined using the linear wave theory. With an average water depth (h) of 5 meter it appears the waves fall within transitional waters. The corresponding governing wave length contains $L_w = 21.4 \ m$.

The required length and width of the caisson to ensure the dynamic stability against sway is $l_e = b_e > \frac{L_w}{0.7} = 30.58 \ m$. This means both the length and the width of the caissons are sufficient to ensure the dynamic stability against sway.

NATURAL OSCILLATION

When the natural oscillation period of the element lies close to the period of the water movements, the dynamic stability might be endangered as well. One should ensure the natural oscillation period of the element will be significantly larger than that of the waves or swell. Calculations in appendix B.5.2 have shown a natural oscillation period $T_0 = 6.35 \, sec$. Transportation will be solely allowed when the natural oscillation period lies significantly higher than the wave period. Since the wave period for wind waves has been calculated in extreme conditions, there are no problems during transportation expected regarding the natural oscillation.

5.5.3 STABILITY OF HYDRAULIC STRUCTURES ON SHALLOW FOUNDATIONS

To determine the stability of the Tidal Power Plant in commission, three stability checks will be performed. The load situation in commission will be considered governing here.

HORIZONTAL STABILITY

Using a friction coefficient, the horizontal stability has been checked. The friction coefficient multiplied by the dead weight, including the equipment for tidal power operations, requires exceedance of the horizontal forces. The horizontal forces are delivered by the extreme water conditions at both Lake Grevelingen and the North Sea. The calculations show the friction multiplied by the dead weight exceeds the horizontal forces by a factor 3. Hence, the horizontal stability has been guaranteed.

ROTATIONAL STABILITY

Within the soil, solely compressive stresses are allowed, tensile stresses cannot be absorbed by the subsoil. If the resulting action force intersects with the structure's core, this requirement will be met. The core has been defined as the area extending to 1/6 of the structure's width on both sides adjacent to the structure's midsection.

Compliance with this requirement will be achieved if the moment centre to the intersection point of the resulting force and the bottom line of the structure (e_R) does not exceed 1/6 of the structure's width ($52.676/6 = 8.86 \, meter$).

Applying the Tocardo free-stream Tidal Power plant $e_R = 3.89 \, m$ and lies within the margin. Applying the much heavier PFN bi-directional turbine leads to $e_R = 10.98 \, m$ which extends the core width. The turbine's weight makes a huge difference here. The applied mass formula obtained from PFN; $M = 2500 * D^3 \, (kg)$ with D the turbine diameter in meters, provides an indication of the turbine's mass. As PFN has not manufactured full scale turbines yet, the credibility of the equation is quastionable.

In case the mass formula is correct, measures should be taken to overcome rotational stability problems. Applying extension of the slucie bottom plate could be considered as one of these measures.

VERTICAL STABILITY

To overcome soil failure, the vertical effective soil stress, required to resist the acting loads ($\sigma_{k;max}$), should not exceed the maximum bearing capacity of the soil (p'_{max}). The bearing capacity has been calculated using Brinch Hansen. Calculations have shown the vertical stability will be easily achieved, with both the PFN and the Tocardo turbine.

5.5.4 CONCLUSION STABILITY CHECKS

The conclusions from the previous subparagraphs have been summarized in Table 16

	Requirement	Result	Complies?
Static stability floating elements			
Equilibrium of vertical forces	$\sum V = 0$	Draught = 6.62 meter	*yes*
Equilibrium of moments	$\sum M = 0$	Ballast layer of 1.97 meter	*yes*
Metacentric height	$h_m > 0.5\ m$	$30.28 < h_m < 17.39$	*yes*
Dynamic stability floating elements			
Sway	$l_e < \frac{l_w}{0.7} = 30.58\ m$ $b_e < \frac{l_w}{0.7} = 30.58\ m$	$l_e = 157.82\ m$ $b_e = 52.676\ m$	*Yes*
Natural oscillation	$T_0 < 3.99$	$T_0 = 6.44$	*Yes*
Stability of hydraulic structure on shallow foundation			
Horizontal stability	$\frac{\sum H}{f \sum V} < 1.0$	$\frac{\sum H}{f \sum V} = 0.3$	*Yes*
Rotational stability	$e_R < \frac{52.676}{6} = 8.86\ m$	Tocardo: $e_R = 3.89\ m$ PFN: $e_R = 10.98\ m$	*Yes* *No*
Vertical stability	$\sigma_{k;max} < p'_{max}$	Tocardo: $151.62 < 3311.4\ kN/m^2$ PFN: $181.06 < 3346.3\ kN/m^2$	*Yes* *Yes*

TABLE 16: SUMMARY CONCLUSIONS STABILITY CHECKS

From Table 16 it appears the stability of the structure will be guaranteed for almost every criterion. Solely the rotational stability of the PFN turbine does not comply with the requirement. Measures such as extending the bottom slab of the sluiceway could be applied to reach compliance. A note must be made here, the PFN turbine weight strongly influences the rotational stability, whereas the mass equation obtained from PFN concerns an estimation. PFN has not manufactured full scale turbines yet, the credibility of the equation is quastionable. Therefore, extending the bottom slab of the sluiceway has not been further elaborated in this thesis.

Including the ballast layer wihtin the ballast housing, the final transverse cross-sectional has been illustrated in Figure 54 on the succeeding page. The longitudinal cross-section will not differ from the in Paragraph 5.4 presented illustration, except for an additional ballast layer in Figure 51.
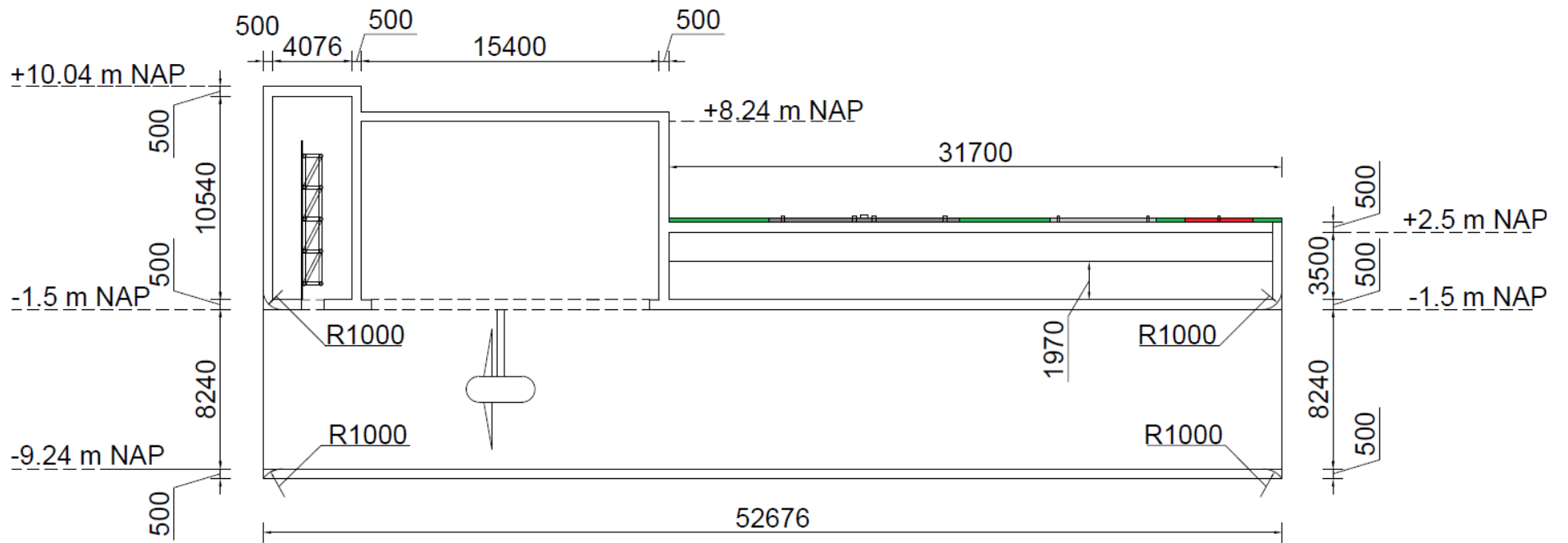
FIGURE 54: CROSS-SECTION PRELIMINARY POWERHOUSE DESIGN INCLUDING BALLAST LAYER (1.97 METER) UNDERNEATH INFRASTRUCTURE

5.6 CONCLUSION PRELIMINARY POWERHOUSE DESIGN

The previous sections have been used to determine the preliminary powerhouse dimensions. Transverse and longitudinal length have been computed according to the required functions of and on top of the Tidal Power Plant. These dimensions have been summarized in Table 17:

	Inner dimensions	Outer dimensions (incl. walls)	Bottom with respect to NAP	Top with respect to NAP
Gate housing			-1.5 m	+10.04 m
Transverse length	4.076 m	5.076 m		
Longitudinal length	8.24 m	9.24 m		
Height	10.54 m	11.54 m		
Turbine housing			-1.5 m	+8.74 m
Transverse length	15.4 m	15.9 m		
Longitudinal length	8.24 m	9.24 m		
Height	9.24	10.24		
Ballast housing			-1.5 m	+3.0 m
Transverse length	31.2 m	31.7 m		
Longitudinal length	8.24 m	9.24 m		
Height	3.5 m	4.5 m		
Sluiceway			-10.24 m	+1.5 m
Transverse length	52.676 m	52.676 m		
Longitudinal length	8.24 m	9.24 m		
Height	8.24 m	8.74 m		
Total Longitudinal length			157.82	m
Total Transverse length			52.676	m
Total weight concrete elements			571964.1	kN
Total weight water in sluiceways			643783.3	kN
Total weight gate			182.15	kN
Total weight turbine	Tocardo		2313.2	kN
	PFN		246980.8	kN
Total weight infrastructure			50028.94	kN
Total weight ballast			4532.7	kN
Total vertical load	Tocardo		1272804	kN
	PFN		1517472	kN
Load per square meter	Tocardo		153.1	kN/m^2
	PFN		**182.53**	kN/m^2

TABLE 17: OVERVIEW DIMENSIONS PRELIMINARY POWERHOUSE DESIGN

Except for one requirement, all the requirements within the stability checks have been met. The rotational stability of the Tidal Power Plant in scenario two will be jeopardized due to the weight of the PFN turbine. The weight equation of the PFN turbine requires some additional attention, as these turbines have not been developed on full scale yet. Measures, such as extending the bottom plate of the sluiceway could result in a positive rotational stability check. However, as the PFN turbine's weight remains uncertain, this measure has not been further elaborated.

Sub-paragraphs 5.4.2 and 5.5.4 have provided cross-sectional illustrations together with top view illustrations of the Tidal Power Plant. Still to be considered is the integration of the Tidal Power Plant in the currently existing Brouwersdam. The next chapter will therefore be dedicated to the integration of the Tidal Power Plant in the Brouwersdam.

6 INTEGRATION TIDAL POWER PLANT IN BROUWERSDAM

In the preliminary powerhouse design each component has been elaborated and the full dimensions of the powerhouse are known. In chapter 2 the optimal site location was qualitatively determined; resulting in the northern section. Integrating the complete Tidal Power Plant into the northern section of the Brouwersdam becomes the main topic in this chapter.

The Tidal Power Plant's position within the northern section will be determined using the construction method. For a construction method in the dry, the final location of the Tidal Power Plant will lie within the boundaries of the current dam. On the other hand, construction in the wet results in a final location at the Lake side of the dam. These options are discussed in the third paragraph from which a final conclusion is drawn.

Constructing the Tidal Power Plant in the Brouwersdam is one of the challenges arising the Tidal Power Plant design approach. The construction method of the tidal power plant strongly influences the definite location of the Tidal Power Plant within the Brouwersdam. Multiple approaches are available regarding the construction method of the Tidal Power Plant, these will be discussed in paragraph one.

With the definite location of the Tidal Power Plant in the Brouwersdam, the entry shape Tidal Power Plant upstream inlet can be determined. Paragraph two will be dedicated to upstream inlet system design.

High flow velocities at the outlet induce erosion. Preventing instability due to erosion, a bed protection will be applied. Head losses at the inlet and within the sluiceway influence the required bed protection. Therefore the head losses and incoming velocities will be elaborated to come up with a bed protection result in paragraph three.

Prevention of scour underneath the structure and during closure, will be achieved by applying a proper foundation bed. The composition of the foundation bed will be elaborated in paragraph 4.

Combining the four paragraphs will result in the Tidal Power Plant integrated into the Brouwersdam. Final sketches will therefore be provided in paragraph 5.

6.1 CONSTRUCTION METHOD

Two main methods may be described for the construction of the Tidal Power Plant. First, referring to the construction of the current dam, construction in the wet. The second considered method is construction in the dry. Two construction method will be described for construction in the dry. In Appendix C.3.2 the alternatives are elaborated in more detail, this paragraph provides a short description.

6.1.1 CONSTRUCTION IN THE WET

Construction in the wet contains one main option; casting the Tidal Power Plant elements at a precast yard relatively close to the final position. The location used for the construction of the caisson in the current dam could be considered as an option.

After casting the concrete elements, the yard will be filled with water and the elements will be towed towards its final position on top of a rubble foundation adjacent to the Brouwersdam. Removal of the dam and excavation to the preferred depth will start thereafter. Meanwhile, the road connection will be finalized.

6.1.2 CONSTRUCTION IN THE DRY

CONSTRUCTION PIT LAKE SIDE

Water retaining sheet pile walls are used to ensure a dry construction pit and provides protection against piping and heave. The dry construction pit will be located at the lake side of the dam just behind the top level of the dam. Hence, part of the dam will remain in-tact conducting its water retaining function.. The probability of flooding will thus be guaranteed during execution of the project. Applying natural relatively steep slopes, the stability of the dam will remain unaffected. Drainage shall be applied to ensure the full drought of the construction pit. Due to the location of the current highway, infrastructure will be redirected over a small reconstructed dam at the lake side of the construction pit. The construction will be finalized by removing remnants of the dam and the caissons in the wet.

CONSTRUCTION PIT AT CAISSON

The third option contains a construction pit at the caisson location. The dam will be partly demolished while a temporary water retaining structure has been built in front of the site to ensure flood protection. Water retaining sheet pile walls will be used to ensure a dry construction pit and provides protection against piping and heave. Infrastructure will be redirected over a part of the unaffected dam. The caissons will be demolished in a dry construction pit, excavated to the required depth. Casting of the Tidal Power Plant will be executed in-situ. After finalizing the construction of the Tidal Power Plant, the remnants of the dam will be excavated and dredged to the required depth.

6.1.3 CONCLUSION

The alternatives are appreciated based on three criteria as described in Appendix C.3.3 and C.3.4:

- Costs based on previous studies
- Feasibility
- Disturbance environment (roads, Flora and Fauna)

Due to the uncertainties it is hard to make a clear statement regarding the most attractive construction method. However, due to the uncertainties regarding the ability to reach a dry construction pit, and the possible additional costs to completely ensure construction in the dry, for now the construction in the wet has been considered as the optimal alternative.

Disturbance to the surroundings will be expected to occur at each construction method, whereas construction in the wet will probably result in increased disturbances. However, costs and feasibility have been appreciated as more important. Therefore, construction in the wet remains the most attractive one. An overview of the cross-sectional area of the construction pit has been provided in Figure 55 on the next page.
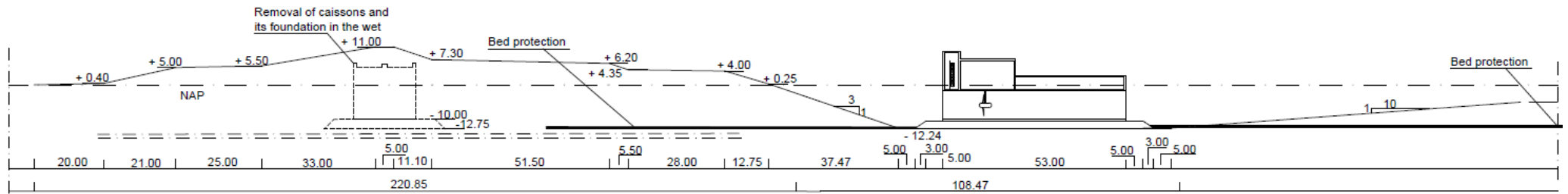
FIGURE 55: CONSTRUCTION IN THE WET

Turbulent flows reduce the energy production of the tidal power plant. Therefore, the generation of turbulent flows will be minimized as much as possible. Since the Tidal Power Plant will be constructed at the lake side of the Brouwersdam, a large area of the dam will be demolished and excavated to the required depth. The inlet system from the North Sea will therefore be located within the Brouwersdam. The sluiceway shape has already been adapted in order to reduce inlet losses, the exact similar approach will be applied to the inlet shape. From Stuwo Modeling Studio [2005], Figure 47, the equation to determine the required entry sluice rounding has been obtained:

$$\varepsilon_e = \left(\frac{2d}{3d+25r}\right)^2$$

The value for 'd' has been determined by the Tidal Power Plant's longitudinal length ($= 157.82\ m$). Entry losses are considered negligible at an entry loss coefficient smaller than 0.01. The corresponding radius equals:

$$0.01 = \left(\frac{2*157.82}{3*157.82+25r}\right)^2 \rightarrow r > 107.3\ m$$

A top view of the applied radius has been presented in Figure 56 and Figure 57. The required bed protection length, computed in the succeeding paragraph, has been included in these figures as well.
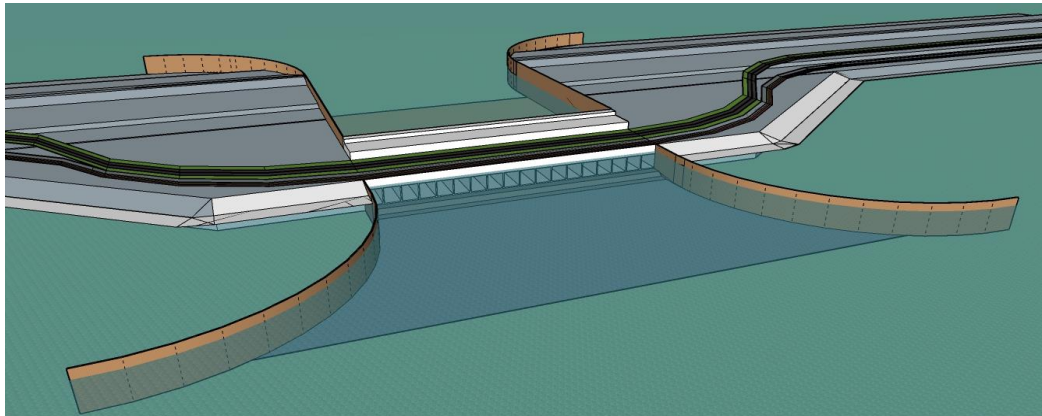
FIGURE 56: TOP VIEW TIDAL POWER PLANT FROM LAKE GREVELINGEN SIDE
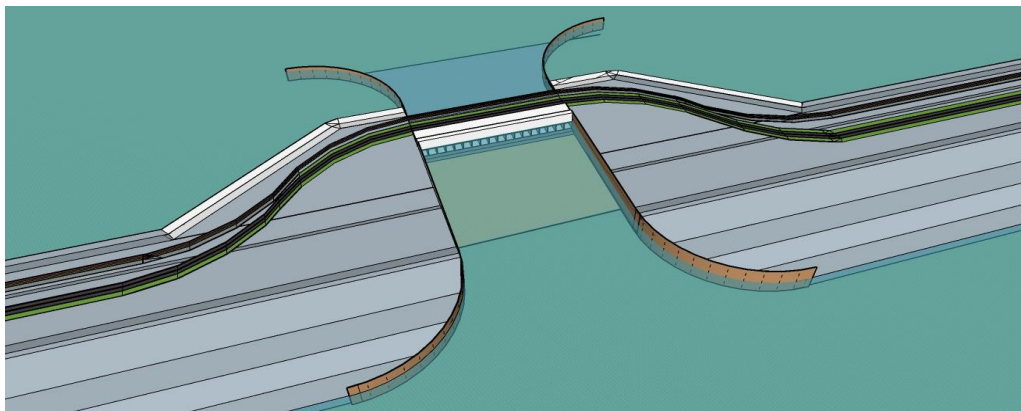
FIGURE 57: TOP VIEW TIDAL POWER PLANT INTEGRATED IN BROUWERSDAM, VIEW FROM NORTH SEA SIDE.

6.3 BED PROTECTION

Since the Tidal Power plant becomes part of a primary flood defence system, the structure's stability will be essential. Turbulent out-flow induce scour of loosely packed bed material at the downstream side of incoming flow. If the stability of the structure is endangered, scour protective measures are taken. Therefore, in order to decide whether measures are to be taken, the degree of scour without protection will be determined.

The scour development is proportional to the flow velocities of water leaving the sluiceway. Therefore, prior to any scour development calculations, the flow velocities are computed in subparagraph 6.3.1. Head losses emerging along the water flowing through the sluiceway reduce the outgoing flow velocity. Subparagraph 6.3.2 will therefore be dedicated to determine these head losses.

The scour development without scour protection provides a conclusion whether the structure remains stable over time. The scour process will therefore be described in subparagraph 6.3.3.

Finally a bed protection design will be elucidated based on the incoming flow velocities reduced by the head losses. The location of this bed protection has already been simply indicated in Figure 58. Subparagraph 6.3.4 provides the elaboration of the bed protection design.

In each section a distinction will be made between the two flow directions. From here on, the flow directions are indicated by: flow direction 1 and flow direction 2, see Figure 58. The flow direction from North Sea towards the lake will be assigned as flow direction 1. Water flowing from Lake Grevelingen towards the North Sea will be assigned as flow direction 2. Subscript '1' and subscript '2' will be used to account for flow direction 1 and 2 respectively.
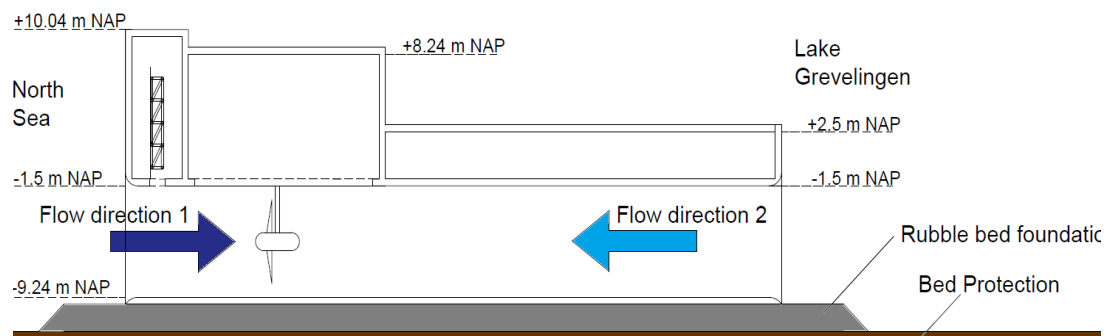
FIGURE 58: SCHEMATIZATION FLOW DIRECTION

6.3.1 FLOW VELOCITIES

The scour development will mainly be determined by the outflow velocities. This section will therefore be dedicated to the determination of the outflow velocities. The dimensions of the sluiceway and the obtained tidal data contribute to the computation of the incoming flow velocities from both directions. These incoming flow velocities will therefore be treated first. Furthermore, due to contraction, turbine losses and friction losses, the flow velocity in the sluiceway decreases. These losses are treated secondly. Finally, the influence of the head losses to the incoming velocity result in a final outflow velocity, computed in the last section.

The incoming flow velocities of the Free-stream turbine are considered with the hydraulic conditions described in Scenario 1 from chapter 4.4.2. The incoming flow velocity per sluiceway follows from:

$$U_{in,j,i} = \frac{Q_{in}}{A_s} = \frac{A_s\sqrt{2*g*H}}{A_s}$$

In which:

Q_{in} represents the incoming discharge

H   represents the head difference

A_s represents the wet cross − sectional area of the slucieway

      $= 8.24 * 8.24 = 67.9 \text{ m}^2$

g   represents the gravitational constant $= 9.81 \text{ m/s}^2$

Subscript 'j' represents the free-stream ('f') or turbine bulb ('b'), whereas subscript 'i' indicates flow direction 1 or 2.

The average head difference over the lifetime of the free-stream turbine will be determined using the following steps:

- Provide tidal data from 1 year from Waterbase.nl (year 2016)
- Determine the water level sequence at Lake Grevelingen using equations from paragraph 4.2.5.
- Maintaining a water level at Lake Grevelingen between +0.05 meter NAP and -0.45 m NAP.
- Compute the average difference over the considered time span.

With the obtained data from October 2015 to October 2016 (waterbase.nl) a maximum head difference of 1.91 meter was found in flow direction 1. However, over the lifetime of the free-stream turbine a sea level rise of 25 cm will be expected, as was described in paragraph 4.4.2. The governing maximum head difference is computed by adding 0.25 meter to the obtained one year data. Following the above described steps, the maximum head difference over one year becomes 2.07 meter for flow direction 1, leading to $U_{in,f,1} = 6.37 \text{ m/s}$.

The maximum head difference in flow direction 2 reduces over time due to the sea level rise. Hence, head differences obtained from the tidal data (waterbase.nl) have been used to determine the governing head difference. It resulted in a maximum head difference of 1.21 meter, leading to $U_{in,f,2} = 4.87 \text{ m/s}$.

This approach has been applied to determine the governing maximum incoming flow velocities for the bulb turbines as well. However, the sea level rise, with respect to the initial levels from 2016, is expected to reach a value of 40 cm during the bulb turbine's lifetime. The resulting maximum incoming flow velocity in flow direction 1 contains 2.13 meter, leading to $U_{in,b,1} = 6.46 \text{ m/s}$.

The bulb turbine maximum head difference for flow direction 2 equals 1.20 m, leading to $U_{in,b,2} = 4.85 \text{ m/s}$.

6.3.2 HEAD LOSSES

The sluiceway has been designed as a straight smooth ducted concrete box. The applicable head losses in such ducted rectangle box are discussed and computed in this section. The four main types of head losses are:

- Contraction at the entry point of the sluiceway
- Friction
- Sudden expansion at the exit point
- Turbine losses

For each head loss, the computed governing flow velocities are applied.

Entry losses

The entry losses have been determined in the sluiceway shape, paragraph 5.1.5. a one meter radius has been applied to the entry top and bottom slab, leading to a head loss coefficient of $\varepsilon_e = 0.11$.

The governing entry loss for flow direction 1 and 2 are:

$\Delta H_{E,f,1} = 0.11 \left(\frac{6.37^2}{2*9.81} \right) = 0.227 \ m$
$\qquad\qquad\qquad \Delta H_{E,f,2} = 0.11 \left(\frac{4.87^2}{2*9.81} \right) = 0.133 \ m$

$\Delta H_{E,b,1} = 0.11 \left(\frac{6.46^2}{2*9.81} \right) = 0.234 \ m$
$\qquad\qquad\qquad \Delta H_{E,b,2} = 0.11 \left(\frac{4.85^2}{2*9.81} \right) = 0.132 \ m$

Exit losses

The sluiceway functions as inlet from both directions, at both sides the shape of the inlet is adapted. In addition, when flowing through a tube into a still standing reservoir (as the lake or sea may be considered) the exit coefficient becomes 1. The exit losses are, however, not of importance for scour development. The scour development will be a result of the outflow velocity and thus the exit losses do not yet apply to this outflow velocity.

Friction losses

A smooth wall reduces the friction between the incoming flow and wall. The flow can be considered as a turbulent flow, according to the Reynolds number:

$$Re = \frac{ul}{v}$$

In which 'u' represents the flow velocity, 'l' the characteristic sluiceway length and 'v' the kinematic viscosity ($v = 1.05 * 10^{-6} \ m^2/s$ at 20°C). substituting the flow velocity values into the Reynolds equations results in an exceedance of the turbulent flow criterion; (Re>3500). Applying the White-Colebrook equation, the head loss for turbulent flow follows from:

$$\Delta H_{f,j,i} = c_f \left(\frac{L}{R} \right) \left(\frac{U^2}{g} \right)$$

In which:

c_f represents the friction coefficient $= 0.003$ for smooth concrete

U represents the average velocity in the tube

R represents the hydraulic radius $= \frac{A}{P} = 2.06$

L represents the tube length $= 52.676$

Assuming presence of the average velocity through the complete sluiceway, the length of the tube becomes 52.676 m. Applying the computed governing flow velocities, the friction losses in flow direction 1 and 2 are:

$$\Delta H_{f,f,1} = 0.003 * \left(\frac{52.676}{2.06}\right)\left(\frac{6.37^2}{9.81}\right) = 0.32 \; m \qquad \Delta H_{f,f,2} = 0.003 * \left(\frac{52.676}{2.06}\right)\left(\frac{4.87^2}{9.81}\right) = 0.185 \; m$$

$$\Delta H_{f,b,1} = 0.003 * \left(\frac{52.676}{2.06}\right)\left(\frac{6.46^2}{9.81}\right) = 0.33 \; m \qquad \Delta H_{f,b,2} = 0.003 * \left(\frac{52.676}{2.06}\right)\left(\frac{4.85^2}{9.81}\right) = 0.184 \; m$$

Turbine losses

The flow velocity directly behind the turbines will be computed by:

$$\mu_{free-stream} = \frac{u_2}{u_1} = \sqrt[3]{\frac{A_s - \eta * C_p * A_{turb}}{A_s}}$$

Where:

u_1 represents the velocity in front of the turbine

u_2 represents the velocity behind the turbine

A_s represents the total wet cross $-$ sectional area of the sluiceway

A_{turb} represents the cross $-$ sectional area of the turbine $= 19m^2$

$\eta * C_p$ represents the efficiency of the turbine $= 0.415$

Mooyaart and Noortgaete [2010] proposed this equation for computing the influence of a free-stream turbine in the flow velocity. This equation seems quite reasonable, but is majorly influenced by the unknown efficiency of the free-stream turbine. The notation $'\eta'$ represents the Betz-limit, which has been defined as the maximum efficiency of wind turbines and equals 59.3%. Whether this limit can be applied in the hydrodynamics remains doubtful, however the effects on free-stream turbines may be compared with the conditions wind turbines are subject to. Therefore, the Betz limit is applied in the first estimation. Laboratory tests should give more clearance regarding this assumption. The turbine's efficiency of the Tocardo free-stream turbines remain uncertain due to a lack of information provided by Tocardo. In previous studies a value between 60 and 70 percent has been applied. By means of determining the bed protection, the excessive efficiency leads to the governing flow velocity. The total turbine efficiency has, consequently, been assumed to be equal to 0.415.

The influence of the bulb turbine on the flow velocity has been defined in a different manner. Mooyaart and Noortgaete [2010] also performed discharge calculations for

bulb turbines. Their method accommodates the use of reference bulb turbines in Alphen aan de Maas, The Netherlands. The applied turbine diameter at Alphen aan de Maas equals 4 meter.

$$Q_d = \frac{Q_{d,Alphen}\sqrt{H_{rated}}}{\sqrt{H_{rated,Alphen}}} * \frac{D^2}{D^2_{Alphen}} = 100 * \frac{\sqrt{H_{rated}}}{\sqrt{4}} * \frac{D^2}{4^2} = 3.125\sqrt{H_{rated}}D_{turb}^2$$

Where:

H_{rated} $Turbine\ rated\ head = 1.1\ m\ (obtained\ from\ Section\ 4.5.1)$

D_{turb} $Turbine\ diameter = 8.23\ m$

The incoming discharge applied to the determine has been determined using:

$$Q_{in,turb} = Q_d * \sqrt{\frac{H_s}{H_{rated}}}$$

The loss induced by the turbine's energy generation from the incoming discharge has been calculated using the discharge coefficient. The discharge coefficient represents the ratio of the incoming turbine discharge over the total incoming discharge at the sluice:

$$\mu_{bulb} = \frac{Q_{in,turb}}{A_s\sqrt{2gH_s}}$$

Where:

Q_d $\qquad represents\ the\ design\ discharge$

H_s $\qquad represents\ the\ head\ difference$

Since the head loss has been determined using the average velocities in both flow directions. Applying the average head difference to the above mentioned equations leads to the final discharge coefficient. The ratio of flow velocity in front of the turbine and behind the turbine is set equal to $(1 - \mu_{bulb})$

As for both turbines the velocity decrease will be determined, the head losses are computed using:

$$\Delta H_{j,i} = (1 - \mu_j)\frac{U^2}{2g}$$

The results of the loss coefficient for each turbine are:

$$\mu_{f,1} = \mu_{f,2} = \sqrt[3]{\frac{67.9 - 0.415 * 19}{67.9}} = 0.96 \qquad\qquad \mu_{b,1} = \mu_{bulb,2} = \frac{3.125D_{turb}^2}{A_s\sqrt{2g}} = 0.704$$

The influence on the incoming flow for the free-stream turbine is much lower compared with the bulb turbine. This is similar to what would be expected, as the bulb turbine has a much higher efficiency.

The head loss for the free-stream turbine in both flow direction 1 and 2 is:

$$\Delta H_{f,1} = (1 - 0.96) * \frac{6.37^2}{2*9.81} = 0.083\ m \qquad\qquad \Delta H_{f,2} = (1 - 0.96) * \frac{4.87^2}{2*9.81} = 0.048\ m$$

The head loss for the bulb turbine in both flow direction 1 and 2 is:

$$\Delta H_{b,1} = (1 - 0.704) * \frac{6.46^2}{2*9.81} = 0.63 \; m \qquad \Delta H_{b,1} = (1 - 0.704) * \frac{4.85^2}{2*9.81} = 0.35 \; m$$

The governing turbine head losses result from the bulb turbine.

Outflow velocity

The initial head will reduced by each of the head losses computed in the sections above. The final maximum outflow velocity follows from:

$$U_{out,i} = \left(U_{in} - \sqrt{2g \sum \Delta H_i} \right)$$

The computation of the final maximum outflow velocity in both flow directions has been summarized in Table 18:

		Flow direction 1	Flow direction 2	
Inflow velocity	$U_{in,f,i}$	6.37	4.87	m/s
	$U_{in,b,i}$	6.46	4.85	m/s
Entry loss	$\Delta H_{E,f,i}$	0.227	0.133	m
	$\Delta H_{E,b,i}$	0.234	0.132	m
Friction loss	$\Delta H_{f,f,i}$	0.32	0.184	m
	$H_{f,b,i}$	0.33	0.185	m
Turbine loss	$\Delta H_{f,i}$	0.083	0.048	m
	$\Delta H_{b,i}$	0.63	0.35	m
Total head loss	$\sum \Delta H_{f,i}$	0.63	0.592	m
	$\sum \Delta H_{b,i}$	1.194	0.667	m
Outflow velocity	$U_{out,f,i}$	**2.85**	**1.46**	m/s
	$U_{out,b,i}$	1.62	1.32	m/s

TABLE 18: RESULTS HEAD LOSSES AND MAXIMUM OUTFLOW VELOCITY

In further calculations, such as the scour development over time, the average outflow velocity becomes of importance as well. The computation of these velocities is similar to the approach above. Table 19 provides a summary of the obtained values.

		Flow direction 1	Flow direction 2	
Inflow velocity	$U_{in,f,i}$	4.20	3.16	m/s
	$U_{in,b,i}$	4.20	2.87	m/s
Entry loss	$\Delta H_{E,f,i}$	0.099	0.056	m
	$\Delta H_{E,b,i}$	0.099	0.046	m
Friction loss	$\Delta H_{f,f,i}$	0.137	0.078	m
	$H_{f,b,i}$	0.137	0.064	m
Turbine loss	$\Delta H_{f,i}$	0.036	0.020	m
	$\Delta H_{b,i}$	0.270	0.124	m
Total head loss	$\sum \Delta H_{f,i}$	0.272	0.154	m
	$\sum \Delta H_{b,i}$	0.506	0.234	m
Outflow velocity	$U_{out,f,i}$	**1.89**	**1.42**	m/s
	$U_{out,b,i}$	1.05	0.73	m/s

TABLE 19: RESULTS AVERAGE OUTGOING VELOCITY

6.3.3 SCOUR PROCESS

Local sediment transport exceeding the supply from upstream results in scour. Due to a difference in either velocity or in turbulence the transport difference will be acquired. Due to turbulence motion or velocities higher than the critical velocities, sediment is suspended in the water and is carried along with the main flow. An upstream slope develops, reaching an equilibrium after a time 't'. The flow separates as a consequence of the originated slope, causing a mixing layer in the scour hole and recirculation zone against which water flows against the main flow direction. Hence, the scouring process is influenced by the scour hole itself. The final scour depth will reached when the velocity in the scour hole decreases to values below the critical value [Schiereck and Verhagen, 2012].

Scour itself is not necessarily a problem, only if the stability of the structure is endangered a bed protection will be required. It is assumed scour protection is required due to both turbulence and the velocity at the outflow of the sluiceway.

In Kessel et al. [2015] soil analyses have been performed at Lake Grevelingen. The aim of these soil analysis was to determine the magnitude of silt suspension into the water and the sensitivity to erosion of the silt bed top layer, bearing in mind a discharge structure will be constructed at the Northern Section of the Brouwersdam. Therefore, the obtained results include measurements at the location of the Tidal Power Plant.

6.3.4 BED PROTECTION PROPERTIES

At the scour depth equilibrium point the sedimentation from the scour hole is equal to the incoming sediment transport. With the equilibrium scour depth the final required bed protection properties will be determined. The required bed protection will be obtained using the guidelines of bed protection for locks [Rijkswaterstaat, 2000].

6.3.4.1 POINT OF ATTACHMENT TO BED

Due to the vertical distance between the sluiceway and the bed, the outgoing flow expands over a distance $'x_{bn}'$ where it 'touches' the bed. The angle of the outgoing flow towards the bed is set equal to 5.7°. Applying the parameters as shown in Figure 59, x_{bn} follows from:

$$x_{bn} = e_n/\tan(\alpha + 5.7)$$

Where

α *represents the angle of the flow axis, which is assumed to be equal to* 0

e_n *represents the vertical distance of flow axis to bed*
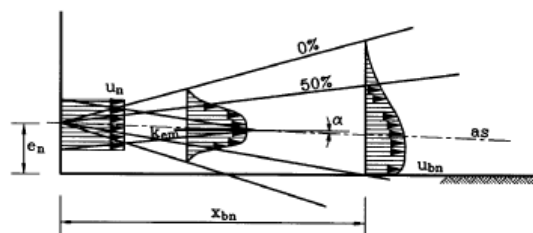
FIGURE 59: FLOW REDISTRIBUTION OVER LENGTH x_{bn}

The depth of the bed is set equal to the bed of the rubble foundation layer, determined in the succeeding section. For now a rubble bed layer thickness of 1.6 meter has been set. The sand bed will be located at a level of -11.84 m NAP. The centre of the flow equals the centre line of the sluiceway, located at -5.62 m NAP. The value of the horizontal distance to the attachment point equals:

$$x_{bn} = \frac{6.22}{\tan(0+5.7)} = 62.3 \; m$$

The maximum velocity at the bed will now be computed using the equation below.

$$u_{bn,i} = 2.5 u_{n,i} \sqrt{\frac{d_{n,i}}{x_{bn}}}$$

Where

$u_{bn,i}$ *represents the maximum flow velocity at the bottom in flow direction i*

$u_{n,i}$ *represents the maximum outgoing flow velocity in flow direction i*

$d_{n,i}$ *represents the height of the outgoing flow* $= 8.24 \; m$

In flow direction 1, the maximum flow velocity at the bed equals:

$$u_{bn,1} = 2.5 * 2.85 \sqrt{\frac{8.24}{62.3}} = 2.59 \; m/s$$

In flow direction 2, the maximum flow velocity at the bed equals:

$$u_{bn,2} = 2.5 * 1.46 \sqrt{\frac{8.24}{62.3}} = 1.33 \; m/s$$

The composition of the top layer of the bed protection is proportional to the intensity of the turbulent flow near the bed. The provided preferred approach to compute the composition of the top layer will be described in the next section.

6.3.4.2 REQUIRED NOMINAL DIAMETER TOP LAYER

The stability relation for sluices been most properly by an adapted Shield formulation. The formulation is adapted to the presence of a concentrated flow, which is the case at the exit point of the sluiceway. The stability relation reads:

$$D_{n,i} = \left(\left(\frac{0.8}{\Delta h^{\frac{1}{3}}} \right) * \frac{u_{b,i}(1 + 3r)^2}{2g} \right)^{\frac{3}{2}}$$

In which:

Δ $represents\ the\ relative\ density = \frac{\rho_s - \rho_w}{\rho_w} = \frac{2650 - 1025}{1025} = 1.59$

D_n $represents\ the\ nominal\ stone\ diameter\ in\ flow\ direction\ i.\ D_{n,i} = 0.84 D_{50}$

h $represents\ the\ total\ water\ depth = -0.45 - (11.84) = 11.39$

r $represents\ the\ turbulence\ intensity$

$u_{b,i}$ $represents\ the\ maximum\ velocity\ neer\ the\ bed\ in\ flow\ direction\ i$

The diameter of the required horizontal bed protection rock material is thus depending on:

- Near Bed flow velocity
- Turbulence intensity
- Bed roughness

The governing value of the required nominal diameter is found by assuming the roughness of the bed is considered rough ($r = 0.3$). In-situ tests should provide a better estimation of this roughness factor.

The water depth in flow direction 1 has been determined using the minor water level at the lake minus the bottom level of the rubble foundation bed. The similar approach has been used for the North Sea side, the minor water level here is similar to the low sea water level; -1.91 m NAP.

The resulting required nominal diameter in flow direction equals:

$$D_{n,1} = \left(\left(\frac{0.8}{1.59 * 11.39^{\frac{1}{3}}} \right) * \frac{(2.59 * (1 + 3 * 0.3))^2}{2 * 9.81} \right)^{\frac{3}{2}} = 0.15\ m$$

$$D_{n,2} = \left(\left(\frac{0.8}{1.59 * 11.39^{\frac{1}{3}}} \right) * \frac{(1.33 * (1 + 3 * 0.3))^2}{2 * 9.81} \right)^{\frac{3}{2}} = 0.020\ m$$

Bed protection length

Preventing the Tidal Power Plant structure from deflecting into the eroded hole, the bed protection requires a certain length. The minimum required bed protection length will be obtained from Figure 60 and:

$$L_{b,i} = 0.5 * h_{e,i}\big(cotg(\gamma) - cotg(\beta)\big)$$

In which:

$L_{b,i}$ *represents the minimum required bottom protection length in flow*

   direction i

$h_{e,i}$ *represents the maximum scour hole depth in flow direction i*

γ_i *represents the bottom slope due to scour, reaches* 1: 15 *over time for*

   loosely packed sand and 1: 6 *for densely packed sand*

β *represents the slope of the scour hole*

Since the Tidal Power Plant will be constructed at the lake side of the Brouwersdam, the sand is assumed to be loosely packed here. The bed protection at the sea side is assumed to be partially densely packed since it has been subject to the self-weight of the Brouwersdam for many years. Since the required bed protection length increases for loosely packed sand, the sand is assumed to be fully loosely packed at the North Sea side. The slope due to scour has been assumed equal to the angle of response of the soil (=30°), the validity of this assumption should be determined using in-situ tests at for example the Brouwerssluice.
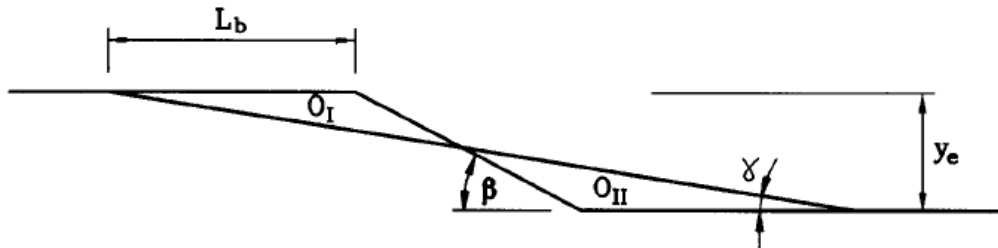
FIGURE 60: BED SCOUR DEVELOPMENT [RIJKSWATERSTAAT, 2000]

As was mentioned before, the scour depth develops over time leading to a certain equilibrium depth. From Schiereck [2015] the derived equation for uniform flow behind a bed protection is written as:

$$h_{s,i}(t) = h_{0,i}\left(\frac{t}{\big(330\Delta^{1.7}h_{0,i}{}^2(\alpha\bar{u}_\iota - \bar{u}_c)^{-4.3}\big)}\right)^{0.38}$$

Where:

$h_s(t)$ *represents the maximum depth in the scour hole as a function of time in*

   the flow direction i

$h_{0,i}$ *represents the initial water depth in the flow direction i*

$\bar{u}_\iota$ *represents the vertically averaged velocity at the end of the protection in*

   flow flow direction i

$\bar{u}_{cr}$ *represents the critical averaged flow velocity for particle motion of the*

114

   bed protection

α *represents, among other things, turbulence and increase the effective*

   velocity

t *represents time in hours*

The value for $'\alpha'$ is defined in two ways. When $\bar{u}$ is defined as Q/A, the influence of a locally increased velocity must be included in α. When $\bar{u}$ is defined locally, α represents the amplification factor due to turbulence. In the case of the Tidal Power Plant, the outflowing water discharges into a large body of water, there is no clear horizontal or vertical constriction. In that case the scour can be approximated to the α-value for a vertical vortex-street which lies around 4 for a bed protection that is $10h_0$ long.

It has been assumed the vertical average flow velocity over the full water depth is equal to the governing average exit flow velocities at the sluiceway. Since these flow velocities enter a large water body, a reduction in flow velocity would be obvious. Calculate the averaged vertical flow velocity regressively from the near bed velocity would lead to an even higher flow velocity with respect to the exit velocities which seems incorrect. Therefore, the value of the exit velocities has been chosen. This will clearly lead to a much higher calculated scour development over time.

The initial water depth ($h_{0,i}$) has been determined applying the average water level at both side of the Brouwersdam. At the lake side, flow direction 1, the average level lies at -0.2 m NAP. At the North Sea side, flow direction 2, the average water level equals the mean sea water level: +0.0 m NAP.

The critical average vertical velocity, introducing particle motion of the bed material, will be computed using D_{50} of the bed material. In the boundary conditions, paragraph 3.3 has been presented, showing the particle size distribution of sand near the Brouwersdam. The corresponding D_{50} reads: $D_{50} = 3.5 * 10^{-4} \, m$. Similarity between the bed composition of the Lake and the North Sea side of the Brouwersdam has been assumed.

$$u_{cr} = 1.4 \left(\frac{h}{D_{50}}\right)^{\frac{1}{6}} \sqrt{\Delta g D_{50}}$$

$$u_{cr} = 1.4 * \left(\frac{11.39}{3.5 * 10^{-4}}\right)^{\frac{1}{6}} \sqrt{1.59 * 9.81 * 3.5 * 10^{-4}} = 0.58 \, m/s$$

The scour depth will now be computed at each flow direction:

$$h_{s,1}(t) = h_{0,1} \left(\frac{t}{\left(330\Delta^{1.7} h_{0,1}{}^2 (\alpha\overline{u_1} - \bar{u}_c)^{-4.3}\right)}\right)^{0.38} =$$

$$= 11.19 \left(\frac{t}{(330 * 1.59^{1.7} * 11.19^2 (4 * 1.89 - 0.58)^{-4.3})}\right)^{0.38} = 3.49t^{0.38}$$

$$h_{s,2}(t) = h_{0,2} \left(\frac{t}{\left(330\Delta^{1.7} h_{0,2}{}^2 (\alpha\overline{u_2} - \bar{u}_c)^{-4.3}\right)}\right)^{0.38} = h_{s,i}(t)$$

$$= 11.39 \left(\frac{t}{(330 * 1.59^{1.7} * 11.39^2 (4 * 1.42 - 0.58)^{-4.3})}\right)^{0.38} = 2.10t^{0.38}$$

Mainly due to the high averaged vertical velocities the scour development over time is extremely fast. This approach seems to be inappropriate while using the outgoing velocities at the exit point of the sluiceway.

The equilibrium scour hole will be determined by:

$$h_{e,i} = h_i(\bar{u} - u_{cr})/u_{cr}$$

The required parameters have been determined in earlier stages. Since the value for the vertical average velocity ($\bar{u}$) seems to be taken too large, the value of the equilibrium scour hole becomes strongly over-dimensioned. However, the next step provides an estimation of the required bed protection length. The vertical average velocity will be determined while including the bed protection length. Hence, the required bed protection length and average vertical velocity at the end of the protection will be determined iteratively. The average vertical velocity at the end of the bed protection will be computed with (provided $L_{b,i} > 8h_{0,i}$):

$$\bar{u}_i = \frac{u_{0,i} * A_s}{h_{0,i}\left(b_s + 0.1 * \left(L_{b,i} - 8h_{0,i}\right)\right)}$$

Where:

$u_{0,i}$ *represents the initial maximum outgoing flow velocity at the sluice exit in*

       flow direction i

A_s *represents the cross − sectional area of the sluiceway* $= 8.24^2 = 67.9 \ m^2$

$h_{0,i}$ *represents the average water depth in flow direction i*

b_s *represents the with of the sluiceway* $= 8.24 \ m$

$L_{b,i}$ *represents the bed protection length*

Combining the equations for the required bed protection length, the scour equilibrium depth and the average vertical velocity at the end of the bed protection, the equilibrium depth will be obtained. The combined equation reads:

$$ph_{e,i}^2 + \left(20b_s + ph_{0,i} - 16h_{0,i}\right)h_{e,i} + \left(20b_s h_{0,i} - 16h_{0,i}^2 - 20u_{0,i}A_s/u_{cr}\right) = 0$$

Where:

$$p = cotg(\gamma) - cotg(\beta)$$

The results of the equilibrium scour depth and required bed protection in flow direction 1 and 2 are:

$h_{e,1} = 14.21 \ m$ $h_{e,2} = 12.0 \ m$

$L_{b,1} = 94.0 \ m$ $L_{b,2} = 79.85 \ m$

$\bar{u}_1 = 1.32 \ m/s$ $\bar{u}_2 = 1.19 \ m/s$

The length of the bed protection at the North Sea side, flow direction 2, does not comply with the requirement of $L_{b,2} > 8h_{0,2}$. It has been assumed the bed is loosely packed,

which might not even be the case for a large part underneath the current Brouwersdam. The validity of this assumption should therefore be tested and investigated. For now, a bed protection length of $8h_{0,2} = 91.12\ m$ will be applied.

Hence, the bed protection lengths at the North Sea side and Lake side are 91.12 meter and 94.0 meter respectively.

6.3.4.3 COMPOSITION BED PROTECTION

As computed in the previous section, the required nominal stone diameter at the Lake side and the North Sea side equals $D_{n,1}$ =0.15 meter and $D_{n,2}$ =0.02 meter respectively. Applying $D_{n,i} = 0.84D_{50}$, the nominal diameter corresponds to $D_{50,1} = 0.18\ m$ and $D_{50,2} = 0.024\ m$.

To ensure the stability of both the bed material and the top layer of the bed protection material, the composition of the bed protection should comply with several criteria.

The interface stability, the filter stability at the interface of two different granular materials, is described with the geometrically tight criterion. A layer is geometrically tight if no smaller grains are transported through the filter layer. If both materials are well-graded and comply with the criterion described above, the geometrically tight criterion reads:

$$\frac{D_{f15}}{D_{b85}} < 5$$

The subscript "f" and "b" are used to express the top filter layer and base layer respectively.

Corresponding to the required nominal diameter is 5-40 kg ($D_{50,1} = 0.20\ m$) quarry rock at the lake side and 45/125 mm coarse grading $\left(D_{50,2} = 0.08\ m\right)$ at the North Sea side, obtained from Figure 134, Appendix C.4. To comply with the above mentioned geometrically tight criterion, the underlying layer at the Lake side becomes:

$$\frac{0.15}{5} < D_{b85} = 0.03\ m$$

The corresponding coarse grading size equals 45/125 mm ($D_{b85} = 105\ mm$). The particle size at the Brouwersdam, obtained from CPN tests close to the Brouwersdam, equals D_{b85} =0.6 mm (Figure 19, Section 5.3.3.1). Hence a fine gravel layer will be placed between the coarse grading and the sand bed. The properties will be:

$$\frac{0.050}{5} < D_{b85} = 0.01\ m$$

The criterion for permeability of the filter, to prevent pore pressures contributing to instability of the structure reads:

$$\frac{D_{f15}}{D_{b15}} > 4\ to\ 5$$

With the properties of each layer summarized in Table 20 the required properties of each layer are summarized at both sides of the Tidal Power Plant.

Lake Side	$D_{50}[m]$	required $D_{15}[mm]$	required $D_{85}[mm]$	Chosen material	Actual $D_{15}[mm]$	Actual $D_{85}[mm]$
Top layer	0.18	-	-	5-40 kg	150	30
First under layer	0.08	<55	>55	45/125 mm	55	105
Filter	-	$1.25<D_{15}<30$	>10	Gravel	-	-
Bed material	-	-	-	Sand	0.25	0.6
North Sea side						
Top layer	0.024	-	-	45/125 mm	55	105
Filter	-	$1.25<D_{15}<30$	>10	Gravel	-	-
Bed material	-	-	-	Sand	0.25	0.6

TABLE 20: REQUIRED MATERIAL PROPERTIES

The bed protection will be construction in the wet. The layers consisting of 5-40 kg mm will be constructed with thickness of $1.5D_{50}$, whereas the smaller gradation will be constructed with a thickness of 0.25 meter. The bed protection cross-section including the layer thickness has been illustrated in in the succeeding paragraph.

6.3.5 RESULTS

The approaches required to determine the final bed protection length and top layer diameter are provided in this paragraph. Due to a difference in flow velocity in flow direction 1 and flow direction 2, a difference in bed protection length has been found. It has resulted in a bed protection length of 94.0 meter at the Lake Grevelingen side and 91.12 meter at the North Sea. The required top layer nominal stone diameter at the Lake side equals 0.18 meter, whereas a nominal diameter of 0.24 meter will be required at the North Sea side. For compliance to the geometrically tight criterion and permeability, an under filter layer will be applied at the lake side whereas at the North Sea side solely a filter layer will required between the bed material and the top layer. An overview of the full cross-sectional area of the bed protection has been provided in Figure 61.
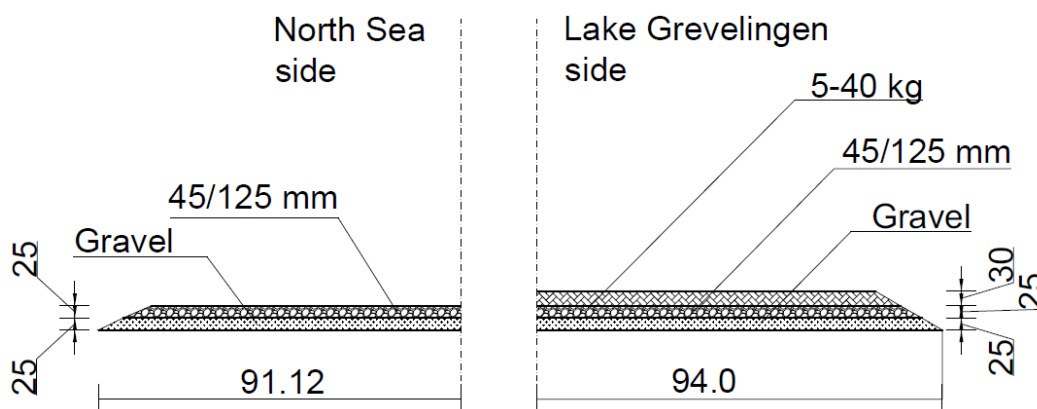
FIGURE 61: CROSS-SECTION BED PROTECTION

Protection against scour underneath the structure will be provided by constructing the rubble foundation bed like a filter. Preventing basic material to be flushed out or moved away through the filter layer reduces the damage to the foundation. Therefore, the foundation should comply with the geometrically closed filter criteria. Ensuring the flow velocity in superjacent filter layers to become sufficiently low, any further damage is controlled. This second method implies that during the operational phase of the Tidal Power Plant the erosion becomes adequately small, damage to the foundation will be prevented.

The rubble foundation bed shall be constructed according to the filter requirements and criteria. These prescribed criteria are described in the succeeding section. From the criteria the final rubble foundation bed composition is computed. On top of the rubble foundation bed the Tidal Power Plant will be sunk.
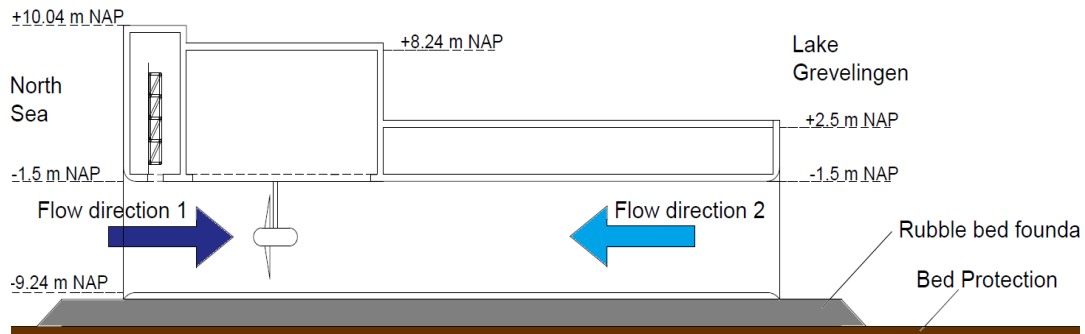
FIGURE 62: SCHEMATIZATION FLOW DIRECTION

6.4.1 REQUIRED MATERIAL

For the armour stone under layer a strict criterion is set by the shore protection manual [CERC, 1984], this criterion reads:

$$\frac{D_{n50a}}{D_{n50u}} = 2.2 \; to \; 2.5$$

The subscript "a" and "u" are used to express the armour layer and under layer respectively.

With the calculated governing armour size of $D_{n50a} = 0.76 \, m$ from Appendix C.4, the corresponding armour size has been determined using Figure 134 Appendix C.4. The available armour units best matching with this nominal diameter is 1000-3000 kg, $D_{n50} = 0.93 \, m$. The required diameter of the first under-layer lies between $0.37 \, m < D_{n50u} < 0.42 \, m$.

The rubble mound material average weight is calculated using:

$$d_{n50u} = \left(\frac{M}{\rho}\right)^{\frac{1}{3}} \rightarrow 134.4 \, kg < M_{50} < 196.3 \, kg$$

This corresponds to rubble material class 60-300 kg light armour stone, with a nominal diameter of $d_{n50u} = 0.41 \, m$, obtained from Figure 134. The slope of the rubble mound

material is set to 1:2 at the sea side and 1:2 at the Lake side [Goda, 2010]. The 60-300 kg light armour stone will be located directly underneath the caisson. Hence, the caisson and light armour stone are in direct contact during the Tidal Power Plants lifetime.

The interface stability, the filter stability at the interface of two different granular materials, is described with the geometrically tight criterion. A layer becomes geometrically tight if no smaller grains are transported through the filter layer. If both materials are well-graded and comply with the criterion described above, the geometrically tight criterion reads:

$$\frac{D_{f15}}{D_{b85}} < 5$$

The subscript "f" and "b" are used to express the filter layer and base layer respectively. For the 60-300 kg under-layer a $D_{f15} = 0.32\ m$ is obtained. Hence the base layer requires $D_{b85} > 0.065\ m$. The corresponding coarse grading filter layer is 45/125 mm. The nominal diameter of this material is $d_{n50} = 80\ mm$. These values are based on Figure 134, Appendix C.4.

To guarantee stability while placing the filter material at a depth of more than -10 m NAP, it is necessary to make any separate layer thick enough. This means a filter layer thickness of at least 0.5 meter should be constructed [Verhagen et al. 2012].

As a consequence of widely graded material, internal instability may occur. The criterion for internal stability of geometrically tight filter is given in Pilarczyk [1998]. This criterion limits the grading width and the coefficient of uniformity of the filter layer and is described as:

$$\frac{D_{60}}{D_{10}} < 10$$

The different layers are due to comply with this criterion. It is up to the supplier to ensure this criterion is met.

The filter functions as a medium water flowing through. The general criterion for permeability of the filter layer is to prevent pore pressures contributing to instability of the structure, by ensuring a certain flow resistance. This requirement on permeability is simplified to:

$$\frac{D_{f15}}{D_{b15}} > 4\ to\ 5$$

The filter layer shall be constructed on top of an assumed to be loosely packed sand layer. In the boundary conditions, paragraph 3.3, the particle size close to the Brouwersdam has been presented. From the Figure 19in the Bourndary condtions, paragraph 3.3, it has been concluded, D_{b85} =0.6 mm.

D_{f15} of 45/145 mm coarse grading is 50 mm. This means the geometrically tight criterion is not met, therefore a gravel bed will be applied. The characteristics of this gravel bed is similar to the gravel bed charactertics of the bed protection. Hence the bed protection filter layer, located on the sand bed, will be applied over the full length of the Tidal Power Plant as well.

The constructability of geotextile underneath the Tidal Power Plant is questionable, since a very large area should be protected and placing a geotextile is not necessarily easy. Especially the buoyancy and air bulbs underneath the geotextile make it hard to sink it properly. However, since no large currents are expected at the lake side of the Brouwersdam, the constructability of geotextile increases and it therefore assumed geotextile is applicable.

A common geotextile criterion, according to the geometrically tight principal reads:

$$D_{min} \leq O_{90,w} \leq D_t$$

In which $O_{90,w}$ represents the filtration opening size of the geotextile filter measured according to EN ISO 12956:1999. D_t represents the indicative diameter of the soil particles to be filtered, corresponding to the soil skeleton to be stabilized (m).

D_{min} represents the minimum value of the geotextile opening size corresponding to the largest fine particles being transported in suspension (m).

Giroud et al. [1998] estimated the minimum value of $D_{min} \cong 50 \mu m$. The standard NF G38061:1993 defined D_t as given here:

$$D_t = CD_{b85}$$

The construction in the wet allows the construction side to be partly at the toe of the current Brouwersdam and partly behind it. Whether this assumption is valid should be investigated at site. For now the value C for loosely packed sand is assumed to suffice with the construction situation. For $D_{60b}/D_{10b} < 5$ the coefficient C for dense packed soil is $C = 0.4$. The required filtration opening of the geotextile is:

$$50 \mu m \leq O_{90,w} \leq 0.4 * 0.6 \; mm$$

The permeability criterion for the geotextile at coastal protection structures reads [Giroud, 1996]:

$$k_f \geq 100 k_b$$

Sinking the geotextile to its proper position becomes a challenge when the geotextile is light and the buoyancy is oversized. Therefore, a composite geotextile or mattress should be applied, which sink easily to its final position. The proper geotextile should be found using scaled tests, which is not within the scope of this thesis.

6.4.2 LAYER THICKNESS

The effective layer thickness of both the armour and first under-layer are calculated by:

$$t = nk_t d_{n50}$$

In which n represents the number of stones across the layer, k_t represents the thickness and d_{n50} represents the nominal diameter of the considered layer. The value for k_t is assumed to be 1.0 for the first under-layer. For a double standard placed armour layer the value of k_t is set to 0.91 [Rock Manual, 2007]. This value is obtained from a spherical food staff method for blocky rock. For both it has been assumed, stability will be ensured

for $n = 2$. An overview of the rubble foundation bed cross-section layers is given in Table 21:

Layer	Material	Nominal diameter d_{n50} (m)	Thickness k_t	Effective layer thickness t (m)
Armour	1000-3000 kg	0.93	0.91	1.38
First under-layer	60-300 kg	0.42	1.0	0.84
Filter layer	45/125 mm	0.065	-	0.5

TABLE 21: EFFECTIVE LAYER THICKNESS CROSS-SECTION RUBBLE FOUNDATION BED

6.4.3 BED PROTECTION COMPOSITION

The final rubble foundation bed cross section is shown in Figure 63.
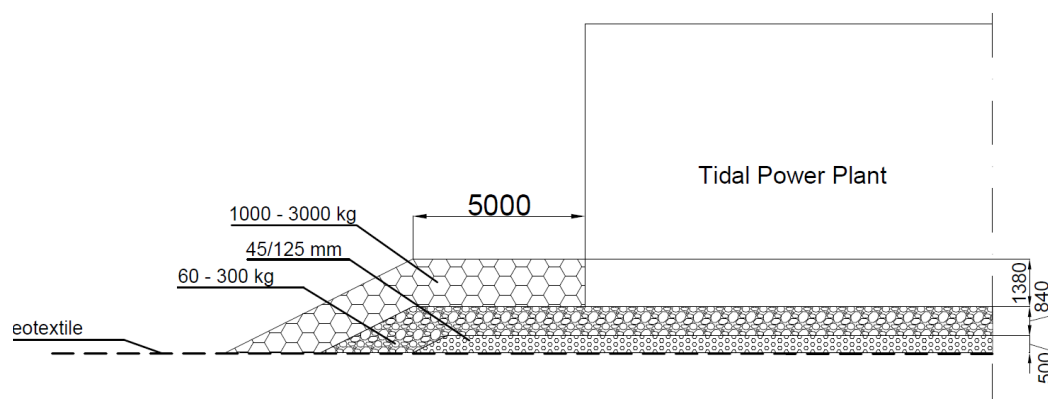
FIGURE 63: RUBBLE FOUNDATION BED TRANSVERSE CROSS SECTION

Including the bed protection results from section 6.3.5 has resulted in Figure 64 and Figure 65 displayed on the next page.

NAP

- 11.58 m NAP

Bottom protection

86.12   5.0   52.676   5.0   89

237.8
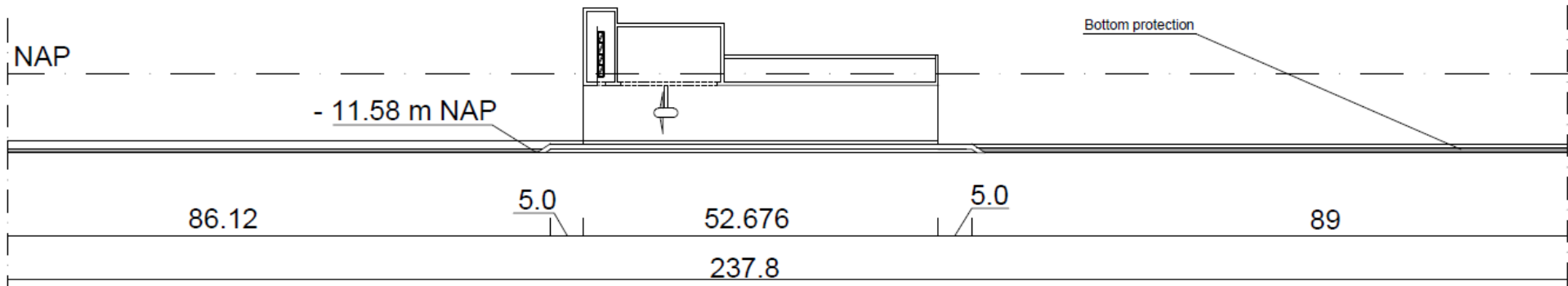
FIGURE 64: TRANSVERSE CROSS-SECTION TIDAL POWER PLANT INCLUDING THE BED PROTECTION LENGTHS

NAP

1000-3000 kg
60-300 kg
45/125 mm
Gravel

5-40 kg
45/125 mm
Gravel
60-300 kg

25
25

30
25
25

FIGURE 65: CROSS-SECTION BED PROTECTION AND RUBBLE FOUNDATION BED

6.4.4 STIFFNESS OF ROCKFILL

For structural calculation purposes the stiffness of the rockfill will be a key parameter. However, information regarding the stiffness of a rockfill is very limited. The values for virgin loading and cyclic loading largely depend on the crushing potential of the grains. For excellent quality rockfill the material parameters fall in the same range as for quartz sand or gravel. Lower quality rock on the contrary is more compressible, especially at high effective stress and at strong cyclic loading [Rock Manual, 2007].

Large scale oedometer tests should be performed to determine the actual stiffness of the rockfill. Information obtained from these tests the deformation of the rockfill during and after construction is computed. Hence, the quality of the rock is defined and appraised to the required standards.

For design purposes a value of the compressibility of the quarry run rock has been assumed, based on the available data regarding quartz sand from the Rock Manual [2007]. A value between 10 and 100 MPa for plastic loading has been described. Therefore, an average value of 50 MPa is assumed to be reasonable.

6.4.5 CONSTRUCTION METHOD OF THE RUBBLE FOUNDATION BED

The chosen construction method in the wet obligates the construction works to be performed from the water. Since all construction works are executed at the lake side of the Brouwersdam, while the dam conducts it flood defending function, the water conditions are mild. Hence, waterborne equipment should be able to execute the construction works at any time within certain precision.

Especially an uneven bedding would mean high unwanted local forces on the bottom slab of the Tidal Power Plant. Therefore, the precision of work execution will be the principal endeavour for determining the construction method.

The placement of the coarse material does already require some precision. With small currents the particles sink to a distance of the actual location. Moreover, to counteract transportation costs of the required equipment, it is wise to use similar equipment for each layer.
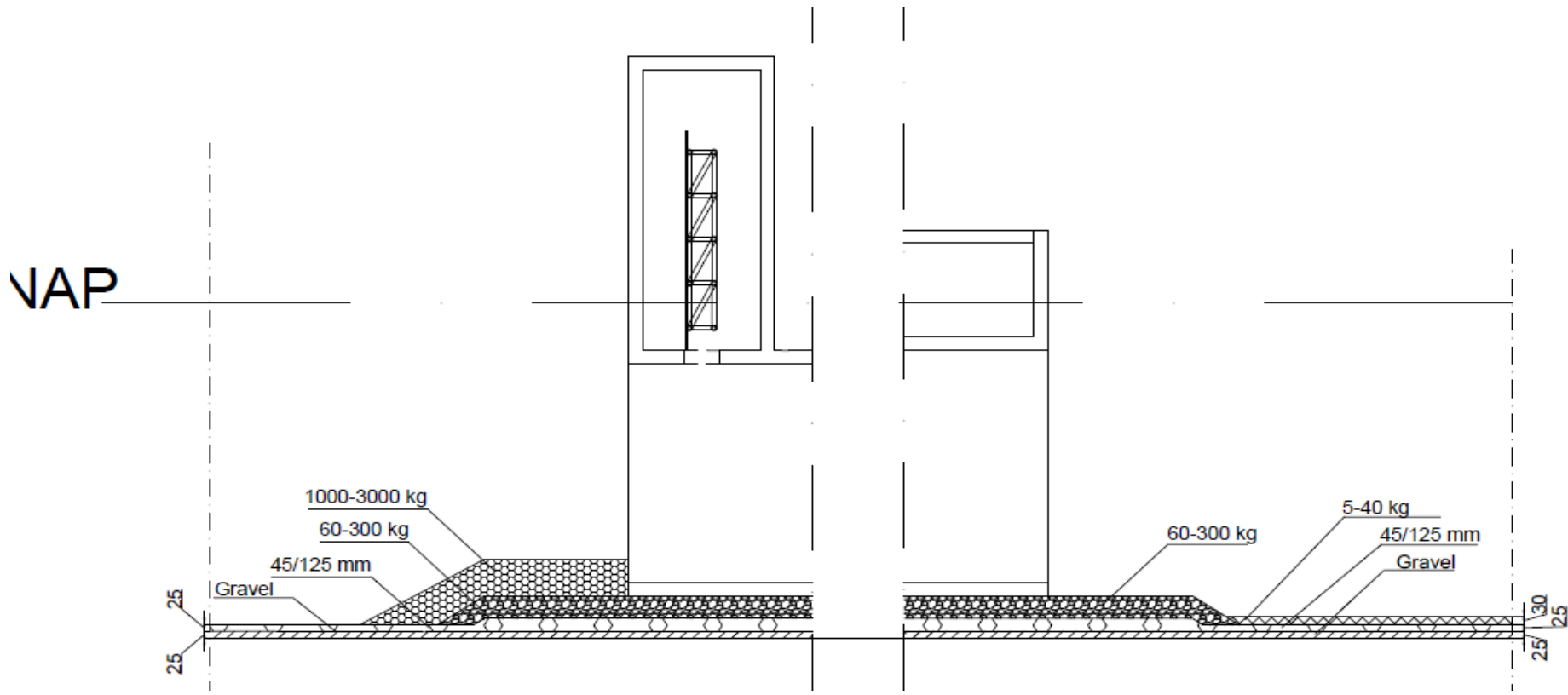
For controlled placement three types of waterborne placement equipment are possible:

- Side stone-dumping vessel or barge (Figure 67)
- Flat-top barges with wheel loader or excavator (Figure 66)
- Pontoon or vessel with a wire-rope crane

The latter one is mainly used for heavy armour material. The armour at the Tidal Power Plant does not require such heavy machinery. The best option would be a combination of the first two types of equipment. The side stone-dumping vessel or barge enables to place a large amount of material at the same time. Placement of the coarse material and the light armour stone could be quick and quite accurate. With a flat-top barge accommodated with excavator, the final height of each layer could be easily controlled. Especially when using large range excavators provided with GPS systems. These GPS systems give the operator the ability to behold the actual depth of the layer. Uneven spots are easily flattened by the bucket of the excavator. Moreover, the placement of the armour material requires precision as well. Dumping armour rock on top of the 60-300 kg layer could lead to damage to the Tidal Power Plant which, an on its turn, could lead to a reduction in durability of the Tidal Power Plant.

During the placement process, tolerances are strict and therefore extensive monitoring will be required. Though, the structure should be able to bear local forces as a consequence of uneven bedding.

FIGURE 66: EXCAVATOR ON FLAT TOP BARGE [VAN OORD]

FIGURE 67: SIDE STONE-DUMPING VESSEL [ROCK MANUAL, 2007]

The figures provided in this section give an overview of the Tidal Power Plant constructed in the Brouwersdam.
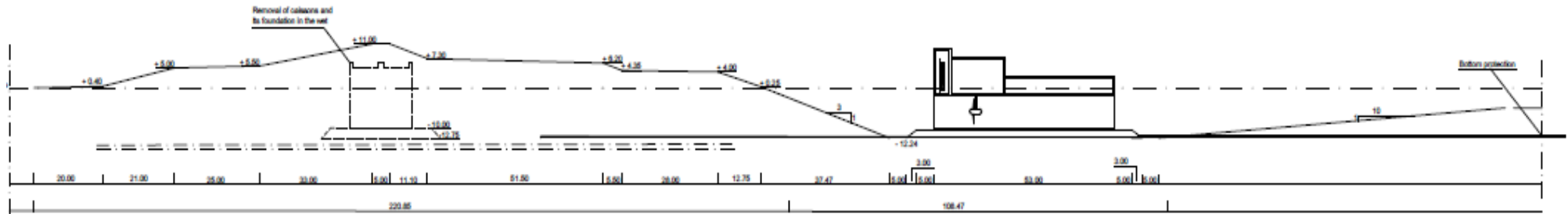

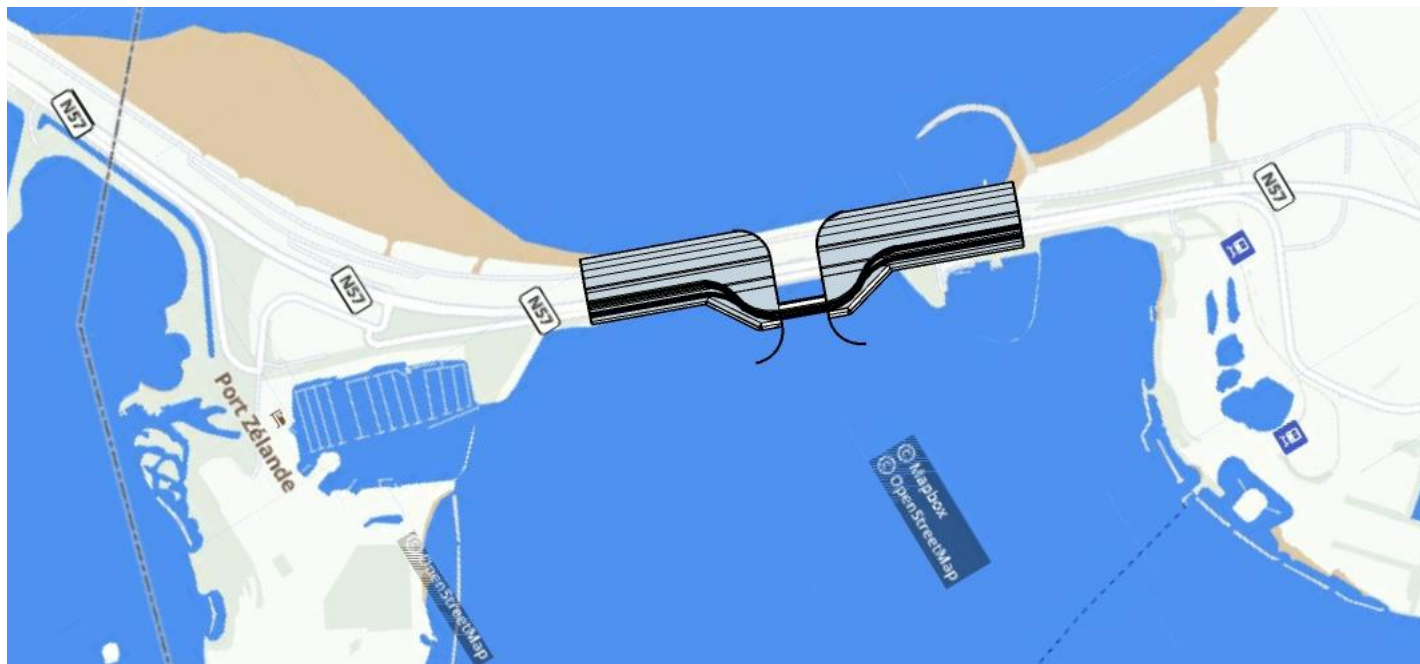FIGURE 68: SKETCH CROSS-SECTION TRANSVERSE DIRECTION CONSTRUCTION METHOD IN THE WET

FIGURE 69: SCHEMATIZATION TOP VIEW LOCATION TIDAL POWER PLANT FROM LAKE GREVELINGEN SIDE[SKETCH-UP]

7 CONCEPTUAL DESIGN STRUCTURAL ELEMENTS

Chapter 6 provided the integration of the Tidal Power Plant in the Brouwersdam. Due to many uncertainties the construction method in the wet has been chosen as best applicable. This construction method induces the final location of the Tidal Power Plant adjacent to the current Brouwersdam. Therefore a new foundation will be constructed. The layout of this foundation has also been described in chapter 6. On top of a rubble foundation bed the Tidal Power Plant will be sunk after towing it from an external construction dock towards its final position.

A rubble foundation bed is subject to level and stiffness deviations. The Tidal Power Plant should be able to bear the effects of these deviations. This chapter will therefore be dedicated to determine the effects of the rubble foundation bed deviations.

With checks obtained from the EN-1992-1-1 the assumed wall and slab thickness of 500 mm will be examined. The assessment will be executed from a global simplistic level towards a more detailed local level.

The design of structural elements should, according to EN-1992-1-1, be performed regarding several limit states. These limit stated will be described in paragraph one. Within the conceptual approach in this thesis the concrete members will be considered in the ultimate limit state (ULS).

The conceptual design of the Tidal Power Plant starts with considering the Tidal Power Plant as a monolithic structure located on homogeneous stiff bedding and subject to extreme external conditions, such as wave impact and high hydraulic pressures. In a first simplistic check, the resistance of the monolithic structure to these extremes will be determined using a simplistic approach. Both the shear and bending resistance will be elaborated on a global level in paragraph 7.2.

The second check concerns the approach to determine the resistance to locally applied external loads or the concrete element's self-weight. Combining this local approach with the simplistic global approach provides a first estimation whether the concrete thickness requires increments or not. The local approach will therefore be discussed in paragraph 7.3.

The third step will be the appliance of the primary deviations. From classical beam theories it has been decided the beam on elastic foundation theory is best applicable to the Tidal Power Plant constructed on top of rubble material bed. Having considered the rubble material bed as a homogeneous elastic foundation, the first deviations apply; external forces. The extreme weather conditions result in large hydraulic pressures in transverse direction. Moreover, the adjacent dike executes large lateral earth pressures in longitudinal direction. The emerging forces within the monolithic structure are therefore considered in paragraph 7.4. From the monolithic structure a more detailed approach will be applied, determining the required reinforcement in slabs and inner walls.

Fourth, the second deviation applies; uneven bedding. The rubble material bed induces an uneven bedding constant as a consequence of uneven bedding or variations in the rubble material stiffness. Subparagraph 7.4.2 describes the influence of two base cases in a one dimensional model.

The succeeding step concerns considering the beam on non-homogeneous foundation in a 2 dimensional model. Torsional moments will arise, which results in additional shear reinforcement. Subparagraph 7.4.3 will be dedicated to the 2 dimensional approach.

Finally a conclusion will be made regarding the assumed thickness of the concrete elements based on the simplistic global approach, the beam on homogeneous foundation and the beam on non-homogeneous foundation.

7.1 LIMIT STATES OF CONCRETE MEMBERS

The ability to resist external loads determine the cross sectional composition of the structural components in the caisson. The capacity of each cross section is verified using EC 2. In total five types of limit state situations are considered here.

Bending Moment Capacity in the ultimate limit state (ULS) of each member with their effective reinforced are in both horizontal as vertical, at mid span and the support ends. The design bending moment is obliged to be smaller than the resisting moment of the concrete cross section($M_{ed} < M_{Rd}$).

Shear capacity in **ULS** is checked based on the ability to resist shear forces without using reinforcement. Applying shear reinforcement is required when resisting shear capacity is lower than the actual shear capacity:($V_{Rd} > V_{ed}$).

Torsion capacity is checked where the static equilibrium of a structure depends on the torsional resistance of elements of the structure. This might be the case for the load conditions during wave impact. A full torsional design covering both ULS and Serviceability limit states (SLS). Calculating the torsional resistance of a section is performed on the basis of a thin-walled closed section, in which equilibrium is satisfied by a closed shear flow. The maximum resistance of a member subjected to torsion and shear is limited by the capacity of the concrete struts. In order not to exceed this resistance $\frac{T_{Ed}}{T_{Rd,max}} + \frac{V_{Ed}}{V_{Rd,max}} \leq 1.0$.

Stress capacity in SLS is checked whether the stress in a concrete member does not exceed the critical stress capacity of the structure. Exceeding the stress capacity, leads to cracking of the concrete and a reduction in the structure's durability. If it does, the required amount of reinforcement steel is calculated for that cross section, allowing absorbing the stress.

Crack control in SLS shall be limited to an extent that will not impair the proper functioning or durability of the structure or cause its appearance to be unacceptable. As a consequence of certain crack width reinforcement steel starts eroding and loses its strength and capacity. Therefore, crack widths in hydraulic structures exposed to sea water should be reduced to almost zero.

The Eurocode provides a limitation to the maximum crack width. In the environmental conditions of class XS2 and XS3 the maximum allowed crack width is $w = 0.1\ mm$, obtained from EN 1992-1-1-2004.

Maximum deflection in SLS is checked in order to ensure the structure is able properly function. The appearance and general utility of the structure could be impaired when the calculated sag of a beam, slab or cantilever subjected to quasi-permanent loads exceeds span/250. For the deflection after construction, span/500, is normally an appropriate limit for quasi permanent loads [EN-1992-1-1-2004].

The checks performed in this thesis will solely be based on the ULS checks and torsion capacity. Therefore, in further research the SLS checks will have to be included.

7.2 SIMPLISTIC GLOBAL RESISTANCE CHECKS

The global resistance checks provides a first estimation whether the assumed element thickness of 500 mm suffices the required resistance to global forces. The checks will be executed for bending, in 7.2.1 and shear, in 7.2.2.

7.2.1 BENDING RESISTANCE

As a starting point the global equilibrium of a monolith structure will be considered. A monolithic structure will simply be constructed on a stiff rubble foundation bed. The influence of the rubble material will thus not be taken into account (yet). The Tidal Power Plant preliminary design will be simplified within the monolith structure, this results in the following assumptions:

- Powerhouse outer dimensions apply
- Hollow sections will be left out for simplicity
- The powerhouse full weight, including filled sluiceways, will apply to the monolith structure. Without safety factor it contains $181.87 \ kN/m^2$.

A schematization of the monolith structure has been illustrated in Figure 70.
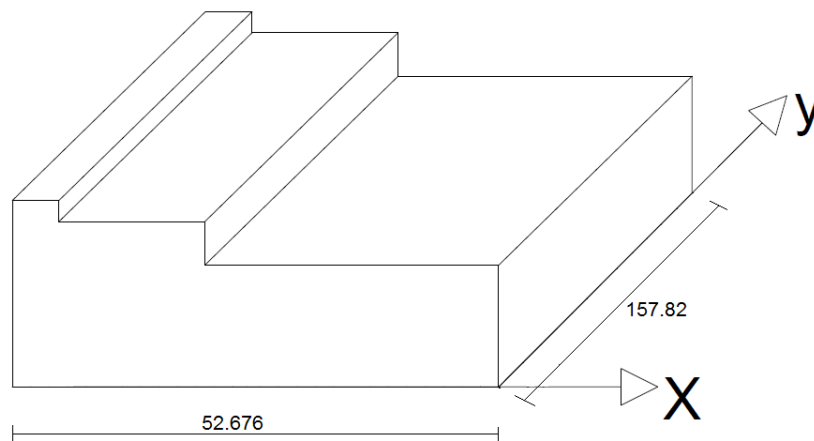
FIGURE 70: MONOLITHIC STRUCTURE WITH TIDAL POWER PLANT DIMENSIONS (METER), NOT TO SCALE

Since the Tidal Power Plant will be constructed at an external construction dock, transported towards its final position and sunk on top of the rubble foundation bed, the structure will be subject to multiple load scenarios. The distinguishable load scenarios are defined as specific phases during the lifetime of the Tidal Power Plant. These phases and corresponding load scenarios have been elaborated in Appendix D.5. In transverse direction, the governing load scenario has been obtained from the Operational phase, illustrated in Figure 71.
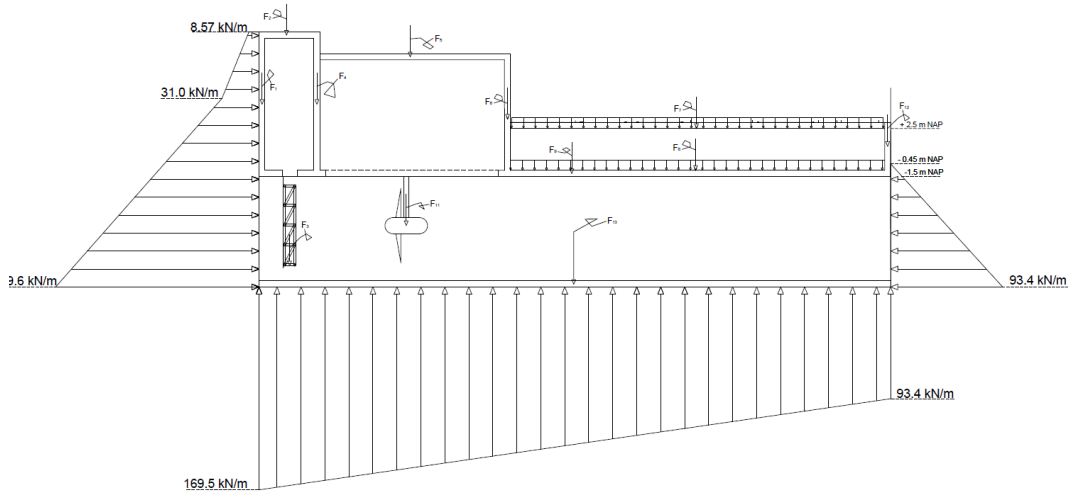
FIGURE 71: RESULTING LOAD DISTRIBUTION EXTREME CONDITIONS TRANSVERSE DIRECTION

The governing stresses within the monolithic structure can be found by considering three distinguishable sections inclined by the adjacent sections. An overview of these sections has been presented in Figure 72. Hence, three inclination situations are described:

a) Section 1 inclined by the combination of section 2 and 3.
b) Section 2 and 3 inclined by section 1
c) Section 3 inclined by section 1 and 2
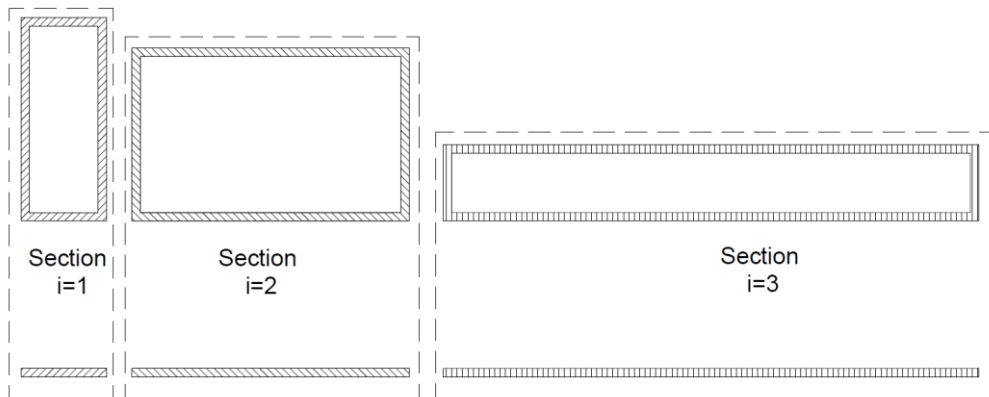
FIGURE 72: OVERVIEW SECTIONS 1, 2 AND 3 IN THE TRANSVERSE CROSS-SECTION

The governing moment will be determined by assuming an average upward water pressure over the full transverse length of the monolithic structure:

$$q_w = \frac{q_{w1} + q_{w2}}{2} = \frac{169.6 + 93.4}{2} \, 131.5 \, kN/m^2$$

The uniform distributed design load in ULS, resulting from the Tidal Power Plant's self-weight equals:

$$q_{Ed} = q_G * \gamma_G = 182.53 * 1.35 = 246.4 \, kN/m^2$$

A vertical equilibrium is reached for upward foundation pressures equal to:

$$q_f = q_{Ed} - q_w = 114.9 \; kN/m^2$$

The governing situation will appear for inclination situation (c), the resulting uniform load will now be computed by sketches from Figure 73:
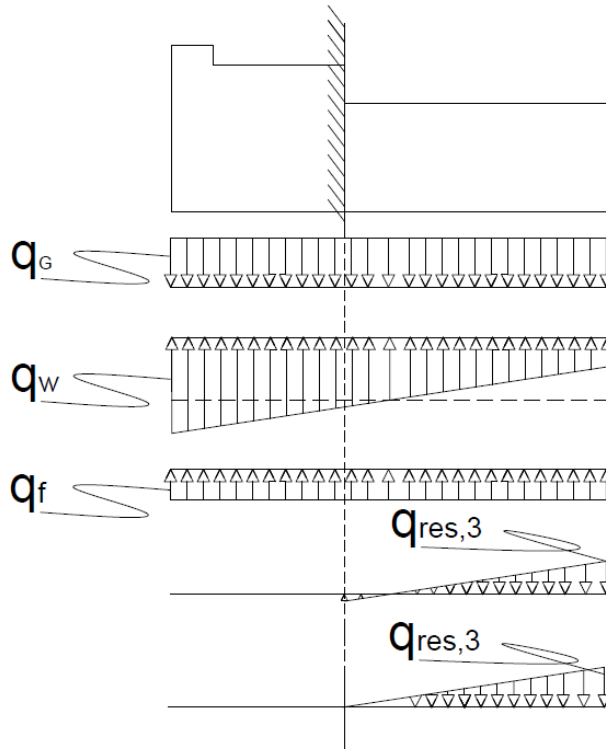
FIGURE 73: SKETCH DETERMINE UNIFORM LOAD

It may be noticed the load has been simplified by assuming no upward forces are present at section 3. This increases the governing moment and results in a small overestimation.

$$q_{res,3} = q_{Ed} - q_f - q_{w3} = 246.4 - 114.9 - 93.4 = 38.1 \; kN/m^2$$

The moment at the intersection between section 2 and 3 equals:

$$M_3 = \left(\frac{2}{3}\right) l_3 * 0.5 * q_{res,3} l_3 = \left(\frac{2}{3}\right) * 31.7 * 0.5 * 38.1 * 31.7 = 12762.1 \; kNm/m$$

From here on the subscript 'y' will be applied when considering the cross-section in longitudinal direction. The transverse direction will be appointed with subscript 'x'.

With the longitudinal length the governing moment in longitudinal direction (y) results in:

$$M_{y,3} = 12762.1 * 157.82 = 2.01 * 10^6 \; kNm$$

A very simplistic method will now be applied to determine the stresses in a bottom slab with a thickness of 500mm. The moment divided by the section's height (h_3)results in a force F_3:

$$F_{y,3} = \frac{M_{y,3}}{h_3} = \frac{2.01 * 10^6}{13.24} = 1.52 * 10^5 \; kN$$

132

The stress in a 500 mm thick slab over the full length becomes:

$$\sigma_{y,3} = \frac{F_3}{A_{slab,3}} = \frac{1.52 * 10^5}{157.82 * 0.5} = 1923.87 \; kN/m^2 = 1.92 \; N/mm^2$$

The tensile stress according to this very simplistic approach reaches a value of $1.92 \; N/mm^2$. The design yield stress equals $f_y = 435 \; N/mm^2$. The total required cross-sectional area of reinforcing steel now becomes:

$$A_{s,3} = \frac{F_{y,3} * 10^3}{f_y} = \frac{1.52 * 10^5}{435} * 10^3 = 3.49 * 10^5 mm^2$$

The reinforcement ratio in longitudinal direction accordingly equals:

$$\rho_{y,3} = \frac{A_{s,3}}{A_c} = \frac{3.49 * 10^5}{157.82 * 10^3 * 0.5 * 10^3} = 0.44 \; \%$$

As mentioned, this approach can be considered very simplistic. The reinforcement ratio remains below the economic reinforcement ratio of 1%, which would mean the assumed slab thickness may be considered acceptable.

In transverse direction (x) the similar resulting uniform load $q_{res,3}$ applies. However, this load will now be considered over a one meter thick strip, applying over the transverse length of section 3.

The corresponding governing moment results from:

$$M_{x,3} = \left(\frac{2}{3}\right) l_3 * 0.5 * q_{res,3} l_3 * 1 = \left(\frac{2}{3}\right) * 31.7 * 0.5 * 38.1 * 31.7 * 1 = 12762.1 \; kNm$$

Applying the simplistic method, the stresses at the bottom and top slab are determined by:

$$\sigma_{x,3} = \frac{M_{x,3}/h_3}{A_{slab,3}} = \frac{\frac{12762.1}{13.24}}{31.7 * 0.5} = 0.061 \; N/mm^2$$

The required cross sectional of reinforcing steel becomes:

$$A_{s,3} = \frac{M_{x,3}/h_3 * 10^3}{f_y} = \frac{12762.1}{13.24} * \frac{10^3}{435} = 2215.87 \; mm^2$$

The transverse reinforcement ratio results in:

$$\rho_{x,3} = \frac{A_{s,3}}{A_c} = \frac{2215.87}{31.7 * 10^3 * 0.5 * 10^3} = 0.014 \; \%$$

In transverse direction the governing required reinforcement ratio seems to be minimal, and no modifications to the slab thickness are required.

The next step in the global computation will be a more detailed approach. The initial dimensions of the Tidal Power Plant are reintroduced.

The above computed moment will remain unchanged, the stress will however be determined using the second order of inertia and the heart to heart distance 'd' between the top and bottom slab, see Figure 74.
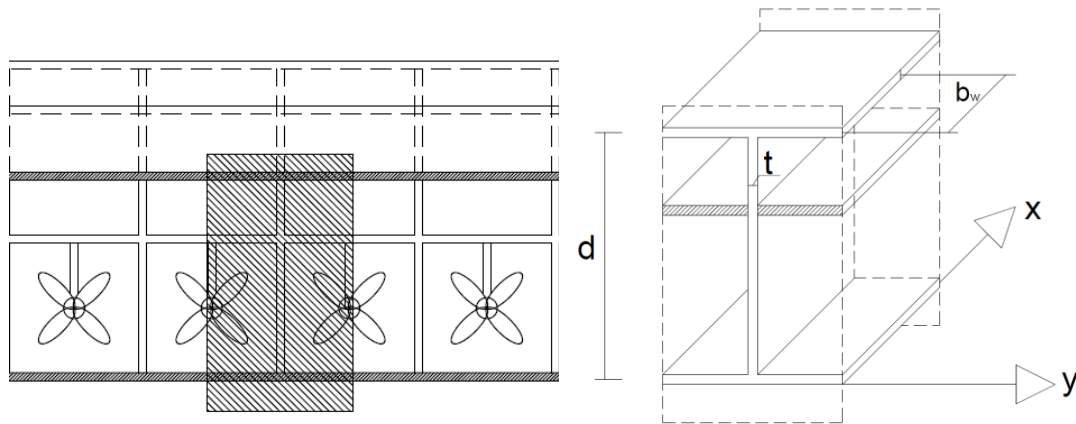
The actual dimensions and layout of the Tidal Power Plant will now be used. The above calculated moment applies in longitudinal direction (y-direction).

$$\sigma_{y,3} = \pm \frac{M_{y,3} * d_3}{I_{y,3}}$$

Where:

d_3 *represents the heart to heart distance between the top and bottom slab*

       within section 3.

$I_{y,3}$ *represents the second order moment of inertia of the longitudinal cross −*

       section in section 3

It has been assumed the governing moment will be absorbed by the top and bottom slab of the cross-section. In this situation the tensile stress will emerge at the bottom slab.

The second order of elasticity has been calculated for the full longitudinal cross sectional with the Steiner rule.

$$\sigma_{y,3} = \pm \frac{M_{y,3} * z_3}{I_{y,3}} = \frac{2.01 * 10^6 * 12.74}{8385.29} = 3.05 \ N/mm^2$$

From a horizontal equilibrium the tensile force in the reinforcement steel should be equal to the concrete compression force:

$$N_s = N_c \rightarrow A_s * f_y = N_c$$

It is assumed the concrete compression zone equals the top slab thickness with a width of 1 meter in transverse direction (x):

$$N_c = 500 * 3.05 * 1000 = 1.525 * 10^6 \ N$$

This results in a required cross-sectional area of reinforcing steel of:

$$N_s = N_c \rightarrow 1.525 * 10^6 = A_s * 435 \rightarrow A_s = 3505.7 \ mm^2$$

The reinforcement ratio now becomes:

$$\rho_{y,3} = \frac{A_{s,3}}{A_c} = \frac{3505.7}{500 * 1000} = 0.7\%$$

Hence the reinforcement ratio in longitudinal direction lies below the 1% economical value of the reinforcement ratio and thus the thickness remains sufficient with regard to solely bending.

In transverse direction a similar approach will be applied with the governing moment $M_{x,3} = 12762.1 \ kNm$.

$$\sigma_{x,3} = \pm \frac{M_{x,3} * z_3}{I_{x,3}} = \frac{12762.1 * 12.74}{1297.6} = 0.125 \ N/mm^2$$

It is assumed the concrete compression zone equals the top slab thickness with a width of 1 meter in longitudinal direction (y):

$$N_s = N_c \rightarrow 500 * 0.125 * 1000 = A_s * 435 \rightarrow A_s = 144.02 \ mm^2$$

The corresponding reinforcement ratio reads:

$$\rho_{x,3} = \frac{A_{s,3}}{A_c} = \frac{144.02}{500 * 1000} = 0.03\%$$

In transverse direction the required reinforcement ratio is minimal. This reinforcement ratio should however been taken into account when considering the total reinforcement ratio in the slab.

In sections 1 and 2 the reinforcement ratio will decrease due to the height of each section. Since the height will be used in the stress calculation, where it reduces the stress as the height increases, the reinforcement ratio from section three becomes governing.

One side note regarding the detailed approach should be made, the compression zone has now been taken at the full thickness of the top slab. In reality the inner walls will contribute to the compression zone.

7.2.2 SHEAR RESISTANCE

At first a simplistic method will be applied to determine the required shear reinforcement. The structure is considered in y-direction. From the preliminary powerhouse design it appeared in total 18 turbines will be applied in the Tidal Power plant. Hence in total 19 walls are present in the longitudinal cross-section.

Section 3 inclined by section 2 will be considered again. The governing resulting load $q_{res,3}$ will be assumed to be fully present in 1 meter thick strip over the full longitudinal length of the cross section, the total governing shear force emerges:

$$F_{l,3} = q_{res,3} * 157.82 * 1 = 5018.7 \ kN$$

This force accounts for the shear force over the full cross-section in y-direction. Since in total 19 walls are present with an effective length of the height 'd' and a wall thickness 't' mm, the shear stress in each wall becomes:

$$\sigma_{shear,l} = \frac{F_{l,3}}{d_3 * 19 * t} = \frac{5018.7}{12.74 * 19 * 0.5} = 0.041 \ N/mm^2$$

The shear resistance of concrete subject to shear is calculated using the minimum shear resistance equation, obtained from EN 1992-1-1:

$$v_{min} = \left(0.035 k^{\frac{3}{2}} f_{ck}^{\frac{1}{2}} \right)$$

Where:

$$f_{ck} = 45 \ N/mm^2$$

$$k = 1 + \sqrt{\frac{200}{d_3}} = 1 + \sqrt{\frac{200}{12.74*10^3}} \approx 1$$

Resulting in:

$$v_{min} = \left(0.035 k^{\frac{3}{2}} f_{ck}^{\frac{1}{2}} \right) = 0.035 * 1 * 45^{\frac{1}{2}} = 0.235 \ N/mm^2$$

The minimum shear resistance has not been exceeded by $\sigma_{shear,l}$. Shear reinforcement will thus not be required.

A note must be made with regard to this approach, the influence of the top mid and bottom slab attached to the inner walls, see Figure 74, has not been taken into account. It is expected the influence of these slabs will be small due to its height of thickness of 500 mm with respect to the effective thickness of the walls; 12.74 m at section 3.

7.2.3 CONCLUSION SIMPLISTIC GLOBAL APPROACH

As a starting point the governing load situation in a global approach has been applied to section 3 of the transverse cross-section. Due to the height of this cross-section, the results may be considered as governing. A resulting 0.7% reinforcement ratio does not imply the thickness of the structural elements should be increased. The applied approach will furthermore be used in any further bending resistance calculations.

In the first estimation shear reinforcement will not be required in the inner walls of the longitudinal cross section. Hence, the assumed wall thickness of 500 mm seems to be able to resist the global shear forces. Moreover, the applied shear resistance approach will be used in further shear resisting calculations.

In this simplistic situation the structural elements within the Tidal Power Plant will not solely be subject to global forces, therefore the succeeding paragraph will determine the resistance to local forces.

7.3 SIMPLISTIC APPROACH TO RESISTANCE OF LOCAL BENDING MOMENTS

From the detailed step made in the global approach an even more detailed step will be made in the local approach. This section will describe the approach of local emerging forces at structural elements within the structure. Due to external and local load situations, such as self-weight from structural elements, these structural elements require local steel reinforcement as well. A distinction between structural elements will be made, see Figure 75.

- Top slab
- Mid slab
- Bottom slab
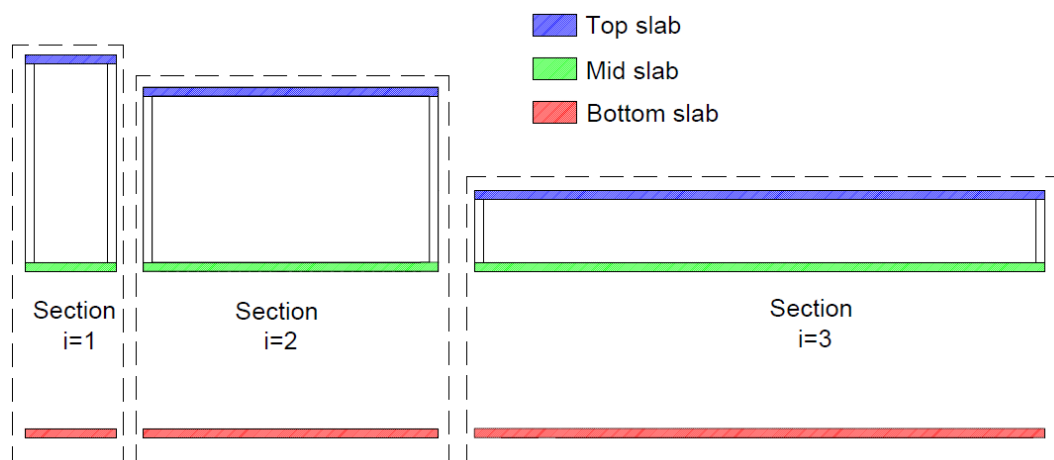
FIGURE 75: OVERVIEW SLABS WITHIN CROSS-SECTION

The bending reinforcement as a consequence of the element's self-weight or local external loading will become governing for each slab, where the influence of inner walls will be included as well. Hence this approach might be considered as a more detailed approach of the bending reinforcement. Each slab will therefore be considered separately later. A general approach will however be applied to determine the required reinforcement:

7.3.1 GENERAL APPROACH

The general approach will consist of a number of steps to be elaborated. These steps will be provided here, equations are obtained from EN-1992-1-1.

1. Consider a slab inclined at all four edges, due to the stiff connection with the inner walls.
2. Determine the governing slab load distribution direction using Figure 76.
   It is assumed, when the ratio $\frac{l_y}{l_x} > 1.5$ or $\frac{l_y}{l_x} < 2/3$, the load will be mainly distributed in one direction; ($k_j = 1$). The perpendicular direction absorbs in that case 20% of the total moment is absorbed ($k_j = 0.2$).

FIGURE 76: LOAD DISTRIBUTION CONSTANT FOR PARTICULAR INCLINATIONS [WALRAVEN, 2011]

3. Determine the governing uniform load in the governing direction
4. Compute the governing moment using:

$$M_{Ed,j} = \frac{1}{12} k_j q_{ed,j} l_j^2$$

Where

q_j *represents the uniform load in the governing direction* $(j = x \text{ or } y)$

k_j *represents the load distribtution constant in direction j*

l_j *represents the span in direction j*

The governing moment will be located at the slab's edges.

5. Determine the stresses over the slab's cross section with:

$$\sigma_j = \pm \frac{M_{Ed,j}}{W_j}$$

Where W_j represents the section modulus for a slab with $b = 1\,m$ representing the slab length one meter in perpendicular direction to the considered, and thickness t: $W_j = \frac{1}{6} b t^2$

6. Compute the compression zone and the corresponding steel reinforcement cross section with the following steps:
   a. Check the strain of concrete:

$$\varepsilon_c = \sigma / E_c$$

If $\varepsilon_c < 1.75‰$, the stress distribution over the slab thickness will be similar to Figure 77. The height of the compression zone 'x' will be found with:

$$\frac{\varepsilon_c}{\varepsilon_s} = \frac{x}{d - x}$$

$'d'$ represents the reduced slab height: $d = t_{slab,i} - c - \frac{1}{2}\phi_{main} - \phi_{stirrup.}$

ε_s represents the steel strain, $\varepsilon_s = \frac{f_{yd}}{E_s} = \frac{435}{2.0*10^5} = 2.175\ ‰.$

$\phi_{stirrup}$ represents the stirrup diameter and has been assumed at 12 mm.

139

b. The horizontal equilibrium between steel force and concrete compression force will be applied:

$$N_c = N_s \rightarrow \frac{1}{2} b x \varepsilon_c E_{cm} = A_s E_s \varepsilon_s$$

With $b = 1\,m$ representing the slab length one meter in perpendicular direction to the considered.

The reinforcement ratio becomes:

$$\rho_j = \frac{A_s}{t * b}$$

c. If $\varepsilon_c > 1.75‰$ a different approach will be applied and the slab starts cracking.
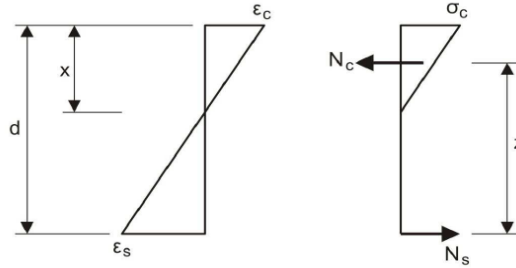
FIGURE 77: STRESS-STRAIN DISTRIBUTION ALONG SLAB [WALRAVEN, 2011]

7.3.2 TOP SLAB

Top slabs in each section are subject to the similar load; its self-weight. The top slab at section 3 will also be subject to an additional load from the road structure: $q_{road} = 10\,kN/m^2$. The governing reinforcement ratio will thus be found for a slab with the largest governing span:

- In transverse direction: top slab section 3 (31.7 meter)
- In longitudinal direction: all equal 8.74 meter

The load distribution constant in transverse direction for section 3 becomes $k_x = 0.2$, whereas the load distribution in longitudinal direction becomes $k_y = 1.0$.

The governing uniform load is defined as:

$$q_{ed} = t * \gamma_c * \gamma_G + q_{road} * \gamma_G = 0.5 * 25 * 1.35 + 10 * 1.35 = 30.38\,kN/m^2$$

In which $'\gamma_G'$ represents the partial factor for permanent actions, prescribed by NEN-1990: $\Gamma_G = 1.35$

$$M_{Ed,x} = \frac{1}{12} k_x q_{ed} l_x^2 = \frac{1}{12} * 0.2 * 30.38 * 31.7^2 = 508.7\,kNm/m$$

$$M_{Ed,y} = \frac{1}{12} k_y q_{ed} l_y^2 = \frac{1}{12} * 1 * 30.38 * 8.74^2 = 193.4\,kNm/m$$

Let's first consider the moment in transverse direction (x):

$$\sigma_x = \pm \frac{M_{Ed,x}}{W_x} = \pm \frac{508.7}{\frac{1}{6} * 1 * 0.5^2} = 12.2\,N/mm^2$$

The concrete strain contains: $\varepsilon_c = \frac{12.2}{30000} = 4.07 * 10^{-4} = 0.4‰$

The compression zone height, assuming reinforcement bar diameter of 20 mm, follows from:

$$\frac{\varepsilon_c}{\varepsilon_s} = \frac{x}{d-x} \rightarrow \frac{0.4}{2.175} = \frac{x}{(500-55-10-12)-x} \rightarrow x = 66.67 \ mm$$

The required reinforcement cross-sectional area follows from:

$$N_c = N_s \rightarrow \frac{1}{2}bx\varepsilon_c E_{cm} = A_s E_s \varepsilon_s$$

$$\frac{1}{2} * 1000 * 66.67 * 0.4 * 10^{-3} * 30000 = A_s * 2.0 * 10^5 * 2.175 * 10^{-3} \rightarrow A_s$$
$$= 933.41 \ mm^2$$

The required reinforcement ratio contains:

$$\rho_x = \frac{A_s}{t * b} = \frac{933.41}{500 * 1000} = 0.19\%$$

Similar steps will be taken longitudinal direction, resulting in a required reinforcement ratio in longitudinal direction:

$$\rho_y = 0.03\%$$

7.3.3 MID SLAB

In section 3 the mid slab will be subject to a 1.97 meter thick ballast load ($\gamma_{ballast} = 16 \ kN/m^2$). Together with its length, the mid slab in section will be governing. The steps from the general approach will be applied to the mid slab as well. The calculation method therefore becomes similar to the top slab.

The uniform distributed load equals:

$$q_{ed} = t * \gamma_c * \gamma_G + q_{road} * \gamma_G = 0.5 * 25 * 1.35 + 16 * 1.35 = 38.5 \ kN/m^2$$

This results in a required reinforcement ratio in transverse direction (x) and longitudinal direction (y):

$$\rho_x = 0.29\% \qquad\qquad \rho_y = 0.05\%$$

7.3.4 BOTTOM SLAB

In longitudinal direction, the bottom slab will be inclined by the stiff connections from the inner walls. In transverse direction, no walls are present, making the bottom slab two parallel sided inclined. With a transverse length of $l_x = 52.676 \ m$ and a longitudinal length of $l_y = 8.74 \ m$ (heart to heart distance between inner walls), the load distribution constants are obtained:

$$k_y = \frac{5l_x^4}{l_y^4 + 5l_x^4} \approx 1$$

Hence the load will be fully distributed in longitudinal (y) direction.

The value of the uniform load will be obtained in a load situation during sluiceway maintenance. No water will be present in a single sluiceway. The total uniform load will be reduced from $245.5 \, kN/m^2$ to $239.7 \, kN/m^2$. The bottom slab between the inner walls of the sluiceway will be subject to a foundational pressure of $239.7 \, kN/m^2$. the downward pressure from the bottom slab solely exists of its self-weight, hence the governing load now becomes:

$$q_{ed} = 240.6 - 0.5 * 25 * 1.35 = 223.7 \, kN/m^2$$

Following the steps from the general approach will lead to a moment of:

$$M_{Ed,y} = \frac{1}{12} k_y q_{ed} l_y^2 = \frac{1}{12} * 1 * 222.8 * 8.74^2 = 1424.2 \, kNm/m$$

The concrete strain becomes:

$$\varepsilon_c = \frac{(1424.2/(0.5^2/6))}{30000} = 1.13 * 10^{-3} = 1.14 \, ‰$$

The provided steps may still be followed as the concrete strain remains below 1.75‰.

It results in a required reinforcement of:

$$\rho_y = 1.14 \, \%$$

The economical reinforcement ratio has been exceed by solely the contribution of the upward pressures. Increasing the bottom slab thickness becomes inevitable.

7.4 TIDAL POWER PLANT ON RUBBLE BED FOUNDATION

The Tidal Power Plant will be placed on a rubble foundation bed as imposed in section 6.4. The rubble material bed will be constructed in the wet. Hence, it becomes inevitable deviations in the material bed level arise. The influence of these deviations allow computation. Therefore, a beam theory will be applied. The beam theory should include the characteristics of the bed and the influence of these characteristics on the Tidal Power Plant. Four beam theories have been elaborated in D.2. It was concluded the beam on elastic foundation theory provides the best solution to the influence of discrepancies in the rubble material bed.

The influence of the rubble material bed on the structure will be investigated in this paragraph. This will be performed using the following steps:

1. Determine the influence of a rubble foundation bed without any deviations; an homogeneous foundation, considered in subparagraph 7.4.1.
2. Apply forces resulting from the governing load situation
3. Determine the bending and shear resistance of a monolithic structure
4. Determine the bending and shear resistance of a structure conform the preliminary powerhouse design
5. Conclude the suitability of the assumed structural element thickness of 500 mm.
6. Apply deviations in the bedding constant k_d, this will be considered in subparagraph 7.4 .2
7. Reconsider step 2 to 5

The described steps determine the influence in two decoupled directions. Therefore, after finishing step 7, a coupled analysis will be performed. The coupled analysis will result in torsional moments. Subparagraph 7.4.3 will consider this 2 dimensional approach and determines the designed structure's ability to resist torsional moment.

7.4.1 TIDAL POWER PLANT ON HOMOGENEOUS FOUNDATION

The Tidal Power Plant will again be considered as a monolith structure, provided with properties from the Tidal Power Plant, will be considered resting on a rubble bed foundation. Considering the monolithic structure as a beam on elastic foundation, see Figure 78, the beam on elastic foundation theory will be applied.
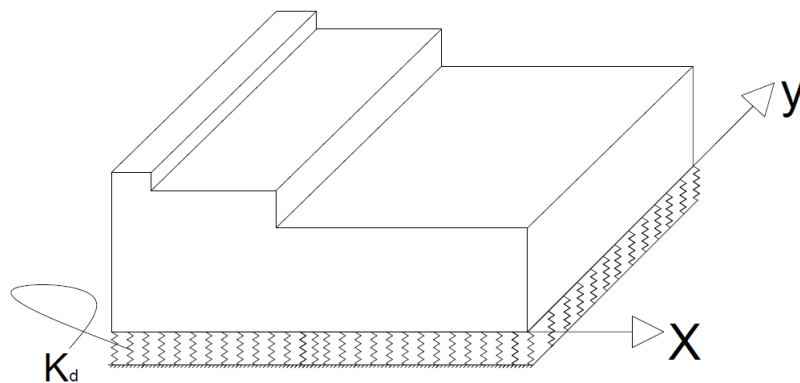
FIGURE 78: MONOLITHIC STRUCTURE ON ELASTIC FOUNDATION

The force distribution in transverse direction on the monolithic structure are illustrated in Figure 79.
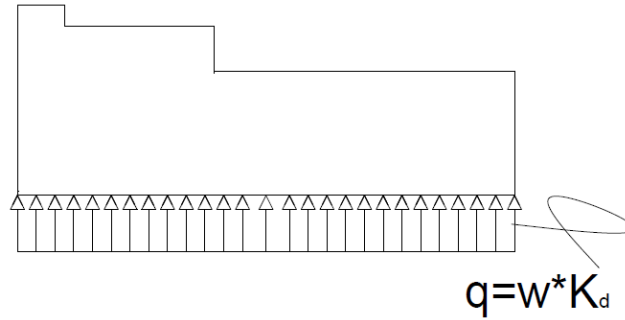
FIGURE 79: LOAD DISTRIBUTION ON MONOLITHIC BEAM ON ELASTIC FOUNDATION

The beam is subject to an equal load over its full length. The deflection following from the beam on elastic foundation theory, described below, provides a solution with four unknowns. To determine the deflection of the beam, boundary conditions are required.

$$w_i(x) = \exp(\lambda_i x)\left(C_1 \cos(\lambda_i x) + C_2 \sin(\lambda_i x)\right) + \exp(-\lambda_i x)\left(C_3 \cos(\lambda_i x) + C_4 \sin(\lambda_i x)\right) + \frac{q_1}{k_{d,i}}$$

With: $$\lambda_i = \sqrt[4]{\frac{k_{d,i}}{4EI_i}}$$

The beam will be considered as freely supported. The corresponding boundary conditions at the beam ends are; $M = 0$ and $V = 0$. Considering the beam in transverse direction, hence x-direction results in the boundary conditions described as:

At $x = 0$: $$V(0) = -EI * \frac{\partial^3 w(0)}{\partial x^3} = M(0) = -EI * \frac{\partial^2 w(0)}{\partial x^2} = 0$$

At $x = L$ $$V(L) = -EI * \frac{\partial^3 w(0)}{\partial x^3} = M(L) = -EI * \frac{\partial^2 w(L)}{\partial x^2} = 0$$

Two interface will be required to find a solution for w(x). The beam characteristics are assumed to be equally distributed over the beam. Hence, splitting the beam at the midsection will lead to two equal sections. Two deflection equations arise:

For $0 < x < L/2$:

$$w_1(x) = \exp(\lambda_1 x)\left(C_1 \cos(\lambda_1 x) + C_2 \sin(\lambda_1 x)\right) + \exp(-\lambda_1 x)\left(C_3 \cos(\lambda_1 x) + C_4 \sin(\lambda_1 x)\right) + \frac{q}{k_{d,1}}$$

For $L/2 < x < L$:

$$w_2(x) = \exp(\lambda_2 x)\left(C_5 \cos(\lambda_2 x) + C_6 \sin(\lambda_2 x)\right) + \exp(-\lambda_2 x)\left(C_7 \cos(\lambda_2 x) + C_8 \sin(\lambda_2 x)\right) + \frac{q}{k_{d,2}}$$

At $x = L/2$ the interface conditions read:

$$w_1(x) = w_2(x) \qquad \frac{\partial w_1(x)}{\partial x} = \frac{\partial w_2(x)}{\partial x} \qquad \frac{\partial^2 w_1(x)}{\partial x^2} = \frac{\partial^2 w_2(x)}{\partial x^2} \qquad \frac{\partial^3 w_1(x)}{\partial x^3} = \frac{\partial^3 w_2(x)}{\partial x^3}$$

Combining the above equations has resulted in the Maple worksheet presented in Appendix D.3.1 for a beam on elastic foundation.

A solution will be found when the characteristics of the beam are inserted. These characteristics are summarized in Table 22.

144

Parameter	Symbol	Value		Obtained from
Length	L	52.676	m	5.6
Weight Tidal Power Plant	q	246.4[1]	kN/m^2	5.6
Soil stiffness rubble bed foundation	k_d	50000	kN/m^2	6.4.4
Second order moment of inertia	I	276.23	m^4	Appendix D.4.1
Young's modulus	E	30000[2]	N/mm^2	Appendix D.4.2

TABLE 22: INPUT PARAMETERS BEAM ON ELASTIC FOUNDATION IN TRANSVERSE DIRECTION

Inserting these characteristics results in the beam deflection illustrated in Figure 80.
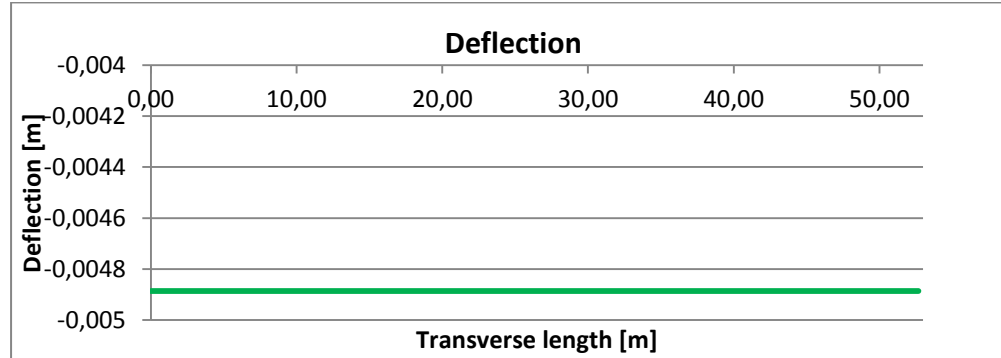
FIGURE 80: DEFLECTION (GREEN LINE) TRANSVERSE DIRECTION HOMOGENEOUS FOUNDATION

From Figure 80 the presence of homogeneous foundational pressures along the beam may be noticed. The corresponding moments and shear forces equal zero. Hence, the beam will not be subject to any external loads and remains in full vertical equilibrium.

However, in reality the beam will be subject to external forces. The governing load situation in transverse direction has been presented in paragraph 7.2 and was obtained from Appendix D.5. External moments emerge due to the eccentric point of engagement of the hydraulic pressures from the North Sea and Lake Grevelingen, with respect to monolithic structure's centre-line, see figure Figure 81. The internal lever arm, distance between point of engagement and centre-line, multiplied by the resulting pressure results in the external moment.

In longitudinal direction, external moments emerge due to the lateral earth pressures. It has been assumed the dike body ($y_{soil} = 20\ kN/m^3$) adjacent to the Tidal Power Plant will reach a similar height as the top level of each section. Hence for each section a different external moment will be obtained.

In both transverse and longitudinal direction, the point of engagement of the resulting pressure lies below the structure's centre line. The moments on the structure are therefore directed in the direction illustrated in Figure 81. The governing moments in transverse and longitudinal direction are summarized in Table 23.

---

[1] The total vertical load per square meter has been multiplied by a partial factor of 1.35 for permanent loads [NEN-1990].

[2] The nominal stiffness of slender compression members will be calculated by

$$EI = K_c E_{cd} I_c + K_s E_s I_s$$

The value for EI, required in the beam on elastic foundation, will be reduced by K_c. Appendix D.4.3 describes the result of this value.
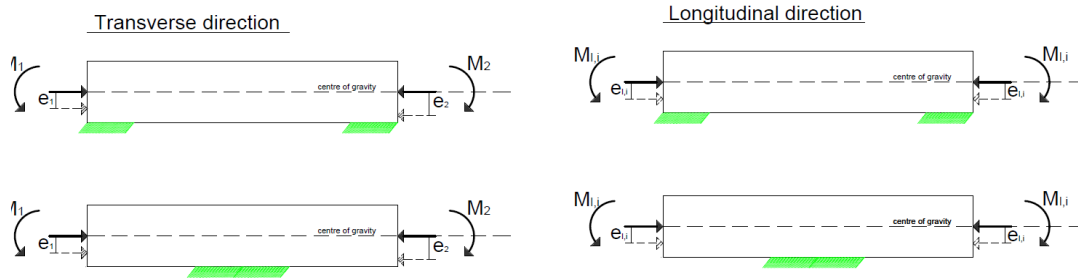
FIGURE 81: EXTERNAL FORCES BEAM ON ELASTIC FOUNDATION

Transverse direction		L_x	52.676	$[m]$
External moment North Sea		$M_{Ed,sea}$	17099	$[kNm/m]$
External moment Lake Grevelingen		$M_{Ed,lake}$	2356	$[kNm/m]$
Longitudinal direction		L_y	157.82	$[m]$
External moments	Section 1	$M_{Ed,earth,1}$	28409.8	$[kNm/m]$
	Section 2	$M_{Ed,earth,2}$	15978.3	$[kNm/m]$
	Section 3	$M_{Ed,earth,3}$	6240.8	$[kNm/m]$

TABLE 23: GOVERNING LOADS ON BEAM ON ELASTIC FOUNDATION

The influence of the external moment on the monolithic structure will be determined by reconsidering the boundary conditions at the beam ends. In transverse direction, the new boundary condition read:

$$At \; x = 0: \qquad V(0) = -EI * \frac{\partial^3 w(0)}{\partial x^3} = 0, M(0) = -EI * \frac{\partial^2 w(0)}{\partial x^2} = 17099 \; kNm/m$$

$$At \; x = L \qquad V(L) = -EI * \frac{\partial^3 w(0)}{\partial x^3} = 0, M(L) = -EI * \frac{\partial^2 w(L)}{\partial x^2} = 2356 \; kNm/m$$

Inserting the conditions in the Maple worksheet from Appendix D.4.1, the influence of the external moment on the deflection will be obtained, see Figure 82.
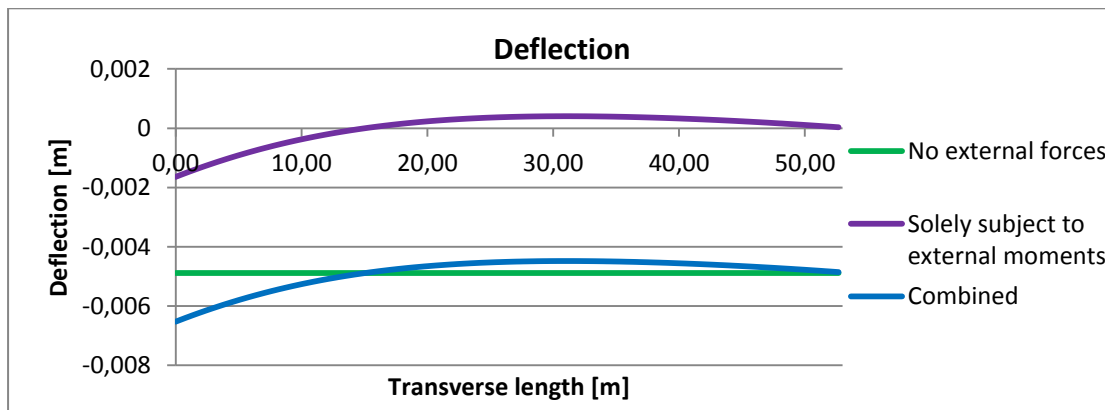
FIGURE 82: DEFLECTION TRANSVERSE DIRECTION HOMOGENEOUS FOUNDATION

The governing moment and shear force follow from the expressions:

$$V(x) = -EI * \frac{\partial^3 w(x)}{\partial x^3} \qquad\qquad M(x) = -EI * \frac{\partial^2 w(x)}{\partial x^2}$$

The bending and shear resistance of the beam will be appreciated with the results of the beam on elastic foundation subject to external moments in the succeeding sections.

146

7.4.1.1 BENDING RESISTANCE

The bending resistance of the beam on an homogeneous foundation subject to external moments will be elaborated in this section. First, external moment in transverse direction will be applied. With these external moment the required reinforcement will be determined. Second, the governing longitudinal moment for each section will be computed and the bending resistance to the longitudinal moment shall be determined.

TRANSVERSE DIRECTION

Figure 83 provides the results of the moment distribution in transverse direction along the beam respectively. The governing moments obtained from these figures allows to calculate the bending resistance of the monolithic beam using a similar approach as in 7.2.1.
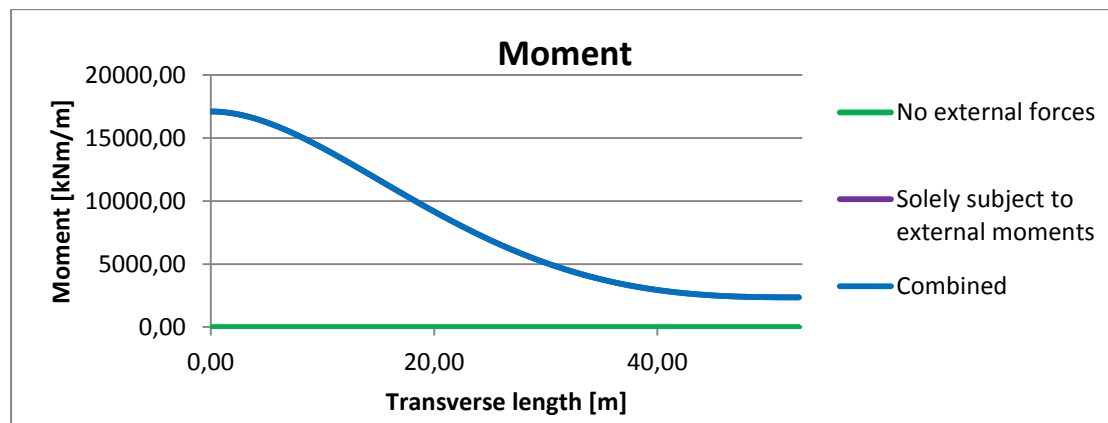
FIGURE 83: MOMENT TRANSVERSE DIRECTION HOMOGENEOUS FOUNDATION

The structure will be divided in three sections, see figure Figure 84.
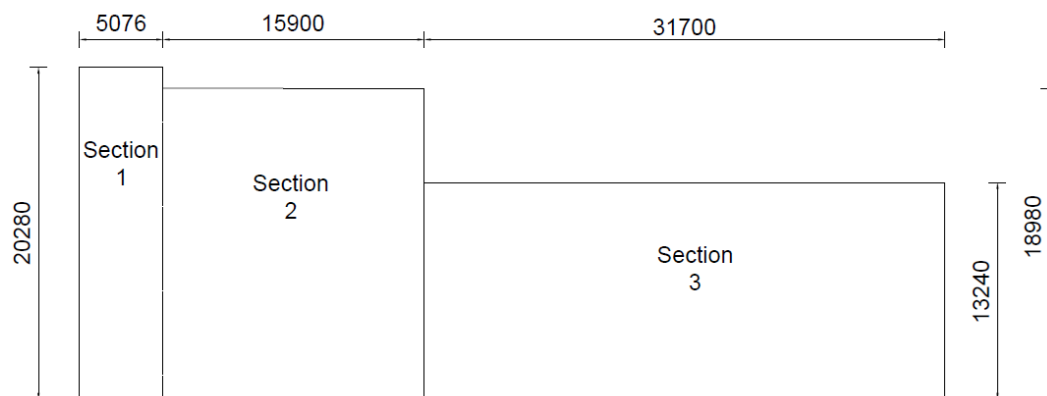
FIGURE 84: DISTINGUISHABLE SECTIONS MONOLITH STRUCTURE

The governing moment in the monolithic beam arises at section 1, containing 17099 kNm/m. Applying the very simplistic global bending resistance approach from paragraph 7.2.1, the governing moment on the structure becomes:

$$M_{y,1} = 17099 * 157.82 = 2.7 * 10^6 \ kNm$$

Stresses at the bottom and top slab are determined by:

$$\sigma_{y,1} = \frac{M_{y,1}/h_1}{A_{slab,1}} = \frac{\frac{2.7 * 10^6}{20.28}}{157.82 * 0.5} = 1.69 \; N/mm^2$$

The required cross sectional of reinforcing steel becomes:

$$A_{s,1} = \frac{M_{y,1}/h_1 * 10^3}{f_y} = \frac{2.7 * 10^6}{20.28} * \frac{10^3}{435} = 3.1 * 10^5 \; mm^2$$

The transverse reinforcement ratio results in:

$$\rho_{y,1} = \frac{A_{s,1}}{A_c} = \frac{3.1 * 10^5}{157.82 * 10^3 * 0.5 * 10^3} = 0.39 \; \%$$

These steps will be elaborated for section 2 and 3 as well. The governing moment for section 2 contains 16210 kNm/m and at section 3, 8839 kNm/m (obtained from Figure 83). The corresponding reinforcement ratios contain: $\rho_{y,2} = 0.39\%$ and $\rho_{y,3} = 0.31\%$.

Applying the more detailed approach; considering the beam provided with initial Tidal Power Plant dimensions. The above mentioned governing moments remain unchanged. A calculation for section 1 will be elaborated:

$$\sigma_y = \pm \frac{M_{y,1} * z_1}{I_1} = \pm \frac{17099 * 157.82 * 19.78}{21169.5} = 2.52 \; N/mm^2$$

'The second order of elasticity has been calculated for the full longitudinal cross sectional with the Steiner rule, results are provided in Appendix D.4.1.

From a horizontal equilibrium the tensile force in the reinforcement steel should be equal to the concrete compression force:

$$N_s = N_c \rightarrow A_s * f_y = N_c$$

It is assumed the concrete compression zone equals the top slab thickness with a width of 1 meter in transverse direction (x):

$$N_c = 500 * 2.52 * 1000 = 1.525 * 10^6 \; N$$

This results in a required cross-sectional area of reinforcing steel of:

$$N_s = N_c \rightarrow 1.525 * 10^6 = A_s * 435 \rightarrow A_s = 2897 \; mm^2$$

The reinforcement ratio now becomes:

$$\rho_{y,1} = \frac{A_{s,3}}{A_c} = \frac{2897}{500 * 1000} = 0.58\%$$

Following these steps, the results in section 2 and 3 are respectively $\rho_{y,2} = 0.6\%$ and $\rho_{y,3} = 0.49\%$.

The reinforcement will be located in the top slab as the external moment produces tensile stresses in the top slabs.

In transverse direction (x) similar steps are taken. However, instead of applying the computed moments over the longitudinal length it will be considered over a one meter thick strip in transverse direction: $\rho_{x,1} = 0.11\%$, $\rho_{x,2} = 0.04\%$ and $\rho_{x,3} = 0.19\%$

The reinforcement ratio's in both directions remain below the economical 1%. The computed values will be combined with the local reinforcement ratio's from subparagraph 7.2.1. This will be treated in the conclusion 7.4.1 .3 below.

LONGITUDINAL DIRECTION

The results of the beam subject to moments arising from the lateral earth pressures have been presented in
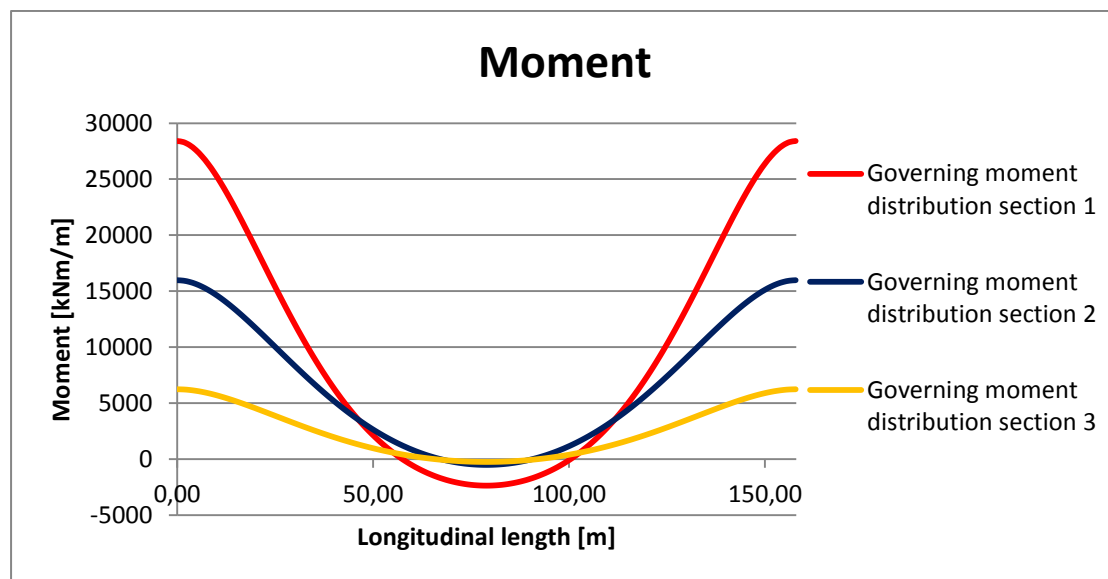
FIGURE 85: GOVERNING MOMENTS IN THE SEPERATE SECTIONS

The governing moments for each section read:

$$M_{y,1} = 28409 \ kNm/m \qquad M_{y,2} = 15978 \ kNm/m \qquad M_{y,3} = 6240 \ kNm/m$$

In longitudinal direction (y), the moments are assumed to apply on a one meter thick strip. The approach will be similar to the in 7.2.1 applied approach in transverse direction. Resulting in: $\rho_{y,1} = 0.006\%$, $\rho_{y,2} = 0.004\%$ and $\rho_{y,3} = 0.002\%$.

Hence, minimal reinforcement will be required in longitudinal direction as a consequence of the external moments in longitudinal direction. The required reinforcement in transverse direction (x) on the other hand increases:

$\rho_{x,1} = 0.66\%$, $\rho_{x,2} = 0.4\%$ and $\rho_{x,3} = 0.45\%$.

These reinforcement ratios are required in the top slabs, since tensile stresses will arise as a consequence of the external moments.

The reinforcement ratio's in both directions remain below the economical 1%. The computed values will be combined with the local reinforcement ratio's from subparagraph 7.2.1. This will be treated in the conclusion 7.4.1 .3below.

7.4.1.2 SHEAR RESISTANCE

The computation of the shear resistance will be similar to the computation provided in section 7.2.2. The governing shear force has been determined in both transverse and longitudinal direction. Figure 86 and Figure 87 provide the shear forces in transverse and longitudinal direction respectively

The maximum shear force in each direction obtained from Figure 86 and Figure 87 are:

$$F_{x,1} = 318.7 \ kN/m \qquad F_{x,2} = 516.9 \ kN/m \qquad F_{x,3} = 477.8 \ kN/m$$

$$F_{l,1} = 698.1 \ kN/m \qquad F_{l,2} = 341.2 \ kN/m \qquad F_{l,3} = 135.0 \ kN/m$$

It has been assumed the shear force will be resisted by the inner walls present in longitudinal direction. Hence, the governing shear force in longitudinal direction
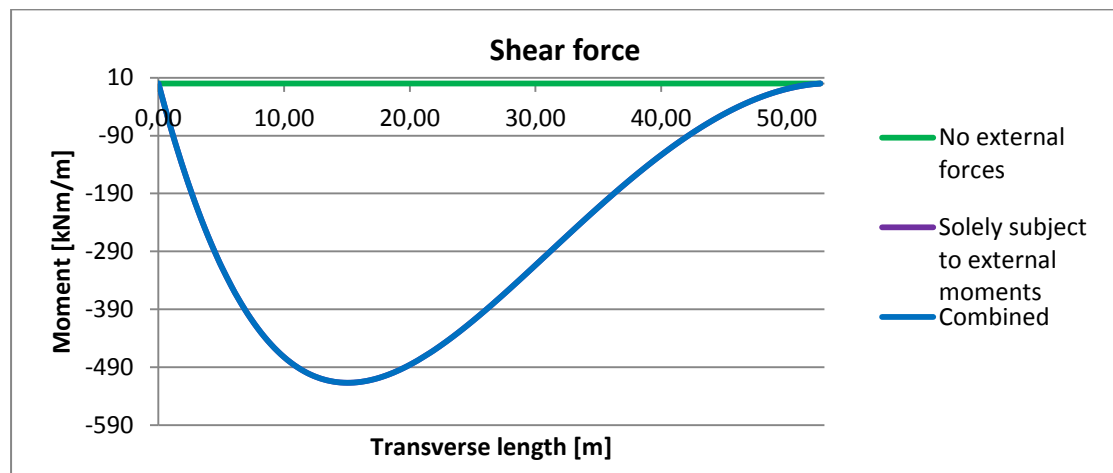
FIGURE 86: SHEAR FORCE TRANSVERSE DIRECTION HOMOGENEOUS FOUNDATION
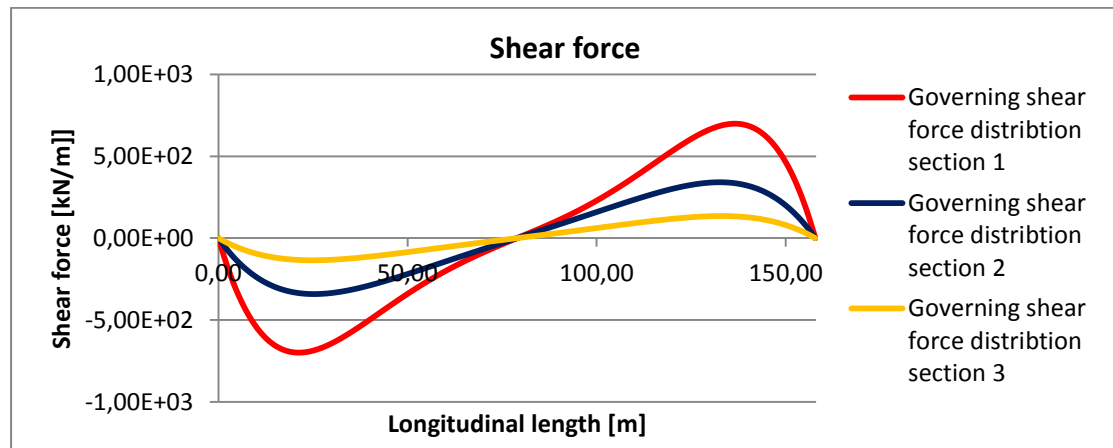
FIGURE 87: SHEAR FORCE DISTRIBUTION LONGITUDINAL DIRECTION SEPERATE SECTIONS

$F_{l,j}$ would be applied over total 19 walls and will not result in a governing situation. Therefore, the transverse directed shear force will be used to determine the shear resistance. Section 1 will be briefly elaborated here:

$$F_{Ed,1} = F_{x,1} * L_y = 318.7 * 157.82 = 50297.2 \ kN$$

With $F_{Ed,1}$ representing the design shear force.

$$\sigma_{shear,1} = \frac{F_{Ed,1}}{d_1 * 19 * t} = \frac{50297.2}{19.78 * 0.5 * 19} = 0.27 \; N/mm^2$$

The concrete shear resistance without shear reinforcement has been determined in section 7.2.2: $v_{min} = 0.235 \; N/mm^2$

The shear resistant stress of concrete has been exceeded. Shear reinforcement will be required. The cross-sectional area of shear reinforcement is calculated by the lower value of:

$$V_{Rd,s} = \frac{A_{sw}}{s} d f_{ywd} \cot(\theta)$$

And:

$$V_{Rd,max} = \frac{\alpha_{cw} b_w z_j v_1 f_{cd}}{\cot(\theta) + \tan(\theta)}$$

Where:

A_{sw} *represents the cross sectional area of the shear reinforcement*

s *represents the spacing of the stirrups*

b_w *represent the minimum width between tension and compression chords*

f_{ywd} *represents the design yield strength of the shear reinforcement*

v_1 *representsa strength reduction factor for concrete cracked in shear = 0.6*

α_{cw} *represents a coefficient taking account of the state of the stress in the*

       compression chord = 1

θ *represents the angle between the concrete compression strut and the*

       beam axis perpendicular to the shear force = 45° as upper limit and 21.8°

       as the lower.

z_j *represents the heart to heart distance between the top and bottom slab*

       within section 3 = d in this approach.

Applying the minimum angle θ, and considering the wall thickness as b_w, the maximum shear resistance in section 1 becomes:

$$V_{Rd,max} = \frac{\alpha_{cw} b_w z_3 v_1 f_{cd}}{\cot(\theta) + \tan(\theta)} = \frac{1 * 500 * 19.78 * 10^3 * 0.6 * 30}{\cot(21.8) + \tan(21.8)} = 6.14 * 10^7$$

The design shear force should not exceed the resisting shear force $V_{Rd,s}$. Applying a shear reinforcing bar diameter of 25 mm, the stirrup spacing becomes:

$$s = \frac{A_{sw} d f_{ywd} \cot(\theta)}{V_{Ed}} = \frac{0.25 * 25^2 * \pi * 19.78 * 10^3 * 435 * 2.5}{50297.2 * 10^3} = 209.9 \; mm$$

Hence at every in-plane meter (x-direction) at least 4.76 bars should be placed. The total shear reinforcement ratio is calculated using:

$$\rho_{shear} = \frac{A_{sw}}{s * b_w * \sin(\alpha)}$$

Where:

α *represents the angle between shear reinforcement and the longitudinal*

axis with a lower limat at 45° and a upper limit of 90°

The angle $'\alpha'$ has been set at 90 degrees, the shear reinforcement ratio becomes:

$$\rho_{shear,1} = \frac{A_{sw}}{s * b_w * \sin(\alpha)} = \frac{0.25 * 25^2 * \pi}{209.9 * 1000 * \sin(90)} = 0.22\ \%$$

Applying a similar approach to the shear forces in section 2 and 3, results in:

$$\sigma_{shear,2} = 0.465$$

$$\sigma_{shear,3} = 0.623$$

At both sections shear reinforcement will be required:

$$\rho_{shear,2} = 0.41\%$$

$$\rho_{shear,3} = 0.54\%$$

The shear reinforcement ratios do not exceed the economic value of 1%. The inner walls do thus not require an increase in wall thickness. Moreover, from the global equilibrium it appeared no shear reinforcement was required. In both approaches the influence of the self-weight of the top, mid and bottom slab has not been taken into account. However, due to the height of the walls, it has been assumed the contribution of the 0.5 meter thick slabs becomes almost negligible.

Shear forces transfer in a closed circuit. Hence, the required reinforcement ratio's obtained for the inner walls, will also be required in the top and bottom slab. The influence of the mid slab on the shear reinforcement has been assumed negligible.

The obtained shear reinforcement will be located in the inner walls in the longitudinal cross-section. Hence it contributes to the reinforcement ratio in y-direction:

From both the bending and shear resistance calculations it has appeared the economic reinforcement value of 1 % will not be exceeded. However, these values have been considered for particular structural element subject to shear or bonding only. The longitudinal and transverse external moment resulted in reinforcement in both direction for each case. The required reinforcement in similar structural elements in equal direction are combined and inserted in Table 24. Table 24 summarizes the governing results of this section.

	Top slab			Mid slab			Bottom slab			Inner walls		
Longitudinal direction (ρ_y)												
Section	1	2	3	1	2	3	1	2	3	1	2	3
Local bending	0.03	0.03	0.03	0.05	0.05	0.05	1.14	1.14	1.14	-	-	-
Global Bending	0.59	0.6	0.49	-	-	-	-	-	-	-	-	-
Shear forces	0.22	0.41	0.54	-	-	-	0.22	0.41	0.54	0.22	0.41	0.54
Sum	0.84	1.04	1.06	0.05	0.05	0.05	1.36	1.55	1.68	0.22	0.41	0.54
Transverse direction (ρ_x)												
Section	1	2	3	1	2	3	1	2	3	1	2	3
Local bending	0.19	0.19	0.19	0.29	0.29	0.29	-	-	-	-	-	-
Global Bending	0.77	0.44	0.64	-	-	-	-	-	-	-	-	-
Shear forces	-	-	-	-	-	-	-	-	-	-	-	-
Sum	0.96	0.63	0.83	0.29	0.29	0.29	-	-	-	-	-	-

TABLE 24: RESULTS REQUIRED REINFORCEMENT RATIO HOMOGENEOUS BEDDING

It may be concluded the top slab and bottom slab require an increment in concrete thickness. Since the results have shown the required reinforcement ratio slightly exceeds the economic value of 1% at the top slab, the modification will not concern a significant magnitude. The governing bottom slab reinforcement ratio, however, exceeds the economic value with 0.68%. An increase in concrete thickness is therefore recommended.

7.4.2 TIDAL POWER PLANT ON NON-HOMEOGENEOUS RUBBLE BED IN A ONE DIMENSIONAL APPROACH

The first discrepancy to the beam on elastic foundation has now been elaborated. The next step concerns a second discrepancy; variances in the bedding constant.

Deviations in the rubble foundation bed, induce the non-homogeneity of the elastic foundation. The influence of the non -homogeneous bed on the Tidal Power Plant will be elaborated in this subparagraph. Deviations in the rubble foundation bed, may be caused by:

a. Rock stiffness variations.
b. Bed level aberration due to construction tolerances or settlement.

The ROK [Rijkswaterstaat, 2017], provides guidelines to the design of civil structures, and describes an approach to determine the influence of foundation deviations to tunnel segments. The computation of the influence of foundational deviations on the Tidal Power Plant will be based on this approach. The ROK prescribes the deviations of the rubble foundation bed expressed by an $\alpha - value$. For rubble and gravel foundation layers, an $\alpha - value$ of 0.9 will be applied. Multiplying the $\alpha - value$ by the rock stiffness (or bedding constant) induces a non-homogeneous foundation, see Figure 88.
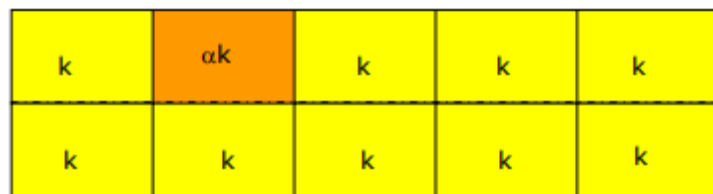
FIGURE 88: DEVIATION IN BEDDING CONSTANT DUE TO A [RIJKSWATERSTAAT ,2017]

The approach described by Rijkswaterstaat [2017] has been defined as dividing the foundation bed into separate sections. Applying the bedding constant deviation value $'\alpha'$ to several sections will lead to local decrease or increase of the upward foundation pressure.

The deviations in bed foundation translated into the elastic foundation properties lead to two foundational load cases; sagging and hogging:

SAGGING

The beam will be subject to a reduced foundational bedding constant at the midsection of the beam, see figure Figure 89. Hence, the beam's edges deliver a higher upward foundational pressure compared with the midsection. Due to the reduced upward foundational pressures at the midsection, the deflection at the midsection tends to become larger compared with the beam's edges.

HOGGING

The beam will be subject to a reduced bedding constant at its edges. Hence, the midsection of the beam delivers a higher upward foundational pressure compared with the edge sections, see Figure 90. The length of the supported area is varied leading to differences in the cross-sectional forces. Due to the higher upward foundational pressures at the midsection of the beam, the edges tend to show more deflection compared with the midsection.

154
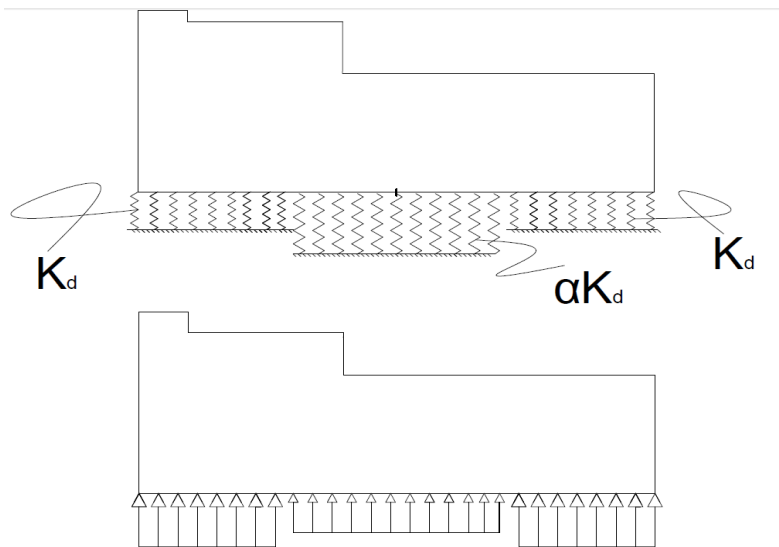
FIGURE 89: SAGGING MONOLITH STRUCTURE ON ELASTIC FOUNDATION
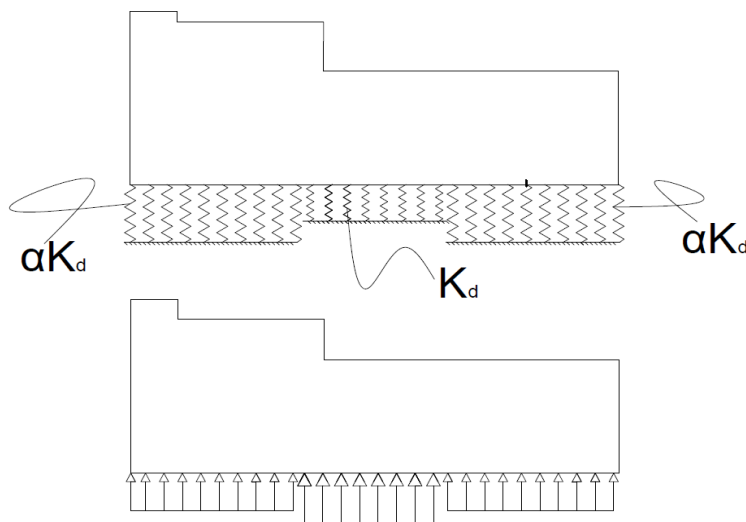
FIGURE 90: HOGGING MONOLITH STRUCTURE ON ELASTIC FOUNDATION

In both cases sagging and hogging the influence of the foundation bedding constant will be determined first. Hence, no additional external moments will be applied.

The computational model for both cases show similarities. Equal interface and boundary conditions apply. In total three deflection equations arise, with interface conditions at two locations and boundary conditions at the beam's edge. Comparing with the beam on homogeneous foundation, the following may be noticed:

- One times four additional interface conditions
- One additional deflection equation $w_i(x)$
- Varying λ_i due to αk_d at reduced supported section

The Maple worksheet for both sagging and hogging are presented in Appendix D.3.2 and Appendix D.3.3 respectively.

155

7.4.2.1 VALIDITY CHECK OF THE COMPUTATIONAL APPROACH

The validity of the applied worksheet will be determined prior to any calculations. The method becomes valid when the total equilibrium of vertical forces equals zero. Hence, the uniform distributed load followed from the structure's self-weight, should be equal to the deflection times the bedding constant over the full length.

Let's consider sagging, where 50% of the transverse length will be supported by a reduced bedding constant αk_d and adjacent to the reduced bedding constant a length of 25% will be normally supported with a bedding constant k_d, see Figure 91.
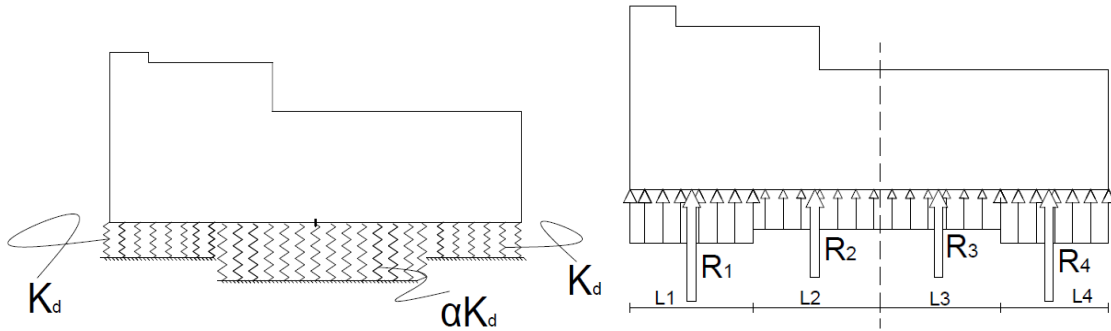
FIGURE 91: LOAD DISTRIBUTION VALIDITY CHECK

The deflection line has been illustrated in Figure 92.
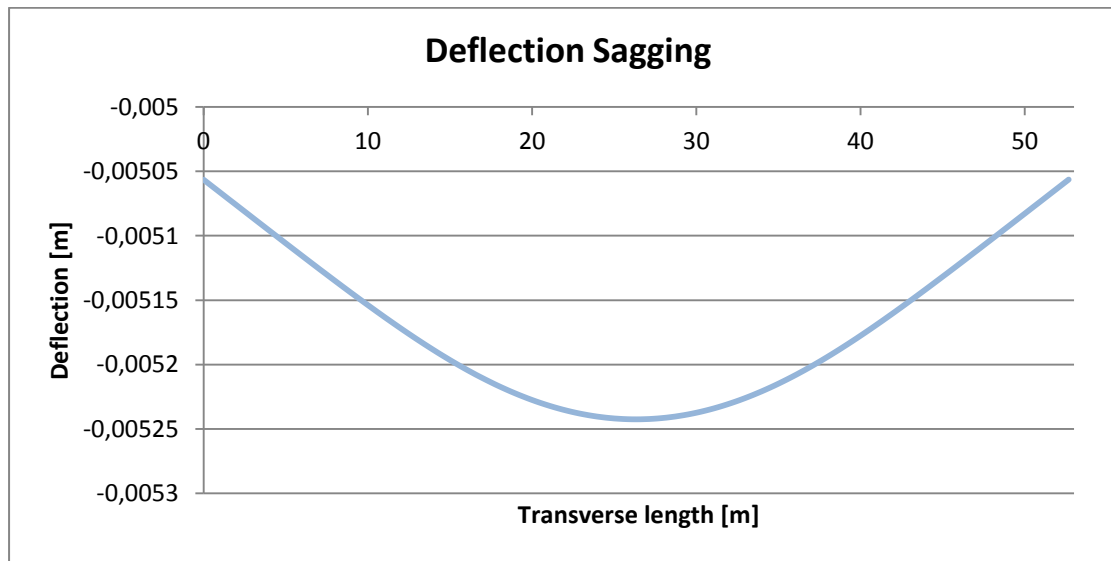
FIGURE 92: DEFLECTION SAGGING WITH REDUCED BEDDING CONSTANT BETWEEN $13.169 < x < 39.507\ m$

The resulting foundational pressures for the sections supported by k_d and the sections supported by αk_d are determined by:

$$R_1 = -k_1 \int_0^{13.169} w_1(x)dx = 3371.7 kN/m \quad R_2 = -k_2 \int_{13.169}^{26.338} w_2(x)dx = 3094.3\ kN/m$$

$$R_3 = -k_2 \int_{26.338}^{39.507} w_2(x)dx = 3094.3\ kN/m \quad R_4 = -k_2 \int_{39.507}^{52.676} w_3(x)dx = 3371.7\ kN/m$$

These results are obtained from the Maple worksheet in Appendix D.3.4. The resulting uniform load for each area results from:

156

$$q_1 = \frac{R_1}{L_1} = \frac{3371.7}{13.169} = 256.03 \; kN/m^2 \qquad\qquad q_2 = \frac{R_2}{L_2} = \frac{3094.3}{(26.338-13.169)} = 234.97 \; kN/m^2$$

$$q_3 = \frac{R_3}{L_3} = \frac{3371.7}{(39.507-26.338)} = 256.03 \; kN/m^2 \qquad q_4 = \frac{R_4}{L_4} = \frac{3094.3}{(52.676-39.507)} = 234.97 \; kN/m^2$$

The average load per considered area has been increased by almost 4.3% in area L1 and L4, whereas a decrease of the average load of 4.3% has been present at area L2 and L3. In theory an increase of 5 % should have resulted, the Maple Worksheet deviated from this theory. Probably due to the non-rectangle deflection of the beam. On the positive side, the vertical equilibrium will be ensured in this approach. Even with the small deviation compared to the expected theoretical, the approach may be considered valid.

7.4.2.2 BASE CASE SCENARIOS

With the computational model considered as valid, the influence of the support length αk_d will be determined. The structure on an elastic foundation will be considered as monolith again.

For both, sagging and hogging, the effect of the supported length with a non-reduced bedding constant, will be elaborated for 6 support length scenarios; starting with a support length of 20% of the total length, which increases by ten percent for each successive scenario. Figure 93 gives a clear representation of the proposed supporting lengths of the 6 scenarios for the two base cases.
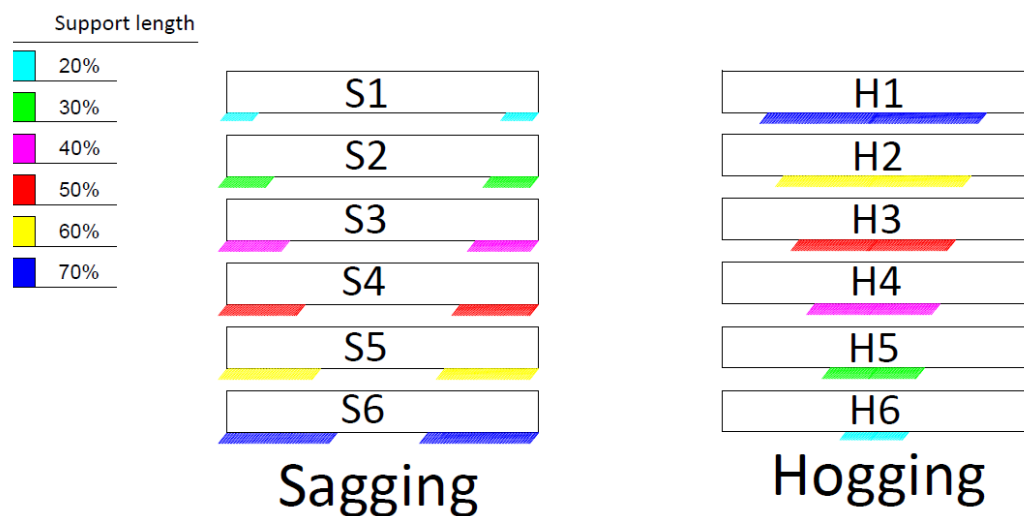
FIGURE 93: SUPPORT LENGTH k_d (COLOURED) BASE CASES

Initially the monolith beam on elastic foundation will be considered without any external loadings. The moment and shear force distribution results have been provided in Appendix D.6. The initial step of considering the beam without any external loadings and determine the required reinforcement will be skipped. Appendix D.6, provides the load distributions including the external forces as well. From the presented figures, the governing moments and shear forces are obtained.

The governing moments have been summarized in Table 25 a distinction has been made between positive (tensile stresses at top) and negative moments (tensile stresses at bottom). The positive moments comply with governing moments from 7.4.1.1. Hence similar reinforcement ratio are required. However, at the bottom slab the governing reinforcement has not been determined. The required reinforcement ratios due to negative moments will therefore be elaborated below.

Governing positive moments	Section 1	Section 2	Section 3	
Transverse direction				
Sagging	17099	16210	8839	kNm/m
Hogging	28409.8	15978.3	6240.8	kNm/m
Longitudinal direction				
Sagging	28409.8	15978.3	6240.8	kNm/m
Hogging	28409.8	15978.3	6240.8	kNm/m
Governing negative moments				
Transverse direction				
Sagging	-243.2	-1537.4	-1669.4	kNm/m
Hogging	0	0	0	kNm/m
Longitudinal direction				
Sagging	-2944.7	-4267.8	-4461	kNm/m
Hogging	-1382.9	-606.9	-602	kNm/m

TABLE 25: SUMMARIZED GOVERNING MOMENTS FROM BASE CASES HOGGING AND SAGGING

The corresponding governing required reinforcement ratios follow from the negative moments for sagging. The approach from paragraph 7.2.1 will be applied.

The approach of considering the beam as a monolithic structure and the more detailed approach will be applied.

Considering the beam as a monolithic structure, the moments from transverse direction require reinforcement ratios of:

$\rho_{y,1} = 0.006\ \%$ $\qquad \rho_{y,2} = 0.04\%$ $\qquad \rho_{y,3} = 0.06\%$

Reinforcement ratios corresponding to moments from the longitudinal direction result in:

$\rho_{x,1} = 0.07\%$ $\qquad \rho_{x,2} = 0.1\%$ $\qquad \rho_{x,3} = 0.15\%$

Applying a more detailed approach, the required reinforcement ratios from the transverse moments read:

$\rho_{y,1} = 0.008\ \%$ $\qquad \rho_{y,2} = 0.06\%$ $\qquad \rho_{y,3} = 0.26\%$

The reinforcement ratios in x-direction becomes negligible.

Reinforcement ratios corresponding to moments from the longitudinal direction result in:

$\rho_{x,1} = 0.097\%$ $\qquad \rho_{x,2} = 0.18\%$ $\qquad \rho_{x,3} = 0.30\%$

The above obtained reinforcement ratios apply to the bottom slab.

Similar to the bending resistance, the governing shear forces for in both direction for each section will be determined using the figures from Appendix D.6. For sagging the governing shear force when applying the external moments will be increased as a consequence of the uneven bedding constant. In case of hogging the opposite applies. The governing shear forces are provided in Table 26.

Governing shear forces	Section 1	Section 2	Section 3	
Transverse direction				
Sagging	426.6	642.9	546	kN/m
Hogging	298.3	460.5	440.9	kN/m
Longitudinal direction				
Sagging	821.5	501.6	302.8	kN/m
Hogging	716.9	351.7	229.8	kN/m

TABLE 26: GOVERNING SHEAR FORCES RESULTING FROM BASE CASES

The shear forces exceed the determined shear forces for a beam on homogeneous foundation. The required reinforcement ratios will therefore be calculated using the governing shear forces for each section in each direction:

$$F_{x,1} = 426.6 \; kN/m \qquad F_{x,2} = 642.9 \; kN/m \qquad F_{x,3} = 546 \; kN/m$$

$$F_{l,1} = 716.9 \; kN/m \qquad F_{l,2} = 501.6 \; kN/m \qquad F_{l,3} = 302.8 \; kN/m$$

The shear resistance approach from section 7.3.1.2 will be applied. Since the shear forces exceed the governing forces from section 7.3.1.2, which required shear reinforcement, shear reinforcement will be required. Applying 25 mm diameter stirrups the following shear reinforcements are obtained:

$$\rho_{shear,1} = 0.31\% \qquad \rho_{shear,2} = 0.50\% \qquad \rho_{shear,3} = 0.62\%$$

From both the bending and shear resistance calculations it has appeared the economic reinforcement value of 1 % will not be exceeded. However, these values have been considered for the particular structural element subject to shear or bending only. The required reinforcement in similar structural elements in equal direction are combined and inserted in Table 27. Hence, Table 27 summarizes the governing results of the required reinforcement for a beam on a non-homogeneous elastic foundation in the one dimensional approach.

	Top slab			Mid slab			Bottom slab			Inner walls		
Longitudinal direction (ρ_y)												
Section	1	2	3	1	2	3	1	2	3	1	2	3
Local bending	0.03	0.03	0.03	0.05	0.05	0.05	1.14	1.14	1.14	-	-	-
Global Bending	0.59	0.6	0.49	-	-	-	0.008	0.06	0.15	-	-	-
Shear forces	0.31	0.50	0.62	-	-	-	0.31	0.50	0.62	0.22	0.41	0.54
Sum	0.93	1.13	1.14	0.05	0.05	0.05	1.46	1.7	1.91	0.22	0.41	0.54
Transverse direction (ρ_x)												
Section	1	2	3	1	2	3	1	2	3	1	2	3
Local bending	0.19	0.19	0.19	0.29	0.29	0.29	-	-	-	-	-	-
Global Bending	0.77	0.44	0.64	-	-	-	0.097	0.18	0.3	-	-	-
Shear forces	-	-	-	-	-	-	-	-	-	-	-	-
Sum	0.96	0.63	0.83	0.29	0.29	0.29	0.097	0.18	0.3	-	-	-

TABLE 27: RESULTS REQUIRED REINFORCEMENT RATIO NON-HOMOGENEOUS BEDDING

Similar to the beam on a homogeneous foundation, the top and bottom slab require an increment in concrete thickness. Since the results have shown the economic reinforcement ratio of 1% has been slightly exceeded within the top slab, the modification will not concern a significant magnitude. Due to the non-homogeneous base cases, sagging and hogging, the required reinforcement ratio in the bottom slab has even increased more, compared to the homogeneous case. Especially the bottom slab at section 3 requires a serious reconsideration. The reinforcement ratio here almost reaches a value twice the recommended. In further calculations adaptations to the slab thickness should be provided.

7.4.3 TIDAL POWER PLANT ON NON-HOMEOGENEOUS RUBBLE BED IN A TWO DIMENSIONAL APPROACH

The one dimensional model has formed the basis for the two dimensional model described in this subparagraph. The influence of the deviations in the rubble foundation bed in each direction, transverse and longitudinal, will now be coupled into a two dimensional model. Hence, the Tidal Power Plant will be again considered as a beam on an elastic foundation.

The major difference with the 1D computations is the influence from a second direction on the beam deflection. As a consequence, torsional moments arise. The reactions of the beam to these torsional moments will be considered in two base cases.

As a consequence of the arising torsional moments, shear forces emerge in concrete members, The aim of this paragraph is to determine the torsional moments and the corresponding required shear reinforcement to bear the emerges shear forces.

Prior to any calculations, the concept torsion will be briefly described in section 7.4.3.1.

The approach of computing the torsional moments will be described in the second section of this subparagraph, 7.4.3.2. Two base cases will be introduced, both with varying lengths of the reduced bedding constant. In base case T1, the beam will be supported over half its length by k_d in both transverse and longitudinal direction. The bedding constant of the other half will be reduced with a factor α. Section 7.4.3.3. will be fully dedicated to base case T1.

The second base case, T2, elaborated in section 7.4.3.4, will be supported by bedding constant k_d for 50% of its length, whereas the remaining support length will be supported by a reduced bedding constant, αk_d. In longitudinal direction the foundation will be divided into two parts. The first part will be subject to a bedding constant k_d applying to 66.6% of the beam's longitudinal length. The bedding constant of the remaining 33.3% will be reduced by the bedding constant factor α. The second part of the beam will be supported in a opposite manner; 33.3% by the bedding constant k_d and 66.6% by a reduced bedding constant αk_d. The top view of both base cases has been illustrated in Figure 94.
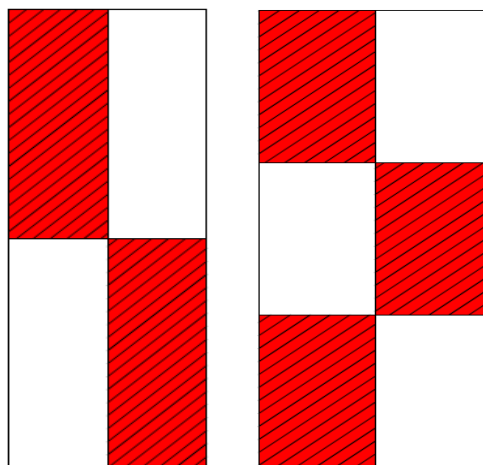
FIGURE 94: BASE CASES T1 (LEFT) AND T2 (RIGHT). THE RED SECTION INDICATES THE AREA SUPPORTED BY α BEDDING CONSTANT k_d. THE BEDDING CONSTANT OF THE WHITE AREA IS REDUCED BY α.

Considering the beam equally supported in both directions, results in a vertical equilibrium between the rubble foundation bed and Tidal Power Plant's weight. Applying discrepancies to the foundation's stiffness, or bedding constant, at certain sections the beam behaves inconsistently. From previous sections, it already appeared the Tidal Power Plant will be considered as a beam on an elastic foundation.

Variances in the supporting length epitomize the bedding constant irregularities and variances along the beams length in both directions. Consequently, to preserve the vertical equilibrium between the Tidal Power Plant and the rubble foundation bed, torsional moments emerge, see Figure 95.
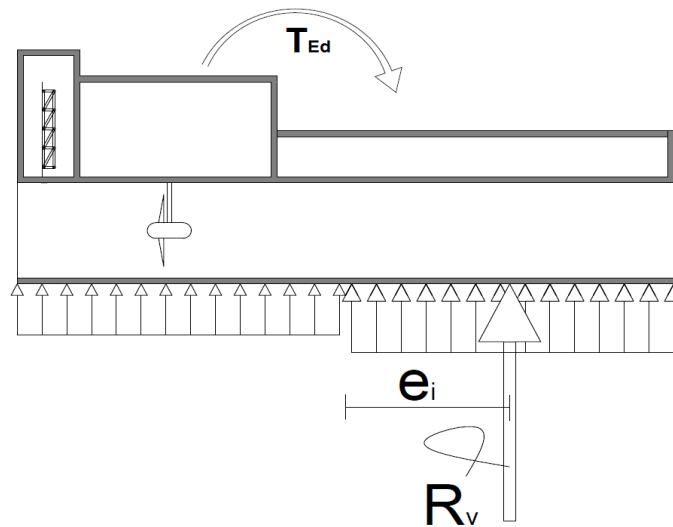
FIGURE 95: RESULTING TORSIONAL MOMENT FROM UNEVEN BEDDING FORCES

The torsional moment is coherent with the deflection at the supported part of the beam. The total deflected area times the bedding constant results in the total reaction force of the rubble foundation bed.

The part with an initial bedding constant k_d is now obliged to counteract the deflections of the part with a reduced bedding constant αk_d. Hence, when assuming the deflection of the beam towards the beam edge decreases linearly, the torsional moments towards the supported part will increase linearly. In other words, the homogeneous supported part will fully absorb the torsional moments along the uneven bedding length, which increases from zero at the beam's edge to its maximum at the homogeneous supported section. Thus when considering a meter thick strip at the beam edge, the 1 meter thick area of the beam should be able to resist the torsional moment. Simply said, consider a strip at the midsection of the beam, where the beam is considered supported homogeneously, the torsional moment in this strip equals the summation of all torsional moment between the beams uneven supported edge to the homogeneously supported midsection. This situation will become more clear when determine the torsional moment numerically.

Since the cross-section of the Tidal Power Plant in both directions is considered as a closed thin walled 'box', warping and the corresponding horizontal forces do not apply.

The torsional behaviour of the Tidal Power Plant will be determined with the two mentioned base cases T1 and T2 in the succeeding sections.

The deflection of the decoupled strips in both longitudinal and transverse direction is computed using the numerical models for sagging and hogging from the beam on an elastic foundation theory. The deflection allows determining the global in-plane forces of the cross section, for each strip, for each element and in each direction. Along this way the in-plane vertical shear forces are obtained.

The torsional moment is obtained from the coupled deflection in both transverse and longitudinal direction. Due to the deflection, a vertical upward reaction force emerges from the foundation. To remain vertically equilibrated, the torsional moment should be equal to the reaction force (R_j) multiplied by the lever arm (e_j). This lever arm is defined as the distance between the resulting reaction force to the mid of the considered strip. With the computed torsional moment, the final required reinforcement is determined by:

$$T_{Ed,j} = R_j * e_j$$

$$t_{ef,i} = \frac{A}{U}$$

$$V_{Ed,i} = \frac{T_{Ed,j} * z_i}{2A_k}$$

$$\frac{A_{sw,t,i}}{s} = \frac{V_{Ed,i}}{\cot(\theta) * f_{yd} * z_i}$$

In which the subscript 'j' represents the considered strip, whereas subscript 'i' represents the considered structural element. Furthermore,

$t_{ef,i}$ *represents the effective wall thickness, but should not be taken as less than twice the distance between edge and centre of the longitudinal reinforcement. For hollow sections the real thickness is an upper limit.*

$T_{Ed,j}$ *represents the design torsional moment within strip j*

A_k *represents the area enclosed by the centre − lines of the connecting walls, including inner hollow areas.*

z_i *represents the side length of concrete member i defined by the distance between the intersection points within the adjacent walls, see* Figure 96.

$V_{Ed,i}$ *represents the shear force in the concrete member i as a consequence of the torsional moment*

$A_{sw,t,i}$ *represents the required cross − sectional area of the assumed shear force reinforcement bars*

s *represents the heart to heart distance in transverse direction between*

the reinforcement bars.
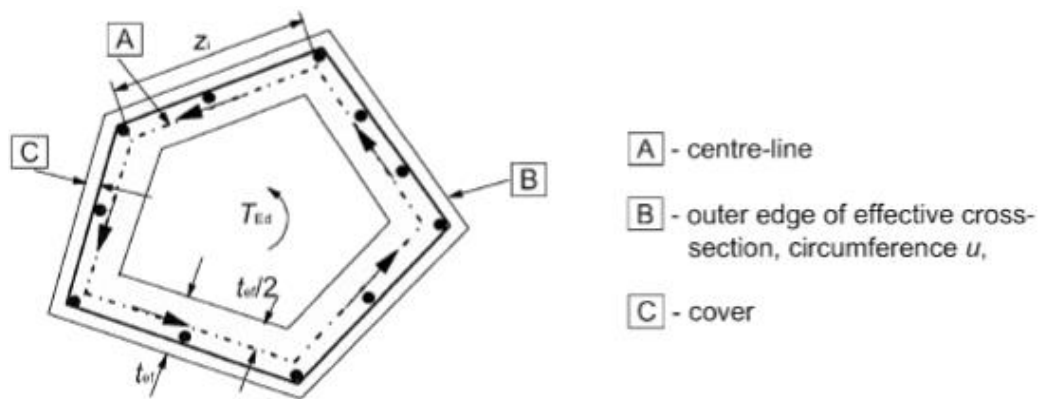
FIGURE 96: NOTIFICATIONS AND DEFINITIONS USED IN TORSION CALCULATIONS [EN 1992-1-1]

One should note that the bottom slab of the cross-section in transverse direction is not coupled to the housing structures. It is, therefore, assumed the bottom slab does not contribute to the torsional resistance.

The closed cross-sectional area in transverse direction has been formed by the upper part of the structure. Solely the closed area contributes to the torsional resistance, hence the sluiceway bottom slab will not be included into torsional resistance calculations.

In longitudinal direction, the closed cross-sectional area has been formed by the full cross-sectional area, thus the sluiceway bottom slab does contribute to the torsional resistance within the longitudinal cross-section.

As mentioned before, the reaction force is obtained by multiplying the deflection times the internal lever arm. Maple will be used to determine this reaction force. For each base case the computational approach is given in the appendices.

For a concrete member in torsion, the required cross-sectional area of the longitudinal reinforcement will be determined using:

$$\frac{\sum A_{sl}f_{yd}}{u_k} = \frac{T_{Ed}}{2A_k}\cot(\theta)$$

With:

$\sum A_{sl}$ *represents the total required cross − sectional area of the longitudinal*

      reinforcement for torsion

u_k *represents the perimeter of the area A_k*

f_{yd} *represents the design yield stress of the longitudinal reinforcementA_{sl}*

θ *represents the angle of compression struts*

The horizontal reinforcement in compressive chords may be reduced in proportion to the available compressive force. For tensile chords on the other hand, the longitudinal reinforcement for torsion should be added to the other reinforcement.

The maximum bearing capacity of a member subject to shear and torsion is limited by the capacity of the concrete struts. In order to not exceed the capacity, the following conditions should be satisfied:

$$\frac{T_{Ed}}{T_{Rd,max}} + \frac{V_{Ed}}{V_{Rd,max}} \leq 1.0$$

In which:

$T_{Rd,max}$ *represents the design torsional resistance moment according to*:

$$T_{Rd,max} = 2v\alpha_{cw}f_{cd}A_k t_{ef,i}\sin(\theta)\cos(\theta)$$

v *represents a strength reduction factor for concrete cracked in shear*:

$$v = 0.6 * \left(1 - \frac{f_{ck}}{250}\right)$$

α_{cw} *represents a coefficient that takes into account the state of the stress in*

            the compression chords. Equals 1 for non − prestressed structures

f_{cd} *represents the concrete design strength* $= 30\ N/mm^2$

$V_{Rd,max}$ *represents the design shear resistance according to*:

$$V_{Rd,max} = \frac{\alpha_{cw}b_w z v_1 f_{cd}}{\cot(\theta) + \tan(\theta)}$$

b_w *represents the minimum width between tension and compression chords*

z *represents the inner lever arm* $= 0.9d$

v_1 *represents the strength reduction factor for concrete cracked in shear* $= v$

The torsion links should be closed and anchored by means of laps or hooked ends, and should form an angle of 90° with the axis of the structural element.

In both of the required reinforcement ratios the minimum allowed shear reinforcement is applied. This value is equal to the value found in the reinforcement ratio:

$$\rho_{min} = 0.08 * \sqrt{f_{ck}}/f_{yd}$$

For Base case T1 the deflection is completely symmetrical along its centre axis in both longitudinal and transverse direction. The behaviour of the beam is elucidated with Figure 97.
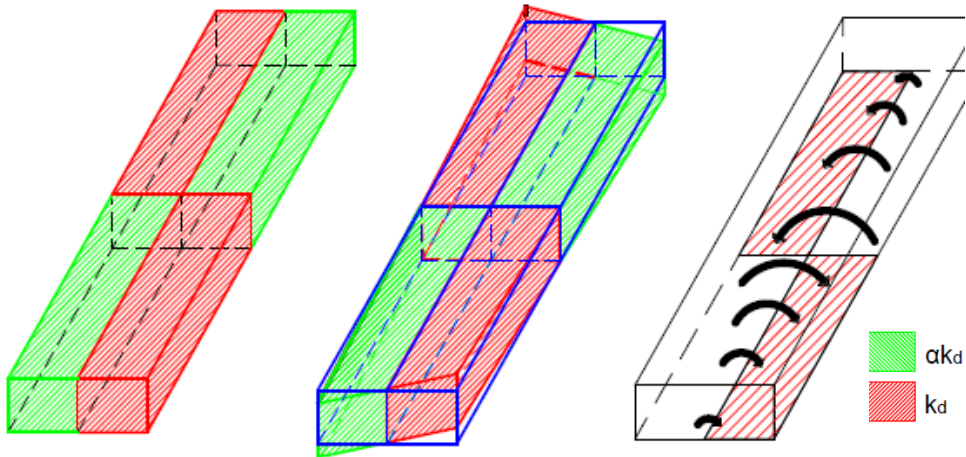
FIGURE 97: TORSIONAL BEHAVIOUR BASE CASE T1

As clearly noticeable from Figure 97 the magnitude of the deflection at of the corners of the beam is much higher compared with the midsection. For that reason the influence of the torsional moments is considered at multiple strips. Figure 98 provides a clear overview of the considered strips for base case T1.
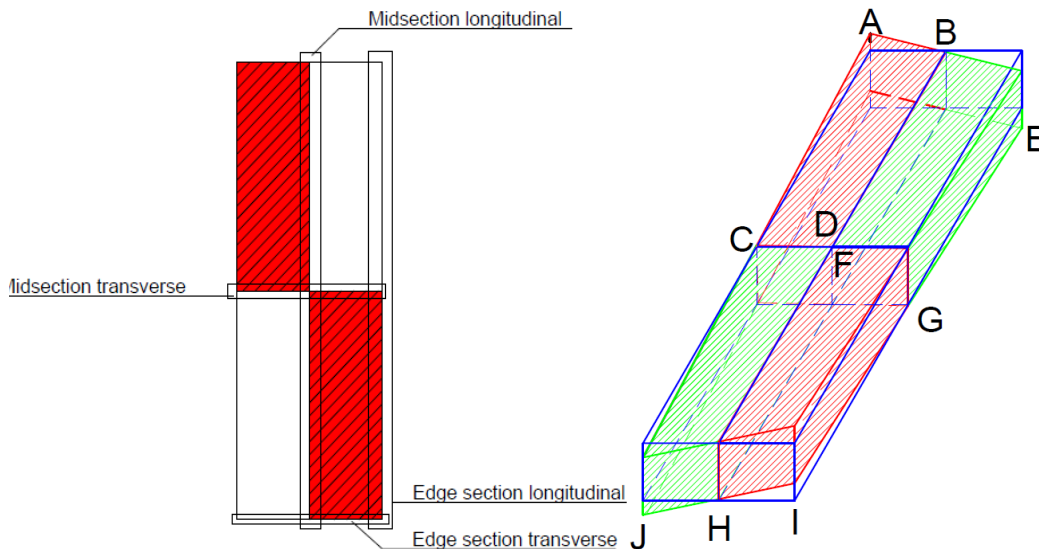
FIGURE 98: CONSIDERED SECTIONS BASE CASE T1 ON THE LEFT SIDE, APPOINTED LABELS OF SPECIFIC POINTS AT THE RIGHT SIDE

The considered strips are labelled by letters; an overview of these labels has been provided in Figure 98. The computational approach for base case T1 has been provided in Appendix D.3.5. This paragraph will determine the required reinforcement in transverse direction; strip A-B-E, C-D-G, C-F-G and J-H-I, and in longitudinal direction: strip A-C-J, B-D-H, B-F-H and E-G-I.

TRANSVERSE DIRECTION

In the calculation example in transverse direction the strips A-B-E and C-D-G will be fully elaborated. This calculation method will be followed for each strip. The position of the considered strips have been illustrated in a 3D model in Figure 99 and Figure 100 and. The calculation approach of strip A-B-E will be elaborated below, followed by the elaboration of strip C-D-G.
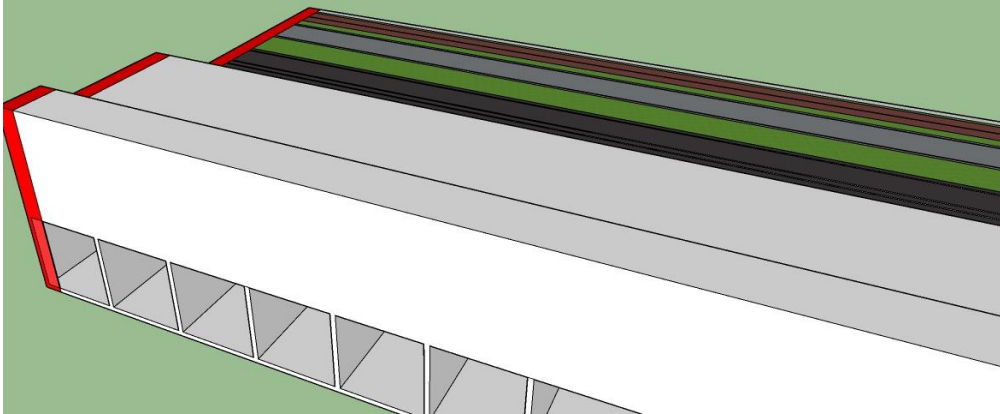
FIGURE 99: ONE METER THICK END STRIP A-B-E (NOT TO SCALE)
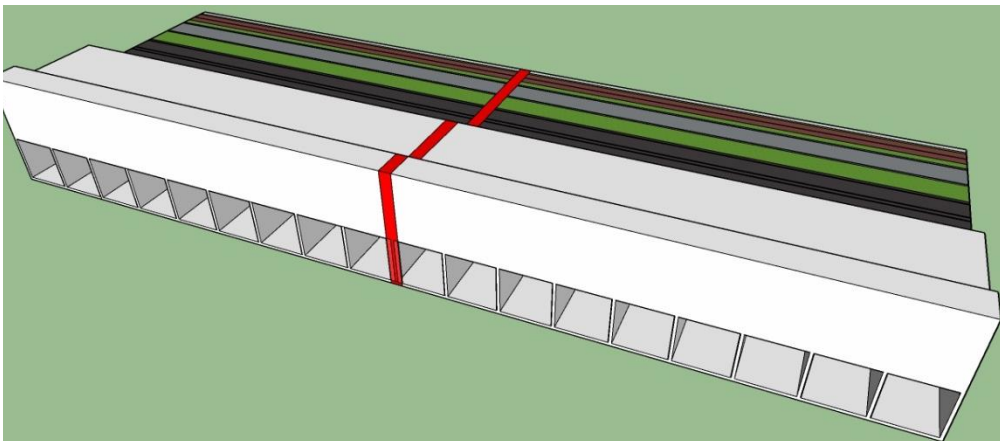
FIGURE 100: STRIP MID SECTION C-D-G (NOT TO SCALE)

The one meter thick end strip J-H-I cross-section has been illustrated in Figure 101 on the next page. The calculation for a one meter thick strip starts with computing the torsional moment. Computing the torsional moment for strip J-H-I, the input parameters as given in Table 28 are required. These parameters will be inserted into the computational model portrayed in Appendix D.3.5.

Parameter	Symbol	Value	
Bedding constant	K_d	50000	kN/m^2
Bedding constant reduction factor	$Alpha$	0.9	−
Moment of inertia	I	74	m^4
External applied moment Sea side	M_{ext_1}	17099	kNm/m
External applied moment Lake side	M_{ext_2}	2356	kNm/m
Uniform distributed load	q	245.5	kN/m^2
Modulus of elasticity concrete (Appendix D.4.3)	E	30000000	kN/m

TABLE 28: INPUT PARAMETERS COMPUTATIONAL MODEL BASE CASE T1
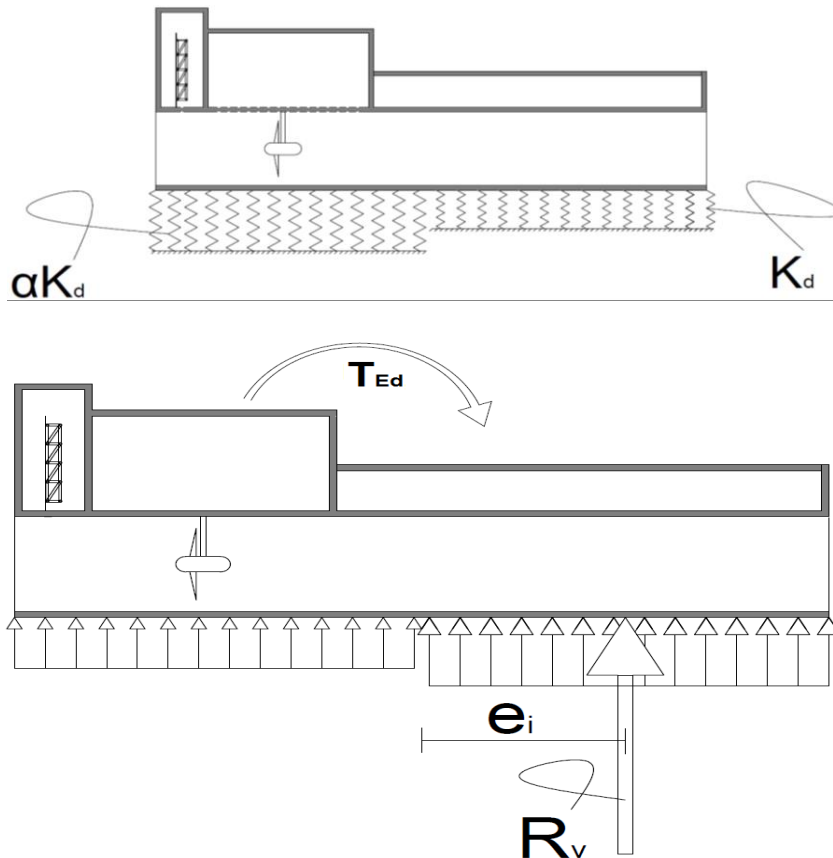
FIGURE 101: CROSS-SECTION J-H-I, WITH BEDDING CONSTANT IN THE UPPER FIGURE AND THE RESULTING UPWARD PRESSURES IN THE BOTTOM FIGURE.

Inserting the parameters from Table 28, the results of the unknowns in the beam on elastic foundation are:

$$C_1 = -1.80 * 10^{-4} \qquad C_2 = -1.03 * 10^{-4} \qquad C_3 = 3.08 * 10^{-4} \qquad C_4 = 5.22 * 10^{-4}$$

$$C_5 = 7.26 * 10^{-5} \qquad C_6 = -1.02 * 10^{-4} \qquad C_7 = 5.99 * 10^{-4} \qquad C_8 = 5.58 * 10^{-4}$$

Substituting these values into the beam deflection equation. With the deflection equation the internal lever arm and resulting reaction force have been determined in the worksheet as well, results will be presented at the succeeding pages.
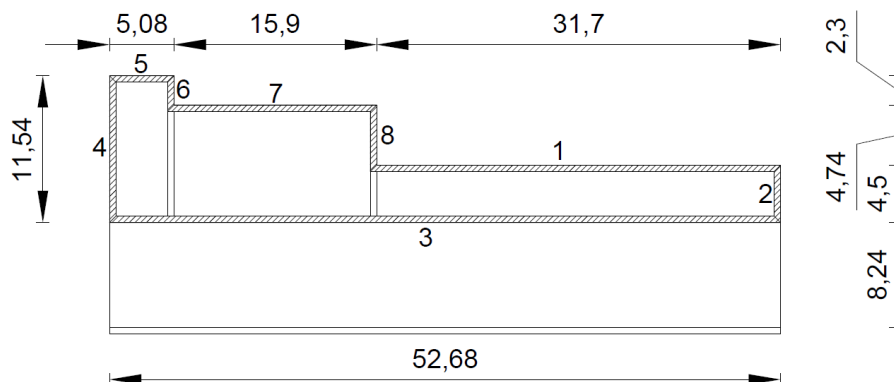
FIGURE 102: APPOINTED STRUCTURAL COMPONENTS CROSS-SECTION IN TRANSVERSE DIRECTION

168

Within the transverse cross-sectional area, a distinction has been made for 8 structural members appointed with numbers 1 to 8, see Figure 102. Let's consider the structural element indicated with '5' at both strips A-B-E and C-D-G:

Calculating the required reinforcement ratio in strip A-B-E:

$$t_{ef} = \frac{A}{U} = \frac{5.08 * 11.54 + 15.9 * 9.24 + 4.5 * 31.7}{31.7 + 4.5 + 52.68 + 11.54 + 5.08 + 2.3 + 15.9} = \frac{348.19}{123.69} = 2.81 \ m$$

The effective wall thickness exceeds the upper limit of the actual wall thickness: 0.5 meter.

$$T_{Ed,ABE} = R_{ABE} * e_{ABE} = 921.24 * 13.83 = 12740.75 \ kNm$$

$$V_{Ed,5} = \frac{T_{Ed,ABE} * z_5}{2A_k} = \frac{12740.75 * 4.576}{2 * 316.34} = 92.15 \ kN$$

$$\frac{A_{sw,t,5}}{s} = \frac{V_{Ed,5}}{\cot(\theta) * f_{yd} * z_5} = \frac{92.15 * 10^3}{2.5 * 435 * 4.576 * 10^3} = 0.018 \ mm^2/mm$$

It has been decided initially to apply 12 mm stirrups bars. The space between the stirrups requires at least:

$$s = \frac{A_{sw}}{\frac{A_{sw,t,5}}{s}} = \frac{0.25 * 12^2 * \pi}{0.018} = 2714.45 \ mm$$

Total number of stirrups per meter:

$$n = \frac{1000}{s} = \frac{1000}{2714.45} = 0.37$$

With these solutions, the required reinforcement ratio results in:

$$\rho_5 = \frac{n * \frac{A_{sw,t,5}}{s} * \cot(\theta)}{b * t} = \frac{0.37 * 0.018 * 2.5}{1000 * 500} = 3.41 * 10^{-8} = 3.41 * 10^{-4} \ \%$$

The total required longitudinal reinforcement results from the governing torsional moment, the area enclosed by the outer walls and its perimeter:

$$\rho_{l,transverse,1} = \frac{\sum A_{sl}}{A_c} = \frac{\frac{T_{Ed,ABE}}{f_{yd}} \frac{u_k}{2A_k} \cot(\theta)}{A_c} = \frac{\left(\frac{12740.75 * 10^6}{435} \frac{126.432 * 10^3}{2 * 316.34 * 10^6} * 2.5 \right)}{63.216 * 10^6}$$
$$= 0.023\%$$

The computed reinforcement ratios do not exceed the economical ratio of 1%. Moreover, the low required ratio at the end strip A-B-E will already be exceeded due to local required reinforcement. Therefore, torsional reinforcement will not have to be added. This will not be the case at the midsection, strip C-D-G. The torsional moment increases towards the equally supported strip C-D-G. Since the deflection has been assumed to decrease linearly towards the midsection, the torsional moment will increase linearly with its maximum at the midsection. The total torsional moment in strip C-D-G has been calculated by taking an average of the torsional moment in 50 considered strips between A-B-E and C-D-G. Multiplying this average by the total length between strip A-B-E and C-D-G (=78.91 m) results in the governing and maximum torsional moment along the beam in transverse direction:

$$T_{Ed,CDG} = \overline{T_{Ed,ABE-CDG}} * 78.91 = 931412.2 \; kNm$$

$$V_{Ed,5} = \frac{T_{Ed,CDG} * z_5}{2A_k} = \frac{931412.2 * 4.576}{2 * 316.34} = 6736.8 \; kN$$

$$\frac{A_{sw,t,5}}{s} = \frac{V_{Ed,5}}{\cot(\theta) * f_{yd} * z_5} = \frac{6736.8 * 10^3}{2.5 * 435 * 4.576 * 10^3} = 1.35 \; mm^2/mm$$

It has been decided to initially apply 20 mm stirrups bars. The space between the stirrups requires at least:

$$s = \frac{A_{sw}}{\frac{A_{sw,t,5}}{s}} = \frac{0.25 * 20^2 * \pi}{1.35} = 232.07 \; mm \qquad n = \frac{1000}{s} = \frac{1000}{232.07} = 4.31$$

$$\rho_{top \; slab, section \; 1} = \frac{n * \frac{A_{sw,t,i,element}}{s} * \cot(\theta)}{b * t} = \frac{4.31 * 1.35 * 2.5}{1000 * 500} = 2.92 * 10^{-5} = 2.92 * 10^{-3}\%$$

$$\rho_{l,transverse,1} = \frac{\sum A_{sl}}{A_c} = \frac{\frac{T_{Ed,CDG}}{f_{yd}} \frac{u_k}{2A_k} \cot(\theta)}{A_c} = \frac{\left(\frac{931412.2 * 10^6}{435} \frac{126.432 * 10^3}{2 * 316.34 * 10^6} * 2.5 \right)}{63.216 * 10^6} = 1.69 \; \%$$

The required longitudinal reinforcement exceeds the economic value of 1%. The applied wall thickness of 500 mm should thus be increased.

The length z_i of each concrete member appointed with 1 to 8, will differ, but combining the equations from the general approach, it will result z_i being cancelled out. Hence, the results of the required reinforcement ratio in each concrete member will be similar to the results from the calculations above:

At the end strip A-B-E: $\rho_i = 3.41 * 10^{-4} \; \%$ $\rho_{l,i} = 0.023 \; \%$

At the mid strip C-D-G: $\rho_i = 2.92 * 10^{-3} \; \%$ $\rho_{l,i} = 1.69 \; \%$

The final check, the bearing capacity of the beam, will be determined at last. The bearing capacity unity check reads:

$$\frac{T_{Ed}}{T_{Rd,max}} + \frac{V_{Ed}}{V_{Rd,max}} \le 1.0$$

The computed torsional moment contains:

$$T_{Ed} = 9.31 * 10^{11} \; Nmm$$

The resisting torsional moment has been defined as:

$$T_{Rd,max} = 2v\alpha_{cw}f_{cd}A_k t_{ef,i} \sin(\theta)\cos(\theta)$$

At first the initial angle of compression struts will be applied:

$$T_{Rd,max} = 2 * 0.6 * \left(1 - \frac{45}{250} \right) * 1 * 30 * 316.34 * 10^6 * 500 * \sin(21.8)\cos(21.8)$$
$$= 2.43 * 10^{12} Nmm$$

$$V_{Ed} = 3.85 * 10^5 \; N$$

$$V_{Rd,max} = V_{Rd,max} = \frac{\alpha_{cw}b_w z v_1 f_{cd}}{\cot(\theta) + \tan(\theta)} = \frac{1 * 500 * 0.9 * 500 * \left(0.6 * \left(1 - \frac{45}{250} \right) \right) * 30}{\cot(21.8) + \tan(21.8)} = 1.15 * 10^6 \; N$$

Substituting in the general unity check equation:

$$\frac{9.31*10^{11}}{2.43*10^{12}} + \frac{3.85*10^5}{1.15*10^6} = 0.74 \leq 1.0$$

Hence, the bearing capacity of the transverse cross-section does comply with the requirement of the unity check ≤ 1.

The values for strips C-F-G and J-H-I differ from C-D-G and A-B-E, due to the difference between the value of the external moment at the north Sea side and the Lake side, the deflection of the supported part in J-H-I and C-F-G is unequal. The calculation approach similar to strips A-B-E and C-D-G will be applied. The results are obtained in Table 29.

Strip transverse direction		J-H-I	C-F-G	
Support length k_d		26.388	26.388	
Support length αk_d		26.388	26.388	
Deflection	At end support k_d	47	48	[mm]
	At interface	47.8	45.09	[mm]
	At end support αk_d	74.1	65.3	[mm]
Resulting reaction force	R_i	629	774.27	[kN]
Lever arm	e_i	13.13	13.33	[m]
Torsional moment	T_{ed}	8255.8	73543.2	[kNm]
Shear Force	V_{Ed}	313.9	385.8	[kN]
Strip		J-H-I	C-F-G	
Member '5'	z_5	4.576	4.576	[m]
Initial thickness member	$t_{5,j}$	500	500	[mm]
Internal shear force	$V_{Ed,5}$	59.7	5298.4	[kN]
Required reinforcement	$\frac{A_{sw}}{s}_5$	0.012	1.06	[mm²/mm]
Assumed stirrup diameter	D_{sw}	10	20	[mm]
h-t-h distance stirrup	s_5	4189.1	295.1	[mm]
Total number of bars per meter	n_5	0.24	3.39	[-]
Required reinforcement ratio	ρ_{x5}	$1.43*10^{-6}$	$1.8*10^{-3}$	[%]
Total Longitudinal reinforcement ratio	ρ_y	0.01	1.33	[%]
Bearing capacity			0.65	[-]

TABLE 29: CALCULATION RESULTS STRIPS IN TRANSVERSE DIRECTION

One would expect a resulting reaction force at strip C-F-G, however, due to the uneven external moments at the North Sea and Lake Side, the deflection over the transverse length will not be equal. This was already shown in Section 7.4.1, Figure 80. Hence, a resulting force will be present in the transverse cross-section.

Table 29 provides positive results regarding the unity check for the bearing capacity and required reinforcement ratios. The required shear reinforcement ratios at the beam edge are below the minimum shear reinforcement ratio. Since the required reinforcement ratios are very low, and the bearing capacity is governed by the shear capacity, the required shear reinforcement will probably be able to bear the torsional moments.

Expect at the midsection, the longitudinal reinforcement requires a ratio of 1.33%, hence additional torsion reinforcement will be required and the economic value exceeded.

LONGITUDINAL DIRECTION

In longitudinal direction, the beam has been divided in three sections, see Figure 103. Each section absorbs a part of the torsional moment. Due to the variances in the external moment the reaction forces for each section differ as well.
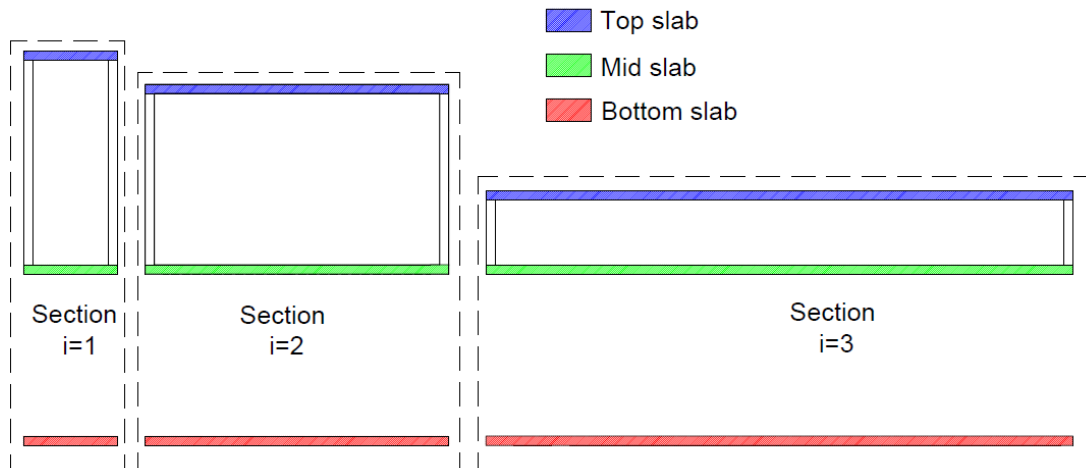
FIGURE 103: THREE SEPERATE SECTIONS

A similar approach as was provided in transverse direction will be applied. The maximum torsional moment in each section will be determined by applying the following steps:

- Determine unknowns for end strip A-C-J and midsection strip B-D-H
- Assume a linear deflection between the two strips
- Take the average of the torsional moments applicable to a single section
- Multiply the average torsional moment by the transverse length of the section:
  - Section 1: 5.076 meter
  - Section 2: 15.9 meter
  - Section 3: 5.362 meter
- Add to the determined torsional moment the maximum torsional moment from the previous section (only for section 2 and 3)
- With the governing torsional moment the required reinforcement ratio allows computation.

Four members may be distinguished in the longitudinal directed cross-section. These members are shown for section 1 in Figure 104:
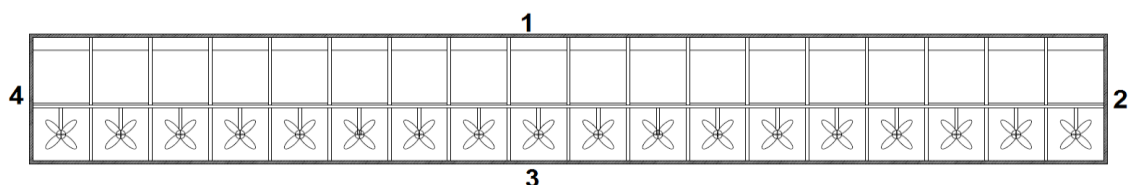
FIGURE 104: CROSS-SECTION SECTION 1. APPOINTED CONCRETE MEMBERS 1 TO 4

A calculation example of the torsional moment in longitudinal direction will be discussed.

At first for section 1 the resulting reaction force and internal lever arm will be determined in both strip A-C-J and B-D-H:

Strip A-C-J: $R_{ACJ,1} = 318\ kN$ $e_{ACJ,1} = 40.7\ m$ $T_{ed,ACJ,1} = 12943.5\ kNm$

Strip B-D-H: $R_{BDH,1} = 0\ kN$ $e_{BDH,1} = 41.04\ m$ $T_{ed,BDH,1} = 0\ kNm$

The maximum torsional moment within this section will be found by assuming a linear decrease of the deflection between strip A-C-J and B-D-H. Hence, the resulting force will increase linearly from B-D-H towards A-C-J. As section 1 has a transverse length of 5.076 meter. The maximum torsional moment within this transverse length will be determined and multiplied by 5.076:

$$T_{ed,1} = \frac{T_{ed,ACJ,1} + \left(T_{ed,ACJ,1} - \frac{T_{ed,ACJ,1} + T_{ed,BDH,1}}{26.338} * 5.076\right)}{2} * 5.076 = 59370.1\ kNm$$

The torsional moment at section 2 will be calculated in a similar manner:

Strip A-C-J: $R_{ACJ,2} = 384\ kN$ $e_{ACJ,2} = 39.885 m$ $T_{ed,ACJ,2} = 15304.8\ kNm$

Strip B-D-H: $R_{BDH,2} = 0\ kN$ $e_{BDH,2} = 40.29\ m$ $T_{ed,BDH,2} = 0\ kNm$

Section 2 lies adjacent to section 1 and has a transverse length of 15.9 meter. Let's say the transverse length is expressed as 'x'. Hence, Between $x_1 = 5.076\ m$ and $x_2 = 20.776\ m$ section 2 will be located. The average torsional moment between $x_1 = 5.076$ and $x_2 = 20.976\ m$ will be found by assuming a linear deflection decrease between strip A-C-J and B-D-H. The torsional moment at both points will thus be found by assuming a linear increase of torsional moment between A-C-J and B-D-H:

At $x_1 = 5.076$:

$$T_{ed,x1,2} = \left(R_{ACJ,2} - \frac{R_{ACJ,2} - R_{BDH,2}}{26.338} * 5.076\right) * \left(e_{ACJ,1} - \frac{e_{ACJ,2} - e_{BDH,2}}{26.338} * 5.076\right)$$
$$= 12388\ kNm$$

At $x_2 = 20.976$:
$$T_{ed,x2,2} = \left(R_{ACJ,2} - \frac{R_{ACJ,2} - R_{BDH,2}}{26.338} * 20.976\right) * \left(e_{ACJ,2} - \frac{e_{ACJ,2} - e_{BDH,2}}{26.338} * 20.976\right)$$
$$= 3143.3\ kNm$$

$$T_{ed,2} = T_{ed,1} + \frac{T_{ed,x1,2} + T_{ed,x2,2}}{2} * 15.9 = 182843.9\ kNm$$

Finally the maximum torsional moment will be calculated for section 3. The transverse length of section 3 between strips A-C-J and B-D-H contains: 26.338-20.976=5.362 meter. Again two points are considered to calculate the maximum torsional moment within section 3; $x_3 = 20.976$ and $x_4 = 26.338$. The resulting reaction force and lever arm at both strips A-C-J and B-D-H are:

Strip A-C-J: $R_{ACJ,3} = 384.7\ kN$ $e_{ACJ,3} = 39.39 m$ $T_{ed,ACJ,3} = 15153.3\ kNm$

Strip B-D-H: $R_{BDH,3} = 0\ kN$ $e_{BDH,3} = 39.79\ m$ $T_{ed,BDH,3} = 0\ kNm$

The torsional moments at x_3 and x_4 follow from:

At $x_3 = 20.976$:

$$T_{ed,x3,3} = \left(R_{ACJ,3} - \frac{R_{ACJ,3} - R_{BDH,3}}{26.338} * 20.976 \right) * \left(e_{ACJ,3} - \frac{e_{ACJ,3} - e_{BDH,3}}{26.338} * 20.976 \right)$$
$$= 3109.9 \ kNm$$

At $x_4 = 26.338$:

$$T_{ed,x4,3} = \left(R_{ACJ,3} - \frac{R_{ACJ,3} - R_{BDH,3}}{26.338} * 26.338 \right) * \left(e_{ACJ,3} - \frac{e_{ACJ,3} - e_{BDH,3}}{26.338} * 26.338 \right)$$
$$= 0 \ kNm$$

$$T_{ed,3} = T_{ed,2} + \frac{T_{ed,x3,3} + T_{ed,x4,3}}{2} * (26.338 - 20.976) = 191181.5 \ kNm$$

The results between strip A-C-J to B-D-H are summarized in Table 30 below.

Strip longitudinal direction:		A-C-J to B-D-H	B-F-H to E-G-I	
Support length k_d		78.91	78.91	[m]
Support length αk_d		78.91	78.91	[m]
Strip A-C-J to B-D-H		Section 1	Section 2	Section 3
Governing torsional moment	T_{ed}	59370.1	182843.9	191181.5 [kNm]
Shear force	V_{Ed}	146.12	173.70	176.85 [kN]
Member '1'	z_1	157.32	157.32	157.32 [m]
Initial thickness member	$t_{1,j}$	500	500	500 [mm]
Required reinforcement ratio	$\rho_{y,1}$	$4.39 * 10^{-6}$	$1.53 * 10^{-5}$	$2.18 * 10^{-5}$ [%]
Total Longitudinal reinforcement ratio	ρ_x	0.01	0.04	0.05 [%]
Bearing capacity		0.13	0.16	0.17
Strip B-F-H to E-G-I		Section 1	Section 2	Section 3
Governing torsional moment	T_{ed}	-	-	200238.4 [kNm]
Shear force	V_{Ed}	-	-	191.39
Member '1'	z_1	-	-	157.32 [m]
Initial thickness member	$t_{1,j}$	-	-	500 [mm]
Required reinforcement ratio	$\rho_{y,1}$	-	-	$2.3 * 10^{-5}$ [%]
Total Longitudinal reinforcement ratio	ρ_x	-	-	0.06 [%]
Bearing capacity		-	-	0.19

TABLE 30: GOVERNING REQUIRED REINFORCEMENT LONGITUDINAL SECTIONS

Table 30 provide positive results regarding the unity check and the required reinforcement ratios. The maximum allowed required reinforcement ratio will not be exceeded. The required shear reinforcement ratios lie below the minim shear reinforcement ratio. Moreover, since the required reinforcement ratios are very low, and the bearing capacity is governed by the shear capacity, the shear required shear reinforcement will probably be able to bear the torsional moments as well.

The asymmetric supporting lengths in the 2D model of base case T2 make the torsional behaviour more complicated compared with T1. In the longitudinal direction a part of the beam is supported by bedding constant k_d for 66.6% of its longitudinal length and a part is supported by a reduced bedding constant αk_d for 33.3% of its longitudinal length. In transverse direction the supported length by bedding constant k_d is 50% of the transverse length. The torsional behaviour of the beam is illustrated in Figure 105. Again several strips in longitudinal and transverse direction are considered, the location of these strips is shown in Figure 106.
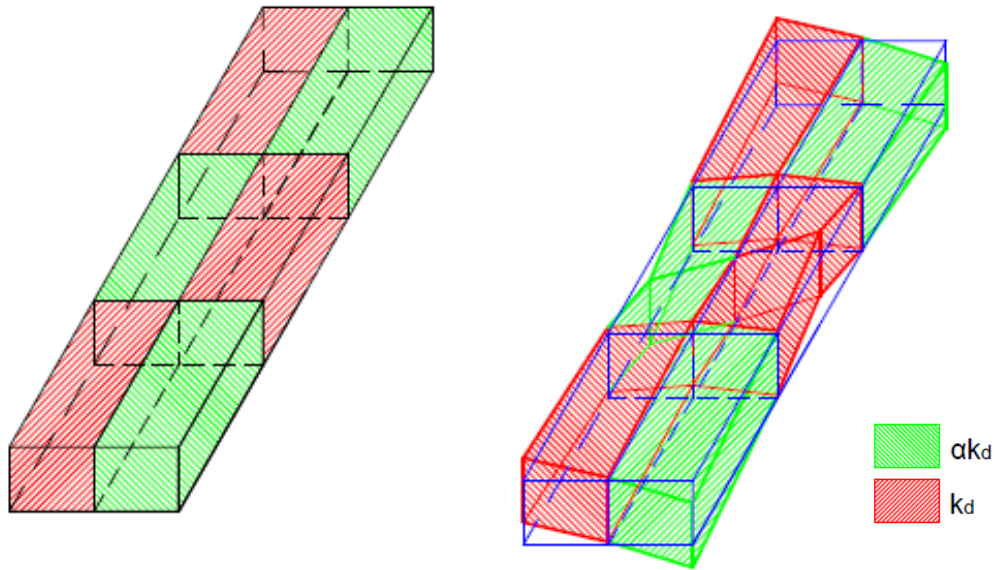
FIGURE 105: TORSIONAL BEHAVIOUR BEAM BASE CASE T2
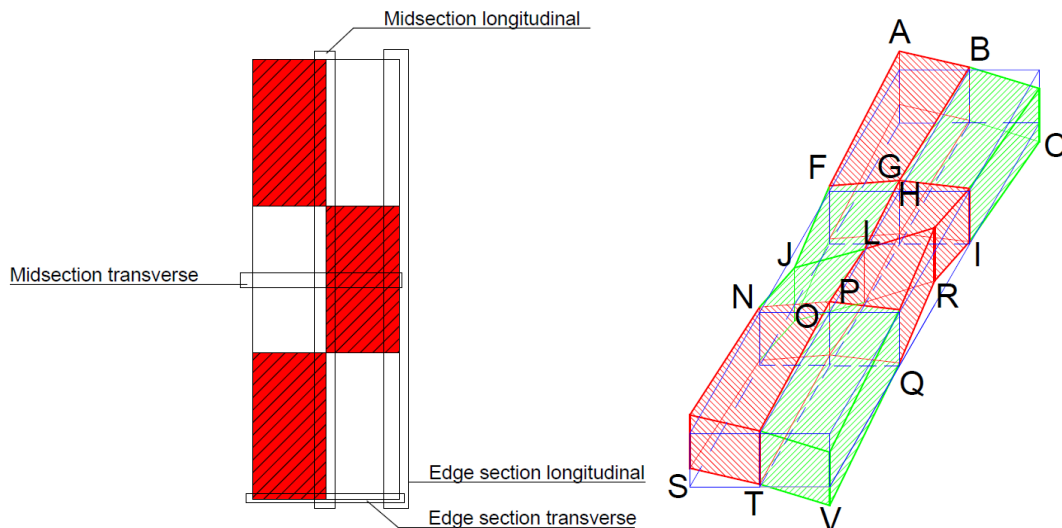
FIGURE 106: INDICATION OF LOCATION CONSIDERED NORMATIVE STRIPS ON THE LEFT SIDE, THE LABELED POINTS ARE SHOWN IN ON THE RIGHT SIDE.

175

The approach used in transverse direction for base case T1 will be applied again. Since this approach has been fully elaborated in the previous section, a summary of the results for base case T2 will be provided in Table 31. Differing from base case T1 is the support length. The value of the average torsional moment is multiplied by a smaller support length (52.61 instead of 78.91), resulting in a lower torsional moment. The considered strips are labelled by letters; an overview of these labels has been presented in Figure 106.

Strip transverse direction		A-B-C	F-G-I	J-L-R	F-H-I	
Support length k_d		26.388	26.388	26.388	26.388	
Support length αk_d		26.388	26.388	26.388	26.388	
Deflection	At end support k_d	47	48	47	48	[mm]
	At interface	47.8	45.09	47.8	45.09	[mm]
	At end support αk_d	74.1	65.3	74.1	65.3	[mm]
Resulting reaction force	R_i	925	774.3	629	774.3	[kN]
Lever arm	e_i	13.81	13.97	13.13	13.3	[m]
Torsional moment	T_{ed}	12779.3	620941.5	8255.8	244181.1	[kNm]
Shear Force	V_{Ed}	460.6	385.8	313.9	385.8	[kN]
Member '5'	z_5	4.576	4.576	4.576	4.576	[m]
Initial thickness member	$t_{5,j}$	500	500	500	500	[mm]
Internal shear force	$V_{Ed,5}$	92.43	251555.9	413.7	12234.7	[kN]
Required reinforcement	$\frac{A_{sw}}{s}\,{}_5$	0.019	0.9	0.012	0.35	[mm2/mm]
Assumed stirrup diameter	D_{sw}	10	20	10	20	[mm]
h-t-h distance stirrup	s_5	4228.5	348.1	6545.4	885.2	[mm]
Total number of bars per meter	n_5	0.24	2.87	0.15	1.13	[-]
Required reinforcement ratio	ρ_{x5}	$2.2 * 10^{-6}$	$1.3 * 10^{-3}$	$9.2 * 10^{-7}$	$2.0 * 10^{-4}$	[%]
Total Longitudinal reinforcement ratio	ρ_y	0.02	1.12	0.01	0.44	[%]
Bearing capacity			0.72		0.49	

TABLE 31: CALCULATION RESULTS STRIPS IN TRANSVERSE DIRECTION

One would expect a resulting reaction force at strip F-G-I and F-H-I, however, due to the uneven external moments at the North Sea and Lake Side, the deflection over the transverse length will not be equal. This was already shown in Section 7.4.1.1, Figure 80. Hence, a resulting force will be present in the transverse cross-section.

Furthermore, from Table 31 it may be noticed the unity check for the bearing capacity complies. In addition the maximum allowed reinforcement ratio will not be exceeded., but the economic value is. The in-plane reinforcement has resulted in a very low value. The required reinforcement from local forces will already be sufficient to bear the torsional moments.

At the mid strip the longitudinal reinforcement requires a ratio of 1.12% and 0.44% at strip F-G-I and F-H-I respectively. Hence additional reinforcement to the local reinforcement will be required. The out-of-plane reinforcement in strip F-G-I exceeds the economic value, therefore structural modifications are recommended.

LONGITUDINAL DIRECTION

In the longitudinal direction the reaction forces are determined by hogging and sagging. As described in base case T1, the torsional moment will be absorbed by the three sections. Hence the governing torsional moment for the three sections will be determined separately, similar steps as described in Base case T1 will be applied:

- Determine unknowns for end strip S-N-J-F-A and midsection strip T-O-G-B
- Assume a linear deflection between the two strips
- Take the average of the torsional moments applicable to a single section
- Multiply the average torsional moment by the transverse length of the section:
  - Section 1: 5.076 meter
  - Section 2: 15.9 meter
  - Section 3: 5.362 meter
- Add to the determined torsional moment the maximum torsional moment from the previous section (only for section 2 and 3)
- With the governing torsional moment the required reinforcement ratio allows computation.

Again four members may be considered, see Figure 104 . Results for member '1' have been elaborated for sagging, strip S-N-J-F-A to T-O-G-B, and hogging, strips V-Q-R-I-C to T-P-H-B in Table 32 and Table 33. Obtaining the torsional moments has been done in a similar method as provided for base case T1.

Strip longitudinal direction:		S-N-J-F-A to T-O-G-B			
Support length k_d		52.607			[m]
Support length αk_d		26.303			[m]
		Section 1	Section 2	Section 3	
Governing torsional moment	T_{ed}	196340	600137	642739	[kNm]
Shear force	V_{Ed}	485.6	418.8	298.1	[kN]
Member '1'	z_5	157.32	157.32	157.32	[m]
Initial thickness member	$t_{5,j}$	500	500	500	[mm]
Required reinforcement ratio	$\rho_{y,5}$	$1.45 * 10^{-5}$	$1.00 * 10^{-4}$	$2.21 * 10^{-4}$	[%]
Total Longitudinal reinforcement ratio	ρ_x	0.04	0.13	0.18	[%]
Bearing capacity		0.44	0.41	0.32	[-]

TABLE 32: RESULTS REQUIRED REINFORCEMENT RATIOS STRIPS S-N-J-F-A TO T-O-G-B.

Strip longitudinal direction:		V-Q-R-I-C to T-P-H-B			
Support length k_d		26.303			[m]
Support length αk_d		56.607			[m]
		Section 1	Section 2	Section 3	
Governing torsional moment	T_{ed}	-	-	228091	[kNm]
Shear force	V_{Ed}	-	-	80.8	[kN]
Member '1'	z_5	-	-	157.32	[m]
Initial thickness member	$t_{5,j}$	-	-	500	[mm]
Required reinforcement ratio	$\rho_{y,5}$	-	-	$5.23 * 10^{-5}$	[%]
Total Longitudinal reinforcement ratio	ρ_x	-	-	0.07	[%]
Bearing capacity				0.09	[-]

TABLE 33: RESULTS REQUIRED REINFORCEMENT RATIOS STRIPS V-Q-R-I-C TO T-P-H-B.

Both tables have shown positive results regarding the required reinforcement ratios and bearing capacity unity check. From Table 32 it may be noticed the unity check value

decreases for each succeeding section. It may be concluded the shear force governs the bearing capacity. Thus, the required reinforcement from the shear force applied at the cross-section will be governing. Due to the low reinforcement ratio it may be expected the shear reinforcement will also be able to bear the torsional moments. Hence, no additional reinforcement will be required to bear the torsional moment due to the low reinforcement ratios.

7.4.3.5 CONCLUSION TORSION

The assumed wall thickness of 500 mm provides positive results regarding the in-plane reinforcement. The longitudinal reinforcement, or out-of-plane reinforcement exceeds the economic value of 1%. Based on this feature the wall thickness, especially in the transverse cross-section should be increased.

Combining the obtained torsional reinforcement ratios and the reinforcement ratios from sections 7.4.2.5, the required reinforcement ratio will be exceeded significantly (indicated with red in Table 34.). The governing ratios are provided in Table 34.

	Top slab			Mid slab			Bottom slab			Inner walls		
Longitudinal direction (ρ_y)												
Section	1	2	3	1	2	3	1	2	3	1	2	3
Local bending	0.03	0.03	0.03	0.05	0.05	0.05	1.14	1.14	1.14	-	-	-
Global Bending	0.59	0.6	0.49	-	-	-	0.008	0.06	0.15	-	-	-
Shear forces	0.31	0.50	0.62	-	-	-	0.31	0.50	0.62	0.22	0.41	0.54
Torsion	1.12	1.12	1.12	-	-	-	1.12	1.12	1.12	-	-	-
Sum	2.05	2.25	2.26	0.05	0.05	0.05	2.58	2.82	3.03	0.22	0.41	0.54
Transverse direction (ρ_x)												
Section	1	2	3	1	2	3	1	2	3	1	2	3
Local bending	0.19	0.19	0.19	0.29	0.29	0.29	-	-	-	-	-	-
Global Bending	0.77	0.44	0.64	-	-	-	0.097	0.18	0.3	-	-	-
Shear forces	-	-	-	-	-	-	-	-	-	-	-	-
Torsion	0.04	0.13	0.8	-	-	-	0.04	0.13	0.8	-	-	-
Sum	1.0	0.76	0.63	0.29	0.29	0.29	0.137	0.31	1.1	-	-	-

TABLE 34: GOVERNING REQUIRED REINFOREMENT RATIOS FROM BASE CASES HOGGING AND SAGGING AND TORSIONAL BASES CASES

The bearing capacity unity check complies for each cross-section and base case. The maximum shear resistance will thus not be exceeded according to the provided calculations.

The red marked values in Table 34 indicate the structural elements that require an significant increase in element thickness. In further research the optimal concrete thickness should be sought for.

7.5 CONCLUSION CONCEPTUAL DESIGN STRUCTURAL ELEMENTS

The results of the performed analyses have been combined in Table 34 on the previous page. The required reinforcement ratios in several structural elements are still to be considered. However, the considered elements almost all exceed the economic reinforcement value of 1%. Especially in the bottom slab requires additional attention. Therefore, in further research an improved slab and wall thickness should be applied. An iterative process will follow to determine the optimal concrete thickness of the structural elements.

Hence, the assumed thickness of 500 mm for the structural elements results in reinforcement ratios exceeding 3%. The assumed thickness has thus be considered as insufficient and requires major adaptations at several structural elements.

Additionally, three more limit state checks should be performed to finalize the conceptual design phase. These checks are described as:

- Stress capacity in SLS
- Crack control in SLS
- Maximum deflection in SLS

Concluding the conceptual design phase by providing these three checks leads to a final conceptual design adapted to all the requirements prescribed by the EC2.

8 CONCLUSIONS

Conclusions drawn from the main sections in this theses are discussed in this chapter.

Main activities at Lake Grevelingen, such as: tourism and recreation, fishery industry and flora and fauna, will suffer from the deteriorating oxygen gradient. Since these three activities contribute to revenues of local enterprises, the entire Lake environment suffers from the reducing water quality.

Introducing a tidal range of 50 cm at Lake Grevelingen will result in an increases water quality. A discharge system should be provided to reach such tidal range. The construction costs of a discharge structure are rather, however, since the Brouwersdam is in direct contact with the North Sea, the tidal range from the North Sea could be used to generate power. Hence, the construction of a low head Tidal Power Plant seems to be an optimal solution.

The preliminary turbine design has provided two optimal turbine types; the PFn and free-stream turbine. Applying a free-stream and modified bulb turbine in the Tidal Power Plant could lead to an annual energy production of 19.22 GWh and 81.54 GWh respectively. Applying the modified bulb turbine would thus result in an increased energy generation. However, due to many uncertainties regarding the properties of a modified bulb turbine with a diameter of 8.24 meter it is chosen to apply proven free-stream turbine prior to the modified bulb turbine.

Within the preliminary powerhouse design the dimensions of the Tidal Power Plant have been obtained. Including a gate and gate housing, turbine housing and a complete infrastructure area, the transverse and longitudinal length contains 52.676 meter and 157.82 meter respectively. All structural elements have been provided with 500 mm thick walls. The resistance to external forces of these structural elements has been elaborated in the conceptual design of the structural elements. From the stability checks it came forward and additional ballast layer will be required within the structure, see Figure 107.

FIGURE 107: TRANSVERSE CROSS-SECTION TIDAL POWER PLANT INCLUDING INFRASTRUCTURE AND BALLAST LAYER UNDERNEATH COLOURED INFRASTRUCTURE.

Since the caissons present at the Brouwersdam could not be reused, removal becomes inevitable. It has been decided to remove the caissons in the wet, while constructing the Tidal Power Plant in the wet as well. The Tidal Power Plant will be located at the Lake side of the current Brouwersdam. A rubble material bed will be applied to function as

foundation to the Tidal Power Plant. Adjacent to this foundation a 94.0 meter and 91.1 meter long bed protection will be constructed at the Lake and North Sea side respectively. Figure 108 provides a three dimensional overview of the Tidal Power Plant implemented in the Brouwersdam.

FIGURE 108: 3D TOP VIEW FROM NORTH SEA SIDE, TIDAL POWER PLANT INTEGRATED IN BROUWERSDAM. INCLUDING THE BED PROTECTION.

Within the conceptual design of the structural elements the resistance to local and external forces has been investigated. The computational approach consisted of a beam on an elastic foundation induces the influence of deviations in the rubble foundation bed. These deviations have been considered in a one dimensional and two dimensional approach. With the rather small thickness of the structural elements, the required reinforcement has been determined accordingly. It has resulted in governing reinforcement ratios exceeding 3%. With an economic reinforcement ratio of 1% is has been concluded the thickness of the structural elements has been assumed insufficient. Therefore in further research, increased concrete element thickness should be applied.

9 RECOMMENDATIONS

First of all, a clear cost estimation should be made, providing a better insight of the feasibility of the project. Included in this estimation should be a revenue estimation from the generated energy by the applied turbines. Therefore, better and more clear information should be provided by turbine manufacturers as well. With the construction of a Tidal Power Testing centre, situated at the Grevelingendam, genuine tests will be performed in the near future. Results from these test may be used to optimize the final turbine type and turbine dimensions.

The concrete members thickness has proven to be insufficient. According to the performed calculations a significant modification will be required. Moreover, more detailed calculations should be performed to reach a final verdict regarding the concrete thickness. It is therefore recommended to apply a more detailed calculation method using the Finite element (FE) method. A 3D Fe method should provide a clear indication of the required cross-sections.

The turbine selection was strongly influenced by the fish mortality rate of turbines. The allowed fish mortality of 0.01%, prescribed by the Dutch Government [Dronkers, 2015] seems to be extremely low. Moreover, the exact definition of the mortality rate is unknown. Hence, it is recommended to provide a clear understanding of the fish mortality requirement.

The width of the road provided in the preliminary powerhouse design has been based on the assumption the current infrastructure present on the Brouwersdam should remain unchanged. Whether this is actually preferred remains unknown. The requirements of the infrastructure should therefore be clearly described. The dimensions of the Tidal Power Plant are strongly influences by these infrastructural requirements.

A subgrade stiffness of 50 MPa has been assumed as an reasonable value, based on information obtained from the Rock Manual [2007]. The subgrade stiffness has a major impact on the response of the rubble foundation to the external loadings. Therefore, tests should be performed to determine the actual stiffness of the applied subgrade material. Also, one could decide to provide proper material having material properties coinciding with the required material properties used in the calculations.

The bed protection has been determined using a water depth obtained from a first assumption of the required rubble material foundation. This value has been adapted afterwards, without adapting the bed protection calculations. It is therefore recommended to determine the bed protection iteratively when more information is available regarding the required bottom slab thickness.

During the design stages of the Tidal Power Plant many assumptions are made. A better and more detailed insight to the important parameters is therefore recommended. Moreover, just a small part of the design of the Tidal Power Plant is performed in this thesis, much work is required to define an actual decent design of the structure, such as:

- The influence of the Tidal Power Plant on the sandy beaches at the North Sea side of the Brouwersdam
- Deciding whether Lake Grevelingen will be used as a storage basin. In this preliminary and conceptual design this has not been taken into account. The

influences of enabling Lake Grevelingen as a storage basin on the Tidal Power Plant is therefore very interesting to investigate.

10 REFERENCES

Andritz. 2016. Bulb Turbines. [Online] Available at: https://www.andritz.com/products-and-services/pf-detail.htm?productid=9213

Autodrill. 2013. Coefficient of Friction. [Online] Available at: http://drill-hq.com/wp-content/uploads/2012/11/CoefficientOfFrictionChart.pdf

Battjes, J.A., Labeur, R.J. 2014. Course CTB3350 Open Channel Flow. TU Delft.

Berkel, van J. Kraassenberg, T., Paulus, P. 2011. MIRT Grevelingen, Tidal Power Plant Brouwersdam, Project Outline

Boon, M.J.J., Roest, F.M. 2008. Notitie civiele aspecten doorlaatmiddel Brouwersdam. Witteveen + Bos.

Bouma, S., Lengkeek, W., Waardenburg, H.W. 2007. Het effect van zuurstof deficiënte op het bodemleven in het Grevelingenmeer. Bureau Waardenburg.

Bouma, S., Lengkeek, W. Boudewijn, T.J., Turlings, L.G., Abma, R. Nieuwkamer, R.L.J. 2008. Notitie knelpunten autonome ontwikkeling. Onderdeel verkenning Grevelingen. Bureau Waardenburg.

CIRIA; CUR; CETMEF. 2007. The Rock Manual. The use of rock in hydraulic engineering (2nd edition). London.

Clark, R.H. 2007. Elements of tidal-electric engineering

Danad, M. 2015. Port of Rotterdam reuse of Caissons. Master thesis TU Delft.

De Deltadienst. 1968. Het ontwerp van de doorlaatcaissons voor het Brouwershavensche Gat. De Deltawerken Feb 1st 1968.

Department of the Army Waterways Experiment Station. Corps of Engineers Coastal Engineering Research Center. 1984. CERC, Shore Protection Manual. US Government.

Dronkers, J.H. 2015. Beleidsregel watervergunningverlening waterkrachtcentrales in rijkswateren.

Erbisti, P.C.F. 2015. Design of Hydraulic Gates, 2nd edition.

Esch, B.P.M. van. 2015. Model based study of fish damage for the Pentair Fairbanks Nijhuis modified bulb turbine and the Water2Energy cross flow turbine. Pro-Tide.

Esch, B.P.M. 2015. Model based study of fish damage for the Pentair Fairbanks Nijhuis modified bulb turbine and the Water2Energy Cross flow turbine. Pro-Tide.

Goda, Y. 2010. Random seas and design of maritime structures. 3rd edition.

Giroud, J.P. 1996. Granular Filters and geotextile filters. In: J. Lafleur and A.L Rolin. Proc Geofilter '96, Montreal, 29-31 May. Bitech Publisching, Richmond, BC.

Giroud, J.P., Delmas, P., Artières, O. 1998. Theoretical basis for the development of a two-layer geotextile filter. In: R.K. Rowe (ed), PROC 6th int conf geosynthetics, Atlanta, Ga.

Grol, C. 2016. Door grotere turbines en lage rentes zijn windparken nu goedkoper dan ooit. Financieel dagblad.

Haag, C. Veenstra, J. Everdij, L. Teuling, W. 2014. Nota Toetsingkaders en beleidsregels voor het watersysteem 2014. Waterschap Hollandse Delta.

Hamsel, R. ter, Boheemen-Gerritsen, S. van, Puts, T.J.A. 2016. Groene Impuls Grevelingen Advisering vogeleilandjes en vismigratievoorzieningen. Witteveen + Bos.

Hetenyi, M. 1979. Beams on elastic foundation. Theory with the applications in the field of civil and mechanical engineering.

Jocobson, P. 2014. Evaluation of survival and behavior of fish exposed to an axial-flow Hydrokinetic Turbine. Electric Power Research Institute.

Kessel, T. van., Verheul, M.R.A., Lucas Pardo, M.A. de. 2015. Resultaten bodemmonsteranalyse Grevelingen en Volkerak-Zoommeer.

Koninklijk Nederland Meteorologisch Instituut (KNMI). 2014. KNMI'14 Klimaatscenario's voor Nederland.

Koninklijk Nederland Meteorologisch Instituut (KNMI). Ziespiegelveranderingen in de toekomst. [Online]. Available at: https://www.knmi.nl/kennis-en-datacentrum/achtergrond/zeespiegelveranderingen-in-de-toekomst.

Knapp, F.H. 1960. Ausfluss, Überfall und Durchfluss im Wasserbau, Verlag G. Braun, Karlsruhe.

Kranenbarg, J., 2004. KRW vis in overgangswateren Antropogene knelpunten en potentiële herstel- en inrichtingsmaatregelen. STOWA

Lammens, L.C., Swolf, W.K., Barrois, J.C., Ruijter, L.M. de, Lauf, J., Balla, A., Tijs, M., Jong, B. de. 2016. Schouwen-Duiveland Brouwerseiland Milieu-effectrapportage. Rho Adviseurs voor Leefruimte.

Lengkeek, W. Bouma, S. Van den Booogaard, W. 2010. De verspreiding van witte bacteriematten en schade aan het bodemleven in het Grevelingenmeer. Onderzoek naar de effecten van zuurstofloosheid. Bureau Waardenburg.

Maldegem, P.J. 1973. Het verlengen van het damvak Kabbelaarsbank en de drempelopbouw in de sluitgaten. OTAR.

Meijnen, R., Arnold, J. 2015. TPP-Brouwersdam. Conceptual design and comparison of Two Propeller Turbine Configurations.

Miller, H. 1978. 'Choice of hydro-electric equipment for tidal energy' (Proceedings Korea Tidal Power Symposium, Sulzer-Esher Wyss, Oct-Nov. 1978)

Ministerie van Verkeer en Waterstaat. 2007. Hydraulische Randvoorwaarden primaire waterkeringen.

MIRT Grevelingen, Berkel, van J., Kraassenberg, T., Paulus, P. 2011. Tidal Power Plant Brouwersdam, Project Outline.

Mooyaart, L.F., Noortgaete, T. Van Den. 2010. Getijcentrale in de Brouwersdam Variantenstudie. RHDHV.

Natuur- en Recreatieschap Grevelingen. 2006. Ontwikkelingsschets; Zicht op de Grevelingen.

Nieuwendijk, G.L. 1968. De Deltawerken (nr. 33). De Ingenieur.

Nolte, A. Troost, T. De Boer, G. Spiteri, C. Van Wesenbeck, B. 2008. Verkenning oplossingsrichtingen voor een betere waterkwaliteit en ecologische toestand van het Grevelingenmeer; verkenning Grevelingen, water en getij. Deltares.

Noortgaete, T. Van Den. 2009. Overzicht stand van techniek kleinschalige waterkracht. Deltares.

Pentair-Nijhuis, R&D department. 2015. Status report Low Head Turbines 06-2015.

Pentair Fairbanks Nijhuis. 2017. Bi-directional Turbine. [Online] Available at: http://www.fairbanksnijhuis.com/EngineeredProduct_Bi-directional_turbine.aspx

Pilarczyk, K.W. 1998. Stability criteria for geosystems – an overview-. 6th Intern. Conference on Geosynthetics, Atlanta USA.

Programmabureau zuidwestelijke Delta. 2014. Ontwerp-rijksstructuurvisie Grevelingen en Volkerak-Zoommeer. Ministerie van Infrastructuur en Milieu

Raabe, J. 1985. Hydropower: 'The design, use and function of hydromechanical, hydraulic and electrical equipment', (VDI-Verlag, Duesseldorf, 1985)

Rijkswaterstaat. 2013. Richtlijnen Beoordeling Kunstwerken.

Rijkswaterstaat. 2015. Richtlijn Ontwerp Autosnelwegen 2014.

Rijkswaterstaat. 2017. Richtlijnen Ontwerp Kunstwerken.

Rijkswaterstaat and Royal Haskoning DHV. 2015. Natura 2000 Ontwerpbeheerplan Deltawateren 2015-2021 Grevelingen. Rijkswaterstaat and RHDHV.

Scheijgrond, P., Schaap, A., Raventos, A. 2014. Scenario analysis of tidal stream generation in an inlet in the Brouwersdam. MET-Support.

Schiereck, G.J., Verhagen, H.J. [2012] Introduction to bed, bank and shore protection.

Simone, A. 2011. An introduction to the Analysis of Slender Structures. Delft University of Technology.

Smale, A.J., Turlings, L.G., Boon, M.J.J., Nieuwkamer, R.L.J. 2008. Notitie optimale locatie(s) doorlaatmiddelen, Onderdeel verkenning Grevelingen. Rijkswaterstaat.

Spengen, J. van, Reijneveld, J.D., Wit, M., Tieleman, O. 2015. Civil Design of a Tidal Power Plant case Brouwersdam. Iv-Groep.

Spiteri, C., Nolte, A.J. 2010. Validatie van het 3D model van het Grevelingenmeer voor hydrodynamica, waterkwaliteit en primaire productie, Deltares.

Stratelligence. 2014. MKBA bij Rijksstructuurvisie Grevelingen en Volkerak-Zoommeer. Leiden.

TATA Steel. 2016. Hybox® 355 Technical Guide, Structural hollow sections.

Tocardo Tidal Power. 2016. Tidal Power Plant in Dutch Delta works. [Online] Available at: http://www.tocardo.com/Project/oosterschelde/

Verhagen, H.J., d'Angremond, K. Roode, F. van. 2012. Breakwaters and closure dams, 2nd edition.

Voorendt, M.Z., Molenaar, W.F., Bezuyen, K.G. 2011. Lecture Notes : Hydraulic Structures, Caissons. TU Delft.

Vrijling, J.K., Duivendijk, J., Jonkman, S.N., Gilles, A., Mooyaart, L.F. 2008. Getijcentrale in de Brouwersdam een verkennende studie.

Vrijling, J.K., Duivendijk, J. van, Jonkman, S.N., Gilles, A., Mooyaart, L.F. 2008. Getijcentrale in de Brouwersdam, een verkennende studie. TU Delft [Vrijling et al, 2008]

Walraven, J.C. Gewapend beton. Dictaat CT2052/3150. TU Delft.

Waterbase.nl

Wardenier, J. 2010. Hollow section in structural applications. TU Delft.

Welsink, M., Yazici, S. 2014. Innovatieve civiele technieken voor de Getijcentrale Brouwersdam. TU Delft.

Wetsteijn, L.P.M.J. 2011. Grevelingenmeer: meer kwetsbaar?. Rijkswaterstaat

Wijsman, J.W.M., Goudswaard, P.C., Kotterman, M.J.J., Smaal, A.C.S. 2014. Quick scan: Effecten zout getij Grevelingenmeer en Volkerak-Zoommeer op visserij en aquacultuur. Wageningen UR.

APPENDIX A

REQUIREMENTS BY MIRT GREVELINGEN

The MIRT Grevelingen, a governmental institute which focusses on multiannual programme for infrastructure, space and transport, has set a number of requirements for the project outline of a Tidal Power Plant in the Brouwersdam. The design provided in this thesis must comply with these requirements in order to have any contribution to future construction of the Tidal Power Plant. The requirements formulated in the MIRT Grevelingen [MIRT Grevelingen, 2011], were set in the year 2011. Hereafter several studies have been performed, therefore the list of requirements is slightly updated according to findings from the relevant studies in a later stadium. The requirements are distinguished in three components:

1. Functional requirements

Water passage	The Tidal power plant needs to allow passage of water from the North Sea to lake Grevelingen and vice versa.
Flow rates	The Tidal Power Plant needs to: • Facilitate passage of minimal 3500 m^3/s (time average) of water in ebb-mode. • Facilitate passage of minimal 3500 m^3/s (time average) of water in flood-mode.
Water barrier	The tidal power plant needs to be incorporated in connecting water barrier number 14 and must at all time function as such. The tidal power plant must be able to withstand (hold) also in case of a 1/4000, the norm-frequency for maximum conditions at the North Sea.
Level Control	During normal operation: • Targeted water level at Lake Grevelingen on average NAP -0.20 m with variation between -0.40 and 0.00 NAP. • Mean water level at North Sea LW-level NAP -1.06 m and HW-level NAP +1.44 m The tidal power plant must facilitate control of the water level in lake Grevelingen, between maximum and minimum level, with prescribed average level.
Traffic	The tidal power plant needs to facilitate road traffic on the Brouwersdam, also from the N57 and parallel road, at least with today's traffic quality.

2. Aspect requirements

Safety	The tidal power plant is to be considered as a machine that to comply with "Machinerichtlijn".
Safe usage	Operators, visitors and others related to control, operation and maintenance must be able to safely stay in and around and make uses of the tidal power plant facility,
Fish friendliness	The tidal power plant fish mortality rate must be lower than 0.01 %.
Availability water passage	Non-availability of the tidal power plant, in relation to water passage, must be less than 0.5 %. Non-availability includes: • Foreseeable non-availability (maintenance). • Non foreseeable, non-availability as a result of closure of the gates due to malfunctioning.
Max. period of non-availability	The maximum time-interval of non-availability in relation to water passage must be less than 12 hours.
Discharge capacity during maintenance	Reduction of water passage capacity due to planned maintenance must be less than 50 %.
Vandalism effect on availability	The tidal power plant must be designed and constructed in a way that vandalism does not affect availability and reliability of the water passage function and water barrier functions.
Availability traffic connection	Non-availability of the tidal power plant in relation to road traffic must be equal or less than 0.5 %.
Life time tidal power plant	The tidal power plant must be constructed with a lifetime for functional use of at least 100 years.
Life time components	Components must have a life time: • Civil works: 100 years • Steel construction components: 50 years • Mechanical engineering components: 50 years.

Max. overtopping flow rate	Maximum overtopping flow rate during MHW must be less than 0.1 m^3/s/m.
Chance of failure (closing)	The tidal power plant must have a chance of failure for closure, less $2.5 * 10^{-5}$ per year.
Re-establish closure after failure	After failure of closure procedure, closure must be restored with 1 day.
Change of mechanical failure	The chance of constructive failure of the tidal power plant in relation to water holding capacity must be less than 1/400.000 year (0,01 x norm)
Reliability constructive safety	Reliability of the tidal power plant, in relation to constructive safety, must comply to safety class RC3 conform the Euro code
Air pollution, hindrance	Regarding air pollution, vibrations and noise, the tidal power plant needs to comply with relevant laws and legislation rules.
Environmental effect	The tidal power plant needs to fulfil the respective conditions in the governing environmental legislation.
Vibration during construction	The chance that vibrations lead to damage of objects must be minimized within the framework of SBR guidance A.
Water safety during construction	During construction of the tidal power plant, the water holding function of the Brouwersdam must at all times be fulfilled.
Temporary barrier function	Temporary measures for water hold-up during construction of the tidal power plant are designated as primary water barriers within the framework of the Waterwet and at all times need to function as such.
Control	The tidal power plant needs to be controllable on-site and remote.
Dismantling	Moving construction components needs to be demountable with reasonable effort

3. External interface requirements

Interface inlet and outlet on ambient	The inlet and outlets need to connect to adjacent streams (outside system boundary) in a way that water passage under free fall conditions is guaranteed.
Flow velocity at end sea bed protection	Maximum flow velocity at the bottom interface between tidal power plant and surrounding water system needs to be less than 0,5 m/s.
Cables and conduits	Functions of existing cables and pipe work on the Brouwersdam must be maintained.
Interface traffic roads	Roads inside the tidal power plant system boundary need to connect to surrounding roads.

.

APPENDIX B:

PRELIMINARY TURBINE DESIGN

B.1 TURBINE TYPE

The best applicable turbine type is, amongst other factors, determined using recent studies performed by several institutes and engineering companies. These recent studies could help giving a clear insight of what the costs of the tidal power plant could become and what kind of turbine would generate the highest amount of energy. Next to that, the Rink method is introduced as an inspiration for the decision of what type of turbine is best applicable, or in what way can we make sure the Tidal Power Plant will keep on generating as much power as possible during its lifetime. . The Rink method works in that way as a kind of inspiration.

B.1.1 RECENT STUDIES TURBINE DESIGN

Below the design of the recent studies are summarized. The recent studies can be used as a reference when determining the best turbine solution for the tidal power plant at the Brouwersdam.

Report A: Vrijling et al. [2008]

Variant	Investment[3]	Energy field	Tide	Type	Location	Specific location	Dock type	Current construction	Turbine type	$D_{turbine}$	Turbine Units
	$(10^6 €)$	(GWh/y)	(m)							(m)	
A 1a	291,2	226	1,0-1,1	Ebb	North	Original caissons	Dry dock	Removing existing caissons	Bulb	3,5	106
A 1b	291,2	203	1,1-1,2	Flood	North	Original caissons	Dry dock	Removing existing caissons	Bulb	3,5	106
A 2a	279,2	226	1,0-1,1	Ebb	North	Original caissons	Dry dock	Removing existing caissons	Bulb	3,5	106
A 2b	279,2	203	1,1-1,2	Flood	North	Original caissons	Dry dock	Removing existing caissons	Bulb	3,5	106
A 3a	457,6	392	1,5	ebb	North & South	Original caissons/ block dam	Dry dock	Removing existing caissons and blocks	Bulb	3,5	106+ 52
A 3b	457,6	280	1,5	Flood	North & South	Original caissons/ block dam	Dry dock	Removing existing caissons and blocks	Bulb	3,5	106+ 52
A 4	228,5	213	0,7	Bi-directional	North	Original caissons	Dry dock	Removing block dam	Bulb	3,5	106
A 5	167,5	145	0,4	Bi-directional	South	Original Block dam	Dry dock	Removing block dam	Bulb	3,5	70
A 6	188,1	162	0,5	Bi-directional	South (2 layers)	Original Block dam	Dry dock	Removing block dam	Bulb	3,5	2*40
A 7	395,95	344	1,0-1,1	Bi-directional	South & North	Original caissons/ block-dam	Dry dock	Removing existing caissons and blocks	Bulb	3,5	106+ 70
A 8	416,55	353	1,1	Bi-directional	South & North	Original caissons/ block-dam	Dry dock	Removing existing caissons and blocks	Bulb	3,5	106+ 2*40

Report B: Boon and Roest [2008]

Variant	Investment	Energy field	Tide	Type	Location	Specific location	Dock type	Current construction	Turbine type	$D_{turbine}$	Turbine Units
	$(10^6 €)$	(GWh/y)	(m)							(m)	
B 1	314	0	0,5	Sluice	South	Inner side dam	Dry dock with temporary dam	Removing existing caissons	-	-	-
B 2	314	0	0,5	Sluice	North	Inner side dam	Dry dock with temporary dam	Removing existing caissons	-	-	-
B 3	1549	344	1,0-1,1	Bi-directional	South & North	Inner side dam	Dry dock with temporary dam	Removing existing caissons and blocks	bulb	3,5	106+70

---

[3] Investment costs without construction costs.

Report C: Mooyaart and Noortgaete [2010]

Variant	Investment	Energy field	Tide	Type	Location	Specific location	Dock type	Current construction	Turbine type	$D_{turbine}$	Turbine Units
	$(10^6$ €$)$	(GWh/y)	(m)							(m)	
C 1a	499	193	0,57	Bi-directional	North	Original caissons	Dry dock	Removing existing caissons	Bulb	3,5	106
C 1b	315	30	1,6	Bi-directional	North	Original caissons	Dry dock	Removing existing caissons	Free-stream	6	20*4
C 1b*	158	10	0,5	Bi-directional	North	Original caissons	Dry dock	Removing existing caissons	Free-stream	6	20*4
C 2a	534	193	0,57	Bi-directional	North	Inner side dam	Dry dock with temporary dam	Removing existing caissons	Bulb	3,5	106
C 2b	350	30	1,6	Bi-directional	North	Inner side dam	Dry dock with temporary dam	Removing existing caissons	Free-stream	6	20*4
C 2b*	175	10	0,5	Bi-directional	North	Inner side dam	Dry dock with temporary dam	Removing existing caissons	Free-stream	6	20*4
C 3a	562	193	0,57	Bi-directional	North	In lake Grevelingen inner side dam	External Wet & building in the wet	Removing existing caissons	Bulb	3,5	106
C 3b	379	30	1,6	Bi-directional	North	In lake Grevelingen inner side dam	External Wet & building in the wet	Removing existing caissons	Free-stream	6	20*4
C 3b*	190	10	0,5	Bi-directional	North	In lake Grevelingen inner side dam	External Wet & building in the wet	Removing existing caissons	Free-stream	6	20*4
C 4a	497	174	0,56	Bi-directional	North	Partly over Original caissons	Dry dock	Reuse existing caissons	Waterpower siphon	3,5	106
C 4b	301	118	0,56	Bi-directional	North	Partly over Original caissons	Dry dock	Reuse existing caissons	Hydro-pneumatic	-	-

Report D: Welsink and Yazici [2014]

Variant	Investment	Energy field	Tide	Type	Location	Specific location	Dock type	Current construction	Turbine type	$D_{turbine}$	Turbine Units
	$(10^6$ €$)$	(GWh/y)	(m)							(m)	
D 1:Base variant	468	213	0.7	Bi-directional	North	Original caissons	Dry dock	Removing existing caissons	Bulb	3,5	106
D 2:Large Diameter	434		0.5	Bi-directional	North	Original caissons	Dry dock, with temporary dam	Removing existing caissons	Bulb	7	26
D 3: VLH	475		0.5	Bi-directional	North	Original caissons	Dry dock	Removing existing caissons	VLH	5,5	192

Report E: Scheijgrond et al. [2014]

Variant	Investment Turbine[4]	Energy field	Tide	Type	Location	Specific location	Dock type	Current construction	Turbine type	$D_{turbine}$	Turbine Units
	$(10^6$ €$)$	(GWh/y)	(m)							(m)	
E 1a: Schottel	17.9	16	0,443	Bi-directional	North	Original caissons	Dry dock	Removing existing caissons	Free stream horizontal axis	3	60
E 1a: Tocardo	18.0	14,8	0,435	Bi-directional	North	Original caissons	Dry dock	Removing existing caissons	Free stream horizontal axis	5,8	15
E 1a: OEU	31.9	28,7	0,425	Bi-directional	North	Original caissons	Dry dock	Removing existing caissons	Free stream vertical axis	10,5	8
E 1b: Schottel	17.9	10,7	0,443	Bi-directional	North	Original caissons	Dry dock	Removing existing caissons	Free stream horizontal axis	3	60
E 1b: Tocardo	18.0	9,9	0,435	Bi-directional	North	Original caissons	Dry dock	Removing existing caissons	Free stream horizontal axis	5,8	15

[4] Costs of the civil construction is not taken into account.

Variant	Investment (10^6 €)	Energy field (GWh/y)	Tide (m)	Type	Location	Specific location	Dock type	Current construction	Turbine type	$D_{turbine}$ (m)	Turbine Units
E 1b: OEU	31.9	19,1	0,425	Bi-directional	North	Original caissons	Dry dock	Removing existing caissons	Free stream vertical axis	10,5	8
E 2: Schottel	28.4	16,2	0,5	Bi-directional	North	Original caissons	Dry dock	Removing existing caissons	Free stream horizontal axis	4	48
E 2: Tocardo	32.7	17,6	0,5	Bi-directional	North	Original caissons	Dry dock	Removing existing caissons	Free stream horizontal axis	5,8	18
E 2: OEU	52.7	34,9	0,5	Bi-directional	North	Original caissons	Dry dock	Removing existing caissons	Free stream vertical axis	10,5	10

Report F: Van Spengen and Reijneveld [2015]

Variant	Investment (10^6 €)	Energy field (GWh/y)	Tide (m)	Type	Location	Specific location	Dock type	Current construction	Turbine type	$D_{turbine}$ (m)	Turbine Units
F 1: Diffuser	318,5		0.5	Bi-directional	North	Original caissons	External dock & Building in the wet	Removing existing caissons	Bulb	3.5	86
F 2: Ducted type	75		0.5	Bi-directional	North	Original caissons	External dock & Building in the wet	Removing existing caissons	Ducted Free stream	7	15
F 3: Linear VETT	138,5		0.5	Bi-directional	North	Original caissons	External dock & Building in the wet	Removing existing caissons	VETT	3.5	16

Report G: BAM Memo

Variant	Investment (10^6 €)	Energy field (GWh/y)	Tide (m)	Type	Location	Specific location	Dock type	Current construction	Turbine type	$D_{turbine}$ (m)	Turbine Units
G 1: BAM 1	294	116.4	0.5	Bi-directional	North	Inner side dam	Dry dock	Removing existing caissons	Bulb	7.5	20
G 2: BAM 2	294	148	0.7	Bi-directional	North	Inner side dam	Dry dock	Removing existing caissons	Bulb	7.5	20
G 3: BAM 12+2	225	84	0.33	Bi-directional & sluice	North	Inner side dam	Dry dock	Removing existing caissons	Bulb & sluice	7.5	12

TABLE 35: OVERVIEW PREVIOUS RESEARCH BULB TURBINES

B.1.2 SUMMARY OF ALL THE RECENT STUDIES

This summary will treat the conclusions that may be drawn from the information given in Table 35. Each type of turbine will be treated separately. Finally a conclusion will be made regarding the outcomes of the recent studies. It should be noted that the information provided in Table 35 is not all based on similar assumptions.

B.1.2.1 BULB TURBINES

The Bulb turbine has been applied in the BAM preliminary design, Vrijling et al. [2008], Boon and Roest [2008], Mooyaart and Noortgaete [2010], Welsink and Yazici [2014] and Spengen et al. [2015. Specifications of these ideas are given in Table 35 from the previous section.

At the moment of the research performed by Vrijling et al. [2008] and Boon and Roest [2008] the required tidal range was still undetermined. Therefore their ideas concerned a large tidal difference at Lake Grevelingen. Moreover, one may notice a large amount of small diameter (3.5 meter) turbines applied in the designs. The energy production is much larger compared with the 7.5 meter diameter turbines, as are the investment costs which seems to comprehend with the number of turbines. In addition, a smaller turbine diameter results in a higher fish mortality rate.

BAM has introduced two almost equal designs, varying in the applied water level limitation in Lake Grevelingen. If the limitation, of a maximum water level of +0.05 meter NAP, would be expanded to a water level of +0.25 m NAP, the energy production would increase by 25%, while the investment costs remain the same. However, as the requirements from MIRT Grevelingen mention, the water level restriction remains unchanged

The total number of turbines seems to have the highest influence on the investment costs. Comparing Vrijling et al. [2008] with the other bulb variants, the investment costs at the southern section are lower opposed to the northern section. However Vrijling et al. [2008] did not take the construction dock into account, which might result in much higher costs compared to the northern section. In addition the costs for construction at the location of the current caissons, using the current dam as a primary flood defence system results in lower costs as can be noticed from Mooyaart and Noortgaete [2010]. Since the investment costs of variant G1 are the lowest, it seems to be most favourable to use 7 meter diameter bulb turbines. This, however, cannot be used as a final conclusion regarding the bulb turbine, since many reports have not given an indication of the energy production. This is probably due to the many uncertainties of the efficiency and the operational hours of the turbines.

In Scheijgrond et al. [2014] the use of free-stream turbines was investigated. Data provided by three free-stream manufactures (Schottel, Tocardo and Ocean Energy Unlimited (OEU)) was used to determine the cost estimation and the impact on the tidal range of Lake Grevelingen. The data provided by two of the three developers is assumed to be reliable, thus successful realization of the project does not depend on a single manufacturer. The manufacturers stated the proposed designs have not yet been fully optimized in terms of impact on tidal range and costs. More detailed study could lead to a reduction in costs and impact. This might, however, require a certain amount of time.

For each developer three scenarios were considered:

     1a.   Minimum inlet and fulltime operation
     1b.   Minimal inlet and seasonal operation
     2.   Larger inlet and fulltime operation

Investment costs of the total power plant are unfortunately not determined. The reason is the simplicity of installing the free stream turbines as was done by Tocardo at the Eastern Scheldt barrier [Tocardo.com]. There were almost no adaptions to the Eastern Scheldt barrier required to install the free stream turbine. The turbines of OEU and Tocardo are supported by a cross beam above the water level, whereas Schottel supports the turbines with vertical pillars to the seabed construction. Downside of the Schottel support system is the moveable parts that are located under water, hence extra measures should be taken to avoid fouling by barnacles, mussels oysters etc. Tocardo rotates the entire supporting beam, whereas OEU has a fixed support structure, on which each turbine-row can be rotated separately. In the efficiency models the Schottel and Tocardo turbines are awarded with the highest score.

Mooyaart and Noortgaete [2010] delivered a number of variants using free-stream turbines. The investment costs of the free-stream turbines at the location of the original caissons seems to be lower compared with the construction at the inner side and in the wet. The total energy generation is mentioned in both Mooyaart and Noortgaete [2010] and Scheijgrond [2010], report C and E respectively. The turbines from report E describe a much lower energy production for a 5.8 meter diameter turbine compared with the 6 meter diameter turbine from report C. Since the energy generation from report E is calculated using the information provided by three manufacturers, this data is assumed to be more reliable.

Finally Spengen et al. [2015] included one free stream turbines in their sketches as well. Comparing the specifications from this free-stream turbine with the turbines mentioned by Scheijgrond et al. the first remark can be made regarding the diameter of the turbines. Spengen et al. [2015] delivered a sketch with a diameter which was not mentioned in report E, 7 meter. The corresponding investment costs delivered by Spengen et al. [2015] are much lower compared with the investment costs of the variant in report E and C. This while report E only mentions the investment costs of the turbines, whereas report F mentions the investment costs of the whole structure. Report E, by Schejjgrond et al. [2010] is assumed to be more reliable since actual manufactures were included in the determination of the costs. This also resulted in an indication of the generated energy, while Spengen et al. [2015] have not given any calculation of the energy production at all.

It may be concluded the report written by Scheijgrond et al. [2014] is assumed to be most reliable and therefore set as a reference study for the free-stream turbines. The energy production is rather low, while investment costs seem to be rather high. The positive side of the free-stream turbines from the three manufacturers is there are not much special modifications

required in order to install the turbines. In other words, when it is decided to construct a sluice instead of a tidal power plant, it may always be possible to apply the tidal free-stream turbines without significantly modifying the sluice.

B.1.2.3 OTHER TURBINE TYPES

As mentioned in the Turbine types section, VedErg has developed a VETT turbine. This turbine still requires a lot of investigation since no clear data is available of the bi-directional turbine. The investment costs from report F seem quite promising. Whether the energy production revenues are significantly high to make the construction of the Tidal Power Plant economically feasible is doubtful. Hence, it is still hard to determine whether this technique is applicable or not.

The VLH turbine was investigated in the literature study before. The literature study had shown the VLH turbine did not suffice all the requirements. It was uncertain whether the turbine could work bi-directionally. However, Report D shows a construction set-up where the turbine can be mounted in multiple positions, in that way the turbine is able to work bi-directionally. Moreover, the fish friendliness of the turbine has been tested with positive results. In addition the efficiency of the turbine is rather high as well, up to 80%. However, this efficiency rate is based on a situation with a constant head, which will not be the case at the Brouwersdam. Hence, the VLH turbine is quite an interesting variant, but the efficiency should be checked at varying water levels. One downside of the turbine is the investment costs according to Report D. Unfortunately the energy production was not determined in report D, but with an efficiency of 80% for a constant head this might be promising.

Report C has included two variants that are able to be constructed over the original caissons. The waterpower syphon turbine is a tube turbine with the generator located outside the tube. The hydro-pneumatic is thanks to the density of the air a much lighter and thus cheaper solution compared with the waterpower syphon. The hydro-pneumatic turbine generates power due to the pressure difference of the air at each end of the tube. The main disadvantage of these turbine types is the lack of possibility to work as a pump. Applying the syphon turbine induces additional pumps are required for bi-directional performance. Therefore these two turbines are assumed insufficiently able to meet all the requirements.

B.1.3 RINK

Due to changing conditions, like climate changes, legislation, organisation composition and usage, quality of civil structures decrease faster than expected. Rijkswaterstaat has come with a programme to inventorize the influence of the changing conditions on the structures and what the corresponding risks are. These risks and their influence on the reliability and future operational availability of the structures are mapped in the program called RINK (Risk inventorization wet structures).

The RINK program had set several goals, these goals are described briefly:

1. Give an indication of the technical and functional state of the structure and give an indication of the remaining lifespan.
2. Criticize the technical and functional state and describe scenarios for a multiannual maintenance plan including the costs
3. Propose a cost efficient set of measures for each object and prioritise the need for maintenance of each object.
4. Ensure the RINK system is carried out

A typical RINK assessment is given in Figure 109. First the inspection and analysis of the object will be performed. The RAMS analysis describes the performance of the structure based on the Reliability (R), Availability (A), Maintainability (M) and Safety (S). Rijkswaterstaat has published guidelines for the RAMS analysis in March 2010, explaining the meaning of RAMS and how to perform a RAMS analysis within Rijkswaterstaat.

Secondly, the object analysis is compared with the required performances of the whole corridor and of the object on itself.

Finally, an optimized maintenance and control plan is described which ensures the object complies with the requirements during its lifetime.

The RINK method is useful for the tidal power plant, since a set of scenarios is set. The scenarios show different conditions regarding the sea level rise and the 'Room for the river' program.

Based on the scenarios a number of alternatives can be described. When describing these alternatives the RINK program is bared in mind. In other words, the tidal power plant should be able adapt itself to the changing conditions as described in the scenario's.

FIGURE 109: RINK ASSESMENT

200
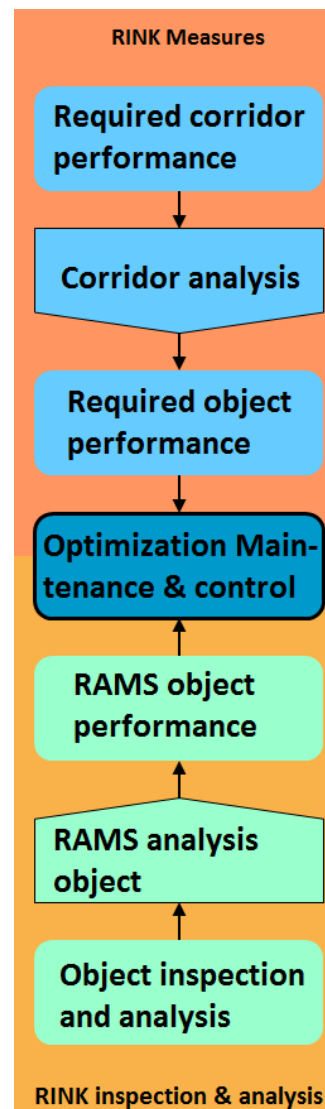
This Appendix will be dedicated to determine the wind influence on the water levels at Lake Grevelingen. Water level restrictions at the lake depend on the wind wave set down or the significant wave height as a consequence of the wind waves towards the dam. The magnitude of both features will be determined in this appendix, resulting in a governing value.

For the wind velocity at Lake Grevelingen, the wind velocity obtained from a measuring point one kilometre offshore of the Brouwersdam has been used (Brouwershavensche gat 02, see Figure 110). Data from this point provides data from in total 18 year and no measuring point delivers a similar amount of data closer to the Brouwersdam.

FIGURE 110: MEASURING POINTS CLOSE TO BROUWERSDAM

B.2.1 WIND SET-DOWN

The wind set up in Eastern direction determines the wave set-down at the Brouwersdam. The wind set-down represents the negative deviation in water level due to wind velocities. For wind blowing over the water surface for an extended period of time, the water volume downwind rises, whereas the water level upwind drops. This is explained by the obligated volume equilibrium of the closed basin. Since Lake Grevelingen can be schematized as a closed basin, the wind set-down at the Brouwersdam is equal to the wave set-up at one of the near shores.

The wind set up will be calculated using the equation below, each parameter will be discussed in this chapter as well:

$$Maximum\ W = C_2 \frac{u^2}{gd} F = 0.57\ meter$$

With:

W represents the *total wind set − up*
u represents the *wind velocity*
C_2 represents the *friction coefficient*
d represents the *average waterdepth*
F represents the *Fetch*

As will be discussed below, the found wind set-down will probably be overestimated due to the available wind data, the fetch and water depth. A more accurate outcome could be found when equation include for example the irregular shapes of the lake and the presence of the shores.

WIND VELOCITY

To determine the extreme value for the wind velocity, data from a direction between 270 and 320 degrees has been obtained (Figure 113, orange dotted line). Using a Gumbel and Weibull distribution the maximum wind velocity will be found. The return period used in these calculations is set to 1/20. This value has been chosen according to the available data of 18 years. If the wind velocity, calculated by Gumbel and Weibull, would be exceeded it will not result in major damage or major energy generation losses. Therefore an extreme value close to the available measured data shall be sufficient. The obtained values are provided in Table 36:

U_{10} (m/s)	No. Of storms per bin	Cum	P	Q	Neg Nat Log	Gumbel	Weibull
9	9918	49760	0,542261	0,457739	0,781455	0,491009	0,92141
10	9465	59225	0,645406	0,354594	1,036781	0,825819	1,012061
11	7787	67012	0,730265	0,269735	1,310314	1,157253	1,093853
12	6507	73519	0,801175	0,198825	1,615329	1,506538	1,172534
13	5064	78583	0,85636	0,14364	1,940444	1,863913	1,246119
14	3832	82415	0,898119	0,101881	2,283951	2,230705	1,315389
15	2838	85253	0,929046	0,070954	2,645727	2,609154	1,381179
16	2254	87507	0,953609	0,046391	3,070655	3,046999	1,451177
17	1729	89236	0,972451	0,027549	3,591792	3,577856	1,528683
18	1181	90417	0,985321	0,014679	4,22134	4,213955	1,612864
19	580	90997	0,991642	0,008358	4,784489	4,780295	1,681315
20	355	91352	0,99551	0,00449	5,405952	5,403703	1,750866
21	233	91585	0,998049	0,001951	6,23959	6,238613	1,836226
22	98	91683	0,999117	0,000883	7,032526	7,032085	1,910605
23	43	91726	0,999586	0,000414	7,789389	7,789182	1,976539
24	22	91748	0,999826	0,000174	8,654387	8,654299	2,046845
25	9	91757	0,999924	7,63E-05	9,481065	9,481027	2,109774
26	5	91762	0,999978	2,18E-05	10,73383	10,73382	2,198494

TABLE 36: EXTREME DISTRIBUTION APPLIED TO NEARSHORE DATA DIVIDED INTO WIND BINS
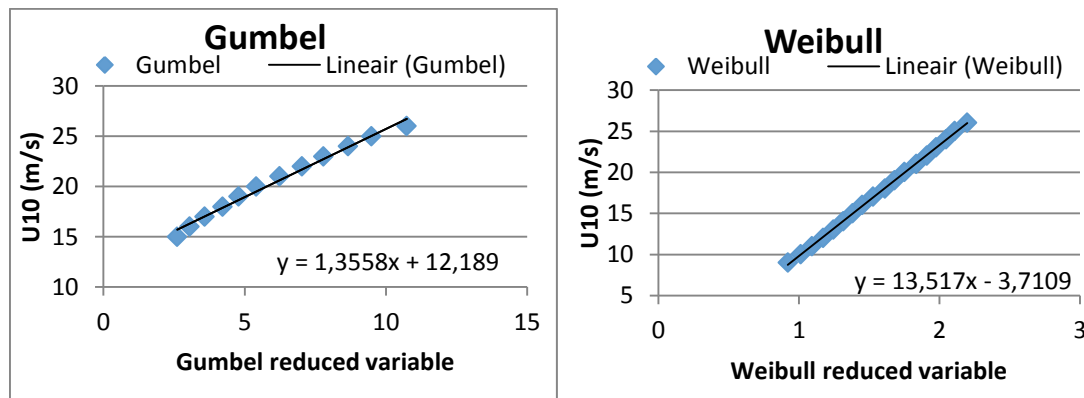
FIGURE 111: GUMBEL AND WEIBULL DISTRIBUTION WIND VELOCITY

	Gumbel	Weibull
β	1.3558	13.517
γ	12.189	-3.7109
α	3.013	3.013
Q_s	1/20	1/20
N_s	91764	91764
U_{10}	27.82	26.72

TABLE 37: OBTAINED PARAMETERS WIND VELOCITY

From Figure 111 the main parameters to calculate the extreme value for the Gumbel and Weibull distribution are obtained. These are provided in Table 37.

The value obtained by the Gumbel distribution has shown to be governing. Therefore the wind set-up will be calculated using a maximum wind velocity of $U_{10} = 27.82 \, m/s$.

FRICTION COEFFICIENT

An important empirical factor that discounts a lot of effects is the friction coefficient. The friction coefficient can be seen as an empirical correction factor for all the imperfections and the shear stress coefficient for the friction between air and water. In the Netherlands a factor of $3.5 * 10^{-6} - 4.0 * 10^{-6}$ applies.

AVERAGE WATER DEPTH

The lake has shown some large deviations regarding the water depth. Shores lying above the mean sea water level are present in the lake, whereas deep gullies have been formed in the lake before the construction of the Brouwersdam. However, to give an indication of the wind set-up, a mean water depth is assumed. Based on Figure 112, the lake bathymetry provided by Deltares [2008], the average water depth is set to 5 meter.
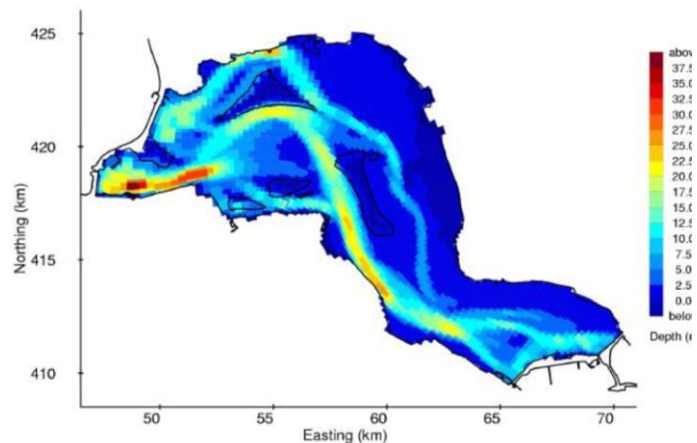
FIGURE 112: BATHYMETRY LAKE GREVELINGEN [DELTARES, 2008]

FETCH

The fetch follows from Figure 113 below. As may be noticed the fetch crosses the dry shores in the lake. Therefore the assumed fetch is an absolute maximum which will almost never be achieved, except for high water levels (above NAP) which will not occur during the first and second scenario. Therefore calculating the wind set-up using this equation and the fetches from the figure, a large overestimating will be made. However, since the wind-set up is required to determine the top level of the inlet tube at the lake side, an overestimation would only result in a lower chance of having turbulent flow entering the inlet tube.

FIGURE 113: WIND DIRECTION AND FETCH LAKE GREVELINGEN

As mentioned earlier, the obtained wind set-up might deviate in practice due to the irregularity of the lake. In addition, the influence of the land around the lake influences wind set-up as well. The land will influence the wind direction and wind speed. Since there is no data available close to Lake Grevelingen, while the wind is measured ten meters above mean water level, the data from Brouwershavensche Gat 02 is assumed to be governing for Lake Grevelingen as well.

B.2.2 SIGNIFICANT WAVE HEIGHT

To determine the significant wave height the fetch, water depth and the wind velocity are required. Both the fetch and the water depth can be obtained from the method above. The wind velocity changes, due to a different wind direction, now 70 to 120 degrees (Figure 113, red dotted line). The wind velocity is, furthermore, calculated as was done for the wind set-up, using the Weibull and Gumbel distribution. The obtained governing wind velocity is equal to: $U_{10} = 22.13 \, m/s$.

The significant wave height caused by wind is calculated using the wind wave formula based on the Sverdup-Munk-Brettschneider method [SPM, 1984] for wave generation. With the water depth and the fetch as limiting factors the equation by Sverdup-Munk-Brettschneider can be rewritten to:

$$\frac{gH_s}{U_w^2} = 0.283 tanh\left(0.578\left(\frac{gh}{U_w^2}\right)^{0.75}\right) tanh\left(\frac{0.0125\left(\frac{gF}{U_w^2}\right)^{0.42}}{tanh\left(0.578\left(\frac{gh}{U_w^2}\right)^{0.75}\right)}\right)$$

The input parameters and the outcome are shown in Table 38:

Input Parameter			
Wind velocity	U_w	22.13	m/s
Fetch	F	10000	m
Depth	h	5	m
Gravitational acceleration	g	9.81	m/s^2
Outcome			
Significant wave height	H_s	1.17	m

TABLE 38: CALCULATION SIGNIFICANT WAVE HEIGHT

APPENDIX C

PRELIMINARY POWERHOUSE DESIGN AND INTEGRATION IN BROUWERSDAM

C.1 GATE DESIGN

Preventing exceedance of the maximum allowed water level at Lake Grevelingen a water retaining gate is designed in this chapter. Also during extreme weather conditions at the North Sea, the gate should be able to fulfil its water retaining as well.

First, the best applicable gate type is determined, based on requirements and the available gate types. Second, the gate dimensioning using a truss system is performed with literature from Erbisti [2015]. Third, the gate lifting forces are computed, though the type of cylinders and their specification is not within the scope of this thesis.

C.1.1 GATE DIMENSIONING

The computation of the gate dimensions is performed in this paragraph. Boundary conditions influence the dimensions of the gate and are therefore elaborated first. With these boundary conditions the governing load combinations are determined. The final gate dimensions are now computed according to the governing load combinations. For cost reducing purposes, an optimization of the gate dimensions is performed, resulting in a final gate design. The remaining gate elements are discussed in the final section of this paragraph.

C.1.1.1 BOUNDARY CONDITIONS

Since the gate will be exposed to tensile forces due to its water retaining function, constructing in steel seems to be best option. Corrosion is one of the main complications for steel submerged in sea water. Therefore, a water resistant cover shall be applied. The water resistant cover is not sufficient to protect the steel components against corrosion. Hence, the urge of maintenance being carried out every five year is inevitable. Maintenance could be done in/situ or when the gate is being removed. In the case of removal a second or temporary gate should be available to ensure the ability of retaining water at any time.

Considering the high material costs of steel, reducing the required material is a preference. Applying a high strength steel class is therefore beneficial. Therefore the steel class S355 is chosen in this design. In addition, providing high strength steel member with minimal material, the gate is designed using hollow tubular beams.

The preliminary dimensions are summarized in chapter 5, Table 39 gives a short recap of the essential values required in the gate design.

Parameter			
Bottom inlet sluice	h_{bot}	-9.74	[m]
Top inlet sluice	h_{top}	-1.5	[m]
Significant wave height	H_s	2.6	[m]
Design water level North Sea	h_{ed}	+5.0	[m NAP]
Minimum water level Lake Grevelingen	$h_{min\,LG}$	-0.45	[m NAP]
Wave period	T_p	7.5	[s]
Gate height	h_{gate}	8.24	[m]
Gate width	W_{gate}	8.24	[m]
Total water depth	d_{tot}	14.74	[m]

TABLE 39: DESIGN PARAMETERS GATE

During the structure's lifetime it is exposed to several load conditions. The three main and possibly governing load conditions are described in this section: the gate in closed position, during removal of the turbine and during closure.

1.   *GATE IN CLOSED POSITION*

The gate positioned in closed position is subject to the governing loads. The extreme wave conditions apply including the hydrostatic pressures. Whether the wave impact will actually have a large influence at the submerged gate is discussable. Regardless, the wave impact is included in the gate design load conditions. The gate might thus be considered over-dimensioned. The hydrostatic loads acting on the gate are computed using the design water level which is given in 'Hydraulische randvoorwaarden 2006 voor het toetsen van primaire waterkeringen' [Ministerie van Verkeer en Waterstaat, 2007]. The resulting forces are given in the figures below.

The load distribution of the hydraulic pressure is shown in the left illustration in Figure 115. The hydraulic pressures from the North Sea side are partly compensated by the hydraulic pressures from the lake side of the gate, resulting in a hydraulic pressure distribution as shown in the right illustration of Figure 115.
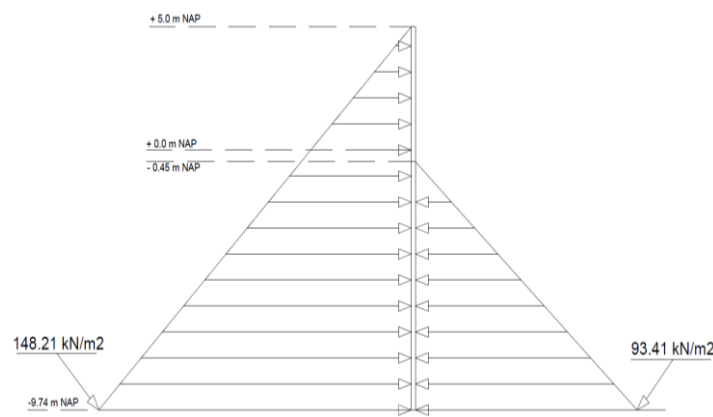
FIGURE 115: HYDRAULIC FORCES ACTING ON THE GATE

The wave impact is calculated with the simplified approach proposed by Sainflou. The structure is considered as a vertical breakwater for which it is assumed the wave is completely reflected at the moment it coincides with the tidal power plant while the gate is situated in closed position. According to Sainflou the wave impact reaches a maximum at the centre line of the wave:

$$p_1 = \frac{\rho g H_s}{2} = 1,025 * 9.81 * \frac{2.6}{2} = 12.57 \ kN/m^2$$

$$p_0 = \frac{\rho g H_s}{2 * \cosh(kd_{tot})} = \frac{1025 * 9.81 * 2.6}{(2 * \cosh(0.0845 * 14.74))} = 6.68 \ kN/m^2$$

FIGURE 114: LOAD DISTRIBUTION WAVE IMPACT

'k' Represents the wave number, this value is iteratively determined using the linear wave theory. The waves are

located in transitional water. The load distribution is sketched in Figure 114.

This corresponds to a final design load combination, in which all the loads are multiplied with a safety factor of 1.5. Since the extreme wave conditions at the North Sea will occur with a very low return period, a safety factor of 1.5 should result in a sufficiently safe design. Three load positions can be distinguished:

$q_{ed1} = 1.5 * P_1 = 19.61 \, kN/m^2$ at +5.0 m NAP

$q_{ed2} = 1.5 * P_1 + 1.5 * \rho g H_1 = 98.42 \, kN/m^2$ At -0.45 m NAP

$q_{ed3} = 1.5 * P_0 + 1.5 * \rho g H_1 = 93.41 \, kN/m^2$ At -9.74 m NAP

In which H_1 represents the difference between the water depth at Lake Grevelingen and the north Sea. The combined load distribution is given in Figure 116.

From Figure 116 it can be noticed the maximum force is located at the low water level of Lake Grevelingen. Since the gate will be located between -1.5 m NAP and -9.74m NAP, the load at -1.5m is governing:

$q_{ed,gate,1} = 98.42 \, kN/m^2$.

2. SLUICEWAY MAINTENANCE

FIGURE 116: RESULTING FORCE LOAD SITUATION 1

During sluiceway maintenance works, the sluiceway will be completely shut off from water. Closure of the sluiceway will be provided by applying temporary removable bulkheads. This means the gate at North Sea side will be solely exposed to the water pressures from the North Sea. During maintenance, the maximum water level at the North Sea as mentioned in scenario 2 (section 4.4.2) has been assumed to be governing (+2.3 m NAP). The corresponding water depth, assuming the tidal power plant will be located at a depth of -9.74 m, becomes 12.04 meter. Additionally, a maximum wave height will be set for which the replacement of the gate is allowed: 1.5 meter. The load situations are illustrated in Figure 117 and Figure 118 on the next page.

FIGURE 117: HYDRAULIC PRESSURES ACTING ON THE GATE
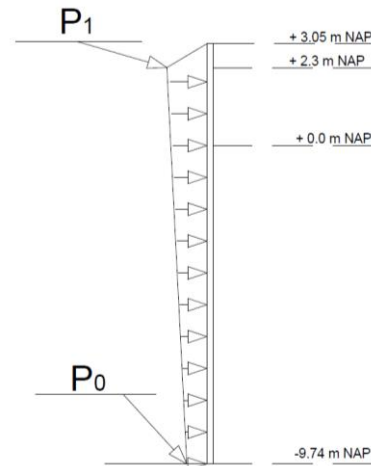
FIGURE 118: WAVE IMPACT ON THE GATE

The approach of calculating the wave impact is similar to the previously used method:

$$p_1 = \frac{\rho g H_s}{2} = 1{,}025 * 9.81 * \frac{1.5}{2} = 7.54 kN/m^2$$

$$p_0 = \frac{\rho g H_s}{2 * \cosh(k d_{tot})} = \frac{1025 * 9.81 * 1.5}{(2 * \cosh(0.09 * 12.04))} = 4.58\ kN/m^2$$

The value for k is changed due to the water depth.

This corresponds to a final design load combination, in which all the loads are multiplied with a safety factor of 1.5. Since safety during maintenance should be guaranteed.

Three load positions are distinguished:

$q_{ed4} = 1.5 * P_1 = 11.31\ kN/m^2$ at +2.30 m NAP

$q_{ed5} = 1.5 * \left(P_1 - \frac{P_1 - P_0}{H_3} H_2\right) + 1.5 * \rho g H_2 = 97.79\ kN/m^2$ at -1.5 m NAP

$q_{ed6} = 1.5 * P_0 + 1.5 * \rho g H_3 = 184.48\ kN/m^2$ at -9.74 m NAP

In which H_2 represents the height between the water surface and top of the inlet sluice at the North side. H_3 represents the total water depth at the North Sea side. The load distribution is illustrated in Figure 119.

From Figure 119 it is noticed the governing load is located at the bottom of the gate at -9.74 m NAP:

$q_{ed,6} = 184.48\ kN/m^2$.
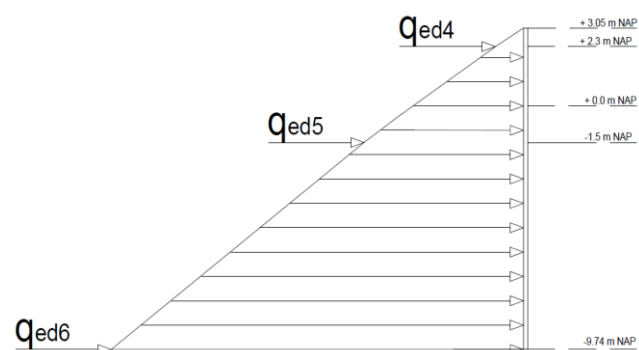
FIGURE 119: RESULTING FORCE LOAD COMBINATION 2

3.   *GATE DURING CLOSURE*

Hydrodynamic forces may emerge during closure of the gate. In that case the load combination during closure consists of a design water level in front of and behind the gate. The head difference between the North Sea and Lake Grevelingen results in water flowing from the Sea towards the Lake or opposite. This situation is set as normative, as the head difference between the maximum water level in Lake Grevelingen and minimum water level of the North Sea is significantly smaller.

The force acting on the gate as a consequence of sea water under flow the gate can be computed using the momentum balance. Due to the pressure difference between the upstream side of the gate and downstream side of the gate , which increases with the velocity flowing under the gate, the

FIGURE 120: VERTICAL LIFT GATE WITH AN UPSTREAM SKIN PLATE [ERBISTI, 2015]

bottom of the gate is subjected to a vertical downward force is. However, Knapp [1960] stated the following rule: 'all surfaces of a gate located in regions of high water velocity and which form a sharp slope with the direction of the corresponding motion, present the possibility of formation of hydrodynamic forces'. Figure 120 shows a vertical lift gate with an upstream skin plate. The skin plate moves in the direction Z-Z', which is similar to the flow direction. Therefore, according to Knapp's rule, there is no formation of low-pressure areas, and consequently, thrust forces are not created [Erbisti, 2015].

C.1.2.3 CONCLUSION

According to the load combination resulting design loads the load combination 2 leads to the governing situation. However, the removal of the turbines is assumed to be done only once in the lifetime of the Tidal Power Plant. The design load from load combination 2 is more than twice as much as the design load from load combination 1. This would mean the gate must become twice as strong, leading to almost double as much steel required to counteract the loads. Therefore, it is decided to design the gates based on the extreme conditions for load combination 1. This means specials panels will have to be constructed for replacement of the turbines, which will not be discussed in this thesis any further.

The steel joints of the gate are of high importance to maintain the gate's stability and strength. The connections between the hollow tubes can be done in various ways [Wardenier et al, 2010]:

- With special prefabricated connectors (Figure 121)
- With end pieces which allow a bolted joint (Figure 122)
- Welded to a plate (Figure 123)
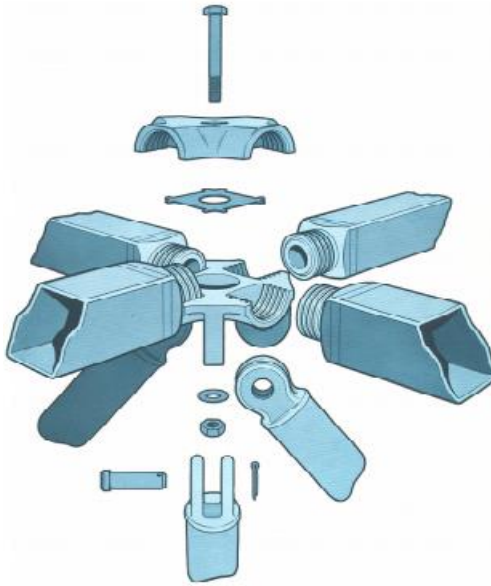- Welded directly to the through member (chord)

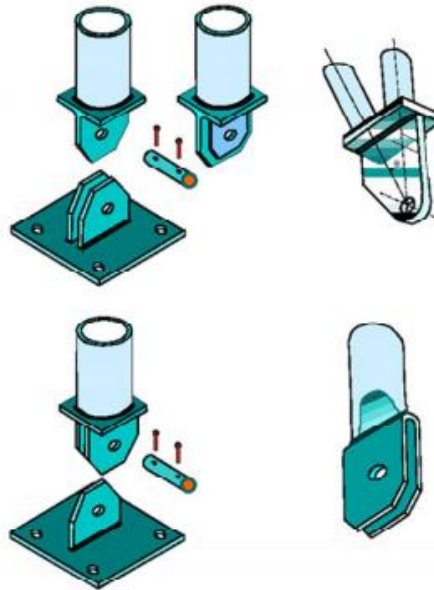FIGURE 121: EXAMPLE OF A PREFABRICATED CONNECTOR [WARDENIER, 2010]

FIGURE 122: JOINTS WITH END PIECES FOR BOLTED JOINTS [WARDENIER, 2010]
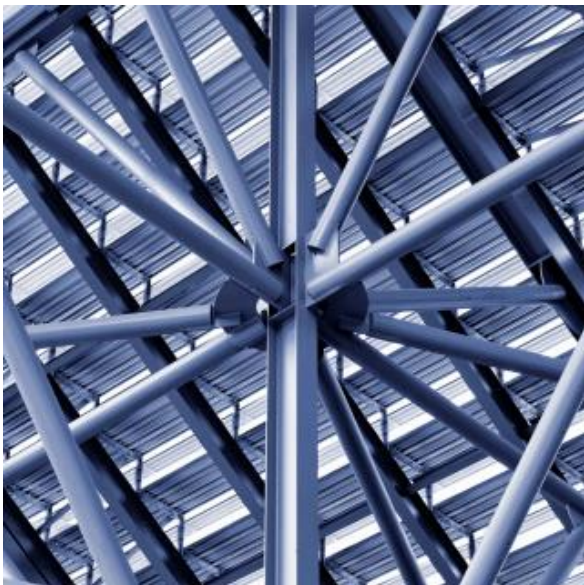
FIGURE 123: WELDED CHS SLOTTED GUSSET PLATE JOINTS [GOOGLE]

Wardenier [2010] states: 'For transport or erection it may be that bolted joints are preferred or required, whereas for space structures prefabricated connectors are generally used. However, the simplest solution is to profile the ends of the members which have to be connected to the through member (chord) and weld the members directly to each other. Nowadays, end profiling does not give any problem and the end profiling can be combined with the required bevelling for the welds'. Since there is enough room for welding at the trusses, it is decided to use welding directly to the through member (chord).

C.1.3 LIFT MECHANISM

Due to the high dead weight of the gate, the lifting mechanism consists of two cylinders. The cylinders can extend, retract and deliver the required force for the movement of the gate by means of oils pressure. Several parameters need to be taken into account to determine the cylinder design. The design of the cylinder will not be treated in this thesis. Anyhow, the gate loads are treated in the succeeding paragraphs accordingly:

- Dead weight
- Buoyancy
- Friction losses

When lowering the gate the gate will have an upward resisting force from the water which becomes dominant. During lifting operations, the cylinders should be able to lift the dead weight of the gate. Due to the different types of loads and the two functions of the cylinders, lifting and pushing, the cylinders should be able to deliver both compressive forces and tensile forces.

C.1.3.1 GATE OPERATION FORCES

During the lifetime of the gate, the cylinders should be able to bear the corresponding gate operation forces. During closure, the water forces, defined as buoyancy of the submerged part of the gate, could become dominant. Other resistance forces are wheel friction, friction forces on seals and downpull (or uplift) forces caused by currents. As mentioned by Knapp [1960] before, the downpull of the gate is not expected to occur since the gate is constructed vertically and manoeuvres vertically. At last the dead weight of the gate should be taken into account for both lifting and 'pushing down'. In equation form a distinction can be made between lifting and closure loads [Erbisti, 2014]:

$$Lifting\ load:\ C_A = (G - E) + F_r + F_v + F_h$$

$$Closure\ load:\ C_F = (G - E) - F_r - F_v + F_h$$

In which:

G *represents the gate's dead weight*

E *represents the buoyancy*

F_r *represents the wheel friction forces*

F_v *represents the seal friction forces*

F_h *represents the hydrodynamic forces*

D.1.3.2 DEAD WEIGHT

The gate's dead weight is obtained from the gate design optimization. Next to the material weight, the weight of additional components should be included as well. These other components are [Erbisti, 2014]:

a) Weight of the gate structure, which has been determined in optimization
b) Weight of accessories and mechanical parts attached to it
c) Weight of paint
d) Weight of debris possibly in the gate structure

e) Weight of water possibly retained in the gate structure
f) Weight of ballast, if any

The portions c, d and e are accounted for when acting unfavourable, which applies to the gate. Debris (d) would lead to severe damage to the turbines and is therefore not taken into account.

The total weight of c and e is computed by multiplying the weight of the gate by a factor 1.05. Including the additional weight of accessories and mechanical parts leads to an estimated multiplication factor of 1.10. It is assumed no additional ballast is required. Moreover, the hollow truss beams and girders are assumed isolated, hence no water enters the hollow sections of these beams and girders. The total dead weight becomes:

$$G = 1.10 * 7.85 * 9.81 * 2.42 = 205.27 \; kN$$

C.1.3.3 BUOYANCY OF THE SUBMERGED PART

The total steel volume of the gate is 2.42 m³. Including the hollow parts of the trusses this becomes, 9.58 m³. The gate will always be completely submerged as the sluiceway sluice is fully accommodated under the lower water levels of Lake Grevelingen and the North Sea. The total gate buoyancy is therefore equal to:

$$E = 9.58 * 10.25 * 0.981 = 96.31 \; kN$$

The dead weight of the gate exceeds the buoyancy and thus no additional ballast is required.

C.1.3.4 WHEEL FRICTION

The friction on supports and hinges is proportional to the water load in the gate and to the friction coefficient of the surfaces in contact. Since the gate is solely moving vertically the resultant of the hydrostatic load is the dominant factor to determine the friction of the wheels. In closed position the gate could reach a maximum head difference of 5.45 meter. The wheel friction is calculated using [Erbisti, 2014]:

$$F_r = \frac{W}{R}(\mu r + f)$$

In which:

F_r *represents the Wheel friction*

W *represents the Wheel load*

R *represents the Radius wheel*

μ *represents the friction coefficient of bearing or brushing* $= 0.003$

r *represents the wheel pin radius or mean radius of bearing*

f *represents the coefficient of rolling* $= 0.02$

The maximum wheel load, governed by the hydraulic pressures is equal to:

$$W = \gamma * B * h * 5.45 = 10.25 * 8.24^2 * 5.45 * 0.981 = 3720.86 \; kN$$

For the wheel radius and wheel on radius of bearing or brushing some values are assumed. These values are based on an example from Erbisti [2014] and should be reconsidered when completely designing the gate operating elements. It results in the value for the wheel friction:

$$F_r = \frac{3720.86*10^3}{(36/2)}(0.003*(22/2)+0.02) = 10.96\ kN$$

C.1.3.5 SEALS

Prior to seal friction calculations, the seal type is determined. The side seals will be attached on both sides of the gate and ensure the gate's water retaining function at all edges. Two applicable seal types are the J-seal and an angled seal. The J-seal is the most common used seal and is therefore applied in this design. Figure 124 shows an example of the J-seal.

It is assumed the seal is located over the whole height and on both sides to make sure no water will flow through. The friction is at maximum when the door closes or opens, this is the situation when there is a maximum water level difference between the North Sea and Lake Grevelingen: 5.45 meter. This leads to a water pressure:

$$p = 10.25 * 5.45 * 0.981 = 54.80\ kN/m^2$$

The equation for seal friction is obtained from Erbisti [2004]:

$$F_v = \mu * N$$

With:

μ *is the friction coefficient between*

           seal and sea

N *is the reaction force of the seal*

The length of the seals is similar to the gate height, 8.24 meter. The friction coefficient of rubber on concrete is 0.6 while the friction coefficient of rubber on concrete is 0.45-0.75 [Autodrill] for sliding. The total maximum friction force than becomes:

$$F_v = 0.75 * 8.24 * 54.801 = 338.67\ kN$$
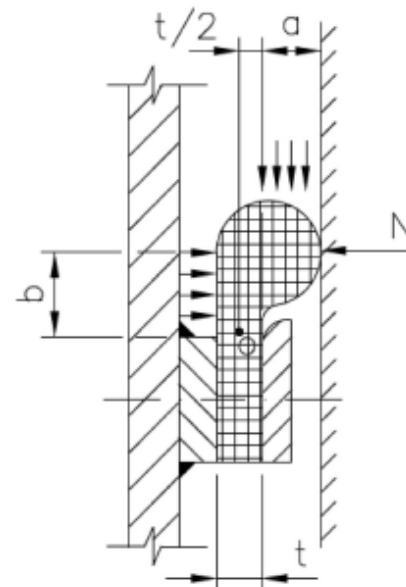
FIGURE 124: J-SEAL

A summary of the obtained loads and forces is given in Table 40. Hence the final lifting and closure loadings are elucidated.

Load Type		Force [kN]
Dead weight	G	205.27
Buoyancy	E	96.31
Wheel Load	F_r	10.96
Seal friction	F_v	338.67
Hydrodynamic force	F_h	0

TABLE 40: OVERVIEW LIFT MECHANISM FORCES

$$Lifting\ load:\ C_A = (G - E) + F_r + F_v + F_h$$

$$Closure\ load:\ C_F = (G - E) - F_r - F_v + F_h$$

The final lifting load for a gate being lifted from its submerged position becomes:

$$C_A = (G - E) + F_r + F_v + F_h = 458.59\ kN$$

The lifting force increases at the moment the buoyancy is almost neglected, but the wheel load is present. Hence, the lifting load just before completely opening the inlet sluice:

$$C_A = G + F_r\ = 216.23\ kN$$

This results in a governing lifting load when the gate is just leaving the water.

The closure load will only be relevant when the gate is entering the water, above this water level the gravity forces will do the lowering job. The closure load becomes:

$$C_F = (G - E) - F_r - F_v + F_h = -240.67\ kN$$

This value is negative; this means the cylinders must be able to push the gate downwards when it is lowered into the water. For clarification, this 'pushing' force applies while lowering the gate. When the gate is in actual final position the dead weight of the gate exceeds the buoyancy and thus the gate remains in position.

The closure load of the just before entering the water in the inlet sluice:

$$C_F = G - F_r = 194.31\ kN$$

Vertical displacement is possible when the applied cylinders are able to bear the obtained forces.

C.2 STABILITY CHECKS

Stability checks are required in order to determine whether the Tidal Power Plant will remain in place or might start moving. Hence, multiple load situations are considered.

It has not been determined yet what the construction will be, this can both be wet and dry. The wet construction method would mean the tidal power plant is constructed externally in segments and towed towards the Brouwersdam where it will be sunk into the final position. The dry construction method indicates the construction at the current Brouwersdam, where part of the dam will be excavated and in-situ the tidal power plant sections shall be casted. For the wet construction an additional stability check is required: stability during transport through the water. In this chapter all the stability checks shall be discussed, so for both wet and dry construction.

Towing of caissons towards its position in the Brouwersdam will results in possible problems during transport. Waves acting on the caissons or wind could influence the stability of the structure. Based on former towing operations of caissons a preferable length, width and height ratio has come forward. This ratio determines the dimensions of one caisson. According to Voorendt et al. [2011] tow tests at the Maritime Research Institute Netherlands (MARIN) showed that a length/width ratio of 3/1 is sufficient for navigation. Also the Length/width ratio for the closure of the Brouwersdam, 3.8/1, proved to be easily navigable. This means the length of the caisson could become between 3 to 3.8 times the caisson width: 159.5 – 202.07 m. The total required length, including the assumed wall thickness of 0.5 meter is 157.82 meter. This implicates the ratio 3/1 is almost reached. Moreover connecting multiple caisson sections will lead to possible weak spots at the connection point. These weak spots could be reinforced using reinforcement steel or special connection methods. However, since the length width ratio is preferred as mentioned above and the connections could lead to damage or failure of the caisson it is decided to construct the caisson as a whole in an external dock. This also positively influences the transport costs, since only one caisson section is due to be transported.

According to [Clark, 2007] manoeuvrability and control requirements during placement of caissons, water velocities greater than 1 m/s would be regarded as unacceptable.

C.2.1 LOAD SITUATIONS

During transport and immersion

During transport the in- and outlet sluice will be closed off from the seawater. In that way the buoyancy of the caisson is increased. To determine the load during transport first the buoyancy should be determined. This is done using the moment equilibrium. A dry sand ballast load is required, underneath the road. For construction simplicity the road will be constructed in situ, meaning the sand deposited on top of the sluice at the lake side. Providing moment equilibrium at the centre point of the caisson, a total ballast sand height of ($\gamma_s = 16 \, kN/m^3$) 1.97 meter is required. The vertical and horizontal forces acting within the caisson are shown in Figure 125, including the centre point of gravity. In this figure represents h_b the water level as a consequence of the buoyancy.

During immersion water will flow gradually into the sluice from both sides of the caisson. This means the total caisson weight increases, while the draught increases as well. It is expected this will not lead to stability problem, this should however be checked in the stability checks as well.
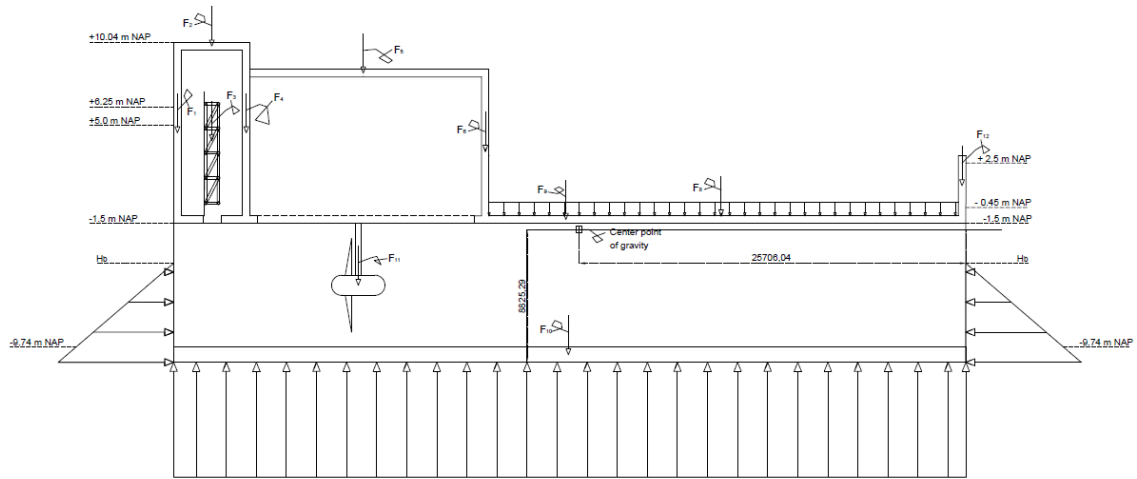
FIGURE 125: LOAD SITUATION DURING TRANSPORT

In commission at extreme conditions

During extreme conditions the gate in the Tidal Power Plant will be lowered. The horizontal loads on the tidal power plant will be at maximum and are equal to the loads mentioned in the gate design, Appendix D.1.2. In this load situation all the elements of the Tidal Power plant are installed. The sluice will be completely filled with still standing water. Additionally, the ballast sand layer shall be filled up to the bottom level of the road.
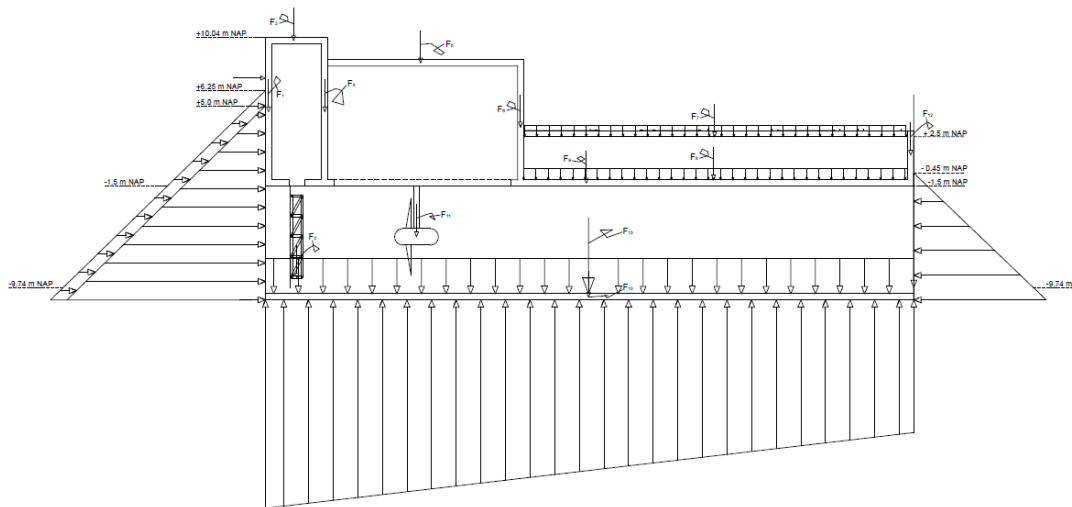
FIGURE 126: LOAD SITUATION AT EXTREME CONDITIONS

C.2.2.1 STATIC STABILITY

In order to maintain the static stability of the caisson during transport the weight of each side of the caisson is due to be equal. Therefore the amount of sand located beneath the N57 shall be as much as required to ensure a horizontal stable situation. In that way the loads on each side of the caisson are equal. So during transport the static stability is checked regarding the equilibrium of forces:

Equilibrium of vertical forces

The equilibrium of vertical forces is reached when the buoyancy is equal to the dead weight of the caisson during transportation. It has appeared a sand layer of 1.97 as ballast sand is required to ensure the equilibrium of moments (explained below), this results in a draught of 6.62 meter. During transport a keel clearance will be required, therefore certain parts of the transportation route are due to be dredged.

Equilibrium of moments

Preventing tilting of the caisson in an unacceptable degree during the transportation or immersion phase, moment equilibrium is required. To enhance this situation the sum of moments around the point of rotation equals zero. This is achieved by applying a sand layer of 1.97 meter as ballast.

Metacentric height

The equilibrium of moments is sufficient when a structure floats in still standing water, this will in reality, however, not be the case. Therefore, the sensitivity to tilting has to be taken into account. The sensitivity is checked by determination of the metacentric height. The required calculation steps are:

- Calculate the weight of the caisson and the position of the gravity centre point of the caisson with reference to the intersection of the Z-axis with the bottom line of the caisson, this distance is KG. $KG = 8.799\ m$.
- Locate the centre of buoyancy and calculate its position above the bottom of the element. This distance is $KB = 3.31\ m$.
- Determine the shape of the area at the fluid surface, and compute the smallest area moment of inertia for that shape$\left(I = \frac{1}{12}lb^3\right)$. Now BM can be computed by dividing the moment of inertia by the volume of displaced fluid, V. $BM = \frac{\left(\frac{1}{12}\right)*157.82*52.676^3}{52.676*6.62*157.82} = 34.90\ m$.
- Now the metacentric height h_m can be computed by: $h_m = KB + BM - KG = 29.41\ m$

If $h_m > 0$ the caisson is theoretically stable, while $h_m > 0.5$ is preferred.

The metacentric height is checked during transport and while in commission. During transportation bulkheads water flowing into the sluiceway, hence the sluiceway is considered empty. While in commission, water flows through the sluiceway, thus the sluiceway is fully filled with sea water. It results in a metacentric height 'h_m' varying between $h_m = 29.41\ m$ during transportation, and $h_m = 17.06\ m$ while in commission. Hence, the static stability with regard to the metacentric height is sufficient in the two considered situations.

Elements transported over water are affected by swell or waves, causing sway. Sway leads to navigability and clearance problems. The caisson is assumed to be prefabricated at an extern construction dock adjacent to Lake Grevelingen. The lake's wave conditions are therefore governing for dynamic stability calculations. Though, the influence of swell waves on the structure is expected to be minimal. However, the dynamic stability should be assured.

Sway

The dimensions of the caisson are compared with the wave length of the swell waves. The following rules of thumb should be applicable to ensure the dynamic stability with respect to sway:

$l_w < 0.7 l_e$ and $l_w < 0.7 b_e$

$l_w = wave\ length\ (m)$

$l_e = length\ of\ the\ floating\ element\ (m)$

$b_e = width\ of\ the\ floating\ element\ (m)$

The wind wave length is determined using the wind velocity from Appendix B.4.1. The wind velocity at ten meter height reads $U_w = 22.13\ m/s$. With this wind velocity the significant wave height and the wave period can be determined. From these two parameters the wave length is determined. The wave period is calculated using the wind wave formula based on the Sverdup-Munk-Brettschneider method [SPM, 1984]:

$$\frac{gT_s}{2\pi U_w} = 1.20 tanh\left(0.833\left(\frac{gh}{U_w^2}\right)^{0.375}\right) tanh\left(\frac{0.077\left(\frac{gF}{U_w^2}\right)^{0.25}}{tanh\left(0.833\left(\frac{gh}{U_w^2}\right)^{0.375}\right)}\right)$$

This results in a wave period, having a fetch (F) of 10 km, of $T_s = 3.99\ sec$. A fetch of 9 km leads to a wave period $T_s = 3.92\ sec$. The governing wave length is now determined using the linear wave theory. With an average water depth (h) of 5 meter it appears the waves are in transitional waters. Hence the wave length is obtained using:

$$L_w = \frac{gT_s^2}{2\pi} * \tanh(kh)$$

The value for the wave number (k) is obtained iteratively, leading to a value of $k = 0.284$. The governing wave length now becomes: $L_{wGrevelingen} = 21.4\ m$.

The wave length of the North Sea is calculated using the wave period of 7.5 sec, obtained from 'Hydraulische randvoorwaarden 2006 voor het testen van primaire waterkeringen' [2006]. This leads to a governing wave length of $L_{wNS} = 87.83\ m$.

The required length and width of the caisson to ensure the dynamic stability against sway is $l_e = b_e > \frac{L_w}{0.7} = 30.58\ m$. This means both the length and the width of the caissons are sufficient to ensure the dynamic stability against sway.

Natural oscillation

When the natural oscillation period of the element is close to the period of the water movements the dynamic stability might be endangered as well. One should ensure the natural oscillation period of the element is significantly larger than that of the waves or swell. The natural oscillation period of the caisson is determined using:

$$T_0 = \frac{2\pi * j}{\sqrt{h_m * g}}$$

Where:

$T_0 = natural\ oscillation\ period$

$h_m = metacentric\ height$

$j = polar\ inertia\ radius\ of\ the\ element = \sqrt{\frac{I_{polar}}{A}}$

$\qquad A = are\ of\ concrete\ in\ a\ vertical\ cross\ section$

$\qquad I_{polar} = I_{xx} + I_{zz}$

$\qquad\qquad I_{xx} = polar\ moment\ of\ inertia\ around\ the\ z-axis$

$\qquad\qquad I_{zz} = polar\ moment\ of\ inertia\ around\ the\ x-axis$

Both I_{xx} and I_{zz} are in relation with the centre of gravity.

This result in a natural oscillation period of $T_0 = 6.44\ sec.$ Transportation is solely allowed when the natural oscillation period is significantly larger than the wave period. Since the wave period for wind waves is not expected to be larger than 3.99 seconds, it is expected the dynamic stability will not be endangered as a consequence of the natural oscillation of the caisson.

C.2.3 STABILITY OF HYDRAULIC STRUCTURES ON SHALLOW FOUNDATIONS

To determine the stability of the Tidal Power Plant when in commission, again several checks should be performed. The load situation described in the load situation while in commission is used. In total three checks are performed:

Horizontal stability

$$\frac{\sum H}{f \sum V} < 1.0$$

The friction coefficient f takes several mechanisms into account. The most critical of these should be used:

Friction between structure and subsoil: $f = \tan(\delta)$, with $\delta \approx \frac{2}{3}\varphi$ (φ is the angle of internal friction of the subsoil). For calculations of the current caissons the angle of internal friction of 30 degrees was used. Based on the available geotechnical data at the Brouwersdam this value seems quite reasonable. This means the friction between structure and subsoil, in case the structure is founded in the sand, becomes $f = \tan\left(\frac{2}{3} * 30\right) = 0.36$. The friction coefficient used

for determining the static stability of the current caissons in 1969 amounts 0.58. This is due to the subsoil of the foundation which is not sand, but a rubble mound layer was used.

For now the friction coefficient between the structure and sand is used to determine the horizontal stability. The horizontal loads are determined according to load situation two, hence when extreme conditions are present at the Tidal Power Plant and the sluice is completely filled with water. The total weight of all the elements, excluding the water weight in the sluice, is multiplied by 1.1. The additional 10 percent accounts for the operational equipment required in the Tidal power Plant. This leads to the values shown Table 41.

Parameter	Value	Unit
$\sum H$	141019.6	kN
$\sum V$	1271057	kN
f	0.364	$(-)$
$\dfrac{\sum H}{f * \sum V}$	0.30	$(-)$

TABLE 41: PARAMETERS HORIZONTAL STABILITY

It is concluded the structure will be horizontally stable during extreme conditions as described in load situation two. This means when applying a new rubble mound layer blow the caisson, for which the friction increases, the horizontal stability will be maintained.

Rotational stability

The sole allowed soil stresses are compressive stresses, tensile stresses cannot be absorbed by the subsoil. This is the case if the resulting action force intersects with the core of the structure. The core is defined as the area extending to 1/6 of the structure width on both sides of the middle of the structure (Figure 127):

$$e_R = \frac{\sum M}{\sum V} \leq \frac{1}{6}b = 8.86 \, m$$

Where:

$e_R = distance\ from\ the\ moment\ centre\ to\ the\ intersection\ point\ of\ the$

$resulting\ force\ and\ the\ bottom\ line\ of\ the\ structure$

$b = width\ of\ the\ structure$

In this stability check the rotational stability of the structure is checked based on solely the self weight of the Tidal Power Plant components. Hence, no external loads from the North Sea and Lake Grevelingen are applied in this check.

For the free-stream turbine $e_R = 3.89 \, meter$ which lies within the margin. However, applying the much heavier PFN turbin, the distance $e_R = 10.98 \, meter$. The Tidal Power Plant tends to rotate towards the North Sea. The weight of the PFN turbine is obtained using the a mass formula $M = 2500 * D^3 \, (kg)$ with D the turbine diameter in meters. This formula, obtained from Pentair Fairbanks, is a first estimate and used for small diameter turbines. Pentair Fairbanks has not created a large diameter turbine yet, and for that reason it is uncertain whether the mass formula is correct or not.

Especially when in commence, and the water level at the North Sea is below the Lake's water level, the rotation towards the North Sea is even increased. With that, and the assumeption the mass formula of the PFN turbine is correct, measures should be taken to overcome rotational stability problems. This can be done by, for example, extending the bottom plate of the sluice.
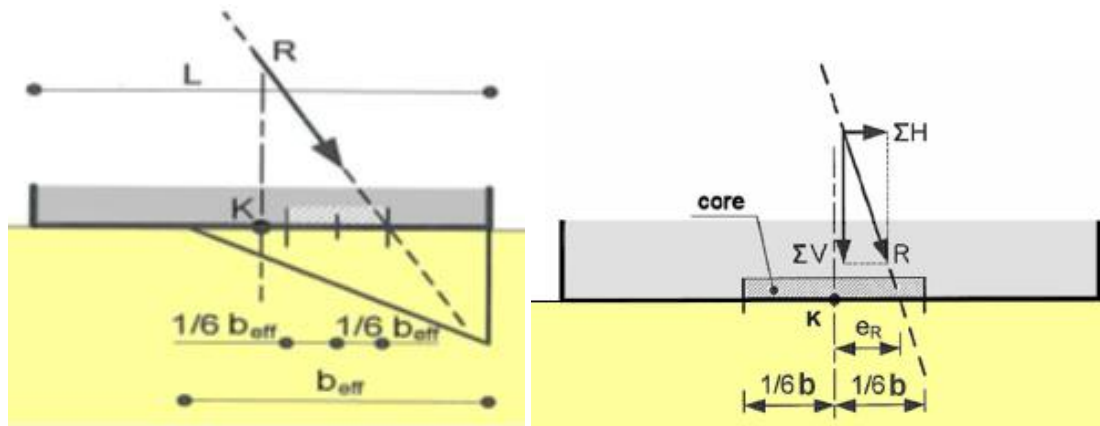

FIGURE 127: ROTATIONAL STABILITY [HYDRAULIC STRUCTURES MANUAL, 2011] .

Vertical stability

The vertical effective soil stress, required to resist the acting loads ($\sigma_{k;max}$), should not exceed the maximum bearing capacity of the soil (p'_{max}), otherwise the soil will collapse:

$$\sigma_{k;max1} = \frac{F}{A} + \frac{M}{W} = \frac{\sum V}{b * l} + \frac{\sum M}{\frac{1}{6}bl^2} = 151.62 \ kN/m^2$$

When applying the PFN turbine with the given mass formula, the maximum bearing capacity becomes $\sigma_{k;max2} = 181.06 \ kN/m^2$

$b = width \ of \ the \ structural \ element = 52.676$

$l = length \ of \ the \ structural \ element = 157.82$

$p'_{max} = brinch \ Hansen \ formula$

$$p'_{max} = c'N_c s_c i_c + q'N_q s_q i_q + 0.5\gamma'N_\gamma W s_\gamma i_\gamma$$

To determine the bearing capacity, several assumptions are made. First, it is assumed the caisson or the whole structure will be constructed on top of a rubble foundation bed. This rubble foundation bed influences the effective soil stress next to the caisson. The sill is not present over the entire width of the sliding plane and it would be too favourable if its effect would be taken fully into account, therefore the effective soil stress is negligible. Additionally, the maximum acting stress on the layer below the sill, and not directly below the caisson, should be compared with the bearing capacity. This means that $\sigma_{k;max}$ due to the caisson weight, reduces with a factor B/W, but an additional pressure as a consequence of the weight of the sill above the area with a width W. For now a rubble foundation bed with a height of 2 meter has been assumed. This means the maximum acting stress becomes:

$$\sigma'_{k;max1} = \frac{b}{W} * \sigma_{k;max} + \gamma'_{sand} * h_{sill} = 165.12 \ kN/m^2$$

$$\sigma_{k;max2} = 194.56 \ kN/m^2$$

Due to the presence of the rubble foundation bed and the absence of cohesion in the sand layer, the Brinch Hansen formula can be reduced to:

$$p'_{max} = 0.5\gamma' W s_\gamma i_\gamma$$

In which the bearing capacity factors are defined as:

$$N_q = \frac{1+\sin(\phi')}{1-\sin(\phi')}\exp(\pi * \tan(\phi')) \quad N_\gamma = 2(N_q - 1)\tan(\phi')$$

The shape factors are:

$$s_\gamma = 1 - 0.3 * \frac{b}{l}$$

The inclination factors to deal with an eventual inclined direction of the resulting force, for drained soil, are:

For H parallel to L and $l/b \geq 2$

$$i_q = i_\gamma = 1 - \frac{H}{F + Ac'cot(\phi')}$$

With:

$\phi' = Angle\ of\ internal\ friction = 30°$

$A = effective\ foundation\ area = 8392.2\ m^3$

$c' = (weighted)cohesion = 0\ for\ sand$

$q' = effective\ stress\ at\ the\ depth\ of, but\ next\ to, foundation\ surface = 0$

$H = shear\ force\ in\ the\ plane\ of\ the\ foundation\ surface$

$F = component\ of\ exerted\ force\ perpendicular\ to\ the\ foundation\ surface$

$W = effecitive\ width\ of\ sliding\ plane\ of\ sill = b + h_{sill} * \tan(45°) = 55.176\ m$

The allowable stress for scenario 1, where the free-stream Tocardo turbine is applied, results in $p'_{max,1} = 3313.4 \frac{kN}{m^2}$. For scenario 2, where the PFN turbine is applied, results in a maximum allowable stress of $p'_{max,2} = 3346.3\ kN/m^2$. Hence one may conclude the bearing capacity of the soil below the Tidal Power plant is sufficient to bear the Tidal Power plant.

C.3 CONSTRUCTION METHOD

The construction method of the tidal power plant strongly influences the final location of the Tidal Power Plant in the Brouwersdam. The construction method may be executed in several manners, these manners are discussed here. Legislation for construction works in a primary flood defence system might be an obstruction for construction manners. Therefore first the legislation for constructing in a primary flood defence system will be discussed. From that, several construction methods can be eliminated. Furthermore, previous research will help to determine construction costs of the construction methods, in that way the final construction method is determined.

C.3.1 LEGISLATION CONSTRUCTION WORKS PRIMARY FLOOD DEFENCE SYSTEM

The Dutch Government has set a Water act for which construction works should comply to receive the required permits. This act describes a lower boundary for the probability of flooding of specific hydraulic structures in The Netherlands. For the Brouwersdam a probability of flooding of 1/1000 per year is the lower boundary. Meaning, during construction works a probability of flooding of 1/1000 should be ensured.

Further legislation for construction works in and around flood defence systems is not given. However, the national guidance for Hydraulic structures does form a base for the design and construction of hydraulic structures in The Netherlands. Therefore the design of the Tidal Power Plant should comply with the norms according to the National Guidance for Hydraulic Structures [Haag et al., 2014].

C.3.2 ALTERNATIVES

Two main methods may be described for the construction of the Tidal Power Plant. The first construction method refers to the construction method of the current dam; construction in the wet. The second method is construction in the dry at its final position. Within these two methods several options are available. These options including its features will be described in this paragraph.

C.3.2.1 FIRST ASSUMPTIONS

For each option the dimensions of the powerhouse are equal, meaning a total length of 157.82 meter, a width of almost 53 meter and the required depth is set to -12.24 meter NAP (assuming a floor thickness of 0.5 meter and a two meter thick rubble foundation bed).

Furthermore the required area at the bottom of the construction pit is depending on the width of the Tidal Power Plant, which is known, and the berm width in front and behind of the Tidal Power Plant. The berm width of the foundation should comply with $0.30 < \frac{B_b}{h_m} < 0.55$ in which B_b represents the berm width and h_m the depth of the bottom of the foundation with respect to NAP [Rock Manual, 2007]. The exact width should however be determined using tests. Since the thickness of the foundation is for now assumed to be 2 meter, the $\frac{B_b}{h_m}$ −ratio is set to 0.41. This results in a berm width of 5.0 meter. Within the construction pit an additional 5 meter of free space at each side to ensure the accessibility of the site.

The bottom of the foundation is assumed to have a total width of 69 meter. A slope steepness of 1:1.5 is applied at the foundation edges. An addition five meter of free space at each side of the

foundation' bottom is assumed to be sufficient to store possible required construction equipment.

To prevent failure as a consequence of piping, water retaining sheet piles are installed. A length of 30 meter should ensure the required safe seepage length is reached. This seepage length is calculated using Lane for coarse sand, Chapter 2.5.2.1.4. Failure might still occur of the connection between the sheet piles and the construction pit is not completely water tight. Therefor the connection requires some extra attention when detailing the construction pit.

Due to the new required bottom protection, as the current bottom protection is not sufficiently large, pneumatic caissons will not be considered in the construction method alternatives.

The dimensions of the armour layer at the North Sea side of the foundation are determined in the Conceptual design.

C.3.2.2 CONSTRUCTION IN THE WET

Construction in the wet contains one main option; casting the Tidal Power Plant elements at a precast yard relatively close to the final position. The location used for the construction of the caisson ns in the current dam could be considered as an option. After casting the yard is filled with water and the elements towed towards its final position at the dam. Where at the lake side of the dam a rubble foundation bed is constructed. On the top of the rubble foundation bed the Tidal Power Plant elements are sunk. The removal of the dam and excavation to the preferred depth can now start. Also redirection of the roads can be finalized. The construction sequence is described as:

- Preparation precast construction dock
  - Installation dike ring
  - Installation drainage system of precast dock
  - Casting Tidal Power Plant and installation of the road
- Dredging and excavation at lake side of the dam
- Installation rubble foundation bed and bottom protection at lake side
- Transport of precast elements towards its final position
- Sinking Tidal Power Plant elements on the rubble foundation bed
- Connecting Tidal Power Plant to the existing dam
- Connecting the existing infrastructure to the infrastructure on the Tidal Power Plant
- Excavation and dredging of remnants dam to required depth
- Removal caissons in the wet
- Installation of bottom protection at North Sea side of the Tidal Power Plant

In Figure 130 a sketch of the location of the construction site is shown.

C.3.2.3 CONSTRUCTION IN THE DRY

Construction pit lake side

Sheet pile water retaining walls are used to ensure a dry construction pit and protects against piping and heave. This dry construction pit is located at the lake side of the dam just behind the top level of the dam. Hence, part of the dam will remain in-tact with its water retaining function as well. The probability of flooding will therefore be guaranteed during execution of the project. Using natural slopes with a relatively steep slope, the stability of the dam will remain unaffected. Drainage shall be applied to ensure the full drought of the construction pit. The construction pit shall be located adjacent to the current highway. Other infrastructure shall be redirected over the same dam section as well. After finishing the Tidal Power Plant the dam

remnants can be removed, meaning the caissons are removed in the wet. The construction sequence is described as:

c. Installation foundation temporary road adjacent to highway and installation road towards construction pit
d. Removal top layer dam
e. Installation construction pit
    o Installation sheet piles
    o Excavating to required depth
    o Applying drainage system
f. Installation rubble foundation bed and part of the bottom protection
g. Cast in-situ Tidal Power Plant
h. Redirecting main roads over Tidal Power Plant and connecting with existing infrastructure
i. Removal of sheet piles
j. Connecting the tidal power plant to the existing dam
k. Removal remnants dam and excavating and dredging to required depth
l. Removal of caissons in the wet
m. Installation of remaining bottom protection.

In Figure 131 a sketch of the location of the construction site is shown.

Construction pit at caisson

The third option contains a construction pit at the location of the caissons, hence at position of the top level of the dam. This method will mean the dam shall be partly demolished while a temporary water retaining structure, a sheet pile wall, is built in front of the construction site to ensure the required probability of flooding. Also the N57 highway road should be redirected. Caissons are able to be removed in the dry, the construction pit excavated to the required depth and the tidal power plant casted in situ. After finalizing the construction of the Tidal Power Plant, the remnants of the dam can be excavated and dredged to the required depth.

n. Redirection of the main roads
o. Removal top layer dam
p. Installation construction pit
    o Installation sheet piles
    o Excavating to required depth
    o Applying drainage system
q. Removal caissons
r. Removal caissons in the dry
s. Installation rubble foundation bed and part of the bottom protection
t. Cast in-situ Tidal Power Plant
u. Removal sheet piles
v. Redirecting main roads over Tidal Power Plant and connecting with existing infrastructure
w. Removal of sheet piles
x. Connecting the tidal power plant to the existing dam
y. Removal remnants dam and excavating and dredging to required depth
z. Installation of remaining bottom protection.

In Figure 132 a sketch of the location of the construction site is shown.

C.3.3 CRITERIA

To determine the final construction method alternatives are appreciated based on the following criteria:

COSTS BASED ON PREVIOUS STUDIES

In previous research many construction method have been described. In multiple cases the construction method is considered in both construction in the wet and construction in the dry. Appendix B.1 will be used to determine the costs of each method.

FEASIBILITY

Within the feasibility the complexity of the alternative is discussed. Complex construction methods bring more and higher risks to failure of the structure or construction pit.

DISTURBANCE ENVIRONMENT (ROADS, FLORA AND FAUNA)

Environmental disturbance focusses on the disturbance for Flora and Fauna. This could for example mean breaching silence areas.

C.3.4 REVIEW OF ALTERNATIVES

This paragraph will determine which construction method is most attractive based on the three named criteria from the previous paragraph.

C.3.4.1 COSTS BASED ON PREVIOUS STUDIES

A cost analysis of the three alternatives is performed based on the previous studies results. Due to the differences in the design assumptions and starting points, many comparisons could not be made. For example, many designs in the literature reuse the current bottom protection, and construct their Tidal Power Plant with as a starting point reusing the current bottom protection, whereas this will not be the case in the design of the Tidal Power Plant in this thesis. However, Van Spengen and Reijneveld [2015] and Mooyaart and Noortgaete [2010] formulated costs sheets where the construction activities are distinguished. This was very helpful in determining the most cost attractive construction method.

In Van Spengen and Reijneveld [2015] and Mooyaart and Noortgaete [2010] considered different construction methods. Unfortunately both reports contradict regarding the costs of building in the wet or in the dry. Moreover, Van Spengen and Reijneveld [2015] did not consider construction at the location of the current caissons. This report does, however, compare the construction at the inner side of the dam with construction in the wet. According to their findings the construction method in the wet resulted in slightly lower construction costs.

Considering the results of Mooyaart and Noortgaete [2010], construction at the current caisson location will lead to lower costs. However, in this report the complete bottom protection is reused. This is not the case for both construction in the dry at the lake side of the dam and construction in the wet. Moreover, the report mentions the removal of caissons in the wet will bring extra costs, compared with removal in the dry. A comment must be made here, since in the cost analysis it is assumed no bottom injection is required to ensure a dry construction pit. Including a bottom injection over the whole construction pit, the construction in the wet becomes, for that matter in both reports, the most cost attractive method.

Concluding, only if the dry construction pit can be assured without additional measures, the construction method at the caisson is the most cost beneficial. In case additional measures are required to ensure a dry construction pit, construction in the wet becomes most cost attractive.

C.3.4.2 FEASIBILITY

The feasibility of construction in the wet is most appealing due to the minimal additional measures required. Since construction in the wet does not require a complete water tight construction area, no bottom protective measures have to be taken. However, a construction dock close to the Brouwersdam should be found, for example Bommenende. This location was used for the construction of the current caissons. The transport route requires sufficient draught as well. Provided insufficient draught in Lake Grevelingen, low-cost measures could be taken to decrease the draught of the Tidal Power Plant Element, for example air cushions or construction weight reducing measures. In the stability checks, Appendix C.2.3, it already appeared the precast Tidal Power Plant is sufficiently stable to transport through the water.

The feasibility of construction in the dry is endangered when the bottom stability is insufficient. Especially the connection between the foundation and water retaining sheet piles with the water retaining soil layer should be sufficiently watertight and stable to prevent piping or heave. As mentioned earlier, ground injections could be applied to accomplish a dry construction pit, resulting in higher construction costs. Furthermore, since relatively simple measures could be taken to ensure the probability of failure against flooding, there are no further risks expected to endanger to feasibility of construction in the dry.

C.3.4.3 DISTURBANCE

Construction in the dry would mean a short time disturbance for traffic when relocating the highway and additional infrastructure. This could be executed in weekends, or moments when the infrastructure is minimally used. Of course for each construction method disturbance to the surrounding will be expected as well, no difference will be expected regarding construction in the wet or dry.

Construction in the wet results in assigning a relatively small part of Lake Grevelingen to the Tidal Power Plant. In addition, construction works at the lake will lead to disturbance of the surroundings at the lake, especially to fauna. This might introduce problems regarding environmentalists. Therefore the construction works should be executed quickly and as environmental friendly as possible.

C.3.4.4 CONCLUSION

Due to the many uncertainties it has become hard to make a clear statement regarding the most attractive construction method. However, due to the uncertainties regarding the ability to reach a dry construction pit, and the possible additional costs to ensure construction in the dry, for now the construction in the wet has been considered as the best option.

Disturbance of the surrounding will be expected to occur at all construction method, where construction in the wet will probably result in higher disturbances. However, the costs and feasibility are of higher importance for determining the construction method than disturbance is. Therefore, construction in the wet remains the most attractive one.

On the next pages cross sections of each alternative are given. Also, the top view of the location of the Tidal Power Plant with respect to its surroundings is given in Figure 129. A 3D sketch is shown in Figure 133, where the height of the Tidal Power Plant with respect to the water level is elaborated.

FIGURE 128: OVERVIEW LOCATION TIDAL POWER PLANT WITH RESPECT TO BROUWERSDAM (YELLOW BOX) FOR CONSTRUCTION IN THE WET [GOOGLE MAPS]
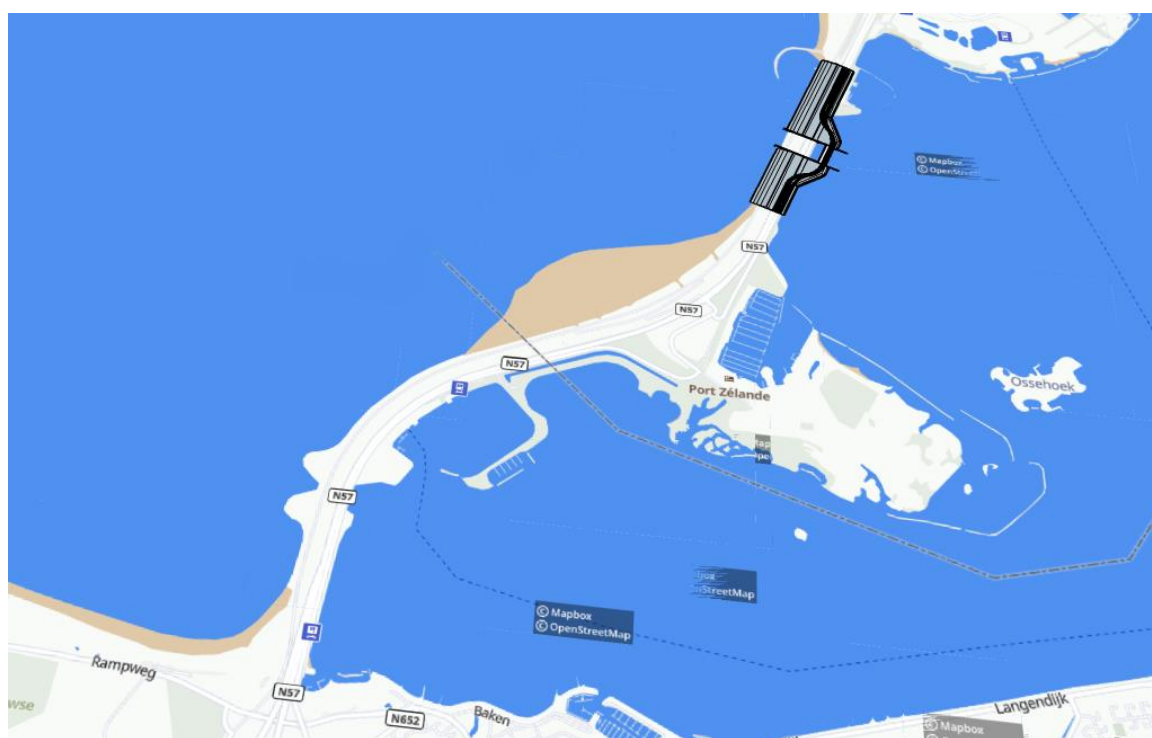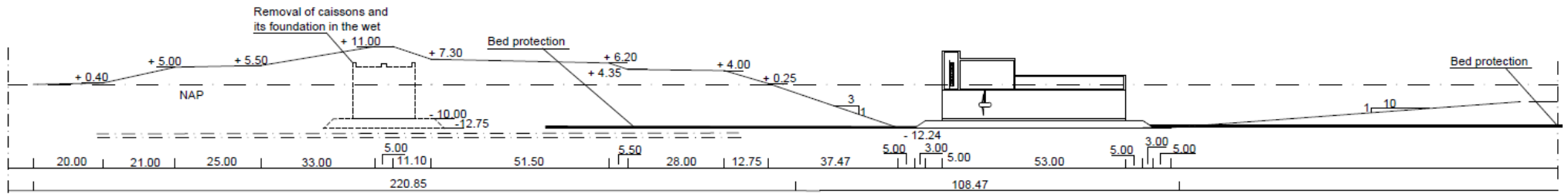

FIGURE 129: SCHEMATIZATION LOCATION TIDAL POWER PLANT

FIGURE 130: SKETCH CROSS-SECTION CONSTRUCTION METHOD IN THE WET
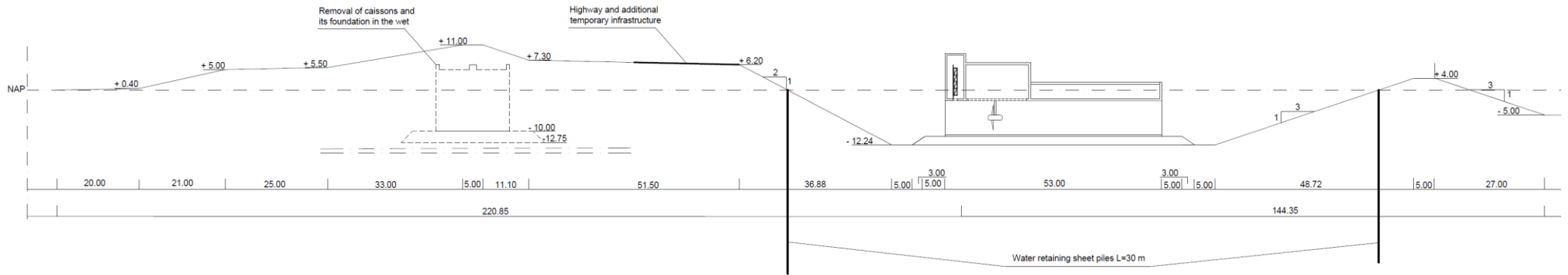
FIGURE 131: SKETCH CROSS-SECTION CONSTRUCTION METHOD IN THE DRY BEHIND CAISSONS
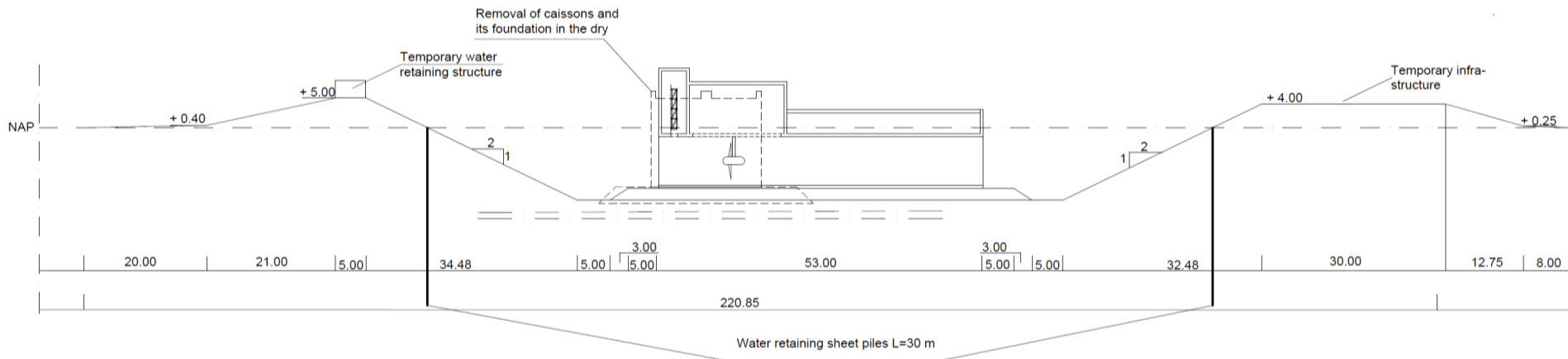
FIGURE 132: SKETCH CROSS-SECTION CONSTRUCTION METHOD IN THE DRY AT CAISSONS

230
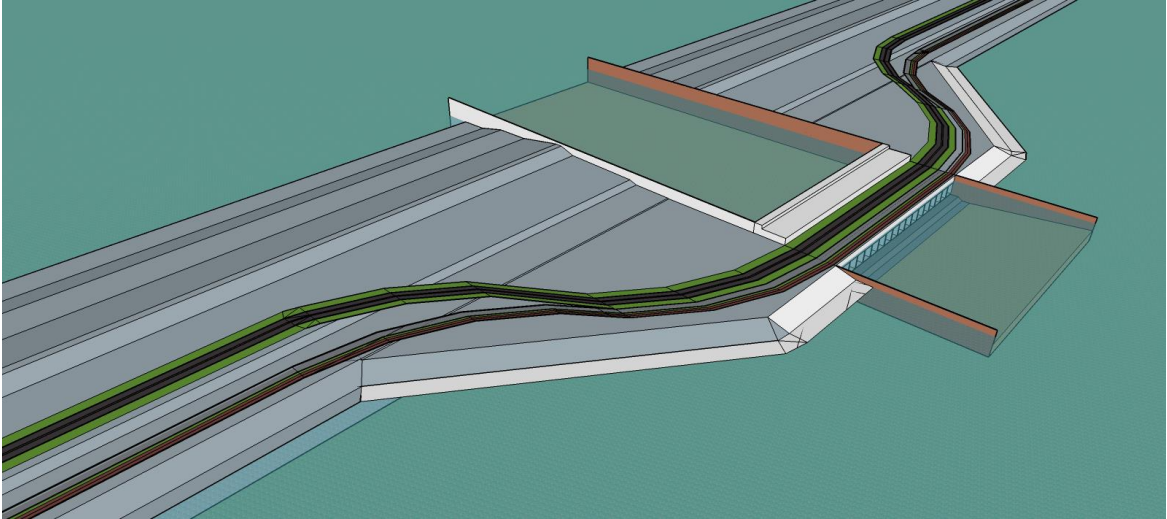
FIGURE 133: 3D REPRESENTATION OF THE TIDAL POWER PLANT WITH RESPECT TO THE AVERAGE WATER LEVEL NAP
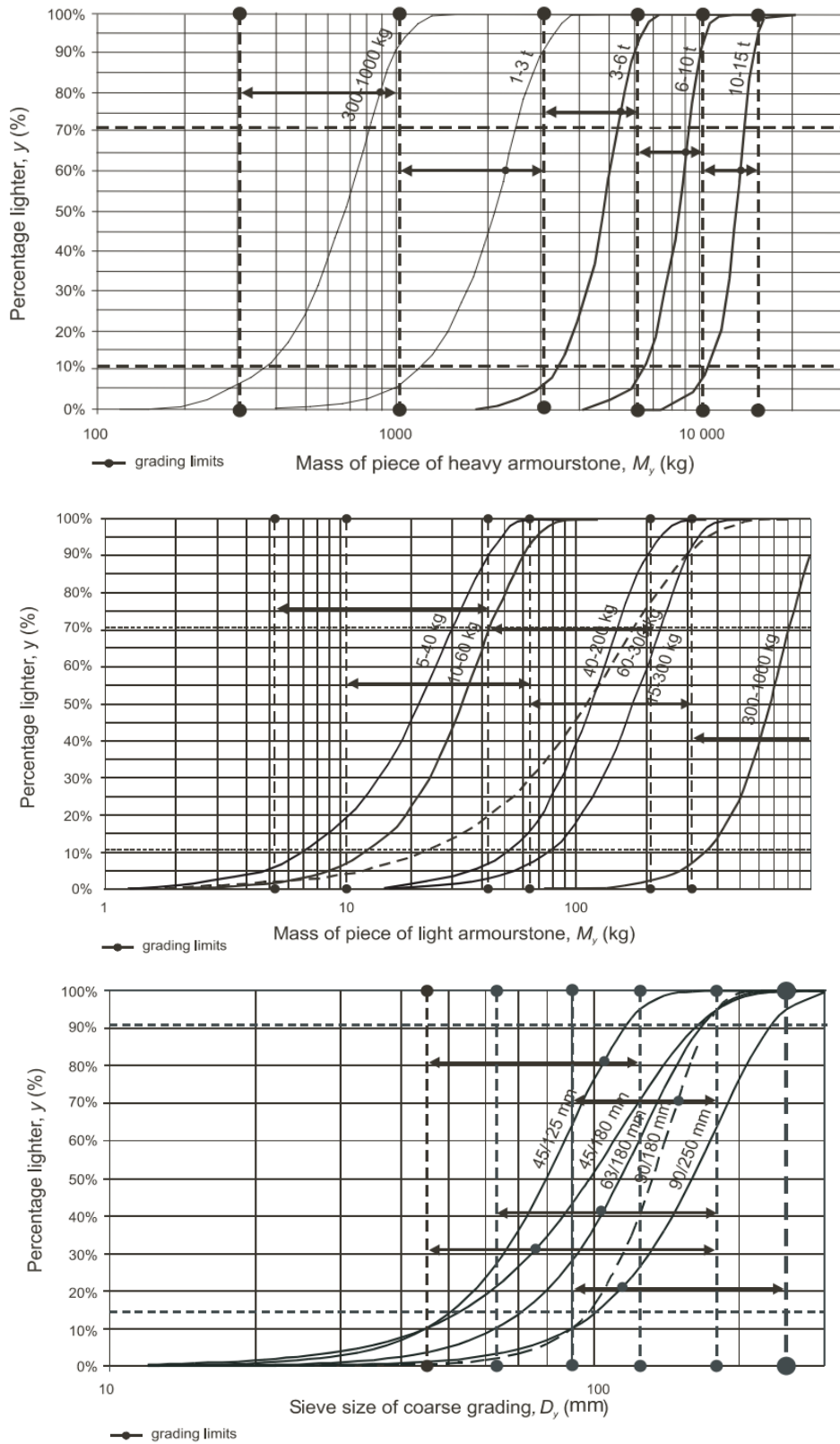
FIGURE 134: ILLUSTRATION OF ALL EN 13383 STANDARD GRADING CURVES USING IDEALISED ROSIN-RAMMLER CURVES DESIGNED TO CONFORM OPTIMALLY TO ALL EN 13383 GRADING REQUIREMENTS [ROCK MANUAL, 2007]

APPENDIX D

CONCEPTUAL DESIGN OF STRUCTURAL ELEMENTS

In the operational phase, the wave impact is the driving factor of the governing wave loads. Combining this with the hydraulic pressures, the governing load combination is discovered during the operational phase. The wave impact is considered in two situations: at extreme conditions, meaning maximum sea water level with a significant wave height and at Mean sea water level with a significant wave height. Although the latter one is very unlikely to occur, it is wise to check each combination.

The wave impact is calculated using Goda-Takahashi. Goda made a general expression for the wave pressure on a caisson on a rockfill sill. This expression can also be used for broken and breaking waves. Goda made use of Figure 135 to determine the wave pressures at several locations in front of the caisson. In case of breaking waves on top of the sill Takahashi adopted a couple of factors obtained by Goda. Combining Goda and Takahashi leads to the following equations [Manual Hydraulic Structures, 2011]:
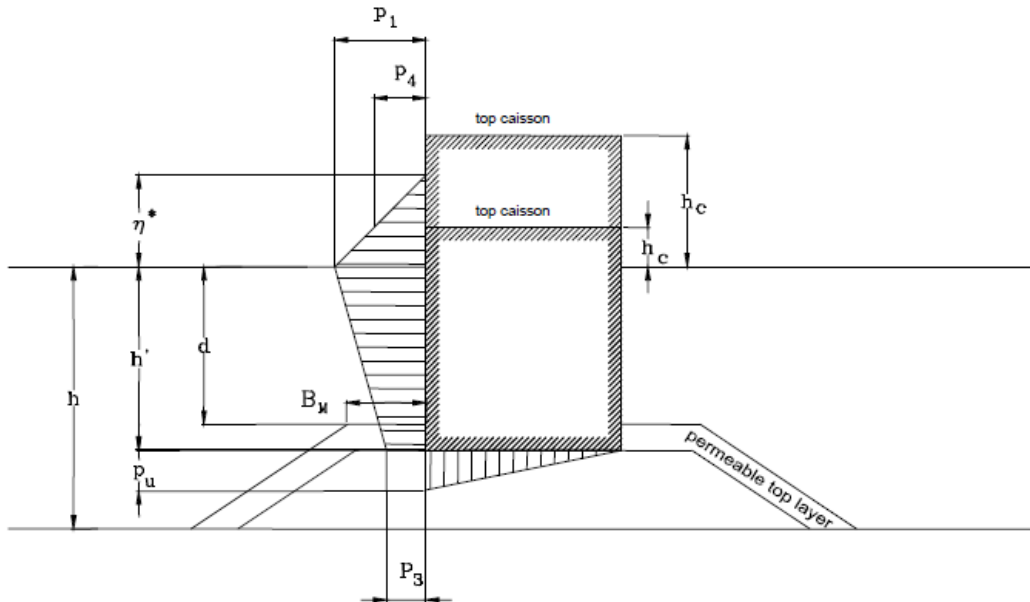
FIGURE 135: GODA (MODIFIED BY TANIMOTO): WAVE PRESSURE [HYDRAULIC STRUCTURES MANUAL, 2011]

$$p_1 = 0.5(1 + \cos(\beta))(\lambda_1 \alpha_1 + \lambda_2 \alpha_2 \cos^2(\beta)) \rho g H_{max}$$

$$p_3 = \alpha_3 p_1$$

$$p_4 = \alpha_4 p_1$$

$$p_u = 0.5(1 + \cos(\beta))\lambda_3 \alpha_1 \alpha_3 \rho g H_{max}$$

In which:

$$\eta^* = 0.75(1 + \cos(\beta))\lambda_1 H_{max}$$

$$\alpha_1 = 0.6 + 0.5\left(\frac{4\pi h/L_D}{\sinh(4\pi h/L_D)}\right)^2$$

234

$$\alpha_2 = min\left(\frac{(1 - d_{sill}/h_b)(H_{max}/d_{sill})^2}{3}, 2d_{sill}/H_{max}\right)$$

$$\alpha_3 = 1 - \left(\frac{h'}{h}\right)\left(1 - \frac{1}{\cosh(2\pi h/L_D)}\right)$$

$$\alpha_4 = 1 - \frac{h_c^*}{\eta^*}$$

β is the angle of incoming wave

h_b water depth at a desitance $5H_{max}$ from the wall $\approx h$

H_{max} desgin wave height $= 1.8H_s$ (if $h/L_D \geq 0$)

d_{sill} water depth above the top of the sill

h' water depth above the wall foundations plane

h waterdepth in front of the sill

h_c^* $min(\eta^*, h_c^*)$

L_D design wavelength which is calculated using the linear wave theory

T wave period $= 7.5$ sec

k wave number

$\lambda_1, \lambda_2, \lambda_3$ factors dependent on the shape of the structure and the wave

         and are elaborated by Takahashi

The design wave length is determined using the linear wave theory. Depending on the water depth-wavelength ratio, the relative water depth characteristics are determined. The wave length is computed by setting the wave length depending on the wave number equal to the wave length determined using the equations in Table 42:

Relative depth characteristics	Shallow water $\frac{h}{l} < \frac{1}{20}$	Transitional water depth $\frac{1}{20} < \frac{h}{l} < \frac{1}{2}$	Deep water $\frac{h}{l} > \frac{1}{2}$
Wave length	$L = T\sqrt{gh}$	$L = \frac{gT^2}{2\pi}\tanh(kh)$	$L = L_0 = \frac{gT^2}{2\pi}$
Wave number		$k = \frac{2\pi}{L}$	

TABLE 42: LINEAR WAVE THEORY COMPUTING THE WAVE LENGTH

The shape depending factors according to Takahashi are computed as follows:

$$\lambda_1 = \lambda_3 = 1$$

$$\lambda_2 = \max\left(1, \frac{\alpha_l}{\alpha_2}\right)$$

Where:

α_l is the impulse coefficeint $= \alpha_n \alpha_m$

$$\alpha_m = \min\left(\frac{H_{max}}{d}, 2\right)$$

$$\alpha_n = \frac{\cos(\delta_2)}{\cosh(\delta_1)} \qquad\qquad if\ \delta_2 \le 0$$

$$\delta_1 = 20\delta_{11} \qquad\qquad if\ \delta_{11} \le 0$$

$$\delta_1 = 15\delta_{11} \qquad\qquad if\ \delta_{11} > 0$$

$$\delta_2 = 4.9\delta_{22} \qquad\qquad if\ \delta_{22} \le 0$$

$$\delta_2 = 3.0\delta_{22} \qquad\qquad if\ \delta_{22} > 0$$

$$\delta_{11} = 0.93\left(\frac{B_M}{L_D} - 0.12\right) + 0.36\left(\frac{h-d}{h} - 0.6\right)$$

$$\delta_{22} = -0.36\left(\frac{B_M}{L_D} - 0.12\right) + 0.93\left(\frac{h-d}{h} - 0.6\right)$$

Where:

B_M *represents the berm width*

The water depth above the sill should be determined to find a reliable value of the wave impact pressure. This is done using Tanimoto et al. [1982]:

$$N_s = \max\left\{1.8, \left[1.3\frac{(1-\kappa)}{\kappa^{\frac{1}{3}}}\frac{h'}{H_s} + 1.8\,exp\left(-1.5\frac{(1-\kappa)}{\kappa^{\frac{1}{3}}}\frac{h'}{H_s}\right)\right]\right\}$$

$$\kappa = \left(\frac{2kh'}{\sinh(2kh')}\right)\sin\left(\frac{2\pi B_M}{L'}\right)$$

$$D_{n50} = \frac{H_s}{N_s}$$

In which:

L' *represents the wave length at the depth h'*

The thickness of the armour stone layer is assumed to be sufficient when two layers of the required nominal diameter are applied. The wave length L' is calculated using the linear wave theory as well.

The input parameters for the two mentioned situations are described in

Parameter	Symbol	Situation 1	Situation 2
Governing water level		+0.0 m NAP	+5.0 m NAP
Bottom level caisson*		-10.24 m NAP	-10.24 m NAP
Bottom level rubble foundation bed**		-12.24 m NAP	-12.24 m NAP
Significant wave height [m]	H_s	2.6	2.6
Angle of incoming wave [°]	β	10	10
Water depth above sill [m]	d	$h' - 2D_{n50}$	$h' - 2D_{n50}$
Water depth above foundation plane [m]	h'	10.24	15.24
Water depth in front of the sill [m]	h	12.24	17.24
Wave period [sec]	T	7.5	7.5
Berm width [m]	B_M	5	5

TABLE 43: INPUT DETERMINE WAVE PRESSURE

* The bottom level of the caisson is assumed to be at the top of the floor of the sluiceway, minus the thickness of 50 cm which is assumed to be the thickness of the sluiceway floor.

** The bottom level of the rubble foundation bed is 2 meter below the bottom level of the sluiceway. A thickness of the rubble foundation bed of 2 meter is assumed to be sufficient.

The results of calculations are summarized in Table 44:

Parameter	Symbol	Situation 1	Situation 2
Wave length at depth h' [m]	L'	65.96	75.10
Design wave length [m]	L	70.17	77.66
Wave number at depth h' [-]	k'	0.09525	0.08366
	κ	0.25953	0.16275
	N_s	3.41	11.83
Nominal armour diameter [m]	D_{n50}	0.76	0.22
Water depth above sill [m]	d	8.69	14.79
Design wave height [m]	H_{max}	4.68	4.68
Shape factor [-]	λ_2	1	1
Height wave impact above water level [m]	η^*	6.97	6.97
Freeboard [m]	h_c^*	6.97	5.04
Pressure [kN/m]	p_4	0.0	8.57
Pressure [kN/m]	p_1	35.03	31.0
Pressure [kN/m]	p_3	23.35	16.39
Pressure [kN/m]	p_u	22.5	16.28

TABLE 44: OUTCOMES GODA, TANIMOTO AND TAKAHASHI EQUATIONS

The known wave pressures lead to a load distribution along the North Sea outer walls in operational phase. Figure 136, Figure 137, Figure 138 and Figure 139 clarify the outcomes on the basis of simple schematizations.
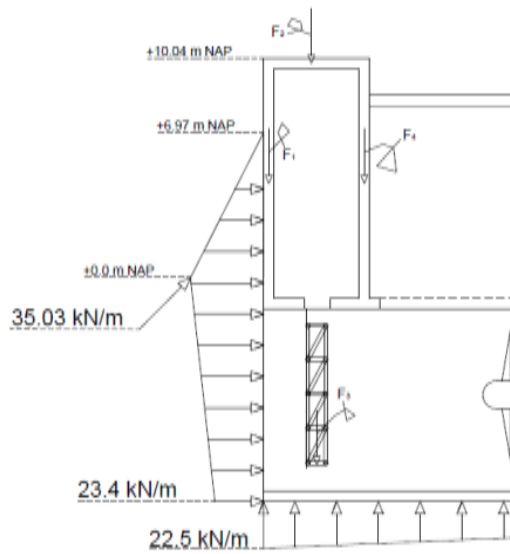
FIGURE 136: LOAD DISTRIBUTION WAVE IMPACT NORTH SEA LEVEL +0.00 M NAP
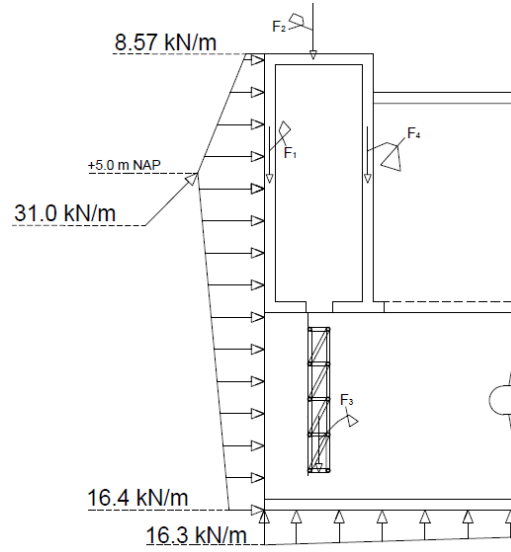

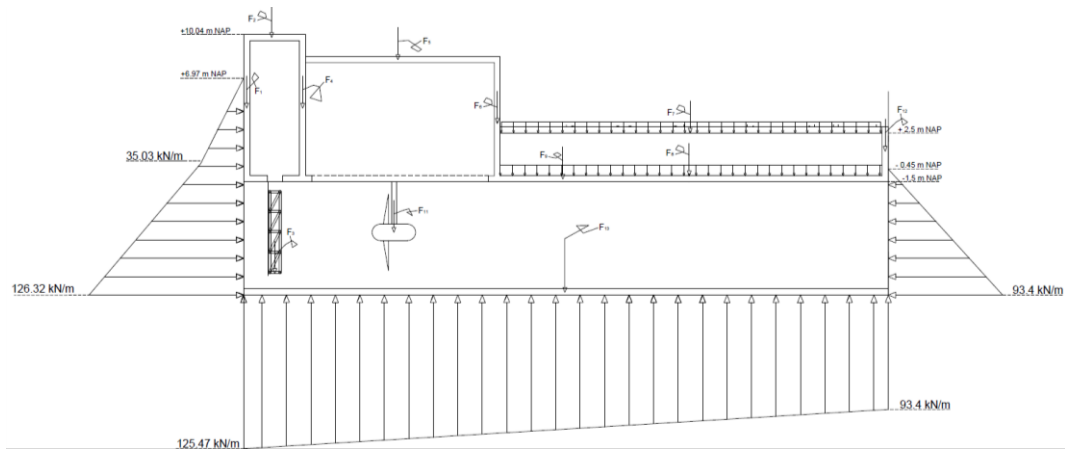FIGURE 137: LOAD DISTRIBUTION WAVE IMPACT NORTH SEA LEVEL +5.00 M NAP

FIGURE 138: LOAD DISTRIBUTION WAVE IMPACT AND HYDRAULIC PRESSURES COMBINED FOR A NORTH SEA WATER LEVEL OF +0.0 M NAP
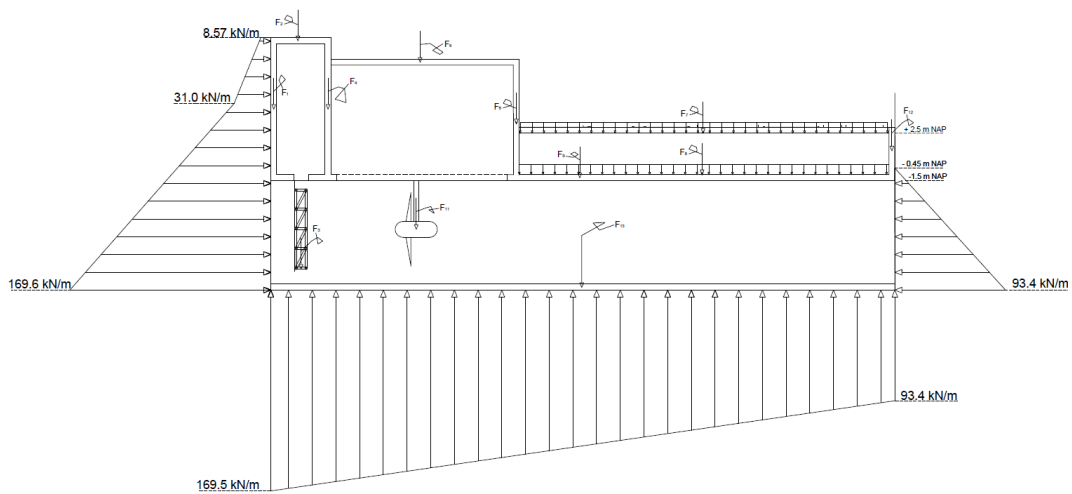

FIGURE 139: LOAD DISTRIBUTION WAVE IMPACT AND HYDRAULIC PRESSURES COMBINED FOR A NORTH SEA WATER LEVEL OF +5.0 M NAP

D.2 CLASSICAL BEAM THEORIES

When computing the force distribution, considering the beam as a rigid beam at first, the proper approach to compute the internal forces should be applied. This paragraph discusses four beam theories describing the motion of one dimensional beams.

D.2.1 EULER-BERNOLLI THEORY

Assuming small displacements, the Euler-Bernoulli theory becomes valid. The Euler-Bernoulli theory assumes the shear strains are approximately zero for each beam problem. It is also assumed the beam has a straight longitudinal axis with cross section of any shape provided it is symmetric about the y-axis, see Figure 140.

The key hypothesis of the Euler-Bernoulli theory claims that the plane cross-section initially perpendicular to the axis of the beam remains plane and perpendicular to the neutral axis during bending. This assumption implies that deformations due to shear and torsion are small compared to those deriving from normal stress and flexural deformation [Simone, 2011] .

With 'w' as the transverse deflection of the neutral axis of the beam, 'E' the Young modulus and 'I' the moment of inertia of the cross-section, the characteristic differential equation for the Euler Bernoulli theory beam subjected to an uniformly distributed load q reads:

$$EI \cdot \frac{d^4 w}{dx^4} = q$$

This equation governs the transverse motion of the beam as t responds to the external loading 'q' and initial conditions.
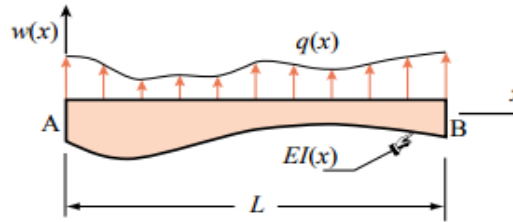

FIGURE 140: EULER BERNOULLI BEAM

D.2.2 PURE SHEAR OF A BEAM

According to the Euler-Bernoulli beam theory, cross sections carry a resultant shearing force 'V', but deformation associated to the corresponding shear stress is not taken into account. Structures containing weak main walls may experience deformations which are very close to pure shear deformations. Due to certain horizontal external cyclic loads, the structure could deflect horizontally. This deflection can be roughly predicted with a model referred to as 'shear beam'. The term pure shear of the beam comes forward from the assumption that the beam solely deforms as a consequence of the shear stress which is constant over the cross section, see Figure 141. Hence flexural deformation has no influence at all.

It is assumed the beam material behaves elastically and follows the simple Hooke's law while experiencing shear deformation. If the beam is inhomogeneous so that that the Shear modulus G does vary with x, the characteristic differential equation for pure-shear reads:
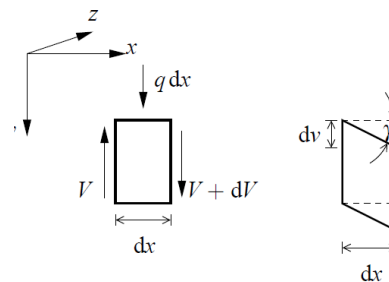

FIGURE 141: PURE SHEAR

$$-GA \cdot \frac{d^2 w}{dx^2} = q$$

D.2.3 TIMOSHENKO BEAM THEORY

Since the Euler-Bernoulli theory assumes shear strains are approximately zero, Timoshenko developed an extension to this assumption as this will not always be the case. The Timoshenko beam theory includes first-order transverse shear effect. The key hypothesis of Euler Bernoulli, claiming that the plane cross-section initially perpendicular to the axis of the beam remains plane and perpendicular to the neutral axis during bending, is relaxed. This relaxation is introduced through an additional degree of freedom which describes the additional rotation to the bending slope which generates shear strain [Simone, 2011], see Figure 142.

The system of differential equations for the Timoshenko beam subjected to an uniformly distributed load "q", constant flexural stiffness "EI" and constant shear stiffness "GA":

$$EI \cdot \frac{d^2\varphi}{dx^2} - GA\left(\frac{dw}{dx} - \varphi\right) = 0$$

$$GA\left(\frac{d^2w}{dx^2} - \frac{d\varphi}{dx}\right) = -q$$

These equations are coupled second order differential equations governing the deflection "w" and the cross sectional rotation "φ" of the Timoshenko beam.
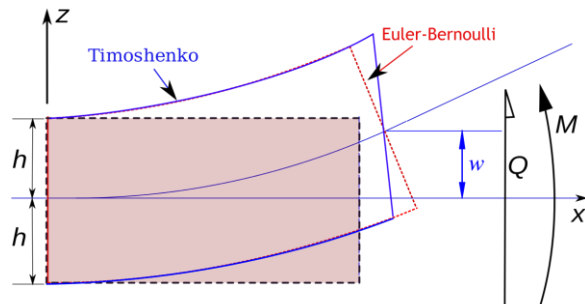

FIGURE 142: TIMOSHENKO VS. EULER-BERNOULLI

D.2.4 BEAMS ON ELASTIC FOUNDATION

The foundation of the caisson structure is formed by a rubble foundation bed. This rubble foundation bed, consists of granular material, schematized as a set of distributed linear elastic springs, see Figure 143. The force related to the elastic springs is proportional and opposite of the displacement. The sole difference with the Euler-Bernoulli beam and the shear beam is the presence of a distributed load proportional to the displacement "w". The distributed load may be considered as the soil stiffness "k_d"[Simone, 2011]. Assuming the bending stiffness is invariant along the beam the equilibrium equation governing the balance of transverse forces acting on a differential element of the beam, reads:

$$EI \cdot \frac{d^4w}{dx^4} + k_d w = q$$
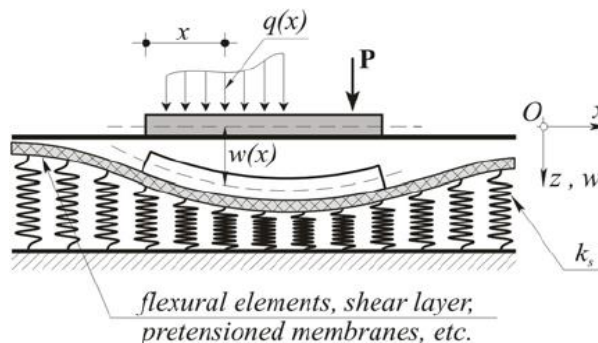
$$-GA \cdot \frac{d^2w}{dx^2} + k_d w = q$$

FIGURE 143: BEAM ON ELASTIC FOUNDATION

240

D.2.5 BEAM THEORY CHOICE

Varying deflections are the result of the differences in beam theory. Whether the beam is subject to pure shear or pure bending is determined using the Timoshenko (exact) beam theory. Timoshenko composed the deflection as a consequence of shear and bending into one equation. The contribution of the flexural deformation and the shear deformation will be determined using the (Timoshenko) exact solution.

The problem is reduced to a beam simply supported on both ends with a span L. The span in transverse direction is equal to 52.676 m, whereas in longitudinal direction the span is equal to 157.82 m. It is assumed the beam is solely subject to its self-weight. The deflection calculated with the pure shear beam theory and the exact solution are accordingly:

$$w = \frac{1}{GA_s}\left(-\frac{1}{2}qx^2 + \frac{1}{2}qxL\right) \qquad \text{(pure shear)}$$

$$w = \frac{1}{EI}\left(-\frac{1}{24}qx^4 + \frac{1}{12}qx^3L - \frac{1}{24}qxL^3\right) + \frac{1}{GA_s}\left(\frac{1}{2}qx^2 - \frac{1}{2qxL}\right) \quad \text{(Timoshenko)}$$

Where in the Timoshenko equation the left part of the equation represents the contribution from the flexural deformation, whereas the right part represents the contribution from the shear deformation.

The final preliminary design is used to determine the values for EI and GA_s. This leads to the final contribution of each theory as shown in Figure 145. In this figure the contribution for four cross-sections is given. X represents the transverse direction, y_i represents the cross-section in longitudinal direction, with subscript 'i' indicating the distinguishable sections 1, 2 and 3 (see figure..)
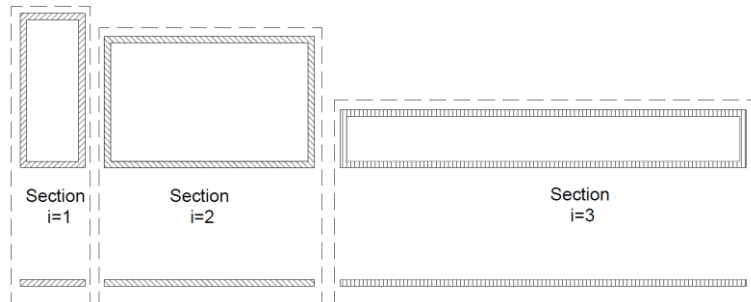

FIGURE 144: SECTIONS i=1, i=2 AND i=3

y_1 cross-section at the location of the gate housing, y_2 the cross section at the location of the turbine housing and y_3 the cross section at the location of the ballast housing. A distinguish between these location has been made due to their differences in the shear cross section area A_s and the moment of inertia I.
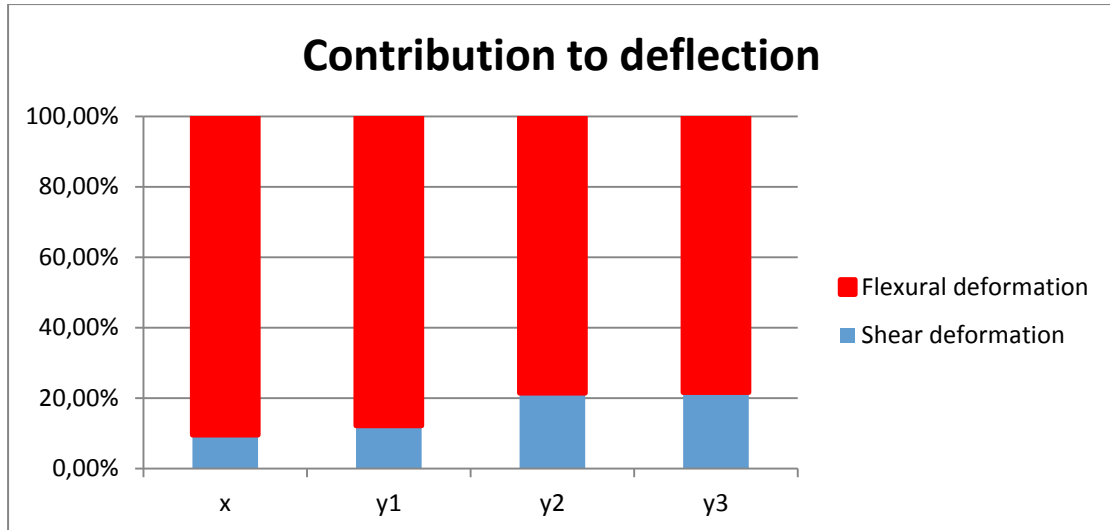
FIGURE 145: CONTRIBUTION SHEAR DEFORMATION VS. FLEXURAL DEFORMATION

From Figure 145 it may be concluded the flexural deformation contributes significantly to the deformation of the beam. Since the beam shall be located on the rubble foundation bed, the governing theory representing the Tidal Power Plant is a beam on an elastic foundation. The contribution to the deflection is governed by the flexural deformation. Therefore, the beam calculations are performed using:

$$EI \cdot \frac{d^4 w}{dx^4} + k_d w = q$$

In which:

w *represents the deformation*

E *represents the Young's Modulus of concrete*

k_d *represents the sill beam subgrade material stiffness*

q *represents the governing load on the beam*

I *represents the Moment of inertia of the beam*

In longitudinal direction the contribution of the shear beam theory increases. The flexural deformation should be compensated for this additional deformation. The magnitude of this compensation is unknown.

D.2.6 BEAM ON ELASTIC FOUNDATION

From the beam theory, beam on an elastic foundation, it already appeared the flexural deformation is governing for the beams' deflection. This section provides the elaborated expressions for the beam deflection, moment and shear force. These expression are required to determine the actual deflection, moment and shear force of the beam.

The equilibrium equation, governing the balance of transverse forces acting on a differential element of the beam, reads:

$$\frac{d^2}{dx^2}\left(EI\frac{d^2}{dx^2}\right) = q_1 - k_d w$$

If the bending stiffness is invariant along the beam, this equation is reduced to:

$$EI\frac{d^4}{dx^4} + k_d w = q_1$$

If additionally, the external force q_1 and the stiffness per unit length k_d of the elastic foundation are also coordinate-invariant, then the general solution of this equation can be readily found. This solution is the superposition of a particular solution, which may be chosen as:

$$w_{part} = \frac{q_1}{k_d}$$

The general solution of the homogeneous part of this equation is to be sought in the form:

$$w_{gen,hom} = \sum_{n=1}^{4} \tilde{C}_n \exp(s_n x)$$

Substituting this into the equation of motion, the following characteristic equation is found:

$$s_n^4 + \frac{k_d}{EI} = 0$$

Solving this characteristic equation leads to:

$$s_1 = (1+i)\lambda, \qquad s_2 = (1-i)\lambda, \qquad s_3 = (-1+i)\lambda, \qquad s_4 = -(1+i)\lambda$$

Where

$$4\lambda^4 = \frac{k_{d,i}}{EI}$$

Substituting the characteristic exponents into the homogeneous part:

$$w = \tilde{C}_1 \exp\big((1+i)\lambda x\big) + \tilde{C}_2 \exp\big((1-i)\lambda x\big) + \tilde{C}_3 \exp\big((-1+i)\lambda x\big) + \tilde{C}_4 \exp(-(1+i)\lambda x)$$

$$= \exp(\lambda x)\left(C_1 \cos(\lambda x) + C_2 \sin(\lambda x)\right) + \exp(-\lambda x)\left(C_3 \cos(\lambda x) + C_4 \sin(\lambda x)\right)$$

Thus the general solution under the condition that EI, k_d, and q_1 are invariant along the beam, reads:

$$w_i(x) = \exp(\lambda_i x)\,(C_1\cos(\lambda_i x) + C_2\sin(\lambda_i x)) + \exp(-\lambda_i x)\,(C_3\cos(\lambda_i x) + C_4\sin(\lambda_i x))$$
$$+ \frac{q_1}{k_{d,i}}$$

Consequently, the expressions for the beam slope, bending moment and shear resistance are:

$$\varphi = \frac{\partial w}{\partial x}$$

$$M = -EI * \frac{\partial^2 w}{\partial x^2}$$

$$V = \frac{\partial M}{\partial x}$$

Substituting the general solution into these expressions results:

$$\varphi = \frac{\partial w}{\partial x} = \lambda_i \exp(\lambda_i x)\,[C_1(\cos(\lambda_i x) - \sin(\lambda_i x)) + C_2(\sin(\lambda_i x) + \cos(\lambda_i x))] + \exp(-\lambda_i x)\,[C_3(-\sin(\lambda_i x) - \cos(\lambda_i x)) + C_4(\cos(\lambda_i x) - \sin(\lambda_i x))]$$

$$M = -EI * \frac{\partial^2 w}{\partial x^2} = 2EI\lambda^2 \left(\begin{array}{l} \exp(\lambda x)(C_1\sin(\lambda x) - C_2\cos(\lambda x)) \\ + \exp(-\lambda x)\,(-C_3\sin(\lambda x) + C_4\cos(\lambda x)) \end{array} \right)$$

$$V = -EI\frac{\partial^3 w}{\partial x^3} = 2EI\lambda^3\{\exp(\lambda x)\,(C_1(\sin(\lambda x) + \cos(\lambda x)) + C_2(\sin(\lambda x) - \cos(\lambda x)))$$
$$+ \exp(-\lambda x)\,(C_3(\sin(\lambda x) - \cos(\lambda x)) - C_4(\sin(\lambda x) + \cos(\lambda x)))\}$$

Solving these equations requires boundary conditions and several simplifications. The method of solving the equation of motion has therefore been described briefly below.

The beam is considered as a free-free beam. The corresponding boundary conditions at the beam each beam edge are therefore:

$$V = -EI * \frac{\partial^3 w}{\partial x^3} = M = -EI * \frac{\partial^2 w}{\partial x^2} = 0$$

Applying the external moments elaborated in the previous sections, the moment at the edges does not equals zero, but equals the external moment.

Furthermore, the beam deflection is assumed to be symmetrical over the considered length. The requirements for symmetry are:

$$w_l = w_r; \qquad \frac{\partial w_l}{\partial x} = \frac{\partial w_r}{\partial x}; \qquad \frac{\partial^2 w_l}{\partial x^2} = \frac{\partial^2 w_r}{\partial x^2}; \qquad \frac{\partial^3 w_l}{\partial x^3} = \frac{\partial^3 w_r}{\partial x^3}$$

In which subscript $'l'$ and $'r'$ represent the left and the right side of the transition point respectively.

The equations for w_l and w_r contain in total 8 unknowns, whereas with the four boundary and four interface conditions in total 8 conditions are described. With the use of a mathematical programme, such as Maple, the unknown constants are obtained. The input parameters are summarized in the succeeding section.

This appendix will provide the Maple worksheets required to determine the influence of the elastic foundation on the Tidal Power Plant.

D.3.1 EQUALLY SUPPORTED BEAM ON ELASTIC FOUNDATION

The beam located on an elastic foundation will not be subject to any external forces. The corresponding Maple worksheet reads:

> *restart; Beam on elastic foundation*

$$\textit{Beam on elastic foundation} \tag{1}$$

> $k1 := kd : k2 := kd : L1 := \dfrac{L}{2} : labda1 := \left(\dfrac{k1}{(4 \cdot EI)} \right)^{(0.25)} : labda2 := \left(\dfrac{k2}{(4 \cdot EI)} \right)^{(0.25)} :$

$w1(x) := \exp(labda1 \cdot x) \cdot (C1 \cdot \cos(labda1 \cdot x) + C2 \cdot \sin(labda1 \cdot x)) + \exp(-labda1 \cdot x)$

$\cdot (C3 \cdot \cos(labda1 \cdot x) + C4 \cdot \sin(labda1 \cdot x)) - \dfrac{q}{k1} : w2(x) := \exp(labda2 \cdot x) \cdot (C5$

$\cdot \cos(labda2 \cdot x) + C6 \cdot \sin(labda2 \cdot x)) + \exp(-labda2 \cdot x) \cdot (C7 \cdot \cos(labda2 \cdot x) + C8$

$\cdot \sin(labda2 \cdot x)) - \dfrac{q}{k2} :$

> $x := -L1 :$

> $V1 := -2 \cdot EI \cdot labda1^3 \cdot (\exp(labda1 \cdot x) \cdot (C1 \cdot (\sin(labda1 \cdot x) + \cos(labda1 \cdot x)) + C2$

$\cdot (\sin(labda1 \cdot x) - \cos(labda1 \cdot x))) + \exp(-labda1 \cdot x) \cdot (C3 \cdot (\sin(labda1 \cdot x) - \cos(labda1$

$\cdot x)) - C4 \cdot (\sin(labda1 \cdot x) + \cos(labda1 \cdot x)))) : M1 := 2 \cdot EI \cdot labda1^2 \cdot (\exp(labda1 \cdot x)$

$\cdot (C1 \cdot \sin(labda1 \cdot x) - C2 \cdot \cos(labda1 \cdot x)) + \exp(-labda1 \cdot x) \cdot (-C3 \cdot \sin(labda1 \cdot x) + C4$

$\cdot \cos(labda1 \cdot x))) :$

> $eq1 := V1 = 0 :$

> $eq2 := M1 = 0 :$

> $x := 0 : eq3 := w1(x) = w2(x) : eq4 := labda1 \cdot (C1 + C2 - C3 + C4) = labda2 \cdot (C5 + C6$

$- C7 + C8) :$

> $eq5 := -(labda1^3) \cdot (-C1 + C2 + C3 + C4) = -labda2^3 \cdot (-C5 + C6 + C7 + C8) : eq6 :=$

$-labda1^2 \cdot (C2 - C4) = -labda2^2 \cdot (C6 - C8) :$

> $x := L1 : V2 := -2 \cdot EI \cdot labda2^3 \cdot (\exp(labda2 \cdot x) \cdot (C5 \cdot (\sin(labda2 \cdot x) + \cos(labda2 \cdot x)) + C6$

$\cdot (\sin(labda2 \cdot x) - \cos(labda2 \cdot x))) + \exp(-labda2 \cdot x) \cdot (C7 \cdot (\sin(labda2 \cdot x) - \cos(labda2$

$\cdot x)) - C8 \cdot (\sin(labda2 \cdot x) + \cos(labda2 \cdot x)))) : M2 := 2 \cdot EI \cdot labda2^2 \cdot (\exp(labda2 \cdot x)$

$\cdot (C5 \cdot \sin(labda2 \cdot x) - C6 \cdot \cos(labda2 \cdot x)) + \exp(-labda2 \cdot x) \cdot (-C7 \cdot \sin(labda2 \cdot x) + C8$

$\cdot \cos(labda2 \cdot x))) :$

> $eq7 := V2 = 0 : eq8 := M2 = 0 :$

> $solution := solve(\{eq1, eq2, eq3, eq4, eq5, eq6, eq7, eq8\}, [C1, C2, C3, C4, C5, C6, C7, C8]) :$

The applied Maple worksheet to determine the unknown constants for sagging from the beam on elastic foundation theory is demonstrated below;

```
> restart; Sagging
> k1 := Kd : k2 := alpha· k1 : k3 := k1 : L1 := Beta·L : L2 := (L −L1) : L3 := L : labda1 :=
```
$$\left(\frac{k1}{(4\cdot EI)}\right)^{(0.25)} : labda2 := \left(\frac{k2}{(4\cdot EI)}\right)^{(0.25)} : labda3 := \left(\frac{k3}{(4\cdot EI)}\right)^{(0.25)} : w1(x) :=$$
$$\exp(labda1\cdot x)\cdot(C1\cdot\cos(labda1\cdot x) + C2\cdot\sin(labda1\cdot x)) + \exp(-labda1\cdot x)\cdot(C3$$
$$\cdot\cos(labda1\cdot x) + C4\cdot\sin(labda1\cdot x)) - \frac{q}{k1} : w2(x) := \exp(labda2\cdot x)\cdot(C5\cdot\cos(labda2\cdot x)$$
$$+ C6\cdot\sin(labda2\cdot x)) + \exp(-labda2\cdot x)\cdot(C7\cdot\cos(labda2\cdot x) + C8\cdot\sin(labda2\cdot x)) - \frac{q}{k2} :$$
$$w3(x) := \exp(labda3\cdot x)\cdot(C9\cdot\cos(labda3\cdot x) + C10\cdot\sin(labda3\cdot x)) + \exp(-labda3\cdot x)$$
$$\cdot(C11\cdot\cos(labda3\cdot x) + C12\cdot\sin(labda3\cdot x)) - \frac{q}{k3} :$$

```
> x := 0 :
```
$$> V1 := 2\cdot EI\cdot labda1^3\cdot(\exp(labda1\cdot x)\cdot(C1\cdot(\sin(labda1\cdot x) + \cos(labda1\cdot x)) + C2$$
$$\cdot(\sin(labda1\cdot x) − \cos(labda1\cdot x))) + \exp(-labda1\cdot x)\cdot(C3\cdot(\sin(labda1\cdot x) − \cos(labda1$$
$$\cdot x)) − C4\cdot(\sin(labda1\cdot x) + \cos(labda1\cdot x)))) : M1 := 2\cdot EI\cdot labda1^2\cdot(\exp(labda1\cdot x)$$
$$\cdot(C1\cdot\sin(labda1\cdot x) − C2\cdot\cos(labda1\cdot x)) + \exp(-labda1\cdot x)\cdot(-C3\cdot\sin(labda1\cdot x) + C4$$
$$\cdot\cos(labda1\cdot x))) :$$

```
> eq1 := V1 = 0 :
> eq2 := M1 = Mext_i :
> x := L1 : eq3 := w1(x) = w2(x) :
```
$$eq4 := labda1\cdot(\exp(labda1\cdot x)\cdot(C1\cdot(\cos(labda1\cdot x)$$
$$−\sin(labda1\cdot x)) + C2\cdot(\cos(labda1\cdot x) + \sin(labda1\cdot x))) + \exp(-labda1\cdot x)\cdot(C3\cdot($$
$$−\cos(labda1\cdot x) −\sin(labda1\cdot x)) + C4\cdot(\cos(labda1\cdot x) −\sin(labda1\cdot x)))) = labda2$$
$$\cdot(\exp(labda2\cdot x)\cdot(C5\cdot(\cos(labda2\cdot x) −\sin(labda2\cdot x)) + C6\cdot(\cos(labda2\cdot x) + \sin(labda2$$
$$\cdot x))) + \exp(-labda2\cdot x)\cdot(C7\cdot(-\cos(labda2\cdot x) −\sin(labda2\cdot x)) + C8\cdot(\cos(labda2\cdot x)$$
$$−\sin(labda2\cdot x)))) :$$

$$> eq5 := -2\cdot EI\cdot labda1^3\cdot(\exp(labda1\cdot x)\cdot(C1\cdot(\sin(labda1\cdot x) + \cos(labda1\cdot x)) + C2$$
$$\cdot(\sin(labda1\cdot x) − \cos(labda1\cdot x))) + \exp(-labda1\cdot x)\cdot(C3\cdot(\sin(labda1\cdot x) − \cos(labda1$$
$$\cdot x)) − C4\cdot(\sin(labda1\cdot x) + \cos(labda1\cdot x)))) = -2\cdot EI\cdot labda2^3\cdot(\exp(labda2\cdot x)\cdot(C5$$
$$\cdot(\sin(labda2\cdot x) + \cos(labda2\cdot x)) + C6\cdot(\sin(labda2\cdot x) − \cos(labda2\cdot x))) + \exp($$
$$−labda2\cdot x)\cdot(C7\cdot(\sin(labda2\cdot x) − \cos(labda2\cdot x)) − C8\cdot(\sin(labda2\cdot x) + \cos(labda2$$
$$\cdot x)))) : eq6 := -2\cdot EI\cdot labda1^2\cdot(\exp(labda1\cdot x)\cdot(C1\cdot\sin(labda1\cdot x) − C2\cdot\cos(labda1\cdot x))$$
$$+ \exp(-labda1\cdot x)\cdot(-C3\cdot\sin(labda1\cdot x) + C4\cdot\cos(labda1\cdot x))) = -2\cdot EI\cdot labda2^2$$
$$\cdot(\exp(labda2\cdot x)\cdot(C5\cdot\sin(labda2\cdot x) − C6\cdot\cos(labda2\cdot x)) + \exp(-labda2\cdot x)\cdot(-C7$$
$$\cdot\sin(labda2\cdot x) + C8\cdot\cos(labda2\cdot x))) :$$

```
> x := L2 : eq7 := w2(x) = w3(x) :
```
$$eq8 := labda2\cdot(\exp(labda2\cdot x)\cdot(C5\cdot(\cos(labda2\cdot x)$$
$$−\sin(labda2\cdot x)) + C6\cdot(\cos(labda2\cdot x) + \sin(labda2\cdot x))) + \exp(-labda2\cdot x)\cdot(C7\cdot($$
$$−\cos(labda2\cdot x) −\sin(labda2\cdot x)) + C8\cdot(\cos(labda2\cdot x) −\sin(labda2\cdot x)))) = labda3$$
$$\cdot(\exp(labda3\cdot x)\cdot(C9\cdot(\cos(labda3\cdot x) −\sin(labda3\cdot x)) + C10\cdot(\cos(labda3\cdot x)$$
$$+ \sin(labda3\cdot x))) + \exp(-labda3\cdot x)\cdot(C11\cdot(-\cos(labda3\cdot x) −\sin(labda3\cdot x)) + C12$$
$$\cdot(\cos(labda3\cdot x) −\sin(labda3\cdot x)))) :$$

$$> eq9 := -2\cdot EI\cdot labda2^3\cdot(\exp(labda2\cdot x)\cdot(C5\cdot(\sin(labda2\cdot x) + \cos(labda2\cdot x)) + C6$$
$$\cdot(\sin(labda2\cdot x) − \cos(labda2\cdot x))) + \exp(-labda2\cdot x)\cdot(C7\cdot(\sin(labda2\cdot x) − \cos(labda2$$
$$\cdot x)) − C8\cdot(\sin(labda2\cdot x) + \cos(labda2\cdot x)))) = -2\cdot EI\cdot labda3^3\cdot(\exp(labda3\cdot x)\cdot(C9$$
$$\cdot(\sin(labda3\cdot x) + \cos(labda3\cdot x)) + C10\cdot(\sin(labda3\cdot x) − \cos(labda3\cdot x))) + \exp($$
$$−labda3\cdot x)\cdot(C11\cdot(\sin(labda3\cdot x) − \cos(labda3\cdot x)) − C12\cdot(\sin(labda3\cdot x) + \cos(labda3$$
$$\cdot x)))) : eq10 := -2\cdot EI\cdot labda2^2\cdot(\exp(labda2\cdot x)\cdot(C5\cdot\sin(labda2\cdot x) − C6\cdot\cos(labda2\cdot x))$$

$+ \exp(-labda2 \cdot x) \cdot (-C7 \cdot \sin(labda2 \cdot x) + C8 \cdot \cos(labda2 \cdot x))) = -2 \cdot EI \cdot labda3^2$
$\cdot (\exp(labda3 \cdot x) \cdot (C9 \cdot \sin(labda3 \cdot x) - C10 \cdot \cos(labda3 \cdot x)) + \exp(-labda3 \cdot x) \cdot (-C11$
$\cdot \sin(labda3 \cdot x) + C12 \cdot \cos(labda3 \cdot x))) :$

> $x := L3 : V3 := 2 \cdot EI \cdot labda3^3 \cdot (\exp(labda3 \cdot x) \cdot (C9 \cdot (\sin(labda3 \cdot x) + \cos(labda3 \cdot x)) + C10$
$\cdot (\sin(labda3 \cdot x) - \cos(labda3 \cdot x))) + \exp(-labda3 \cdot x) \cdot (C11 \cdot (\sin(labda3 \cdot x)$
$- \cos(labda3 \cdot x)) - C12 \cdot (\sin(labda3 \cdot x) + \cos(labda3 \cdot x)))) : M3 := 2 \cdot EI \cdot labda3^2$
$\cdot (\exp(labda3 \cdot x) \cdot (C9 \cdot \sin(labda3 \cdot x) - C10 \cdot \cos(labda3 \cdot x)) + \exp(-labda3 \cdot x) \cdot (-C11$
$\cdot \sin(labda3 \cdot x) + C12 \cdot \cos(labda3 \cdot x))) : eq11 := V3 = 0 : eq12 := M3 = Mext\_j :$

> $solution := solve(\{eq1, eq2, eq3, eq4, eq5, eq6, eq7, eq8, eq9, eq10, eq11, eq12\}, [C1, C2, C3,$
$C4, C5, C6, C7, C8, C9, C10, C11, C12]) :$

In this approach several constants require some attention, as these were not mentioned before:

β *represents the half support length scenario*

K_d *represents the bedding constant*

Alpha   *represents the bedding constant*

I *represents the moment of inertia, varying for each considered section*

$M_{ext,i}$ represents the external applied moment at section i.

The applied Maple worksheet to determine the unknown constants for sagging from the beam on elastic foundation theory is demonstrated below

```
> restart; Hogging
> k1 := beta·Kd : k2 := Kd : k3 := beta· Kd : L1 := Beta·L : L2 := (L −L1) : L3 := L :
```

$$labda1 := \left(\frac{k1}{(4 \cdot EI)}\right)^{(0.25)} : labda2 := \left(\frac{k2}{(4 \cdot EI)}\right)^{(0.25)} : labda3 := \left(\frac{k3}{(4 \cdot EI)}\right)^{(0.25)} :$$

$$w1(x) := \exp(labda1 \cdot x) \cdot (C1 \cdot \cos(labda1 \cdot x) + C2 \cdot \sin(labda1 \cdot x)) + \exp(-labda1 \cdot x)$$
$$\cdot (C3 \cdot \cos(labda1 \cdot x) + C4 \cdot \sin(labda1 \cdot x)) - \frac{q}{k1} : w2(x) := \exp(labda2 \cdot x) \cdot (C5$$
$$\cdot \cos(labda2 \cdot x) + C6 \cdot \sin(labda2 \cdot x)) + \exp(-labda2 \cdot x) \cdot (C7 \cdot \cos(labda2 \cdot x) + C8$$
$$\cdot \sin(labda2 \cdot x)) - \frac{q}{k2} : w3(x) := \exp(labda3 \cdot x) \cdot (C9 \cdot \cos(labda3 \cdot x) + C10 \cdot \sin(labda3$$
$$\cdot x)) + \exp(-labda3 \cdot x) \cdot (C11 \cdot \cos(labda3 \cdot x) + C12 \cdot \sin(labda3 \cdot x)) - \frac{q}{k3} :$$

```
> x := 0 :
```

```
> V1 := 2·EI· labda1³·(exp(labda1·x)·(C1·(sin(labda1·x) + cos(labda1·x)) + C2
      ·(sin(labda1·x) − cos(labda1·x))) + exp(−labda1·x)·(C3·(sin(labda1·x) − cos(labda1
      ·x)) − C4·(sin(labda1·x) + cos(labda1·x)))) : M1 := 2·EI· labda1²·(exp(labda1·x)
      ·(C1·sin(labda1·x) − C2·cos(labda1·x)) + exp(−labda1·x)·(−C3·sin(labda1·x) + C4
      ·cos(labda1·x))) :
```

```
> eq1 := V1 = 0 :
```

```
> eq2 := M1 = Mext_i :
```

```
> x := L1 : eq3 := w1(x) = w2(x) : eq4 := labda1·(exp(labda1·x)·(C1·(cos(labda1·x)
      −sin(labda1·x)) + C2·(cos(labda1·x) + sin(labda1·x))) + exp(−labda1·x)·(C3·(
      −cos(labda1·x)−sin(labda1·x)) + C4·(cos(labda1·x) −sin(labda1·x)))) = labda2
      ·(exp(labda2·x)·(C5·(cos(labda2·x) −sin(labda2·x)) + C6·(cos(labda2·x) + sin(labda2
      ·x))) + exp(−labda2·x)·(C7·(−cos(labda2·x)−sin(labda2·x)) + C8·(cos(labda2·x)
      −sin(labda2·x)))) :
```

```
> eq5 :=−2·EI· labda1³·(exp(labda1·x)·(C1·(sin(labda1·x) + cos(labda1·x)) + C2
      ·(sin(labda1·x) − cos(labda1·x))) + exp(−labda1·x)·(C3·(sin(labda1·x) − cos(labda1
      ·x)) − C4·(sin(labda1·x) + cos(labda1·x)))) =−2·EI· labda2³·(exp(labda2·x)·(C5
      ·(sin(labda2·x) + cos(labda2·x)) + C6·(sin(labda2·x) − cos(labda2·x))) + exp(
      −labda2·x)·(C7·(sin(labda2·x) − cos(labda2·x)) − C8·(sin(labda2·x) + cos(labda2
      ·x)))) : eq6 :=−2·EI· labda1²·(exp(labda1·x)·(C1·sin(labda1·x) − C2·cos(labda1·x))
      + exp(−labda1·x)·(−C3·sin(labda1·x) + C4·cos(labda1·x))) =−2·EI· labda2²
      ·(exp(labda2·x)·(C5·sin(labda2·x) − C6·cos(labda2·x)) + exp(−labda2·x)·(−C7
      ·sin(labda2·x) + C8·cos(labda2·x))) :
```

```
> x := L2 : eq7 := w2(x) = w3(x) : eq8 := labda2·(exp(labda2·x)·(C5·(cos(labda2·x)
      −sin(labda2·x)) + C6·(cos(labda2·x) + sin(labda2·x))) + exp(−labda2·x)·(C7·(
      −cos(labda2·x)−sin(labda2·x)) + C8·(cos(labda2·x) −sin(labda2·x)))) = labda3
      ·(exp(labda3·x)·(C9·(cos(labda3·x) −sin(labda3·x)) + C10·(cos(labda3·x)
      + sin(labda3·x))) + exp(−labda3·x)·(C11·(−cos(labda3·x)−sin(labda3·x)) + C12
      ·(cos(labda3·x)−sin(labda3·x)))) :
```

```
> eq9 :=−2·EI· labda2³·(exp(labda2·x)·(C5·(sin(labda2·x) + cos(labda2·x)) + C6
      ·(sin(labda2·x) − cos(labda2·x))) + exp(−labda2·x)·(C7·(sin(labda2·x) − cos(labda2
      ·x)) − C8·(sin(labda2·x) + cos(labda2·x)))) =−2·EI· labda3³·(exp(labda3·x)·(C9
      ·(sin(labda3·x) + cos(labda3·x)) + C10·(sin(labda3·x) − cos(labda3·x))) + exp(
      −labda3·x)·(C11·(sin(labda3·x) − cos(labda3·x)) − C12·(sin(labda3·x) + cos(labda3
      ·x)))) : eq10 :=−2·EI· labda2²·(exp(labda2·x)·(C5·sin(labda2·x) − C6·cos(labda2·x))
```

$+ \exp(-labda2 \cdot x) \cdot (-C7 \cdot \sin(labda2 \cdot x) + C8 \cdot \cos(labda2 \cdot x))) = -2 \cdot EI \cdot labda3^2$
$\cdot (\exp(labda3 \cdot x) \cdot (C9 \cdot \sin(labda3 \cdot x) - C10 \cdot \cos(labda3 \cdot x)) + \exp(-labda3 \cdot x) \cdot (-C11$
$\cdot \sin(labda3 \cdot x) + C12 \cdot \cos(labda3 \cdot x)))$:

> $x := L3 : V3 := 2 \cdot EI \cdot labda3^3 \cdot (\exp(labda3 \cdot x) \cdot (C9 \cdot (\sin(labda3 \cdot x) + \cos(labda3 \cdot x)) + C10$
$\cdot (\sin(labda3 \cdot x) - \cos(labda3 \cdot x))) + \exp(-labda3 \cdot x) \cdot (C11 \cdot (\sin(labda3 \cdot x)$
$- \cos(labda3 \cdot x)) - C12 \cdot (\sin(labda3 \cdot x) + \cos(labda3 \cdot x)))) : M3 := 2 \cdot EI \cdot labda3^2$
$\cdot (\exp(labda3 \cdot x) \cdot (C9 \cdot \sin(labda3 \cdot x) - C10 \cdot \cos(labda3 \cdot x)) + \exp(-labda3 \cdot x) \cdot (-C11$
$\cdot \sin(labda3 \cdot x) + C12 \cdot \cos(labda3 \cdot x))) : eq11 := V3 = 0 : eq12 := M3 = Mext\_j :$

> $solution := solve(\{eq1, eq2, eq3, eq4, eq5, eq6, eq7, eq8, eq9, eq10, eq11, eq12\}, [C1, C2, C3,$
$C4, C5, C6, C7, C8, C9, C10, C11, C12]) :$

With the Maple Worksheet presented below, the validity of the calculation method using Maple has been determined. The inputs and outcomes of the Maple Worksheet are included as well.

> $restart : Validity\ check\ \ Sagging\ transverse\ direction$

$$\textit{Validity check Sagging transverse direction} \qquad (1)$$

> $k1 := 50000 : k2 := 0.9 \cdot k1 : k3 := k1 : EI := 30000000 \cdot 74.08 : q := 245.5 : D2 := \dfrac{52.676}{4} :$

$L1 := \left(\dfrac{52.676}{2} - D2 \right) : L2 := \dfrac{52.676}{2} + D2 : L3 := 52.676 : labda1 :=$

$\left(\dfrac{k1}{(4 \cdot EI)} \right)^{(0.25)} : labda2 := \left(\dfrac{k2}{(4 \cdot EI)} \right)^{(0.25)} : labda3 := \left(\dfrac{k3}{(4 \cdot EI)} \right)^{(0.25)} : w1(x) :=$

$\exp(labda1 \cdot x) \cdot (C1 \cdot \cos(labda1 \cdot x) + C2 \cdot \sin(labda1 \cdot x)) + \exp(-labda1 \cdot x) \cdot (C3$

$\cdot \cos(labda1 \cdot x) + C4 \cdot \sin(labda1 \cdot x)) - \dfrac{q}{k1} : w2(x) := \exp(labda2 \cdot x) \cdot (C5 \cdot \cos(labda2 \cdot x)$

$+ C6 \cdot \sin(labda2 \cdot x)) + \exp(-labda2 \cdot x) \cdot (C7 \cdot \cos(labda2 \cdot x) + C8 \cdot \sin(labda2 \cdot x)) - \dfrac{q}{k2} :$

$w3(x) := \exp(labda3 \cdot x) \cdot (C9 \cdot \cos(labda3 \cdot x) + C10 \cdot \sin(labda3 \cdot x)) + \exp(-labda3 \cdot x)$

$\cdot (C11 \cdot \cos(labda3 \cdot x) + C12 \cdot \sin(labda3 \cdot x)) - \dfrac{q}{k3} :$

> $x := 0 :$

> $V1 := 2 \cdot EI \cdot labda1^3 \cdot (\exp(labda1 \cdot x) \cdot (C1 \cdot (\sin(labda1 \cdot x) + \cos(labda1 \cdot x)) + C2$

$\cdot (\sin(labda1 \cdot x) - \cos(labda1 \cdot x))) + \exp(-labda1 \cdot x) \cdot (C3 \cdot (\sin(labda1 \cdot x) - \cos(labda1$

$\cdot x)) - C4 \cdot (\sin(labda1 \cdot x) + \cos(labda1 \cdot x)))) : M1 := 2 \cdot EI \cdot labda1^2 \cdot (\exp(labda1 \cdot x)$

$\cdot (C1 \cdot \sin(labda1 \cdot x) - C2 \cdot \cos(labda1 \cdot x)) + \exp(-labda1 \cdot x) \cdot (-C3 \cdot \sin(labda1 \cdot x) + C4$

$\cdot \cos(labda1 \cdot x))) :$

> $eq1 := V1 = 0 :$

> $eq2 := M1 = 0 :$

> $x := L1 : eq3 := w1(x) = w2(x) : eq4 := labda1 \cdot (\exp(labda1 \cdot x) \cdot (C1 \cdot (\cos(labda1 \cdot x)$

$- \sin(labda1 \cdot x)) + C2 \cdot (\cos(labda1 \cdot x) + \sin(labda1 \cdot x))) + \exp(-labda1 \cdot x) \cdot (C3 \cdot ($

$- \cos(labda1 \cdot x) - \sin(labda1 \cdot x)) + C4 \cdot (\cos(labda1 \cdot x) - \sin(labda1 \cdot x)))) = labda2$

$\cdot (\exp(labda2 \cdot x) \cdot (C5 \cdot (\cos(labda2 \cdot x) - \sin(labda2 \cdot x)) + C6 \cdot (\cos(labda2 \cdot x) + \sin(labda2$

$\cdot x))) + \exp(-labda2 \cdot x) \cdot (C7 \cdot (-\cos(labda2 \cdot x) - \sin(labda2 \cdot x)) + C8 \cdot (\cos(labda2 \cdot x)$

$- \sin(labda2 \cdot x)))) :$

> $eq5 := -2 \cdot EI \cdot labda1^3 \cdot (\exp(labda1 \cdot x) \cdot (C1 \cdot (\sin(labda1 \cdot x) + \cos(labda1 \cdot x)) + C2$

$\cdot (\sin(labda1 \cdot x) - \cos(labda1 \cdot x))) + \exp(-labda1 \cdot x) \cdot (C3 \cdot (\sin(labda1 \cdot x) - \cos(labda1$

$\cdot x)) - C4 \cdot (\sin(labda1 \cdot x) + \cos(labda1 \cdot x)))) = -2 \cdot EI \cdot labda2^3 \cdot (\exp(labda2 \cdot x) \cdot (C5$

$\cdot (\sin(labda2 \cdot x) + \cos(labda2 \cdot x)) + C6 \cdot (\sin(labda2 \cdot x) - \cos(labda2 \cdot x))) + \exp($

$-labda2 \cdot x) \cdot (C7 \cdot (\sin(labda2 \cdot x) - \cos(labda2 \cdot x)) - C8 \cdot (\sin(labda2 \cdot x) + \cos(labda2$

$\cdot x)))) : eq6 := -2 \cdot EI \cdot labda1^2 \cdot (\exp(labda1 \cdot x) \cdot (C1 \cdot \sin(labda1 \cdot x) - C2 \cdot \cos(labda1 \cdot x))$

$+ \exp(-labda1 \cdot x) \cdot (-C3 \cdot \sin(labda1 \cdot x) + C4 \cdot \cos(labda1 \cdot x))) = -2 \cdot EI \cdot labda2^2$

$\cdot (\exp(labda2 \cdot x) \cdot (C5 \cdot \sin(labda2 \cdot x) - C6 \cdot \cos(labda2 \cdot x)) + \exp(-labda2 \cdot x) \cdot (-C7$

$\cdot \sin(labda2 \cdot x) + C8 \cdot \cos(labda2 \cdot x))) :$

> $x := L2 : eq7 := w2(x) = w3(x) : eq8 := labda2 \cdot (\exp(labda2 \cdot x) \cdot (C5 \cdot (\cos(labda2 \cdot x)$

$- \sin(labda2 \cdot x)) + C6 \cdot (\cos(labda2 \cdot x) + \sin(labda2 \cdot x))) + \exp(-labda2 \cdot x) \cdot (C7 \cdot ($

$- \cos(labda2 \cdot x) - \sin(labda2 \cdot x)) + C8 \cdot (\cos(labda2 \cdot x) - \sin(labda2 \cdot x)))) = labda3$

$\cdot (\exp(labda3 \cdot x) \cdot (C9 \cdot (\cos(labda3 \cdot x) - \sin(labda3 \cdot x)) + C10 \cdot (\cos(labda3 \cdot x)$

$+ \sin(labda3 \cdot x))) + \exp(-labda3 \cdot x) \cdot (C11 \cdot (-\cos(labda3 \cdot x) - \sin(labda3 \cdot x)) + C12$

$\cdot (\cos(labda3 \cdot x) - \sin(labda3 \cdot x)))) :$

> $eq9 := -2 \cdot EI \cdot labda2^3 \cdot (\exp(labda2 \cdot x) \cdot (C5 \cdot (\sin(labda2 \cdot x) + \cos(labda2 \cdot x)) + C6$

$\cdot (\sin(labda2 \cdot x) - \cos(labda2 \cdot x))) + \exp(-labda2 \cdot x) \cdot (C7 \cdot (\sin(labda2 \cdot x) - \cos(labda2$

$\cdot x)) - C8 \cdot (\sin(labda2 \cdot x) + \cos(labda2 \cdot x)))) = -2 \cdot EI \cdot labda3^3 \cdot (\exp(labda3 \cdot x) \cdot (C9$
$\cdot (\sin(labda3 \cdot x) + \cos(labda3 \cdot x)) + C10 \cdot (\sin(labda3 \cdot x) - \cos(labda3 \cdot x))) + \exp($
$-labda3 \cdot x) \cdot (C11 \cdot (\sin(labda3 \cdot x) - \cos(labda3 \cdot x)) - C12 \cdot (\sin(labda3 \cdot x) + \cos(labda3$
$\cdot x)))) : eq10 := -2 \cdot EI \cdot labda2^2 \cdot (\exp(labda2 \cdot x) \cdot (C5 \cdot \sin(labda2 \cdot x) - C6 \cdot \cos(labda2 \cdot x))$
$+ \exp(-labda2 \cdot x) \cdot (-C7 \cdot \sin(labda2 \cdot x) + C8 \cdot \cos(labda2 \cdot x)))) = -2 \cdot EI \cdot labda3^2$
$\cdot (\exp(labda3 \cdot x) \cdot (C9 \cdot \sin(labda3 \cdot x) - C10 \cdot \cos(labda3 \cdot x)) + \exp(-labda3 \cdot x) \cdot (-C11$
$\cdot \sin(labda3 \cdot x) + C12 \cdot \cos(labda3 \cdot x)))) :$

> $x := L3 : V3 := 2 \cdot EI \cdot labda3^3 \cdot (\exp(labda3 \cdot x) \cdot (C9 \cdot (\sin(labda3 \cdot x) + \cos(labda3 \cdot x)) + C10$
$\cdot (\sin(labda3 \cdot x) - \cos(labda3 \cdot x))) + \exp(-labda3 \cdot x) \cdot (C11 \cdot (\sin(labda3 \cdot x)$
$- \cos(labda3 \cdot x)) - C12 \cdot (\sin(labda3 \cdot x) + \cos(labda3 \cdot x)))) : M3 := 2 \cdot EI \cdot labda3^2$
$\cdot (\exp(labda3 \cdot x) \cdot (C9 \cdot \sin(labda3 \cdot x) - C10 \cdot \cos(labda3 \cdot x)) + \exp(-labda3 \cdot x) \cdot (-C11$
$\cdot \sin(labda3 \cdot x) + C12 \cdot \cos(labda3 \cdot x)))) : eq11 := V3 = 0 : eq12 := M3 = 0 :$

> $solution := solve(\{eq1, eq2, eq3, eq4, eq5, eq6, eq7, eq8, eq9, eq10, eq11, eq12\}, [C1, C2, C3,$
$C4, C5, C6, C7, C8, C9, C10, C11, C12]);$

$solution := [[C1 = -0.0001240012854, C2 = -0.00005074377401, C3 = -0.00002251373742,$ **(2)**

$\quad C4 = -0.00005074377401, C5 = -0.00001340100004, C6 = 0.00003666303346, C7$

$\quad = 0.0003979039132, C8 = 0.0002591974903, C9 = -6.747654251\ 10^{-7}, C10 =$

$\quad -0.000004215227431, C11 = 0.0009924902704, C12 = -0.001432036879]]$

> $assign(solution) : x := 'x' : plot(w1(x), x = 0..L1) : plot(w2(x), x = L1..L2) : plot(w3(x), x = L2$
$..L3) : simplify([C1, C2, C3, C4, C5, C6, C7, C8, C9, C10, C11, C12]) : Rendstrip1 := -k1$
$\cdot evalf(int(w1(x), x = 0..L1)); Rendstrip2 := -k2 \cdot evalf\left(int\left(w2(x), x = L1..\dfrac{52.676}{2}\right)\right);$
$Rendstrip3 := -k2 \cdot evalf\left(int\left(w2(x), x = \dfrac{52.676}{2}..L2\right)\right); Rendstrip4 := -k3$
$\cdot evalf(int(w3(x), x = L2..L3));$

$$Rendstrip1 := 3371.693788$$
$$Rendstrip2 := 3094.285212$$
$$Rendstrip3 := 3094.285212$$
$$Rendstrip4 := 3371.693788$$ **(3)**

The computational approach for a half supported beam has been represented below. Devious from the previous two worksheets, the internal lever arm has been determined as well. The input parameters are furthermore similar to the parameters mentioned in appendix D.4.

> restart; *Transverse direction* :

> $k2 := Kd : k1 := ALpha \cdot k2 : L1 := \dfrac{52.676}{2} : L2 := 52.676 - L1 : labda1 := \left(\dfrac{k1}{(4 \cdot EI)}\right)^{(0.25)} : labda2 := \left(\dfrac{k2}{(4 \cdot EI)}\right)^{(0.25)} : w1(x) := \exp(labda1 \cdot x) \cdot (C1 \cdot \cos(labda1 \cdot x) + C2 \cdot \sin(labda1 \cdot x)) + \exp(-labda1 \cdot x) \cdot (C3 \cdot \cos(labda1 \cdot x) + C4 \cdot \sin(labda1 \cdot x)) - \dfrac{q}{k1} : w2(x) := \exp(labda2 \cdot x) \cdot (C5 \cdot \cos(labda2 \cdot x) + C6 \cdot \sin(labda2 \cdot x)) + \exp(-labda2 \cdot x) \cdot (C7 \cdot \cos(labda2 \cdot x) + C8 \cdot \sin(labda2 \cdot x)) - \dfrac{q}{k2} :$

> $x := -L1 :$

> $V1 := 2 \cdot EI \cdot labda1^3 \cdot (\exp(labda1 \cdot x) \cdot (C1 \cdot (\sin(labda1 \cdot x) + \cos(labda1 \cdot x)) + C2 \cdot (\sin(labda1 \cdot x) - \cos(labda1 \cdot x))) + \exp(-labda1 \cdot x) \cdot (C3 \cdot (\sin(labda1 \cdot x) - \cos(labda1 \cdot x)) - C4 \cdot (\sin(labda1 \cdot x) + \cos(labda1 \cdot x)))) : M1 := 2 \cdot EI \cdot labda1^2 \cdot (\exp(labda1 \cdot x) \cdot (C1 \cdot \sin(labda1 \cdot x) - C2 \cdot \cos(labda1 \cdot x)) + \exp(-labda1 \cdot x) \cdot (-C3 \cdot \sin(labda1 \cdot x) + C4 \cdot \cos(labda1 \cdot x))) :$

> $eq1 := V1 = 0 :$

> $eq2 := M1 = Mext\_1 :$

> $x := 0 : eq3 := w1(x) = w2(x) : eq4 := labda1 \cdot (C1 + C2 - C3 + C4) = labda2 \cdot (C5 + C6 - C7 + C8) :$

> $eq5 := -(labda1^3) \cdot (-C1 + C2 + C3 + C4) = -labda2^3 \cdot (-C5 + C6 + C7 + C8) : eq6 := -labda1^2 \cdot (C2 - C4) = -labda2^2 \cdot (C6 - C8) :$

> $x := L2 : V2 := 2 \cdot EI \cdot labda2^3 \cdot (\exp(labda2 \cdot x) \cdot (C5 \cdot (\sin(labda2 \cdot x) + \cos(labda2 \cdot x)) + C6 \cdot (\sin(labda2 \cdot x) - \cos(labda2 \cdot x))) + \exp(-labda2 \cdot x) \cdot (C7 \cdot (\sin(labda2 \cdot x) - \cos(labda2 \cdot x)) - C8 \cdot (\sin(labda2 \cdot x) + \cos(labda2 \cdot x)))) : M2 := 2 \cdot EI \cdot labda2^2 \cdot (\exp(labda2 \cdot x) \cdot (C5 \cdot \sin(labda2 \cdot x) - C6 \cdot \cos(labda2 \cdot x)) + \exp(-labda2 \cdot x) \cdot (-C7 \cdot \sin(labda2 \cdot x) + C8 \cdot \cos(labda2 \cdot x))) :$

> $eq7 := V2 = 0 : eq8 := M2 = Mext\_2 :$

> $solution := solve(\{eq1, eq2, eq3, eq4, eq5, eq6, eq7, eq8\}, \{C1, C2, C3, C4, C5, C6, C7, C8\}) :$

> $assign(solution) : x := 'x'; plot(w1(x), x = -L1 .. 0) : plot(w2(x), x = 0 .. L1) : simplify([C1, C2, C3, C4, C5, C6, C7, C8]) : Rendstrip1 := -k1 \cdot evalf(int(w1(x), x = -L1 .. 0)) : Rendstrip2 := -k2 \cdot evalf(int(w2(x), x = 0 .. L1)) :$

> $Larm1 := -\dfrac{1}{evalf(int(w1(x), x = -L1 .. 0))} \cdot evalf(int(x \cdot w1(x), x = -L1 .. 0)) : Larm2 := \dfrac{1}{evalf(int(w2(x), x = 0 .. L1))} \cdot evalf(int(x \cdot w2(x), x = 0 .. L1)) :$

Additional to the worksheets presents for hogging and sagging, the reaction force and the internal lever arm are determined. The example below was used to determine torsional moment for hogging in torsion case T2.

> restart; T2 hogging :

> $k1 := 50000 : k2 :=$ alpha· $k1 : k3 := k1 : L1 := \dfrac{L}{3} : L2 := (L - L1) : L3 := L : labda1 :=$

$\left(\dfrac{k1}{(4 \cdot EI)}\right)^{(0.25)} : labda2 := \left(\dfrac{k2}{(4 \cdot EI)}\right)^{(0.25)} : labda3 := \left(\dfrac{k3}{(4 \cdot EI)}\right)^{(0.25)} : w1(x) :=$

$exp(labda1 \cdot x) \cdot (C1 \cdot \cos(labda1 \cdot x) + C2 \cdot \sin(labda1 \cdot x)) + exp(-labda1 \cdot x) \cdot (C3$

$\cdot \cos(labda1 \cdot x) + C4 \cdot \sin(labda1 \cdot x)) - \dfrac{q}{k1} : w2(x) := exp(labda2 \cdot x) \cdot (C5 \cdot \cos(labda2 \cdot x)$

$+ C6 \cdot \sin(labda2 \cdot x)) + exp(-labda2 \cdot x) \cdot (C7 \cdot \cos(labda2 \cdot x) + C8 \cdot \sin(labda2 \cdot x)) - \dfrac{q}{k2} :$

$w3(x) := exp(labda3 \cdot x) \cdot (C9 \cdot \cos(labda3 \cdot x) + C10 \cdot \sin(labda3 \cdot x)) + exp(-labda3 \cdot x)$

$\cdot (C11 \cdot \cos(labda3 \cdot x) + C12 \cdot \sin(labda3 \cdot x)) - \dfrac{q}{k3} :$

> $x := 0 :$

> $V1 := 2 \cdot EI \cdot labda1^3 \cdot (exp(labda1 \cdot x) \cdot (C1 \cdot (\sin(labda1 \cdot x) + \cos(labda1 \cdot x)) + C2$
$\cdot (\sin(labda1 \cdot x) - \cos(labda1 \cdot x))) + exp(-labda1 \cdot x) \cdot (C3 \cdot (\sin(labda1 \cdot x) - \cos(labda1$
$\cdot x)) - C4 \cdot (\sin(labda1 \cdot x) + \cos(labda1 \cdot x)))) : M1 := 2 \cdot EI \cdot labda1^2 \cdot (exp(labda1 \cdot x)$
$\cdot (C1 \cdot \sin(labda1 \cdot x) - C2 \cdot \cos(labda1 \cdot x)) + exp(-labda1 \cdot x) \cdot (-C3 \cdot \sin(labda1 \cdot x) + C4$
$\cdot \cos(labda1 \cdot x))) :$

> $eq1 := V1 = 0 :$

> $eq2 := M1 = Mext\_i :$

> $x := L1 : eq3 := w1(x) = w2(x) : eq4 := labda1 \cdot (exp(labda1 \cdot x) \cdot (C1 \cdot (\cos(labda1 \cdot x)$
$- \sin(labda1 \cdot x)) + C2 \cdot (\cos(labda1 \cdot x) + \sin(labda1 \cdot x))) + exp(-labda1 \cdot x) \cdot (C3 \cdot ($
$- \cos(labda1 \cdot x) - \sin(labda1 \cdot x)) + C4 \cdot (\cos(labda1 \cdot x) - \sin(labda1 \cdot x)))) = labda2$
$\cdot (exp(labda2 \cdot x) \cdot (C5 \cdot (\cos(labda2 \cdot x) - \sin(labda2 \cdot x)) + C6 \cdot (\cos(labda2 \cdot x) + \sin(labda2$
$\cdot x))) + exp(-labda2 \cdot x) \cdot (C7 \cdot (-\cos(labda2 \cdot x) - \sin(labda2 \cdot x)) + C8 \cdot (\cos(labda2 \cdot x)$
$- \sin(labda2 \cdot x)))) :$

> $eq5 := -2 \cdot EI \cdot labda1^3 \cdot (exp(labda1 \cdot x) \cdot (C1 \cdot (\sin(labda1 \cdot x) + \cos(labda1 \cdot x)) + C2$
$\cdot (\sin(labda1 \cdot x) - \cos(labda1 \cdot x))) + exp(-labda1 \cdot x) \cdot (C3 \cdot (\sin(labda1 \cdot x) - \cos(labda1$
$\cdot x)) - C4 \cdot (\sin(labda1 \cdot x) + \cos(labda1 \cdot x)))) = -2 \cdot EI \cdot labda2^3 \cdot (exp(labda2 \cdot x) \cdot (C5$
$\cdot (\sin(labda2 \cdot x) + \cos(labda2 \cdot x)) + C6 \cdot (\sin(labda2 \cdot x) - \cos(labda2 \cdot x))) + exp($
$- labda2 \cdot x) \cdot (C7 \cdot (\sin(labda2 \cdot x) - \cos(labda2 \cdot x)) - C8 \cdot (\sin(labda2 \cdot x) + \cos(labda2$
$\cdot x)))) : eq6 := -2 \cdot EI \cdot labda1^2 \cdot (exp(labda1 \cdot x) \cdot (C1 \cdot \sin(labda1 \cdot x) - C2 \cdot \cos(labda1 \cdot x))$
$+ exp(-labda1 \cdot x) \cdot (-C3 \cdot \sin(labda1 \cdot x) + C4 \cdot \cos(labda1 \cdot x))) = -2 \cdot EI \cdot labda2^2$
$\cdot (exp(labda2 \cdot x) \cdot (C5 \cdot \sin(labda2 \cdot x) - C6 \cdot \cos(labda2 \cdot x)) + exp(-labda2 \cdot x) \cdot (-C7$
$\cdot \sin(labda2 \cdot x) + C8 \cdot \cos(labda2 \cdot x))) :$

> $x := L2 : eq7 := w2(x) = w3(x) : eq8 := labda2 \cdot (exp(labda2 \cdot x) \cdot (C5 \cdot (\cos(labda2 \cdot x)$
$- \sin(labda2 \cdot x)) + C6 \cdot (\cos(labda2 \cdot x) + \sin(labda2 \cdot x))) + exp(-labda2 \cdot x) \cdot (C7 \cdot ($
$- \cos(labda2 \cdot x) - \sin(labda2 \cdot x)) + C8 \cdot (\cos(labda2 \cdot x) - \sin(labda2 \cdot x)))) = labda3$
$\cdot (exp(labda3 \cdot x) \cdot (C9 \cdot (\cos(labda3 \cdot x) - \sin(labda3 \cdot x)) + C10 \cdot (\cos(labda3 \cdot x)$
$+ \sin(labda3 \cdot x))) + exp(-labda3 \cdot x) \cdot (C11 \cdot (-\cos(labda3 \cdot x) - \sin(labda3 \cdot x)) + C12$
$\cdot (\cos(labda3 \cdot x) - \sin(labda3 \cdot x)))) :$

> $eq9 := -2 \cdot EI \cdot labda2^3 \cdot (exp(labda2 \cdot x) \cdot (C5 \cdot (\sin(labda2 \cdot x) + \cos(labda2 \cdot x)) + C6$
$\cdot (\sin(labda2 \cdot x) - \cos(labda2 \cdot x))) + exp(-labda2 \cdot x) \cdot (C7 \cdot (\sin(labda2 \cdot x) - \cos(labda2$
$\cdot x)) - C8 \cdot (\sin(labda2 \cdot x) + \cos(labda2 \cdot x)))) = -2 \cdot EI \cdot labda3^3 \cdot (exp(labda3 \cdot x) \cdot (C9$
$\cdot (\sin(labda3 \cdot x) + \cos(labda3 \cdot x)) + C10 \cdot (\sin(labda3 \cdot x) - \cos(labda3 \cdot x))) + exp($
$- labda3 \cdot x) \cdot (C11 \cdot (\sin(labda3 \cdot x) - \cos(labda3 \cdot x)) - C12 \cdot (\sin(labda3 \cdot x) + \cos(labda3$
$\cdot x)))) : eq10 := -2 \cdot EI \cdot labda2^2 \cdot (exp(labda2 \cdot x) \cdot (C5 \cdot \sin(labda2 \cdot x) - C6 \cdot \cos(labda2 \cdot x))$

$+\exp(-labda2\cdot x)\cdot(-C7\cdot\sin(labda2\cdot x)+C8\cdot\cos(labda2\cdot x)))=-2\cdot EI\cdot labda3^2$
$\cdot(\exp(labda3\cdot x)\cdot(C9\cdot\sin(labda3\cdot x)-C10\cdot\cos(labda3\cdot x))+\exp(-labda3\cdot x)\cdot(-C11$
$\cdot\sin(labda3\cdot x)+C12\cdot\cos(labda3\cdot x)))$:

> $x:=L3:V3:=2\cdot EI\cdot labda3^3\cdot(\exp(labda3\cdot x)\cdot(C9\cdot(\sin(labda3\cdot x)+\cos(labda3\cdot x))+C10$
$\cdot(\sin(labda3\cdot x)-\cos(labda3\cdot x)))+\exp(-labda3\cdot x)\cdot(C11\cdot(\sin(labda3\cdot x)$
$-\cos(labda3\cdot x))-C12\cdot(\sin(labda3\cdot x)+\cos(labda3\cdot x)))):M3:=2\cdot EI\cdot labda3^2$
$\cdot(\exp(labda3\cdot x)\cdot(C9\cdot\sin(labda3\cdot x)-C10\cdot\cos(labda3\cdot x))+\exp(-labda3\cdot x)\cdot(-C11$
$\cdot\sin(labda3\cdot x)+C12\cdot\cos(labda3\cdot x))):eq11:=V3=0:eq12:=M3=Mext\_i:$

> $solution:=solve(\{eq1,eq2,eq3,eq4,eq5,eq6,eq7,eq8,eq9,eq10,eq11,eq12\},[C1,C2,C3,$
$C4,C5,C6,C7,C8,C9,C10,C11,C12]):$

Warning, computation interrupted

> $assign(solution):x:='x':simplify([C1,C2,C3,C4,C5,C6,C7,C8,C9,C10,C11,C12]):$
$Rendstrip1:=-k1\cdot evalf(int(w1(x),x=0..L1)):Rendstrip2:=-k2\cdot evalf(int(w2(x),x=L1$
$..L2)):Rendstrip3:=-k3\cdot evalf(int(w3(x),x=L2..L3)):$

> $Larm1:=L1-\dfrac{1}{evalf(int(w1(x),x=0..L1))}\cdot evalf(int(x\cdot w1(x),x=0..L1)):Larm2:=-L1$
$+\dfrac{1}{evalf(int(w2(x),x=L1..L2))}\cdot evalf(int(x\cdot w2(x),x=L1..L2)):Larm3:=-L2$
$+\dfrac{1}{evalf(int(w3(x),x=L2..L3))}\cdot evalf(int(x\cdot w3(x),x=L2..L3));$

> $Mtorsion1:=Larm1\cdot Rendstrip1;Mtorsion2:=Larm2\cdot Rendstrip2;Mtorsion3:=Larm3$
$\cdot Rendstrip3;$

>

D.4 INPUT PARAMETERS

The input parameters required to determine the influence of the external forces on the beam on elastic foundation are given in this paragraph. Primarily the input dimensions following from the preliminary design are discussed. The design values and material properties are elaborated in the second and third section respectively.

D.4.1 INITIAL DIMENSIONS

The dimensions determined in the preliminary design form the input parameters for any further computations; Table 45 gives a summarization of these initial dimensions.

Parameter		Gate housing	Turbine housing	Ballast housing	
Section	i	1	2	3	-
Top level	$h_{top,i}$	+10.04	+8.74	+3.0	$m\ NAP$
Bottom level	$h_{bot,i}$	-1.5	-1.5	-1.5	$m\ NAP$
Bottom level sluiceway	$h_{bot,s}$	-10.24	-10.24	-10.24	$m\ NAP$
Thickness roof	$t_{roof,i}$	0.5	0.5	0.5	m
Thickness floor	$t_{floor,i}$	0.5	0.5	0.5	m
Height front wall	$h_{front,i}$	11.54	10.24	4.5	m
Height back wall	$h_{back,i}$	11.54	10.24	4.5	m
Thickness front wall	$t_{front,i}$	0.5	0.5	0.5	m
Thickness back wall	$t_{back,i}$	0.5	0.5	0.5	m
Thickness floor sluiceway	$t_{floor,si}$	0.5	0.5	0.5	m
Width incl. inner walls	b_i	5.076	15.9	15.9	m
Thickness inner walls longitudinal direction	$t_{inner,i}$	0.5	0.5	0.5	m
Thickness outer walls longitudinal direction	$t_{outer,i}$	0.5	0.5	0.5	m
h-t-h spacing inner walls longitudinal direction	b_{inner}	8.74	8.74	8.74	m
Concrete cross-sectional area of full housing incl. bottom slab	$A_{c,t,i}$	18.154	172.06	328.11	m^2
Concrete cross-sectional area section longitudinal direction	$A_{c,l,i}$	22.5	21.85	18.98	m^2
Concrete cross-sectional area section transverse	$A_{c,t,i}$	1.5	1.5	1.5	m^2
Concrete cross-sectional area section longitudinal	$A_{c,l,i}$	1.5	1.5	1.5	m^2
Moment of inertia transverse direction section	$I_{z,t,i}$	696.35	1562.13	1392	m^4
Moment of inertia longitudinal direction section	$I_{z,l,i}$	21169.54	18079.79	8382.3	m^4
Moment of inertia full transverse cross section	$I_{z,t,}$		246.72		m^4

TABLE 45: INITIAL DIMENSIONS OF CONCRETE SECTIONS OF THE TIDAL POWER PLANT

Since each section consists of a hollow rectangular box with underneath a half a meter thick concrete slab functioning as the sluiceway floor, the Steiner rule is applied to determine the moment of inertia.

$$I_{section,i} = \frac{1}{12} bh^3 + z^2 A_c$$

255

In which:

b *is the width of the section, for each section a width of* 1 *meter is taken*

h *is the height of each element within the section*

z *is the distance between the center of gravity of the considered component*

           within the section, to the center of gravity of the whole section

A_c *is the cross − sectional are of the considered component within the section.*

In first instance in the cross-sectional areas of section 2 and 3 an additional wall, with equal thickness as the adjacent wall, is placed. The effects on the walls could now be scrutinized in a simplified manner. Hence, compared with the preliminary two additional walls of 0.5 meter thick are inserted.

The centre of gravity varies per section in transverse direction, the moment of inertia is taken about the centre of gravity of the cross-section as a whole. One could decide to determine the centre of gravity for each section separately, this would mean, however, the eccentricity of the external moment varies per section. As this is not the case, using the centre of gravity seems to be the most reasonable solution.

D.4.2 MATERIAL PROPERTIES

Concrete

The durability of the concrete structure is proportional to a number of concrete properties. A durable structure meets the requirements of serviceability, strength and stability throughout its design working life, without significant loss of utility or excessive unforeseen maintenance. Environmental conditions indicate the required concrete cover of steel reinforcement. The cover density and quality is achieved by controlling the maximum water/cement ratio and minimum cement content, it may be related to a minimum strength class of concrete.

The environmental conditions considered the Tidal Power Plant is subject to, are described by environmental class XS 2 and XS 3 from EC2. These classes are defined as a structure located in a zone subject to corrosion induced by chlorides from sea water while permanently submerged (XS2), or at tidal, splash and spray zones (XS3).

The nominal concrete cover corresponding to this environmental class is defined as:

$$c_{nom} = c_{min} + \Delta c_{dev}$$

In which the minimal cover (c_{min}) corresponds to the required minimum cover with regard to the environment class. The minimum cover for the specified environmental classes is 50 mm for XS3 with a structural design lifetime of 100 years. A cover deviation (Δc_{dev}) of 5 mm is allowed in The Netherlands. The resulting nominal concrete cover becomes 55 mm for the caisson, with a concrete strength class ≥C45/55.

The Eurocode prescribes a minimum strength class for corresponding environmental classes as well. In case of the specified environmental classes the recommended minimum strength class is ≥C35/45. This strength class is below the earlier mentioned C45/55 for determining the concrete cover. Since a minimal draught during transport is

preferred, which is achieved by reducing the overall weight of the structure, a concrete strength class of at least C45/55 is chosen.

For reinforced concrete the maximum crack width allowed is 0.1 mm according to EC 2.

More properties of concrete with a strength class C45/55 are summarized in Table 46.

Concrete strength class C45/55					
f_{ck}	45	MPa	ε_{c1}	2.4	‰
$f_{ck,cube}$	55	MPa	ε_{c2}	2.0	‰
f_{cm}	48	MPa	ε_{cu2}	3.5	‰
f_{ctm}	3.8	MPa	η	2.0	‰
$f_{ctk,0.05}$	2.7	MPa	ε_{c3}	1.75	‰
$f_{ctk,0.95}$	4.9	MPa	ε_{cu3}	3.5	‰
E_{cm}	36	GPa			

TABLE 46: PROPERTIES CONCRETE STRENGTH CLASS C45/55

Reinforcing steel

The steel grade used for reinforced concrete is FeB500, having a design yield strength $f_{yd} = 435\ MPa$. The modus of elasticity for reinforcing steel is $E_s = 200000\ MPa$. This steel grade is solely used for reinforcing concrete. Prestressing the concrete has not been assumed to be required.

D.4.3 DESIGN VALUES

The practical factors according to EC2 for materials for ultimate limit states are summarized in Table 47 below:

Design situations	γ_c for concrete	γ_s for reinforced steel
Persistent & transient	1.5	1.15
Accidental	1.2	1.0

TABLE 47: STANDARD DESIGN VALUES CONCRETE AND REINFORCED STEEL

The value of the design compressive strength is defined as:

$$f_{cd} = \frac{f_{ck}}{\gamma_c} = \sigma_c$$

The value of the design tensile strength is defined as:

$$f_{ctd} = \frac{f_{ctk,0.05}}{\gamma_c}$$

The nominal stiffness of slender compression members with arbitrary cross-section"

$$EI = K_c E_{cd} I_c + K_s E_s I_s$$

In which:

E_{cd} is the design value of the modulus of elasticity of concrete

I_c is the moment of inertia of concrete cross section

E_s is the design value of the modulus of elasticity of reinforcement

I_s *is the moment of inertia of reinforcement, about the centre of area of the concrete*

K_s *is a factor for contribution of reinforcement* $= 0$ *for* $\rho \geq 0.01$

K_c *is a factor for effects of cracking, creep, etc. provided* $\rho \geq 0.01$:

$$K_c = \frac{0.3}{1 + 0.5\varphi_{ef}}$$

φ_{ef} *is the effective creep ratio* $= 0.2$

In statically indeterminate structures unfavourable effects of cracking in adjacent members should be taken into account. The concrete stiffness should be based on an effective concrete modulus:

$$E_{cd,eff} = \frac{E_{cd}}{1 + \varphi_{ef}} = \frac{36000}{1 + 0.2} = 30000 \; N/mm^2$$

D.5 LOAD CONDITIONS

Computing the conceptual design of the Tidal Power Plant will be performed using recommendations from Eurocode 2 (EC2), NEN-EN-1992-1-1. Since the caisson will be constructed in an external construction dock and transported towards its final position and sunk to in top of the rubble foundation bed, the structure is subject to multiple load scenarios. The distinguishable load scenarios are defined as specific phases during the lifetime of the Tidal Power Plant.

1. Construction phase:
   o Structure subject to self-weight and foundation pressures.

2. Transport phase
   o Hydrostatic pressure solely on outer walls due to buoyancy.
   o Local tensile forces as a consequence of towing operation, these forces are very specific and hard to determine and therefore not further considered in this thesis.

3. Placement phase
   o Hydrostatic pressure from lake and North Sea, water is flowing into the sluiceway. Hence, hydrostatic pressures on inner and outer walls.

4. Completion phase
   o Final foundation pressures
   o Lateral earth pressure on transverse outer walls

5. Operational phase
   o Water flowing through, hence hydrostatic pressures on inner walls.
   o North Sea extreme wave conditions and wave impact.

6. Maintenance operations
   o At maintenance operations no water flowing through one or more sluices.

D.5.1 CONSTRUCTION PHASE

In the construction phase at the external construction dock, no external forces are expected. Therefore, solely the structures self-weight is governing during this phase.

D.5.2 TRANSPORTATION PHASE

During transportation the hydraulic pressures on the outer walls is governing. The draught strongly influences the hydraulic pressures. Since the Tidal Power Plant is transported through Lake Grevelingen, no significant wave loads are expected to occur. The hydraulic pressures with a maximum at the draught level are therefore expected to be governing. The draught level during transport is calculated in the stability checks of the final design and contains 6.62 meter. Figure 146 gives a simple schematization of the cross-section of the tidal Power Plant subjected to the hydraulic pressures.
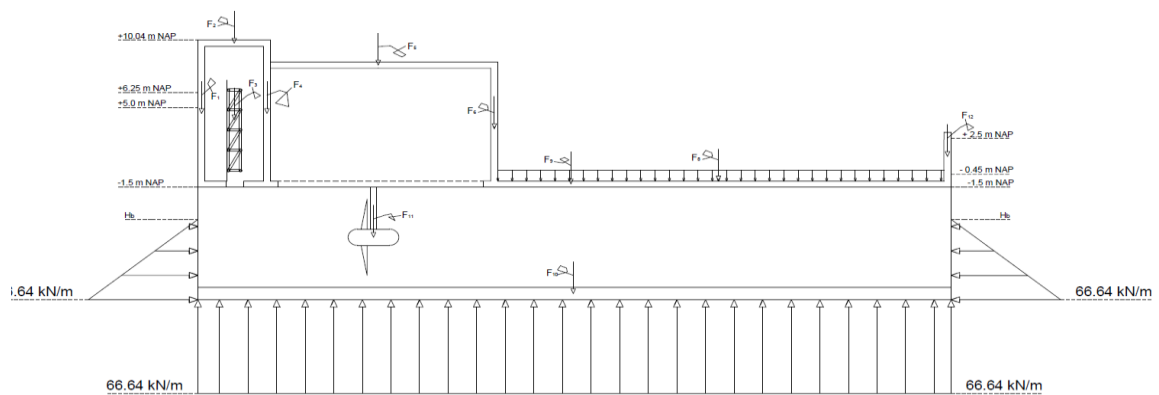
FIGURE 146: LOAD SITUATION DURING TRANSPORT ON CROSS SECTION

D.5.3 INUNDATION AND PLACEMENT PHASE

Establishing the inundation of the Tidal Power Plant, water is obliged to flow into the sluiceways. The outer walls remain subjected to hydraulic pressures from both the in and outside. Hence, as the straight pressure line at outer sides of the sluiceway indicate in Figure 147, the outer hydraulic pressures will slightly be compensated by the hydraulic pressures from the inside. The resulting pressure on the walls will slightly increase comparing it with the transportation phase. In Figure 147 displays an example of the resulting force distribution on the transverse cross-section is shown.
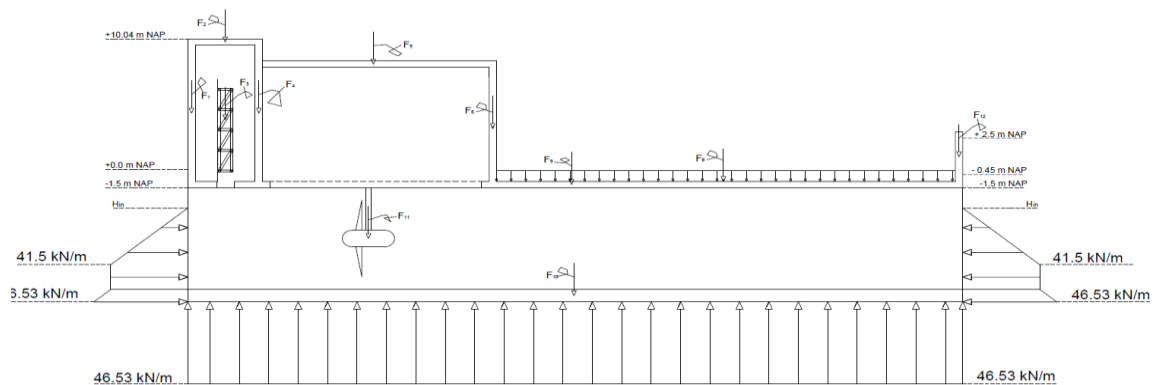
FIGURE 147: RESULTING LOAD DISTRIBUTION ON CROSS-SECTION DURING INUNDATION

D.5.4 COMPLETION PHASE

When submerging the complete Power Plant to its final position the completion phase is introduced. This induces contact with the foundation and thus foundation pressures and lateral earth pressures on the head walls of the plant. Water has flown into each sluiceway. No contact made with the North Sea yet, first the remnants of the dam should be excavated. The load situation after excavation is mentioned in the operational phase. Figure 148 gives a simple representation of the pressures on the longitudinal cross-section.
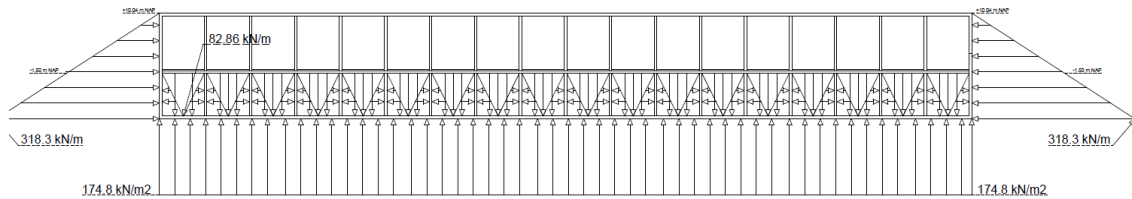
FIGURE 148: LOAD DISTRIBUTION LATERAL PRESSURES ON LONGITUDINAL CROSS-SECTION.

D.5.5 OPERATIONAL PHASE

Whereas the water level at Lake Grevelingen remains within the boundaries of -0.45 m NAP and +0.05 m NAP, at the North Sea side extreme weather conditions arise. This results in asymmetric resulting forces on the Tidal Power Plant. Moreover, extreme weather conditions lead to extreme wave loads. Since the Tidal Power Plant has a length of 157.82 meter, it is assumed the extreme wave loads will not occur at the whole structure the same time. Therefore, when determining the 3D load combinations, extreme wave loads should be applied on just a part of the structure.

The wave loads under extreme conditions are determined using the Goda-Takahashi theory for composite breakwaters. During these extreme conditions the front gate is closed and therefore the Tidal Power Plant acts as vertical breakwater. The governing pressure characterized by the combination of wave impact and horizontal hydraulic pressures. The governing loads during operational phase are checked in two situations; the maximum design water level of +5.00 meter NAP including design wave conditions, and the current average water level including the significant wave height. In both cases the maximum resulting force over the whole caisson occurs at the moment the water level at the Lake Grevelingen side is at minimum (-0.45 m NAP). The wave impact of both situations has been calculated in Appendix D.1. For a North Sea water level of +5.00 m NAP the resulting force of the load distribution is governing, this situation is illustrated in Figure 149.
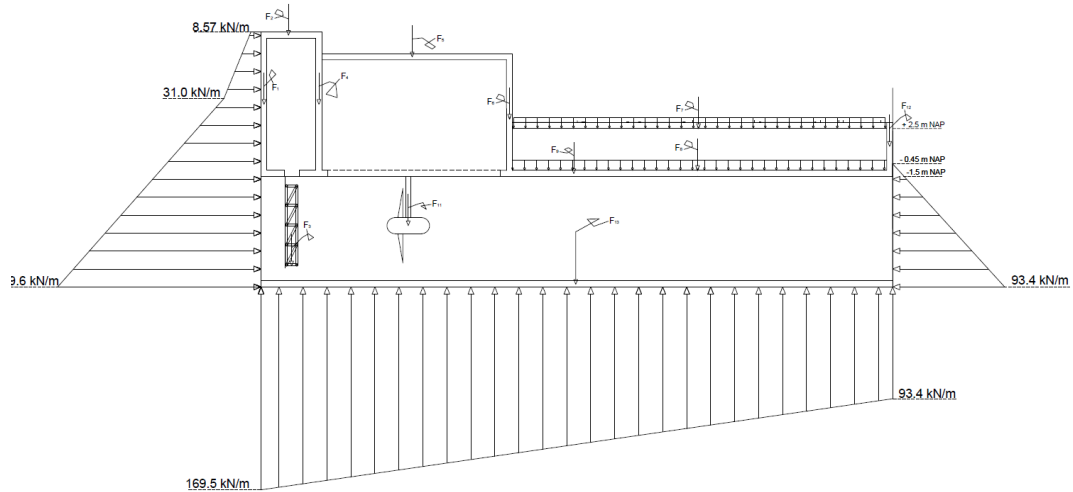
FIGURE 149: RESULTING LOAD DISTRIBUTION EXTREME CONDITIONS TRANSVERSE DIRECTION

D.5.6 MAINTENANCE PHASE

During maintenance one or more sluiceways are closed off. Internal walls are exposed to hydraulic pressures from water flowing in the adjacent sluiceway. Hence the internal walls exhibit pressures from a single side of the wall, this situation is illustrated in Figure 150:
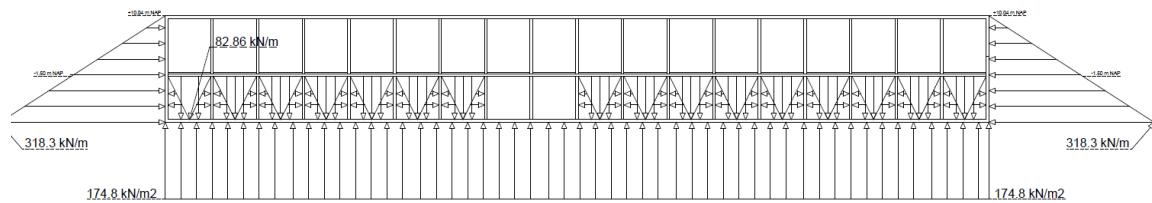
FIGURE 150: LOAD DISTRUBTION DURING MAINTENANCE IN LONGITUDINAL DIRECTION.

D.5.7 GOVERNING LOAD CONDITION

In transverse direction the hydraulic pressures at extreme weather conditions with a design water level at the North Sea side of +5.0 m NAP, and at Lake Grevelingen side of -0.45 m NAP, is defined as the governing load condition. The resulting force from the North Sea contains 1759.2 kN and the point of application lies 6.48 meter from the bottom of the structure. At the Lake Grevelingen side, the resultant force equals 481.9 kN with the point of application at 3.41 meter from the bottom of the structure.

The load condition in longitudinal direction is governing during both maintenance and completion phase. The maintenance phase results in high local forces in inner walls as a consequence of the lack of contra water pressures in one or more sluiceways. In both situations the earth pressures are equal and considered as the governing load in longitudinal direction. The resulting force of the lateral earth pressures will be determined using:

$$F_{earth} = 0.5\gamma_{soil}h_i^2$$

In which:

γ_{soil} *represents the adjacent soil density, assumed at* $16\ kN/m^3$

h_i *represents the total height of section i*

The point of application of the resultant lateral earth pressures equals $\frac{h_i}{3}$

In Ultimate limit state calculations the resultant force from hydraulic pressures will be multiplied by a safety factor of 1.5. The permanently present resulting lateral earth pressures are multiplied by a safety factor of 1.2.

D.6.1 RESULTS SAGGING AND HOGGING

The results of the considered base case S1 to S6 and H1 to H6 will be illustrated in this subparagraph. The Results are obtained by ex- and including the external forces. The Resulting moment and shear distribution in both transverse and longitudinal direction will be used to determine the required reinforcement.

D.6.1.1 RESULTS SAGGING EXCLUDING EXTERNAL FORCES

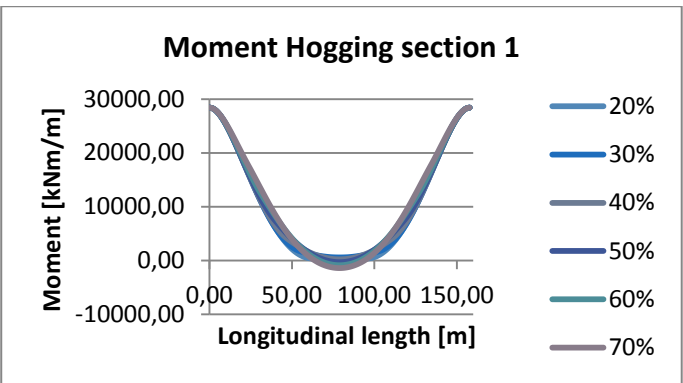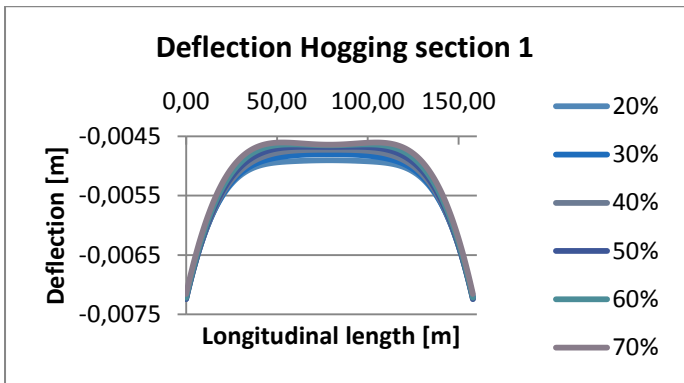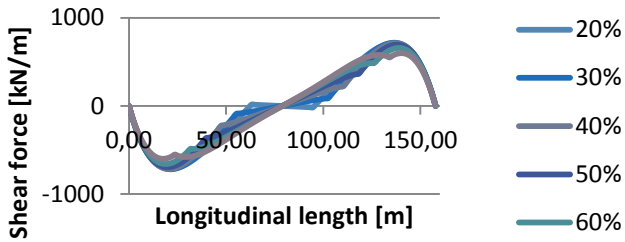*TRANSVERSE DIRECTION*

LONGITUDINAL

TRANSVERSE DIRECTION

LONGITUDINAL DIRECTION

Moment Hogging section 2

Shear force Hogging section 2

Deflection Hogging section 3

Moment Hogging section 3
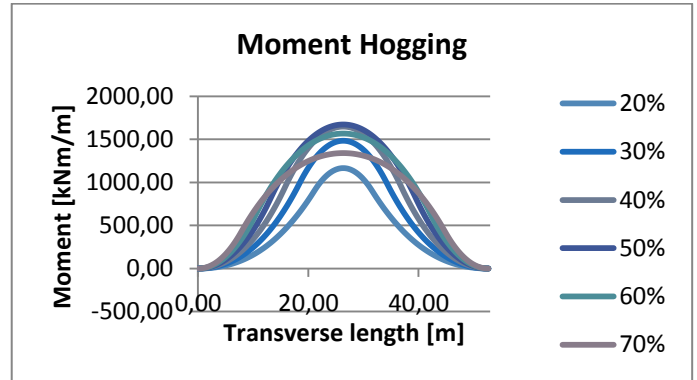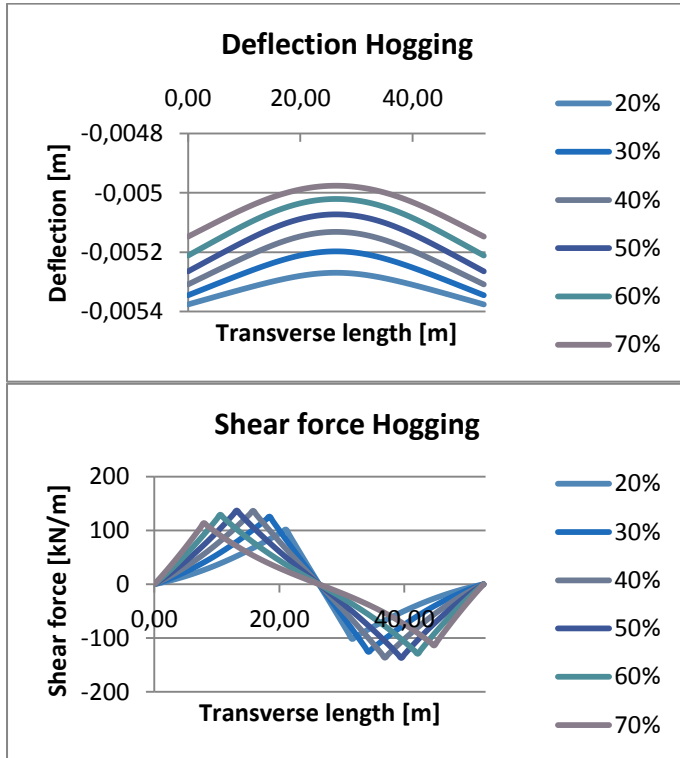
Shear force Hogging section 3
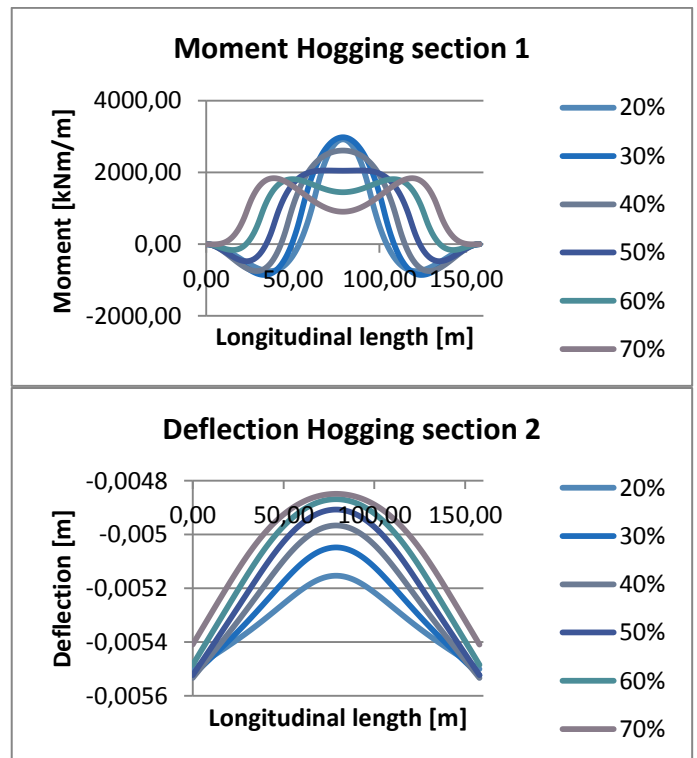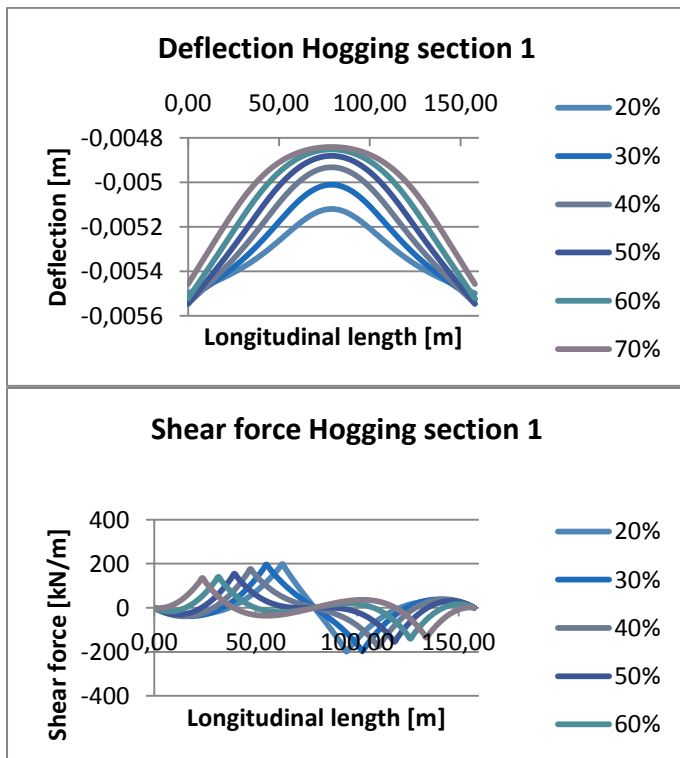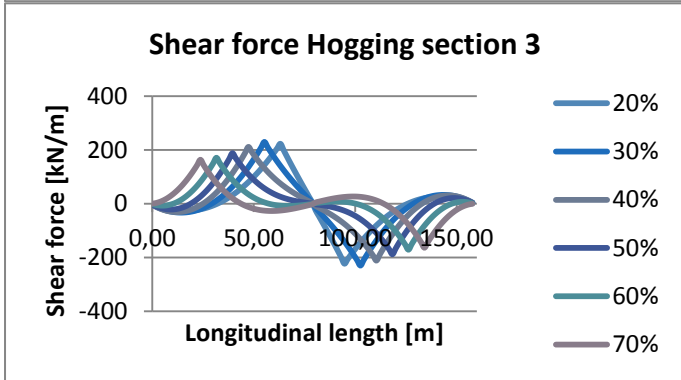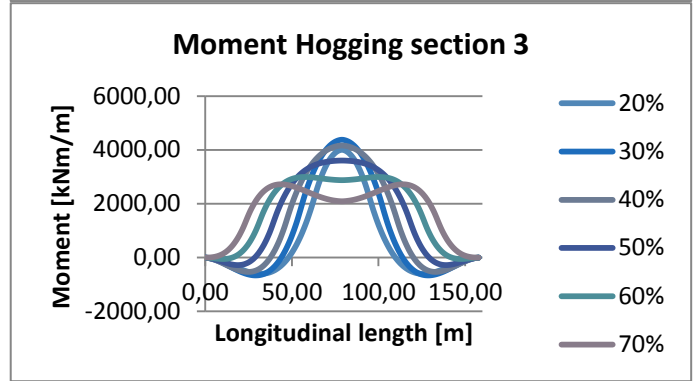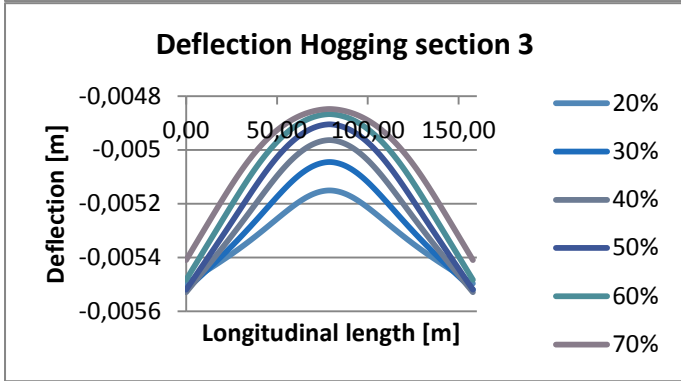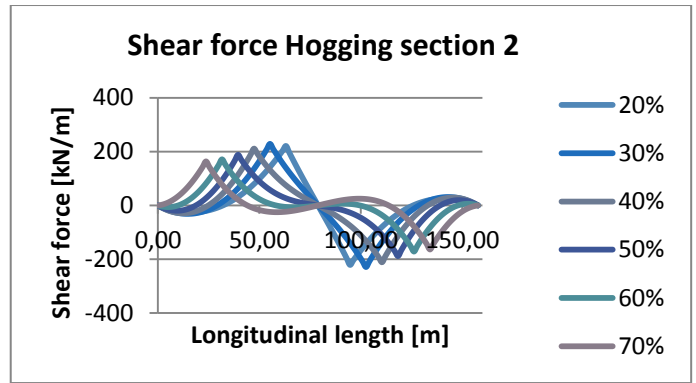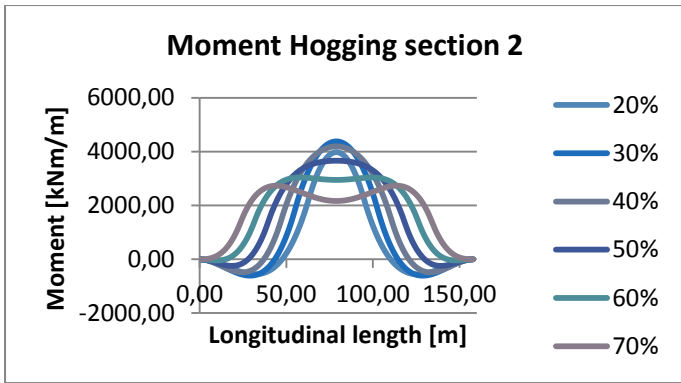
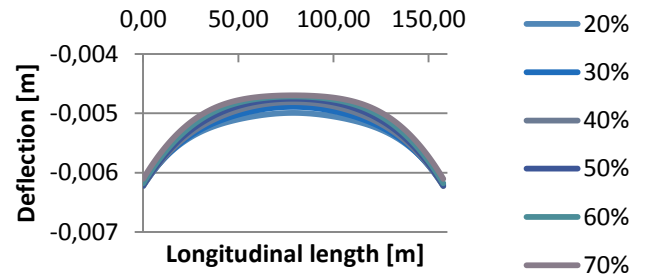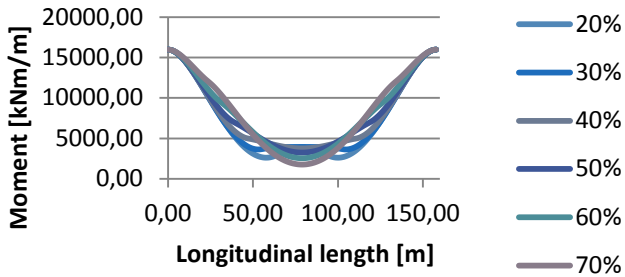## D.6.1.3 RESULTS SAGGING INCLUDING EXTERNAL FORCES

TRANSVERSE DIRECTION

Deflection Sagging

Moment Sagging

267

Shear force Sagging

LONGITUDINAL DIRECTION

Deflection Sagging section 1

Moment Sagging section 1

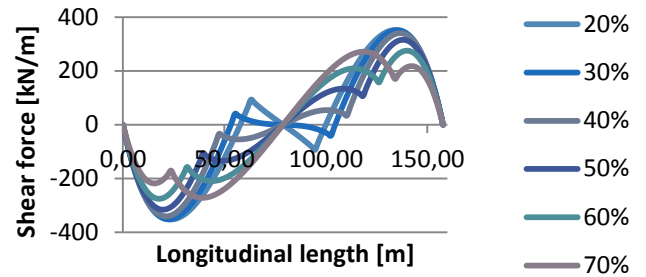**Shear force Sagging section 1**

Deflection Sagging section 2

268

Moment Sagging section 2

Shear force Sagging section 2

Deflection Sagging section 3

Moment Sagging section 3
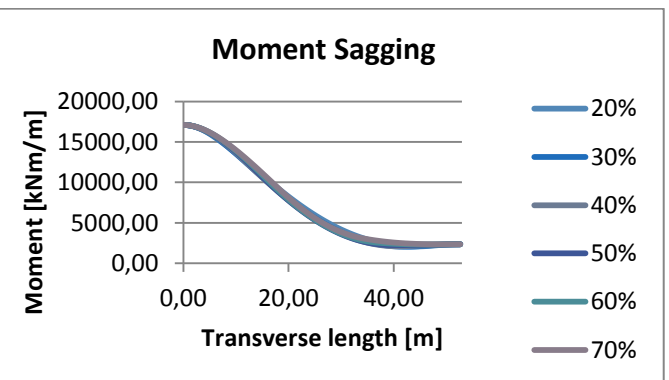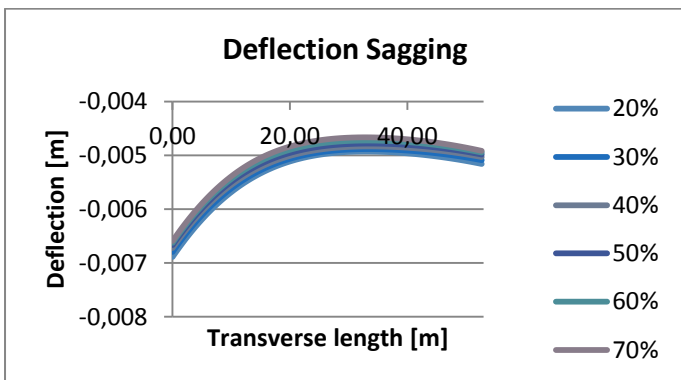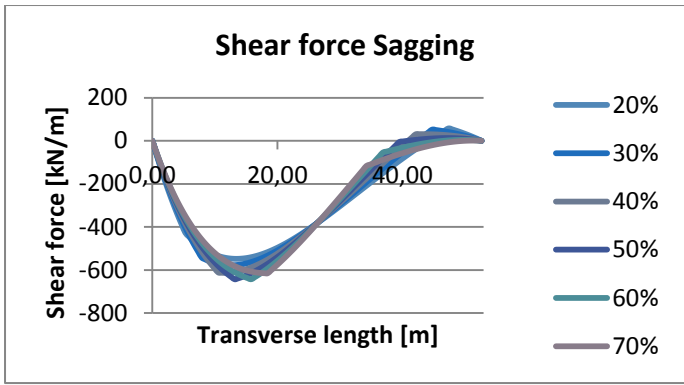
Shear force Sagging section 3
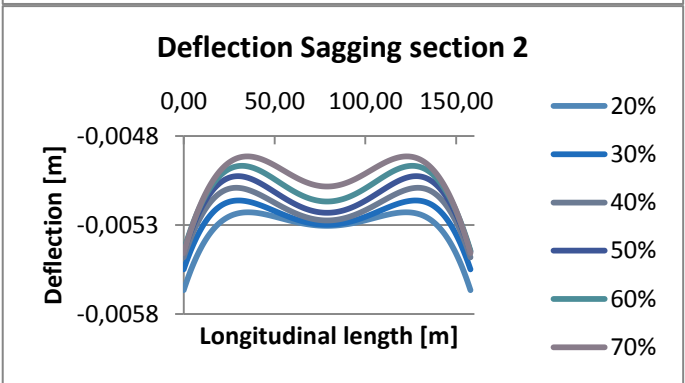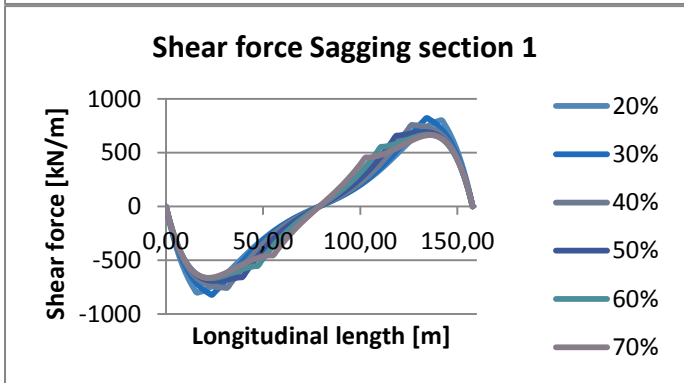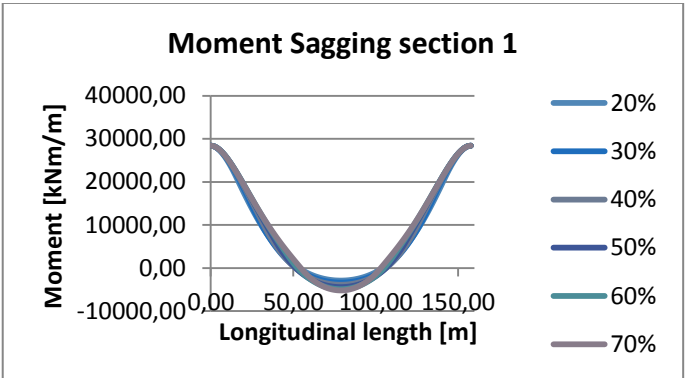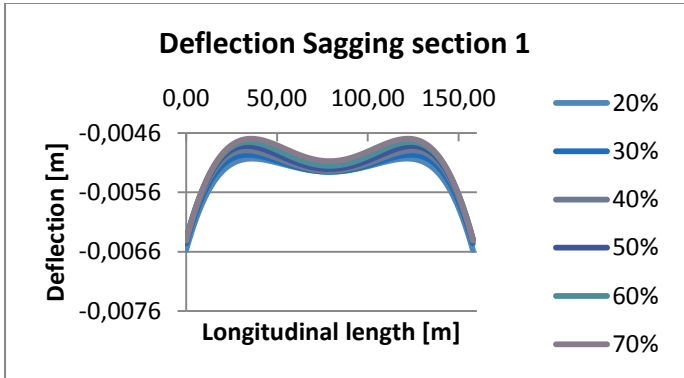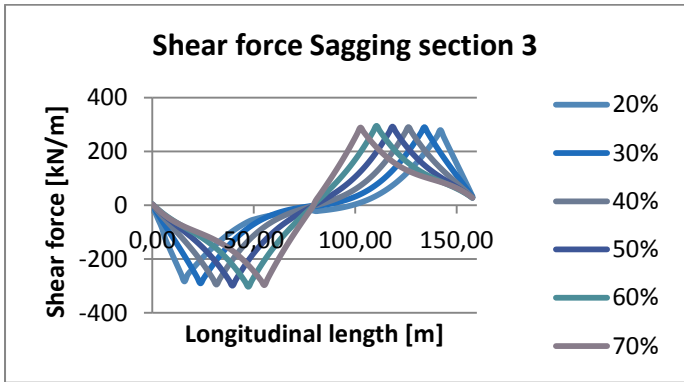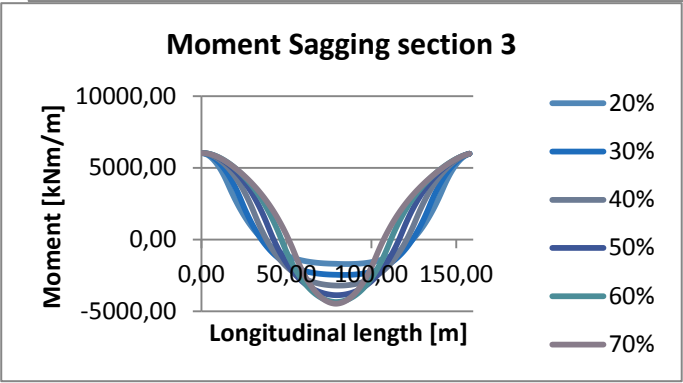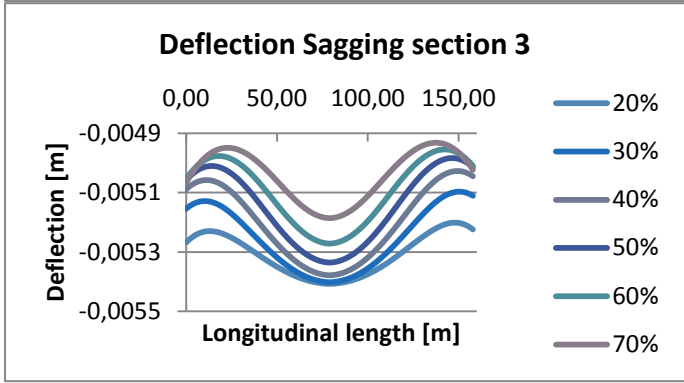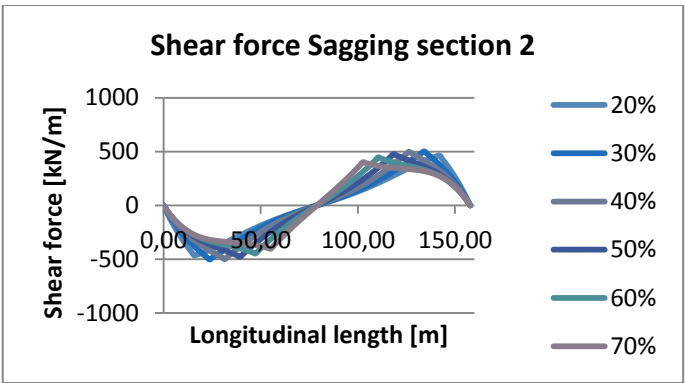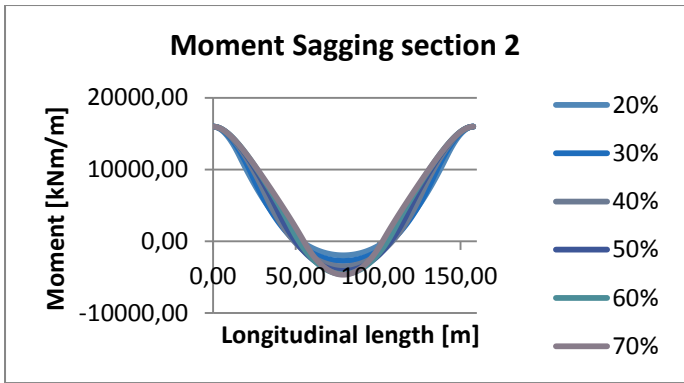
D.6.1.4 RESULTS HOGGING INCLUDING EXTERNAL FORCES

TRANSVERSE DIRECTION

Deflection Hogging

Legend: 20%, 30%, 40%, 50%, 60%, 70%

Moment Hogging

Legend: 20%, 30%, 40%, 50%, 60%, 70%

Shear force Hogging

Legend: 20%, 30%, 40%, 50%, 60%, 70%

LONGITUDINAL DIRECTION

Deflection Hogging section 1

Legend: 20%, 30%, 40%, 50%, 60%, 70%

Moment Hogging section 1

Legend: 20%, 30%, 40%, 50%, 60%, 70%

270
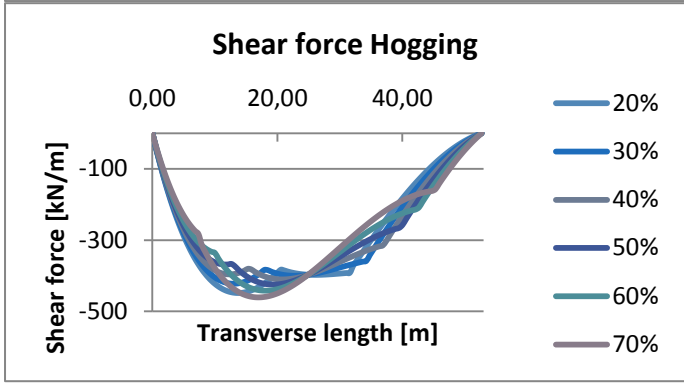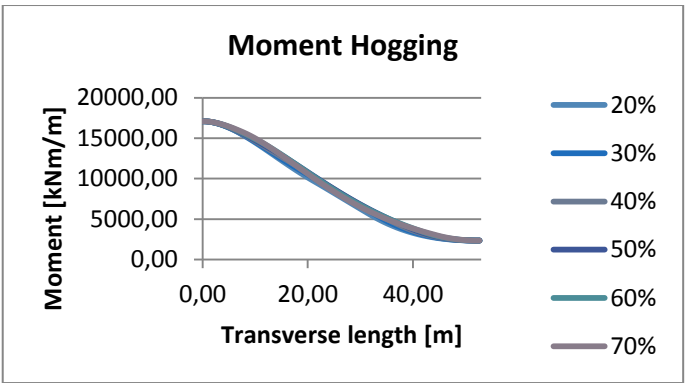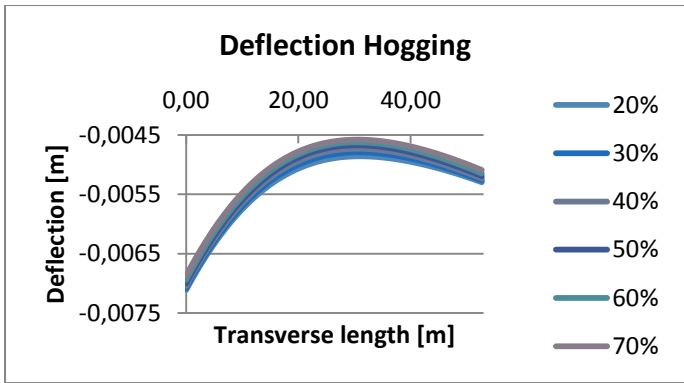
Shear force Hogging section 1

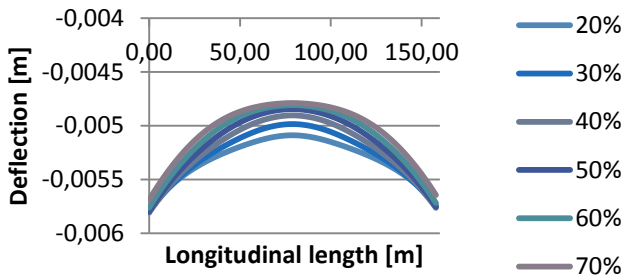
Deflection Hogging section 2
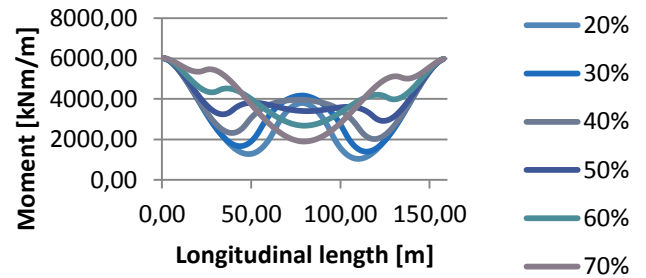

Moment Hogging section 2

Shear force Hogging section 2

Deflection Hogging section 3

Moment Hogging section 3

Shear force Hogging section 3